DEDICATED TO THE ADVANCEMENT OF SCIENCE, EDUCATION, AND EXPLORATION

Front cover: Pictograph from Dunbar Cave, Tennessee. See manuscript by Simek et al. in this issue.

FSC
www.fsc.org
MIX
Paper from
responsible sources
FSC® C006300

CAVE CRICKET EXIT COUNTS: ENVIRONMENTAL INFLUENCES AND DURATION OF SURVEYS

Floyd W. Weckerly[1]

[1]*Department of Biology, Texas State University – San Marcos, San Marcos, Texas, 78666, USA, fw11@txstate.edu*

Abstract: Cave cricket abundance is used as an indicator of integrity of cave ecosystems. One means of monitoring cave cricket abundance is counting crickets as they emerge from cave entrances for two hours after sunset. The influence of cloud cover, relative humidity, and surface temperature on counts is unknown and there might be few cave crickets that emerge during the first hour of the survey. Using mixed effects models, I assessed the influence of these environmental variables on exit counts and estimated when cave crickets emerged within the two-hour survey period. Exit-count surveys were conducted in eleven caves over four years in central Texas, and caves were surveyed up to four times a year across the four calendar seasons. Cloud cover, relative humidity, and temperature influenced counts, but the greatest influence was from temperature. Peaks in cave cricket counts occurred 80 to 90 minutes after the start of a survey and declined thereafter. Cave cricket exit count surveys should record surface temperature, cloud cover, and relative humidity at the start of surveys so that counts can be adjusted for these environmental influences. Also, surveys can be shortened to 1 or 1.5 hours in length.

INTRODUCTION

Cave crickets (*Ceuthophilus*) are often keystone species in cave ecosystems (Fagan et al., 2007; Lavoie et al., 2007; Taylor et al., 2007b). These insects provide inputs of allochthonous resources to caves that are often energy depauperate, the guano from cave crickets sustains invertebrate communities, and there are predators that specialize on the eggs laid by cave crickets (Taylor et al., 2005). Due to the inordinate influence of cave crickets on cave ecosystems, the number of cave crickets (hereafter abundance) that emerge from and return to caves is integral to the conservation of troglobitic endangered species and species of concern (Taylor et al., 2007b).

One means of monitoring abundance and temporal trends in cave crickets is with exit-count surveys (Taylor, et al., 2007b). Beginning at sunset on evenings when the surface temperature is at least 5 °C, two surveyors count cave crickets for two hours as they emerge from a cave entrance. Environmental conditions that might influence cave cricket emergence are the amount of moonlight and the temperature and relative humidity on the surface (Campbell, 1976; Poulson et al., 1995; Yoder et al., 2011). Surface activity of cave crickets is reported to be lower when there is more moonlight, during cool or hot nighttime temperatures, and when relative humidity is lower. But how these environmental variables actually affect the number of cave crickets that emerge from caves has not been examined. Furthermore, cave crickets are rarely active and foraging on the surface during daylight hours (Campbell, 1976; Yoder et al., 2011). In Carlsbad Caverns National Park, Campbell (1976) noted that as many as 50% of the cave crickets that emerged on summer nights did so between one and two hours after sunset. Because cave cricket emergence occurs after sunset, the necessity of conducting counts beginning at sunset is questionable. Perhaps surveys should begin a half hour to one hour after sunset, when most cave crickets emerge. Also, if most cave crickets emerge one to two hours after sunset, need these surveys be conducted for two hours?

The ability of a survey technique to estimate populations is based on the accuracy of actual population estimates in the settings where the survey technique will be applied. Estimates obtained from surveys must be compared to known populations (e.g., Weckerly and Foster, 2010). For cave crickets, it would be quite challenging to know the actual population in caves, and thus, conduct a robust evaluation of the reliability of exit counts. Nevertheless, understanding what influences counts and when to survey, so that counts are conducted when animals are most likely to emerge, can be used to ensure that surveys are standardized. If counts are conducted when most animals emerge, then counts obtained may provide reliable information on cave cricket abundance.

The specific objectives of this study were to determine if and how cloud cover, relative humidity, and temperature influence exit-survey counts, to determine the magnitude of the influence of these environmental variables on counts, and to estimate when cave crickets emerged from cave entrances within the 2-hour survey period.

SURVEYS

Cave cricket exit-count surveys were conducted at eleven small caves in the Balcones Canyonlands Preserve,

Table 1. Features and number of cave cricket exit count surveys conducted from 2006 – 2010 on the Balcones Canyonlands Preserve, Travis County, Texas. Also, the number of surveys with adequate counts (≥20) for analyses of survey length is reported. A dashed line denotes there were no surveys with data.

Cave	Length, m	Depth, m	No. of surveys	No. of surveys for analysis of survey length
Amber	10.2	7.5	10	8
Cotterell	7.9	7.6	11	11
District Park	74.7	13.4	11	11
Flint Ridge	283.0	46.5	11	11
Gallifer	35.0	7.4	11	10
Kretschmarr	7.6	6.1	13	12
Kretschmarr DP	8.0	11.4	6	…
Root complex	15.7	4.3	7	7
Spider	9.0	7.4	12	12
Tardus	6.0	6.3	7	…
Tooth	50.5	5.6	9	6

Travis County, Texas, USA (Table 1). The Balcones Canyonlands Preserve is a discontinuous collection of properties consisting of 5,365 ha managed for endangered species. The surface environment is a mix of ashe juniper (*Juniperus ashei*), hardwoods (mostly oaks, *Quercus* spp.), shrublands, and grasslands with gently sloping to steep-sided canyons. Daytime temperatures are hot (often > 35 °C) in summer and mild (5 to 25 °C) in winter (Watson et al., 2008).

Exit-count surveys were conducted from 2006 to 2010. A survey consisted of two surveyors counting all cave crickets (juveniles, nymphs, and adults) that emerged from a cave opening in a 2-hour period that began at sunset. Red lights were used during surveys to aid in seeing cave crickets and reduce disturbing them. Species of cave crickets were *Ceuthophilus secretus*, sometimes *C. cunicularis*, and a species of *Ceuthophilus* yet to be described (species B, Taylor et al., 2007a). At the beginning of the surveys, the percentage of cloud cover (a visual estimate), the relative humidity, and the temperature were recorded. Percentage cloud cover was a practical way to account for some of the variation in light from the moon and stars. Count surveys were conducted in all four calendar seasons of the year. At each cave six to twelve surveys were conducted.

ANALYSIS–ENVIRONMENTAL INFLUENCES

I analyzed data using mixed-effects models because exit-count surveys were repeatedly conducted at each cave across the four years (Pinheiro and Bates, 2000). Because the response variable was a count, I used a generalized linear mixed-effects model assuming a Poisson distribution (Faraway, 2006).

Fixed factors (hereafter, variables) were cloud cover, temperature, and relative humidity. Variables that potentially influenced the response, counts of emerging cave crickets. Because surface activity of cave crickets should increase from cool to warm temperatures but decline with hot temperatures, I estimated a quadratic relationship between temperature and counts (Poulson et al., 1995). Cloud cover, relative humidity, and temperature were continuous variables (Sokal and Rohlf, 1995). Mixed-effect models can suffer from computational instability. The iterative algorithms and optimization programs that estimate parameters may not converge, parameters are estimated but confidence intervals are not, or the estimated confidence intervals are very wide (Pinheiro and Bates, 2000). To reduce the possibility of computational instability, I centered continuous variables (Cheng et al., 2010) by subtracting the values from the means. z-tests of coefficients of variables were used to assess if a variable had an influence on counts (Faraway, 2006).

To assess the magnitude of influence (MI) of cloud cover, relative humidity, and temperature, I calculated $|Y_{max} - Y_{min}|/|X_{max} - X_{min}|$, where the largest predicted count and its X value were Y_{max} and X_{max} and the smallest predicted count and its X value were Y_{min} and X_{min}. A MI with a large value indicates that the variable had a large influence on counts. I calculated an MI in this manner because it is not possible to assess the magnitude of influence of variables by coefficients or z-tests when the units of predictors are not the same (Sokal and Rohlf, 1995).

Cave was treated as a random factor. Random factors were part of random effects, variances that allow relationships between fixed variables and the response variable to change among caves (Cheng et al., 2010). In the generalized linear mixed-effect model, there was one random effect, the cave. This allowed intercepts of the regressions between variables and counts to vary among the caves (Cheng et al., 2010).

To gauge the variability in the relationships between variables and counts, I estimated an intra-class correlation

Table 2. Quartiles (first-25th percentile, second-median or 50th percentile, third-75th percentile), minimum, and maximum values of percent cloud cover, percent relative humidity, temperature in Celsius, and counts during the 108 cave cricket exit count surveys conducted in 11 caves on the Balcones Canyonlands Preserve, Travis County, Texas.

Percentile	Count	Cloud Cover	Relative Humidity	Temperature
Minimum	1	0	16	7
First quartile	29	0	50	18
Median	149	20	60	24
Third quartile	258	42	75	28
Maximum	1536	100	98	34

coefficient. The coefficient is calculated by dividing the variance of the intercept random effect by the sum of the residual and intercept variances (Pinheiro and Bates, 2000). The residual variance measures the squared deviation between observed and predicted response variables, just like in an ordinary least-squares regression. The quantity can range from 0 to 1, with 0 indicating no variability in relationships across caves and 1 denoting tremendous variation in relationships across caves.

ANALYSIS–TWO HOUR SURVEY PERIOD

Mixed-effects models were also used to estimate emergence of cave crickets in the 2-hour survey period. However, because the response variable was continuous, I used linear mixed effects models. The response variable was the count during a 10-minute interval divided by the 2-hour total and expressed as a percentage. I labeled the response variable percent count. Fixed variables were time, cloud cover, temperature, and relative humidity. Minutes was a discrete variable, coded 1 to 12 to reflect the twelve 10-minute increments in the 2-hour survey period. The continuous variables of cloud cover, temperature, and relative humidity were centered. Minutes were modeled as a cubic relationship with percent counts; minutes had linear ($minutes$), quadratic ($minutes^2$), and cubic ($minutes^3$) coefficients. A cubic relationship allowed for the possibility of a low percent count early in the two hour survey period and a peak and a decline in counts, if they existed, at the end of the survey period. Because I used a linear mixed-effects model, I conducted an analysis of variance to assess which variables were influencing percent count (not possible with a generalized linear mixed-effects model).

In this analysis I modeled random effects so that relationships of fixed variables could vary in *intercepts*, *minutes*, and *minutes²*. Because of the number of random effects, Pearson's correlation coefficients were also estimated to account for possible covariance between random effects. The linear mixed-effects model had correlation coefficients between *intercepts* and *minutes*, *intercepts* and *minutes²*, and *minutes* and *minutes²* (Pinheiro and Bates, 2000). Correlation coefficients estimated between random effects can have wide confidence intervals, indicative of computational instability (Pinheiro and Bates, 2000). In case this occurred, I modeled the random effects assuming there were no correlations (i.e., $r = 0.0$). A preliminary examination of the data indicated the assumption of homoscedasticity was violated. Therefore, a variance function to characterize heteroscedasticity was used (Pinheiro and Bates, 2000). The variance function allowed residual variance to increase with increasing values of *minutes*.

FINDINGS–ENVIRONMENTAL INFLUENCES

There were 108 exit-count surveys conducted in the eleven caves (Table 1). Across these surveys, counts ranged from 1 to 1536 (Table 2). The cloud cover during surveys ranged from open sky (no cloud cover) to complete cloud cover, with a median cloud cover of 20 percent. Relative humidity ranged widely, but half the surveys were conducted when relative humidity was between 50 and 75 percent. The first and third quartiles of temperatures at the start of surveys were 18 °C and 28 °C, respectively.

There was a quadratic relationship between temperature and counts (Table 3). Cloud cover and relative

Table 3. Coefficients, standard errors, and findings from z-tests (z value, P value) for fixed variables and intercept for the generalized, linear mixed effects model. Temperature and temperature² estimated a quadratic relationship.

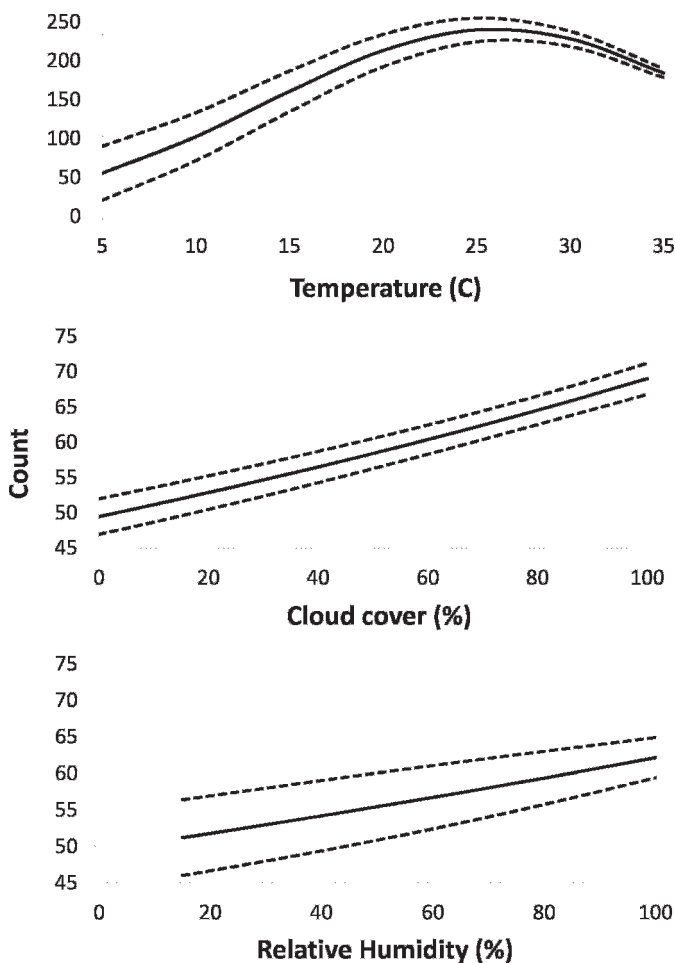| Coefficient	Value	SE	z	P
Intercept	5.169	0.2465	20.97	<0.001
Cloud cover	0.003	0.0002	18.10	<0.001
Relative humidity	0.002	0.0004	−8.96	<0.001
Temperature	0.021	0.0011	20.35	<0.001
Temperature²	−0.001	0.0001	5.27	<0.001

Figure 1. Graphs showing relationships (and 1 standard error envelopes) between relative humidity, cloud cover, temperature, and counts. Note that the scale for counts on the Y axis differs between the temperature graph and the other two graphs.

humidity also influenced counts. Counts increased from cool temperatures (5–10 °C) to warm temperatures (~25 °C) and declined with hotter temperatures (Fig. 1). Both cloud cover and relative humidity had positive relationships with counts.

To estimate the MI for temperature, I multiplied regression coefficients for cloud cover and relative humidity by their respective means. To estimate MI for cloud cover and relative humidity, I likewise multiplied the other coefficients by their means. The MI for temperature, cloud cover, and relative humidity were 9.2, 0.20, and 0.13, respectively.

The residual variance for the generalized linear mixed-effects model was 0.76, and the intra-class correlation coefficient was 0.43. The relationships of cloud cover, relative humidity, and temperature with cave cricket exit counts did vary across caves, but the differences were not dramatic.

INTERPRETATION–ENVIRONMENTAL INFLUENCES

All three environmental variables influenced counts of cave crickets emerging from caves. But temperature clearly had a much greater influence on counts than did cloud cover or relative humidity. The MI for temperature indicated that counts increased over 900 percent for every one degree increase in temperature between 5 and 25 (i.e., counts increased, on average, by nine cave crickets for every one degree increase in temperature), whereas cloud cover and relative humidity increased by only 13 to 20 percent for every one percent increase in these variables. The influence of temperature on counts, however, was not a straightforward linear increase. According to my analysis, cave crickets are most active in the Balcones Canyonlands Preserve when nighttime surface temperatures are between 20 and 30 °C. The reduction in cave cricket emergence on cool and hot nights is consistent with studies indicating hot temperatures are stressful for cave crickets and that cave cricket activity is curtailed when surface temperatures are cool (Poulson et al., 1995; Studier and Lavoie, 1990).

Another finding from the analysis was that relationships between environmental influences on counts varied somewhat across caves. The relationships varied in intercepts but not in slopes. Therefore, the form of relationships did not change across caves. For example, the quadratic relationship between temperature and counts was the same from cave to cave. The variability in intercepts across caves suggests that caves varied in cave cricket abundance.

FINDINGS–SURVEY LENGTH

For the analysis of percent counts I only used surveys where a minimum of twenty cave crickets were counted, consequently there was data from nine caves and 88 exit-count surveys (Table 1). In the initial model there were no influences on percent count from temperature, relative humidity, or cloud cover ($F_{1,1038} < 1.32$, $p > 0.179$). Another model (labeled full random effects in Table 4) was analyzed with these variables removed. The variables in the full random effects model were $minutes$, $minutes^2$, and $minutes^3$. The full random effects model had issues with computational instability. Two of the three correlation coefficients had enormously wide confidence intervals, and I was not confident that this model estimated these parameters reliably. Thus, I ran the final model (subsets random effects in Table 4) without the correlation coefficients between all pairs of random effects (Table 4). Confidence bounds on estimates of all parameters (coefficients) and random effects of the subsets random effects model indicated that computational instability was less of a problem. The three coefficients for $minutes$ (linear, quadratic, cubic) were useful to modeling the relationship between $minutes$ and percent count because every confidence

Table 4. Estimates and 95 percent lower and upper bounds of fixed and random effects of the mixed effects models that estimated relationship between minutes after start of cave cricket exit count survey (minutes) and the percentage of all cave crickets that were counted in 10 minute increments. The full random effects model included all correlations between random components. Because the correlation estimates had wide confidence intervals a subsets random effects model was estimated without correlation estimates. Minutes^2 is a quadratic coefficient and minutes^3 is a cubic coefficient. Standard deviation is denoted by S and R denotes Pearson's correlation coefficient.

Fixed Parameter	Lower Bound	Coefficient	Upper Bound	Random Effect	Lower Bound	Estimate	Upper Bound
			Full Random Effects				
Intercept	9.03	10.69	12.36	S(residual)	2.34	2.66	3.01
Minutes	0.81	1.42	2.04	S(intercept)	1.39	2.38	4.08
Minutes^2	−0.33	−0.20	−0.06	S(minutes)	0.51	0.85	1.43
Minutes^3	−0.03	−0.02	−0.01	S(minutes^2)	0.12	0.20	0.33
…	…	…	…	R(intercept, minutes)	−0.99	−0.94	0.90
…	…	…	…	R(intercept, minutes^2)	−1.00	−0.99	0.73
…	…	…	…	R(minutes, minutes^2)	0.47	0.94	0.99
…	…	…	…	Variance function	0.40	0.47	0.54
			Subsets Random Effects				
Intercept	9.20	10.73	12.25	S(residual)	2.41	2.74	3.10
Minutes	0.81	1.41	2.02	S(intercept)	1.23	2.15	3.76
Minutes^2	−0.32	−0.20	−0.08	S(minutes)	0.51	0.83	1.36
Minutes^3	−0.03	−0.02	−0.01	S(minutes^2)	0.11	0.18	0.30
				Variance function	0.38	0.45	0.52

interval did not overlap zero. Also, it was a good idea to model the heteroscedasticity as increasing residual standard deviation with increasing percent counts because the variance function had confidence intervals that did not overlap zero. The intra-class correlation coefficient was 0.38 for the subsets random effects model. The cubic
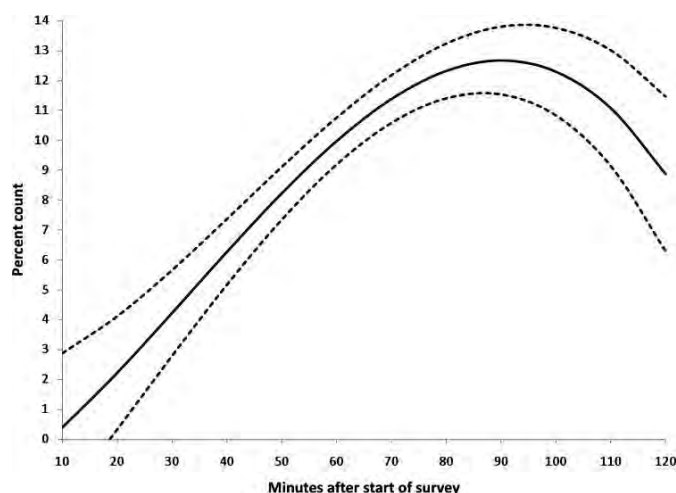

Figure 2. The relationship, and 1 standard error envelope, between minutes after the start of a cave cricket exit-count survey and the percentage of all cave crickets that were counted in the preceding 10-minute interval.

relationship between *minutes* and percent count did vary among caves, but the variation was modest.

The peak in counts occurred between 80 and 90 minutes into the exit-count surveys (Figure 2). Counts increased dramatically from the beginning of the survey to the time of the peak and declined thereafter. I used the predicted percent count at each 10-minute increment to calculate the cumulative percent count. During the last 1.5 hours of a survey, 93 percent of all cave crickets were counted, and during the last 1.0 hours of a count survey, 69 percent of all cave crickets were counted.

The decline in percent counts in the last half hour of surveys indicates that extending surveys beyond 2 hours after sunset will not result in continued high counts, a finding that is consistent with emergence patterns of cave crickets in Carlsbad Caverns National Park (Campbell, 1976). Most crickets in that study emerged one to two hours after sunset. It was not surprising that cloud cover, relative humidity, and temperature did not influence time history of the counts but did influence total counts.

CONCLUSIONS

Proactive conservation of endangered species and species of concern in cave ecosystems requires monitoring of species that indicate the integrity of the cave ecosystem (Lavoie et al., 2007; Taylor et al., 2007b). In central Texas, *Ceuthophilus* cave crickets are the indicator species of cave productivity in the karst environment (Taylor et al.,

2007a). Information gathered from monitoring cave cricket abundance is used to estimate changes over time in the number of cave crickets that emerge from cave entrances, determine the state of cave ecosystems, assess whether goals of a conservation program are met, and implement actions to mitigate degradation of the cave environment. Fundamental to monitoring cave ecosystems is the protocol used to collect data on cave cricket abundance. A standardized survey protocol is merely a set of instructions that dictate that sufficient data are collected that analyses of the data can be done with statistical methods that can account for peculiarities in the data and heterogeneity in environmental conditions that influence cave cricket emergence. Standardization in how the data is collected is fundamental to assessing trends across time, a feature already present in cave cricket exit-count surveys. A feature of these data was that count surveys were conducted periodically across time in the same caves, which required the use of mixed-effects models that can accommodate the grouping of data by caves (Pinheiro and Bates, 2000). It is clear that heterogeneity in counts can be due to temperature, cloud cover, and relative humidity. Of these environmental influences temperature has the greatest influence on cave cricket emergence. To accommodate environmental heterogeneity in surveys there are two options. The first is to restrict surveys to when environmental conditions are most amenable to emergence. A drawback to this option is it will constrain the times when surveys can be conducted. The findings of my analysis suggest that, at the very least, surveys should be conducted when surface temperatures are between 20 and 30 °C. The other option is to retain the existing protocol. By recording temperature, cloud cover, and relative humidity at the start of the survey, the influence of these variables on exit counts can be accounted for in analyses to detect temporal or spatial trends in cave cricket abundance.

In cave cricket exit-count surveys, one aspect of the required survey effort is the length of time to conduct survey. (The other is conducting counts at cave entrances when cave crickets emerge.) Because of logistical and monetary constraints, monitoring programs rarely enumerate the entire targeted population. Instead, a subset of the targeted population is counted. If the count is to reflect the actual population state, surveys should be conducted when individuals in the population are most readily counted. For surveys on the Balcones Canyonlands Preserve, that window of time appears to be 1 to 1.5 hours beginning a half hour to one hour after sunset.

ACKNOWLEDGEMENTS

REFERENCES

Campbell, G.D., 1976, Activity rhythm in the cave cricket, *Ceuthophilus conicaudus* Hubbell: American Midland Naturalist, v. 96, p. 350–366.

Cheng, J., Edwards, L.J., Maldonado-Molina, M.M., Komro, K.A., and Muller, K.E., 2010, Real longitudinal data analysis for real people: building a good enough mixed model: Statistics in Medicine, v. 29, p. 504–520. doi:10.1002/sim.3775.

Fagan, W.F., Lutscher, F., and Schneider, K., 2007, Population and community consequences of spatial subsidies derived from central-place foraging: The American Naturalist, v. 170, p. 902–915. doi:10.1086/522836.

Faraway, J.J., 2006, Extending the Linear Model with R: Generalized Linear, Mixed Effects and Nonparametric Regression Models, New York, Chapman & Hall, CRC Texts in Statistical Science, 312 p.

Lavoie, K.H., Helf, K.L., and Poulson, T.L., 2007, The biology and ecology of North American cave crickets: Journal of Cave and Karst Studies, v. 69, p. 114–134.

Pinheiro, J.C., and Bates, D.M., 2000, Mixed-Effects Models in S and S-PLUS, New York, Springer Verlag, 548 p.

Poulson, T.L., Lavoie, K.H., and Helf, K.L., 1995, Long-term effects of weather on the cricket (*Hadenoecus subterraneus*, Orthoptera, Rhaphidophoridae) guano community in Mammoth Cave National Park: American Midland Naturalist, v. 134, p. 226–236.

Sokal, R.R., and Rohlf, F.J., 1995, Biometry: The Principles and Practice of Statistics in Biological Research, 3rd edition, New York, W.H. Freeman and Company, 887 p.

Studier, E.H., and Lavoie, K.H., 1990, Biology of cave crickets, *Hadenoecus subterraneus*, and camel crickets, *Ceuthophilus stygius* (Insecta: Orthoptera): metabolism and water economies related to size and temperature: Comparative Biochemistry and Physiology, Part A, v. 95, p. 157–161. doi:10.1016/0300-9629(90)90025-N.

Taylor, S.J., Krejca, J.K., and Denight, M.L., 2005, Foraging range and habitat use of *Ceuthophilus secretus* (Orthoptera: Phaphidophoridae), a key trogloxene in central Texas cave communities: American Midland Naturalist, v. 154, p. 97–114. doi:10.1674/0003-0031(2005)154[0097:FRAHUO]2.0.CO;2.

Taylor, S.J., Krejca, J.K., and Hackley, K.C., 2007a, Examining Possible Foraging Differences in Urban and Rural Cave Cricket Populations: Carbon and Nitrogen Isotope Ratios (δ^{13}C, δ^{15}N) as Indicators of Trophic Level: Illinois Natural History Survey Technical Report 2007(59), 97 p.

Taylor, S.J., Weckstein, J.D., Takiya, D.M., Krejca, J.K., Murdoch, J.D., Veni, G., Johnson, K.P., and Reddell, J.R., 2007b, Phylogeography of Cave Crickets (*Ceuthophilus* spp.) in Central Texas: A Keystone Taxon for the Conservation and Management of Federally Listed Endangered Cave Arthropods: Illinois Natural History Survey Technical Report 2007(58), 45 p.

Watson, C.A., Weckerly, F.W., Hatfield, J.S., Farquhar, C.C., and Williamson, P.S., 2008, Presence-nonpresence surveys of golden-cheeked warblers: detection, occupancy and survey effort: Animal Conservation, v. 11, p. 484–492. doi:10.1111/j.1469-1795.2008.00204.x.

Weckerly, F.W., and Foster, J.A., 2010, Blind count surveys of white-tailed deer and population estimates using Bowden's estimators: Journal of Wildlife Management, v. 74, p. 1367–1377. doi:10.1111/j.1937-2817.2010.tb01259.x.

Yoder, J.A., Benoit, J.B., LaCagnin, M.J., and Hobbs, H.H., 2011, Increased cave dwelling reduces the ability of cave crickets to resist dehydration: Journal of Comparative Physiology B: Biochemical, Systemic, and Environmental Physiology, v. 181, p. 595–601. doi:10.1007/s00360-011-0555-5.

INVOLVEMENT OF BACTERIA IN THE ORIGIN OF A NEWLY DESCRIBED SPELEOTHEM IN THE GYPSUM CAVE OF GRAVE GRUBBO (CROTONE, ITALY)

Paola Cacchio[1]*, Claudia Ercole[1], Rosita Contento[1], Giorgio Cappuccio[2], Maria Preite Martinez[3], Maddalena Del Gallo[1], and Aldo Lepidi[1]

Abstract: Microorganisms have been shown to be important active and passive promoters of redox reactions that influence the precipitation of various minerals, including calcite. Many types of secondary minerals thought to be of purely inorganic origin are currently being reevaluated, and microbial involvement has been demonstrated in the formation of pool fingers, stalactites and stalagmites, cave pisoliths, and moonmilk. We studied the possible involvement of bacteria in the formation of a new type of speleothem from Grave Grubbo Cave, the third-largest gypsum cave in Italy. The speleothem we studied consisted of a large aggregate of calcite tubes having a complex morphology, reflecting its possible organic origin. We isolated an abundant heterotrophic microflora associated with this concretion and identified *Bacillus*, *Burkholderia*, and *Pasteurella* spp. among the isolates. All of the isolates precipitated $CaCO_3$ in vitro in the form of calcite. Only one of the isolates solubilized carbonate. The relative abundance of each isolate was found to be directly related to its ability to precipitate $CaCO_3$ at cave temperature. We suggest that hypogean environments select for microbes exhibiting calcifying activity. Isotopic analysis produced speleothem $\delta^{13}C$ values of about – 5.00‰, confirming its organic origin. The lightest carbonates purified from B4M agar plates were produced by the most abundant isolates. SEM analysis of the speleothem showed traces of calcified filamentous bacteria interacting with the substrate. Spherical bioliths predominated among the ones produced in vitro. Within the crystals produced in vitro, we observed bacterial imprints, sometimes in a preferred orientation, suggesting the involvement of a quorum-sensing system in the calcium-carbonate precipitation process.

INTRODUCTION

Few gypsum karst systems in Italy have been studied in detail, but general features that distinguish these systems from limestone systems have nonetheless been identified. These karst systems normally contain small physical and chemical deposits with very similar morphologies and chemical compositions, but they may also contain unusual speleothems and cave minerals characteristic of gypsum caves.

Grave Grubbo Cave (Crotone, Southern Italy) contains two unusual calcite deposits (Forti and Lombardo,1998). The first is a floating calcite speleothem resembling a group of half-bubbles. The second is a newly discovered type of speleothem that was suspected to be of organic origin due to its complex structure composed of a large aggregate of iso-oriented calcite tubes. Poluzzi and Minguzzi (1998) have suggested that the origins of this speleothem may lie in the activities of a troglobitic insect that belongs to the order *Trichoptera* (genus *Wormaldia?*) and dwells in the sulfur compound-rich hypogean water. In theory, these insects would be throphically supported by nutrients synthesized by chemoautotrophic bacteria. In a hypogean environment, the presence of reduced chemical compounds, such as hydrogen sulfide, creates a redox interface between these compounds and the oxygen from the cave atmosphere or from oxygen-rich waters. Chemoautotrophic microorganisms can live at this interface by deriving energy from the oxidation of reduced chemical compounds. Specialized sulphur-oxidizing microbial communities, in particular, use this energy to produce organic matter in situ. Organic matter, in turn, can serve as the basis for a food chain that can sustain invertebrate communities inhabiting the deep recesses of hypogenic caves (Forti et al., 2002). On the other hand, the hypogean environment also hosts bacteria that use or produce large amounts of CO_2 due to their metabolic activities. According to this theory, this CO_2 reacts with the gypsum-saturated water in the presence of Ca^{2+}, resulting in the deposition of calcite around the insect larvae. However, this deposition hypothesis does not account for the absence of insects in the speleothem body, the diameter of the calcite

* Corresponding Author: paolacacchio@yahoo.it
[1] Department of Basic and Applied Biology, Microbiology Laboratory, University of L'Aquila, Coppito, 67010 L'Aquila, Italy
[2] CNR- Institute of Structural Chemistry, POB 10, 00016 Monterotondo Sc., Rome, Italy
[3] Department of Earth Science - La Sapienza University and IGAG - CNR, Rome, Italy

tubes being greater than that of the larvae, and the lack of evidence that continental Trichoptera can accumulate lithoid elements (Poluzzi and Minguzzi, 1998).

Many studies have demonstrated the effects of heterotrophic bacteria, actinomycetes in particular, on the formation of specific speleothems (Baskar et al., 2006, 2009; Cañaveras et al., 1999, 2001; Groth et al., 1999; Laiz et al., 1999, 2000; Le Métayer-Levrel et al., 1997; Melim et al., 2001; Northup et al., 2000). Bacteria can precipitate extracellular calcium carbonate through a variety of processes (Barton and Northup, 2007; Ehrlich, 2002; Riding, 2000; Simkiss and Wilbur, 1989). First, mineralization occurs as a byproduct of microbial metabolism that involves either autotrophic pathways, which can deplete CO_2 locally, or heterotrophic pathways, which release into the environment (Castanier et al., 1999, 2000). In these passive mechanisms, reactions such as the enzymatic hydrolysis of urea, and the ammonification of amino acids cause a rise in pH, which, if free Ca^{2+} is present, results in the precipitation of calcium carbonate.

Second, carbonate nucleation takes place on bacterial cell walls due to ion exchange (i.e., an active process) through the cell membrane by poorly understood mechanisms (Castanier et al., 1999). It may also occur through the adsorption of divalent cations to specific negatively charged functional groups on the cell wall (Rivadeneyra et al., 2000). Nevertheless, once carbonate has begun to precipitate on the cell surface, the cell acts as a nucleation site. This stage is critical in initiating mineral precipitation. Subsequent $CaCO_3$ precipitation may be purely inorganic.

The third possibility involves specific proteins present in the extracellular polymeric substances (EPS) produced by the bacterial communities that can trap sediment and are often essential for a direct deposition of microbial carbonate (Ercole et al., 2007; Riding, 2000).

By growing microorganisms in the laboratory under controlled conditions, it is possible to delineate their ability to alter the chemistry of their microenvironment and produce biominerals. For this reason, we used laboratory-based cultures to investigate the extent to which heterotrophic calcifying bacteria are involved in the formation of the speleothem construction recently discovered in Grave Grubbo Cave. We isolated and characterized culturable heterotrophic microflora from the sample and assessed each isolate for in vitro calcification and carbonate solubilization at various temperatures. We also studied the mineral and isotopic compositions and the morphology of the carbonate concretion and of the purified bioliths obtained in laboratory cultures.

MATERIALS AND METHODS

The Grave Grubbo Cave opens at 158 m above sea level in the gypsum karst of Verzino, on the Calabrian Ionian side, just at the foot of the Silan Massif (Crotone, Southern Italy; Fig. 1). Several deep karst landforms were recently discovered in this area, and the Grave Grubbo-Vallone Cufalo system is the main cave identified (Galdenzi and Menichetti, 1998). Grave Grubbo is the third-largest gypsum cave in Italy and extends to over 2 km. Three galleries branch off from the cave entrance, the Ramo di Cenerentola, the Galleria quadrata, and the Ramo del fiume (Fig. 2; Forti and Lombardo, 1998). An underground river, the water of which contains sulfate and calcium ions, flows through the lower section of the main passage, the Ramo del fiume, and can be followed for about 1.5 km. The temperature of the cave is about 15 °C. The rock formations, structural settlement of the karst formations in this area, and the hydrodynamics of this system are not consistent with the development of large, widespread chemical deposits. Indeed, calcite speleothems are very rare and small, and there are almost no gypsum speleothems.

We studied an unusual and likely biogenic speleothem in the Grave Grubbo Cave. The sample location and sample are shown in Figures 2 and 3, respectively.

The speleothems in Grave Grubbo Cave present as sectional massive or acicular structures, so it was clear, even to the first cavers who visited the cave, that this speleothem was remarkably different from other formations. Forti and Lombardo (1998) were the first to note the peculiar characters of the deposit and described it for a multidisciplinary research program on the Verzino area (Ferrini, 1998). The presence of this kind of speleothem inside Grave Grubbo is limited to a confined area next to a small waterfall and the terminal lake, at about three quarters of the total length of the cave.

The studied speleothem, made of calcite tubes connected together, mantled a limited evaporitic outcrop. From a lithological point of view, the deposit is divided into two separate levels, each having a different direction for its tubes' axes that likely resulted from two different flow directions during its period of deposition. At present, the speleothem has no connection with the actual water flow and appears to be fossilized.

A sample was collected from the upper layer of the speleothem using a sterile chisel and sample bag, and was stored at 4 °C for 24 h until microbiological analysis. From this sample, we obtained two sub-samples under sterile conditions. One contained material from the exterior surface of the speleothem (the ''outer'' subsample) and the other contained material from the speleothem's interior (the ''inner'' subsample).

To isolate the culturable heterotrophic bacteria associated with the outer and inner sub-samples from the upper layer of the speleothem, we ground 1 g of each sample to a powder using a sterile mortar and pestle and suspended this powder in saline solution (0.9% NaCl). Serial dilutions were spread in triplicate on B-4 agar (Boquet et al., 1973) containing 2.5 g calcium acetate, 4.0 g yeast extract, 10.0 g glucose, and 18.0 g Biolife agar per liter of distilled water. The pH was adjusted to 8.0 using NaOH. B-4 medium is an

Figure 1. Geographical location of Grotta Grave Grubbo (Grave Grubbo Cave), Calabria, Southern Italy.

enrichment medium for calcifying bacteria; the acetate ion is an energy source, while the Ca^{2+} cation is used by the calcifying bacteria to precipitate calcium carbonate. The presence of glucose speeds the process. Inoculated plates were incubated at 32 °C for two weeks. Previous studies demonstrated that colonies from cave samples grow very slowly at cave temperature and that the diversity of the culturable genera was similar whether the bacteria were grown at cave temperature (13 °C) or at laboratory temperature (28 °C) (Groth et al., 2001; Laiz et al., 2003). Individual colonies were selected and purified by streaking on B-4 agar. The relative abundance of each isolate, with respect to the total culturable bacterial microflora, was determined by direct counts on B-4 agar plates. Pure calcifying isolates were stored in liquid nitrogen (−196 °C).

Calcifying isolates were characterized using morpho-physiological and biochemical methods. Cell and aggregate morphology was studied under a light microscope. Gram-staining was performed with the Color Gram 2 kit (bio-Mérieux, Marcy-l'Etoile, France).

All physiological tests in which temperature was not a studied variable were carried out at 15 °C. Oxygen requirement was studied by incubating isolates on B-4 agar in an anaerobic chamber. Oxidase activity was assessed using a solution of N,N-dimethyl p-phenylenediamine oxalate, ascorbic acid, and β-naphthol (Oxoid). Catalase production was demonstrated on slides by the formation of bubbles when a suspension of the organism to be tested was mixed with a drop of 3% (v/v) hydrogen peroxide. Acid production was determined by API 50CH, API STAPH, API 20E and API 20NE test strips (bioMérieux) according to the manufacturer's instructions. Urease activity, nitrate reduction, arginine dihydrolase, gelatinase, β-galactosidase, lysine decarboxylase, ornithine decarboxylase, and tryptophan deaminase activities and H_2S indole and acetoin production were also checked by API test strips (bio-Mérieux). APILAB Plus software (update v. 3.3.3) was used for the API test culture identification.

We assessed the calcite production of isolates by culturing them on medium B-4, as described by Boquet et al. (1973). The bacterial isolates were spread in triplicate on
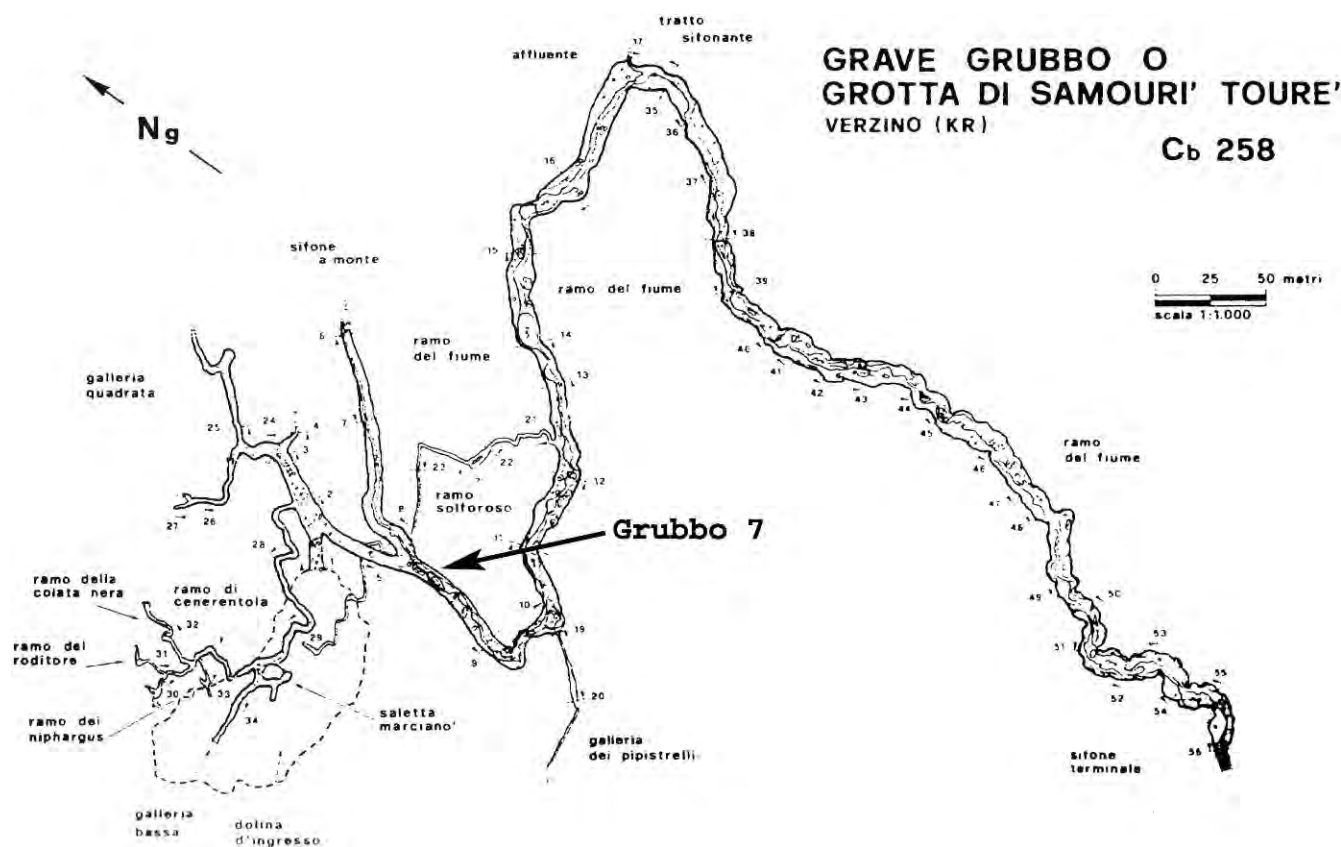
Figure 2. Map of Grave Grubbo Cave (Forti and Lombardo, 1998). Sampling site is at Grubbo 7, shown by the arrow; the entrance is labeled *dolina d'ingresso*.

the surface of agar plates, which were then incubated in the presence of air at 4, 15, 22, and 32 °C. We examined plates periodically under a light microscope to monitor crystal production for up to 40 days after inoculation. For negative controls, we checked for the presence of crystals in

Figure 3. Macroscopic morphology of the newly described speleothem from Grave Grubbo Cave showing the tubes with mean of inner diameter 4.24 mm (Poluzzi and Minguzzi, 1998).

sterile medium and medium inoculated with autoclaved bacteria.

Crystals produced by cultured bacteria were removed from the medium by cutting out agar blocks and placing them in boiling water until the agar dissolved. The supernatants were decanted, and the sediment was resuspended and washed in distilled water until the crystals were free of impurities (Rivadeneyra et al., 1998). The washed crystals were air-dried at 37 °C and then used to determine $CaCO_3$ yield, crystal-phase, stable carbon and oxygen isotope compositions, and morphology.

The carbonate yield of the crystals obtained after three months of incubation was expressed as a percentage of the theoretical dry weight of calcium carbonate by dividing the experimental dry weight of the crystals by the theoretical dry weight. The theoretical dry weight of calcium carbonate was the stoichiometric quantity obtained from the 18 mg Ca^{2+} contained in each plate. The experimental dry weight of $CaCO_3$ was the mean of the values obtained from four independent experiments. Data were analyzed using the Student's t-test.

X-ray diffraction (XRD) measurements were done by a two-circle t/2t diffractometer with a Cu radiation source, secondary graphite monochromator, and scintillation detector (Seifert MZ IV). The supply voltage of the X-ray

P. Cacchio, C. Ercole, R. Contento, G. Cappuccio, M.P. Martinez, M. Del. Gallo and A. Lepidi

Table 1. Identification and culture traits of the calcifying isolates from Grave Grubbo Cave (Calabria, Southern Italy).

Strains	Microorganism	Gram	Catalase	Oxidase	Urease	$NO_3^- \rightarrow NO_2^-$	Anaerobiosis
G1	*Bacillus magaterium*	+	+	−	+	+	+/−
G2	*Burkholderia* sp.	−	+	−	+	+	+/−
G3	*Pasteurella* sp.	−	+	−	+	+	−
G4	*Staphylococcus* sp.	+	+	−	+	+	−
G5	*Burkholderia* sp.	−	+	−	+	+	−
G6	*Brevibacillus brevis*	+	+	−	+	+	−
G7	Not identified	−	+	−	+	+	+/−
G8	*Actinomyces* sp.	+	+	−	+	nd	−

Note: +/− = minimal growth and nd = not determined.

tube was set at 50 kV and 30 mA. The 2t scan range was between 22° and 50°; and each scan was done in steps of 0.05°. A counting time between one and ten seconds per step was selected, depending on the sample density. The crystalline phases were identified using the ICDD (International Center for Diffraction Data) database cards (JCPDS=Joint Commitee on Powder Diffraction Standards).

We used a simple procedure for recognizing the crystalline phases present in each specimen. Cultured solid media samples were dried at 22 °C or 32 °C. Agar medium was cut into 10 × 30 mm flat blocks, 0.5 mm high, and those richest in crystallites were fixed on adhesive tape. This self-supporting film was put into the center of the diffractometer using a U-shaped sample holder to minimize background signals. For crystallite-poor samples, the agar was dissolved and crystals were collected according to the Rivadeneyra et al. method (1998). The washed crystals were air-dried at 37 °C and then supported on a glass slide for X-ray measurements.

Morphology characteristics were studied by scanning electron microscopy (SEM). Cultured solid-media samples were dried at 37 °C; agar medium was cut into flat blocks. For crystallite- poor samples, the agar was dissolved and crystals were collected and purified according to the Rivadeneyra et al. method (1998). To observe the inner portion of the bioliths, crystals were first powdered using a mortar and pestle. All samples were gold-shadowed and observed with a Philips SEM XL30CP.

For $\delta^{13}C$ and $\delta^{18}O$ analyses, carbonates (1 mg) obtained in vitro or from Grave Grubbo Cave were dissolved at 70 °C in a KIEL II carbonate device (modified by McCrea, 1950). The CO_2 produced was analyzed using a Finnigan-Mat 252 mass spectrometer. Data relative to the V-PDB standard are reported using the conventional notation as previously specified (Cacchio et al., 2004).

Bacterial isolates displaying calcification were also tested for calcium carbonate dissolution by growing colonies on Deveze-Bruni medium (pH 6.8) containing 0.14% or 2.5% $CaCO_3$ at 32 °C (NORMAL Commision, 1990). We quantified carbonate solubilization after 7, 15, and 30 days by measuring the diameter of the clear halo that surrounded each colony in response to decreased pH (Martino et al., 1992).

RESULTS AND DISCUSSION

Microbiological analysis of the sample from the upper layer of the calcareous speleothem from Grubbo Cave led to the isolation of sixteen bacterial isolates. Eight of these were obtained from the outer sub-sample and eight were from the inner sub-sample. Based on the colony morphologies of the isolates, we concluded that each sub-sample contained the same eight isolates and numbered them from G1 to G8. These results demonstrate the existence of a microflora of culturable heterotrophic bacteria that was autochthonous to this substrate. The two sub-samples contained similar densities of heterotrophic bacteria culturable in the B-4 medium, 3.4×10^4 cfu g^{-1} (dry weigh) for the outer sample and 2.0×10^4 cfu g^{-1} (dry weight) for the inner sample, which indicated that the isolates were homogeneously distributed throughout the calcareous body. A similar microbial density has been reported for the calcareous speleothems of the Stiffe and Cervo Caves (Cacchio et al., 2003b and 2004, respectively). The abundance of culturable bacterial cells isolated from the Grave Grubbo speleothem suggests that their presence was not accidental.

The isolates were present in similar proportions in the inner and outer sub-samples. The G4 isolate was the most abundant, representing 81% of the population, whereas G5 represented 11%. The contributions of the G1, G2, G3, G6, G7 and G8 isolates to the overall population ranged from 0.3 to 5.4%. These results are interesting, but may not reflect the actual microbial activity taking place in the speleothem, as cultivation techniques are thought to greatly underestimate microbial diversity due to the non-culturability of the large majority of microorganisms (Dojka et al., 2000).

The results of the characterization tests and the species we identified are shown in Table 1. Most isolates were aerobic rod-shaped bacteria, of which 50% were Gram-positive. The most abundant isolate, G4, was an aerobic, spherical-shaped Gram-positive bacterium. It has been reported in the literature that Gram-positive cocci and coccoid forms are extremely common in soil and in undisturbed environments such as the Grave Grubbo and Cervo caves (Cacchio et al., 2004). All the calcifying bacteria reduced nitrate and hydrolyzed urea. Both of these
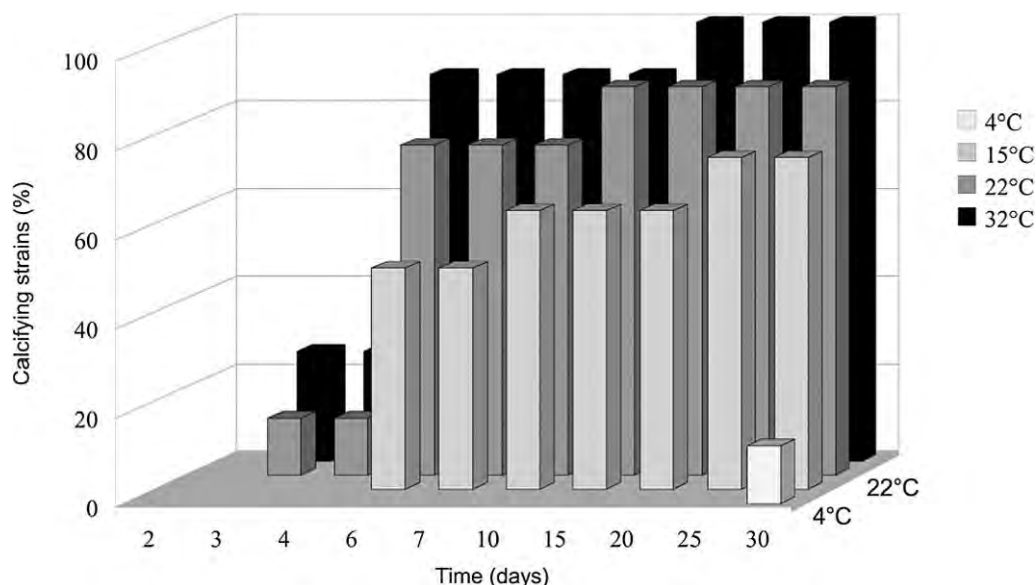
Figure 4. Relationship between the percentage of strains that were calcifying on B-4 solid medium at 4, 15, 22, and 32 °C and the number of days in culture. G7 and G8 did not survive and are not included in the percentages.

metabolic activities might be involved in the precipitation of calcium carbonate in caves (Castanier et al., 1999). Possible sources of nitrates in caves include bat guano, organic-rich ammonia or ammonium ions carried in from surface soils, ammonium-urea from amberat (cave rat urine), bacterial nitrogen fixation, fertilizers, volcanic rocks, and forest litter (Barton and Northup, 2007).

The API System identified seven of the eight calcifying bacterial isolates obtained from the Grave Grubbo speleothem to the genus level (Table 1). The species of 50% of the isolates were scored with low discrimination because the API test bank, which is designed to identify pathogenic species, occasionally misidentifies subsurface isolates (Amy et al., 1992). Isolates G1 and G6 were related to *Bacillus genus* (*Bacillus megaterium* and *Brevibacillus brevis*, respectively). *Bacillus* strains were the most common calcifying bacteria found in the Stiffe Cave (Cacchio et al., 2003b). Isolates G2 and G5 were identified as *Burkholderia sp*. The most abundant isolate, G4, was related to *Staphylococcus* sp. Isolate G7 was not identified. Isolate G8, which was the only one displaying pseudomyceliar growth, was related to *Actinomyces* sp.

Amati and Gualandi (1934) isolated *Bacillus violaceus* and *Micrococcus flavus liquiefaciens* from samples taken from the Gortani Cave, which is in a gypsum outcrop near Bologna. A study of the microbial populations in the Novella Cave (Farneto, Gessi Bolognesi Regional Park) identified many bacterial (*Bacillus* sp., *Serratia* sp., and *Acinetobacter* sp.) and mold (*Cryptococcus* sp., *Penicillium* sp., *Mucor* sp., and *Candida* sp.) species and their connections to the cave.

Under laboratory conditions, 100 percent of the isolates formed crystalline $CaCO_3$ in B-4 medium. This percentage

is higher than what we found in samples from the Stiffe and Cervo Caves (96% and 75%, respectively) (Cacchio et al., 2003a,b, 2004). This result is consistent with those of several other studies and confirms that in appropriate conditions many bacteria are capable of forming $CaCO_3$ crystals (Boquet et al., 1973).

$CaCO_3$ precipitation occurred at all temperatures tested, 4, 15, 22, and 32 °C. The initiation of precipitation by all the calcifying isolates took longer at 4, 15, and 22, than at 32 °C. All of the calcifying isolates began to precipitate $CaCO_3$ after three weeks at 32 °C (Fig. 4) and after six weeks at 4, 15, and 22 °C (data not shown). No crystals were detected in the uninoculated controls or in the controls inoculated with autoclaved bacterial cells.

The relationships between $CaCO_3$ yield and temperature under laboratory conditions depended on the isolate
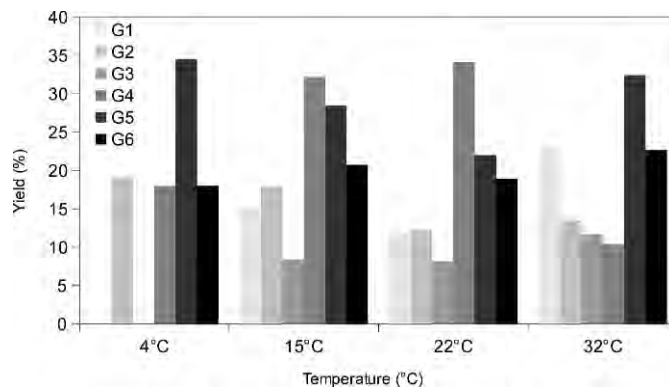

Figure 5. In vitro $CaCO_3$ yield at 4, 15, 22, and 32 °C. The experimental dry weights are the means of four values obtained from independent experiments.
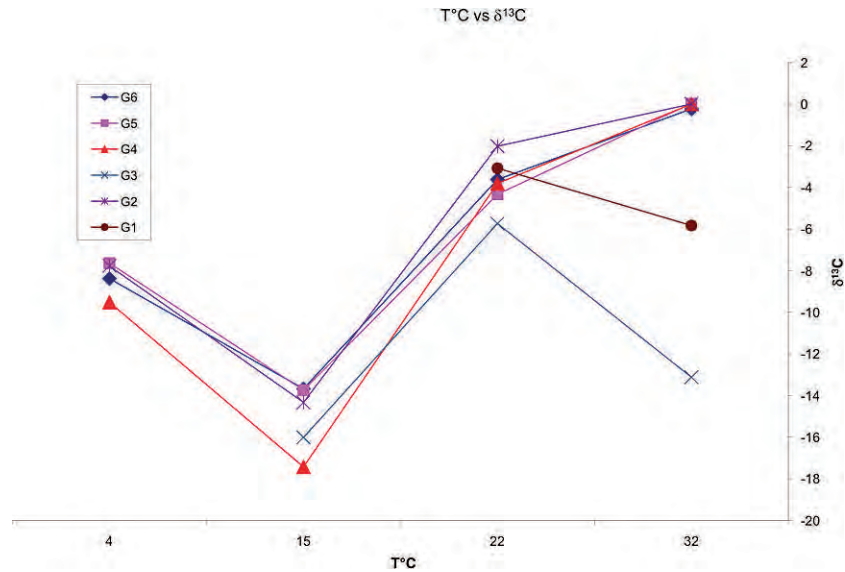
Figure 6. Carbon isotope composition (‰) versus temperature (°C) of calcium carbonates produced in vitro by the calcifying bacterial isolates.

(Fig. 5). The most abundant isolates, G4 and G5, which belonged to the *Staphylococcus* and *Burkholderia* genera, respectively, produced the largest amount of crystals at 15 °C (Fig. 5). In a previous report, we suggested that the ability to precipitate $CaCO_3$ may be advantageous and subject to evolutionary selection in a cave environment (Cacchio et al., 2003b). Calcium carbonate deposition is useful to bacteria cells that remain in situ taking advantage of nutritive molecules present in the water, like corals do. In the case of the speleothem of the Grave Grubbo Cave, carbonatogenesis might keep the calcifying bacteria in place, and calcifying cells may avoid being washed out by the flow of the underground river.

The calcium carbonate yields of the strains G7 and G8 are not available. These isolates suffered during the transition from the starved, oligotrophic conditions of cave environments to the eutrophic conditions of nutrient agar and died before crystals could be recovered. It may be difficult for microorganisms from nutrient-poor cave environments to adapt to the sudden presence of nutrients in a laboratory environment, and they may simply die from osmotic stress (Koch, 1997). In adapting to cave environments, microorganisms employ elaborate mechanisms to pull scarce nutrients into the cell. When these highly-adapted organisms are then exposed to the rich nutrients of laboratory media, these extreme scavenging mechanisms
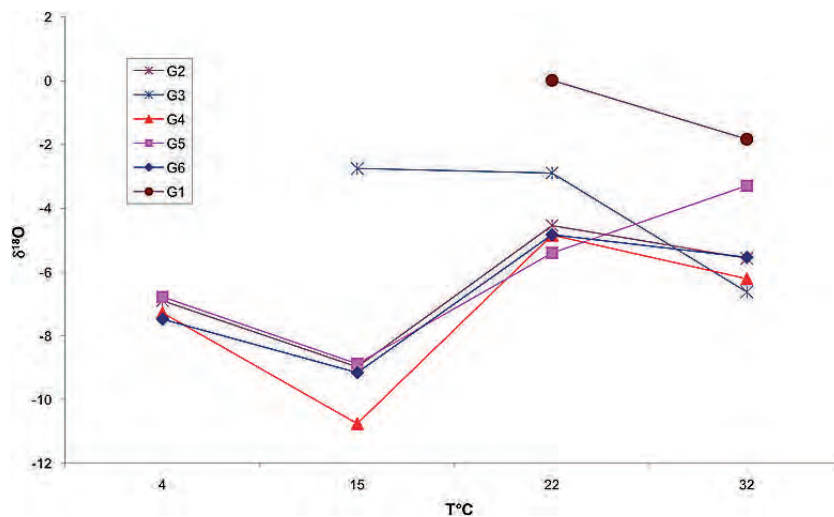

Figure 7. Oxygen isotopic composition (‰) versus temperature (°C) of calcium carbonates produced in vitro by the calcifying bacterial isolates.
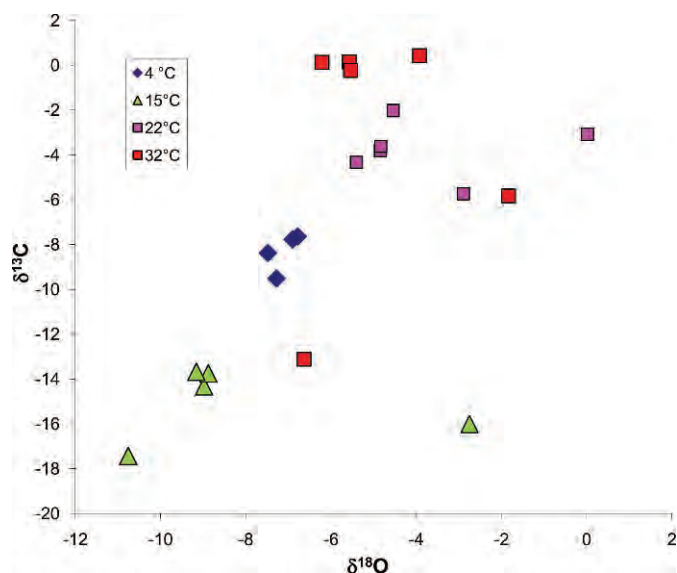
Figure 8. Correlation between $\delta^{13}C$ and $\delta^{18}O$ values (‰) of the calcium carbonates precipitated in vitro by the calcifying isolates.

continue unabated and the bacteria quickly gorge themselves to death (Koch, 1997, 2001).

Xray-diffraction analysis showed that all the calcifying bacteria produced calcite and that *Burkholderia* sp. also deposited vaterite in trace amounts ($< 1\%$) at 15 °C (data not shown). Vaterite precipitation was both species-specific and temperature-dependent. XRD analysis of the speleothem revealed the presence of calcite in large amounts, quartz in small amounts, and aragonite and gibbsite in traces. None of the isolates precipitated calcium carbonate in the form of aragonite.

The isotopic analysis performed on the carbonate concretion of the speleothem has shown medium values for $\delta^{13}C$ and $\delta^{18}O$ of -6.4‰ and -5.7‰, respectively. Previous studies (Turi, 1986) have shown that values for $\delta^{13}C$ lower than -4‰ indicate that in addition to "heavy" carbon from the dissolution of carbonatic rocks, "light" biogenic carbon, which is plant-derived CO_2 dissolved in the soil, must also contribute to calcite precipitation. On the other hand, many of the carbonatic concretions of microbial origin show $\delta^{13}C$ values similar to the values found in the Grave Grubbo speleothem (Andrews et al., 1997). The $\delta^{18}O$ values are compatible with precipitation

at equilibrium from meteoric water at cave temperature (O'Neil et al., 1969). From these observations, oxygen and carbon fractionation due to the presence of calcifying bacteria cannot be ruled out, although the environmental conditions (temperature, $\delta^{18}O$ in the water, carbon derived from inorganic and organic sources, etc.) are essential in defining the isotopic composition of the calcite concretions of caves. In addition, analysis of the carbon and oxygen isotopes of carbonates produced in vitro showed that, first, the isotopic composition of the calcium carbonates produced by the different bacterial isolates depended more on temperature than on the type of bacterial isolate (except for G3) and, second, at cave temperature (15 °C), the most abundant isolate, *Staphylococcus* sp., produced the largest amount of crystals and precipitated the carbonates most depleted in ^{13}C and ^{18}O (Figs. 6 and 7). A positive correlation existed between the $\delta^{13}C$ and $\delta^{18}O$ values of the crystals (Fig. 8).

It was not possible to compare the $\delta^{13}C$ and $\delta^{18}O$ values obtained of the carbonates produced in vitro with the values of the concretions of the cave because the composition of the cave's sources of carbon and oxygen are unknown.

Bacillus megaterium isolates precipitated various biominerals in vitro, predominantly spherulites consisting of isolated spheres or forming groups of spheres (Fig. 9a,b,c). Biofilms were observed as non-calcareous bridges among the crystals (Fig. 9b,c). Hemispherical forms were also present with radial inner surfaces (Fig. 9d,e,f). The outer surfaces of these structures were frequently rough due to the de novo deposition of calcium carbonate (Fig. 9a,d,e). In a previous study, we obtained nine isolates of *Bacillus megaterium* (Cacchio et al., 2003b). SEM analysis revealed that some of those isolates produced spherical or hemispherical crystals similar to those produced by the G1 isolated here. Isolate G6, *Brevibacillus sp.*, also produced spherical crystals. *Pasteurella* sp. precipitated irregularly shaped bioliths that tended to aggregate. *Staphylococcus* sp. deposited globular crystals with a rough outer surface. *Burkholderia* isolates produced elliptical crystals with a scaly surface. The inner portions of these bioliths contained imprints that were similar in size and shape to the bacterial cells (Fig. 9g,h,i,l). We did not analyze the carbonates produced by the G7 isolate and *Actinomyces* sp. by SEM. The different morphologies of the precipitates formed by the different calcifying isolates confirmed that crystal mor-

$\rightarrow$

Figure 9. Scanning electron micrographs of the bioliths precipitated on B-4 agar by *Bacillus megaterium* (a,b,c,d,e,f) and *Burkholderia* sp. (g,h,i,l) isolated from the novel calcite structure in Grave Grubbo Cave, Southern Italy. *a*) Two individual intergrowing bioliths; scale bar 20 μm. *b*) A large aggregate of individual crystals bound by means of non-globular carbonate bridges; scale bar 20 μm. *c*) A higher magnification of the biofilm; scale bar 10 μm. *d*) Radially arranged hemispherical calcium carbonate crystal; scale bar 20 μm. *e*) The outer surface of the biolith characterized by de novo deposition of calcium carbonate; scale bar 20 μm. *f*) Fragment of a crystal showing a three-layered structure; scale bar 20 μm. *g*) The inner surface
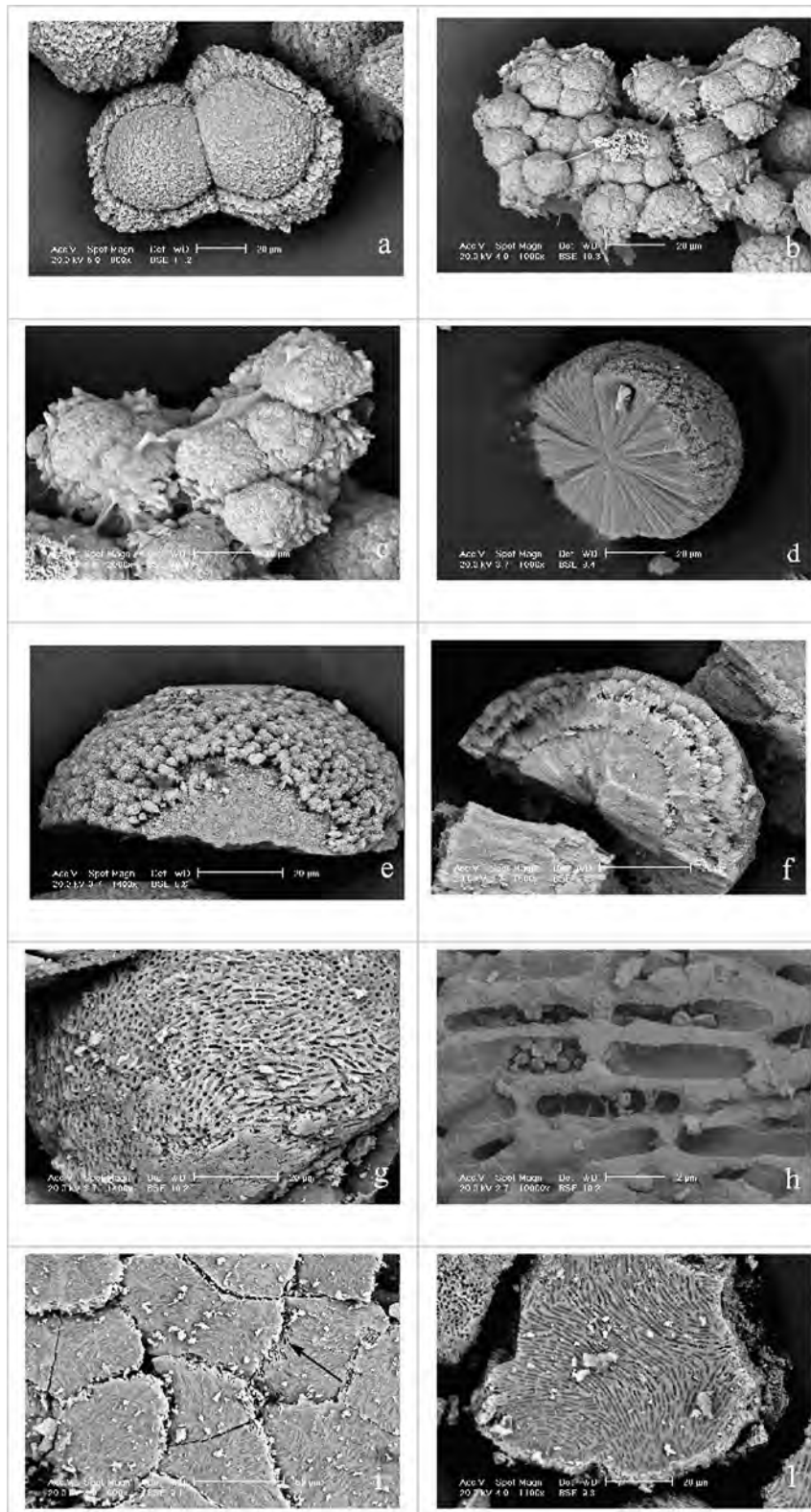
shows microbial imprints similar in size and shape to the microbial rods; scale bar 20 μm. *h)* A higher magnification of the internal porous structure of the biolith; scale bar 20 μm. *i)* Calcium carbonate layer with bacterial imprints arranged in a geometric stream disposition; scale bar 50 μm. *l)* Detail of *i;* scale bar 20 μm.
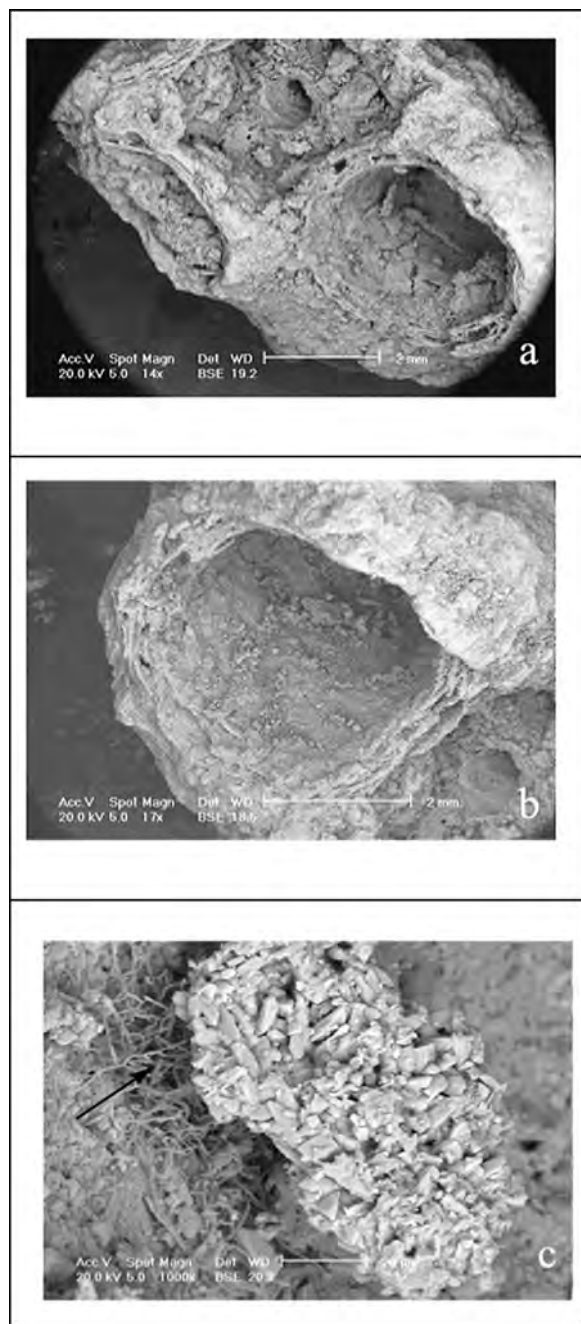
Figure 10. SEM images of cave crystals collected from the speleothem in Grave Grubbo Cave. *a)* Cross-section of the aggregate showing the outer-inner laminae and the middle, sponge-like septa. *b)* Detail of *a*. *c*, Spike crystals deposited after tube formation are likely to occlude the lumen of the tube. Filamentous calcified bacteria interacting with the calcite layer (arrow).

phology was species-specific, suggesting that the bacteria play a major role in the precipitation process.

Some crystals exhibited bacterial imprints arranged in a geometric stream disposition (Fig. 9g,i,l). This particular imprint pattern may be due to the involvement of quorum

sensing in colony growth (Branda et al., 2004). Quorum sensing is a process of cell-to-cell communication that bacteria use to assess their population density to coordinate gene expression of the community (Miller and Bassler, 2001). Quorum sensing requires production, secretion, and detection of extracellular signal molecules called autoinducers, some of which are used for intraspecies communication, while others promote interspecies communication (Federle and Bassler, 2003). Many gram-negative bacterial species use acyl homoserine lactones (AHLs) as autoinducers. Quorum sensing controls several important functions in bacteria, including the production of virulence factors and biofilm formation. We hypothesize that this cell-to-cell communication may be also involved in the calcification process. To this aim, we produced an AHL^- mutant of the strain PHP7 of *Burkholderia cepacia.* The AHL^- mutant grown on B-4 agar plates lost the calcifying capability of the wild type strain (preliminary data not published).

The SEM analysis of the speleothem material confirm the layered organization of the tube body that was apparent upon observation (Fig. 3), supporting the tubular structure of the calcareous body and the spongy structure of the three-layered wall (Fig. 10a,b). Calcified filamentous bacterial cells were detected between the outer wall of the tubes and the deposited calcite (Fig. 10c), which partially occluded the lumen of the tubes (Fig. 10a). Finally, only the G7 isolate was able to solubilize $CaCO_3$ (0.14%), after one week at 32 °C.

CONCLUSIONS

Within the past two decades, growing interest in cave microbiota has helped to recognize and understand the importance of microbial species in caves. Studies of cave microbiology have identified a wide variety of different cave-dwelling microorganisms, revealed how these organisms interact with and adapt to the cave environment, and disclosed their roles in creating and destroying secondary mineral deposits. Most of the research involving the gypsum areas in Italy has been carried out since 2000 on samples from caves located in the large gypsum areas of Sicily, Calabria, and Emilia.

Microbes cycle nutrients within cave environments. The processes of ammonification, nitrification, denitrification, and nitrogen fixation have all been documented to occur in caves. Sulfide and sulfur oxidizers and sulfate reducers are also found in caves. Nitrogen and the sulfur cycles may both occur, separately or concurrently, during heterotrophic bacterial carbonatogenesis in caves.

Microbes are critical to food-limited cave environments because they may act as primary producers in an environment lacking photosynthetic organisms.

Studies of sulfur bacteria have rapidly expanded in the last decade, reflecting the recent discoveries of sulfur-containing caves, including Movile Cave in Romania. The

food web of this cave is based on chemolithotrophic processes involving sulfur and other compounds. Among the Italian caves in the gypsum area, a remarkable number of sulfur bacteria have been isolated in the caves of Santa Ninfa, Sicily. Sulfur bacteria have also been detected in Grave Grubbo Cave, where a subterranean ecosystem driven by these chemoautotrophic microorganisms, as trophic symbionts of troglobitic insects able to agglutinate lithoid elements, has been hypothesized to be indirectly involved in the deposition of the unusual speleothem found in this cave.

We studied this peculiarly structured cave speleothem to determine whether heterotrophic bacterial carbonatogenesis was involved in its formation. The Grave Grubbo speleothem was found to contain a large number of culturable heterotrophic microorganisms, whose presence was likely not accidental. All the isolates obtained from the speleothem samples precipitated $CaCO_3$ in vitro in agar containing calcium acetate. The relative abundance of each isolate was found to be related to carbonate yield at $15°$ C, suggesting that calcification may be a selective advantage.

Isotopic analysis showed that, as previously suspected, the $\delta^{13}C$ values of the Grave Grubbo speleothem were compatible with a biogenic origin and that the $CaCO_3$ bioliths produced in vitro by the *Staphylococcus* sp., the most abundant isolate and the one that produce the largest amounts of carbonates in vitro at $15°$ C, had $\delta^{13}C$ and $\delta^{18}O$ values that were lighter than the carbonates produced in vitro by the other calcifying isolates. In conclusion, these isotopic data were consistent with calcifying bacteria making a significant contribution to the deposition of speleothem carbonates.

SEM images revealed the presence of calcified bacterial cells interacting with the calcite substrate of the speleothem, the presence of a biofilm among the bioliths obtained in vitro, the presence of bacterial imprints in the interior of the $CaCO_3$ bioliths produced in vitro, and different species-specific morphologies among the bioliths obtained in vitro. A typical stream-like organization of the bacterial imprints, observed in some instances, suggests that a quorum-sensing system may be involved in the calcium carbonate precipitation process.

Our data clearly demonstrate that calcifying bacteria isolated from this unusual calcareous speleothem hosted in the Grave Grubbo Cave are able to precipitate $CaCO_3$ in vitro and may play an important role in the deposition of these cave crystals.

Acknowledgements

References

Amati, A., and Gualandi, C., 1934, La microflora di alcune acque cavernicole del sottosuolo bolognese, Naples, Riv. di Fisica, Matematica e Scienze Naturali, ser. 3, 16 p.

Amy, P.S., Haldeman, D.L., Ringelberg, D., Hall, D.H., and Russel, C., 1992, Comparison of identification systems for classification of bacteria isolated from water and endolithic habitats within the deep subsurface: Applied and Environmental Microbiology, v. 58, no. 10, p. 3367–3373.

Andrews, J.E., Riding, R., and Dennis, P.F., 1997, The stable isotope record of environmental and climatic signals in modern terrestrial microbial carbonates from Europe: Palaeogeography, Palaeoclimatology, Palaeoecology, v. 129, p. 171–189, doi:10.1016/S0031-0182 (96)00120-4.

Barton, H.A., and Northup, D.E., 2007, Geomicrobiology in cave environments: past, current and future perspectives: Journal of Cave and Karst Studies, v. 69, no. 1, p. 163–178.

Baskar, S., Baskar, R., Lee, N., and Theophilus, P.K., 2009, Speleothems from Mawsmai and Krem Phyllut caves, Meghalaya, India: some evidences on biogenic activities: Environmental Geology, v. 57, no. 5, p. 1169–1186, doi:10.1007/s00254-008-1413-y.

Baskar, S., Baskar, R., Mauclaire, L., and McKenzie, J.A., 2006, Microbially induced calcite precipitation in culture experiments: Possible origin for stalactites in Sahastradhara caves, Dehradun, India: Current Science, v. 90, p. 58–64.

Boquet, E., Boronat, A., and Ramos-Cormenzana, A., 1973, Production of calcite (calcium carbonate) crystals by soil bacteria is a general phenomenon: Nature, v. 246, p. 527–529, doi:10.1038/246527a0.

Branda, S.S., Gonzáles-Pastor, J.E., Dervyn, E., Ehrlich, S.D., Losick, R., and Kolter, R., 2004, Genes involved in formation of structured multicellular communities by *Bacillus subtilis*: Journal of Bacteriology, v. 186, p. 3970–3979, doi:10.1128/JB.186.12.3970-3979.2004.

Cacchio, P., Contento, R., Ercole, C., Cappuccio, G., Preite Martinez, M., and Lepidi, A., 2004, Involvement of microorganisms in the formation of carbonate speleothems in the Cervo Cave (L'Aquila-Italy): Geomicrobiology Journal, v. 21, p. 497–509, doi:10.1080/01490450490888109.

Cacchio, P., Ercole, C., and Lepidi, A., 2003a, Calcium carbonate deposition in limestone caves: microbiological aspects: Subterranean Biology, v. 1, p. 57–63.

Cacchio, P., Ercole, C., Cappuccio, G., and Lepidi, A., 2003b, Calcium carbonate precipitation by bacterial strains isolated from a limestone cave and from a loamy soil: Geomicrobiology Journal, v. 20, p. 85–98, doi:10.1080/01490450303883.

Cañaveras, J.C., Hoyos, M., Sanchez-Moral, S., Sanz-Rubio, E., Bedoya, J., Soler, V., Groth, I., Schumann, P., Laiz, L., Gonzales, I., and Saiz-Jimenez, C., 1999, Microbial communities associated with hydro-magnesite and needle-fiber aragonite deposits in a karstic cave (Altamira, northern Spain): Geomicrobiology Journal, v. 16, p. 9–25, doi:10.1080/014904599270712.

Cañaveras, J.C., Sanchez-Moral, S., Soler, V., and Saiz-Jimenez, C., 2001, Microorganisms and microbially induced fabrics in cave walls: Geomicrobiology Journal, v. 18, p. 223–240, doi:10.1080/01490450 152467769.

Castanier, S., Le Metayer-Levrel, G., and Perthuisot, J.-P., 1999, Ca-carbonates precipitation and limestone genesis—the microbiogeologist point of view: Sedimentary Geology, v. 126, p. 9–23, doi:10.1016/ S0037-0738(99)00028-7.

Castanier, S., Le Métayer-Levrel, G., and Perthuisot, J.-P., 2000, Bacterial roles in the precipitation of carbonate minerals, *in* Riding, R.E., and Awramik, S.M., eds., Microbial Sediments, Berlin, Springer-Verlag, p. 32–39.

Dojka, M.A., Harris, J.K., and Pace, N.R., 2000, Expanding the known diversity and environmental distribution of an uncultured phylogenetic division of bacteria: Applied and Environmental Microbiology, v. 66, no. 4, p. 1617–1621.

Ehrlich, H.L., 2002, Geomicrobiology, 4th edition, CRC Press, 768 p.

Ercole, C., Cacchio, P., Botta, A.L., Centi, V., and Lepidi, A., 2007, Bacterially induced mineralization of calcium carbonate: the role of exopolysaccharides and capsular polysaccharides: Microscopy and Microanalysis, v. 13, p. 42–50, doi:10.1017/S1431927607070122.

Federle, M.J., and Bassler, B.L., 2003, Interspecies communication in bacteria: The Journal of Clinical Investigation, v. 112, p. 1291–1299, doi:10.1172/JCI20195.

Ferrini, G., ed., 1998, L'area carsica delle vigne (Verzino-Crotone) Studio multidisciplinare (The karst area of ''Le Vigne'' – Verzino Crotone - multidisciplinary researches): Memorie Istituto Italiano di Speleologia.

Ferrini, G., 1998, Litostratigrafia del complesso carsico Grave Grubbo - Risorgiva Vallone Cufalo (Gessoareniti Messiniane del Bacino Crotonese): Memorie dell'Istituto Italiano di Speleologia, ser. 2, v. 10, p. 47–52.

Forti, P., and Lombardo, N., 1998, I depositi chimici del sistema carsico Grave Grubbo – Risorgente di Vallone Cufalo (Verzino, Calabria): Memorie dell'Istituto Italiano di Speleologia, v. 10, p. 83–92.

Forti, P., Galdenzi, S., and Sarbu, S.M., 2002, The hypogenic caves: a powerful tool for the study of seeps and their environmental effects: Continental Shelf Research, v. 22, no. 16, p. 2373–2386, doi:10.1016/S0278-4343(02)00062-6.

Galdenzi, S., and Menichetti, M., 1998, Aspetti morfologici ed evolutivi di un sistema carsico ipogeo nei gessi di Verzino (Calabria): Memorie dell'Istituto Italiano di Speleologia, ser. 2, v. 10, p. 71–82.

Groth, I., Schumann, P., Laiz, L., Sanchez-Moral, S., Cañaveras, C.J., and Saiz-Jimenez, C., 2001, Geomicrobiological study of the Grotta dei Cervi, Porto Badisco, Italy: Geomicrobiological Journal, v. 18, p. 241–258, doi:10.1080/01490450152467778.

Groth, I., Vettermann, R., Schuetze, B., Schumann, P., and Saiz-Jimenez, C., 1999, Actinomycetes in karstic caves of northern Spain (Altamira and Tito Bustillo): Journal of Microbiological Methods, v. 36, p. 115–122, doi:10.1016/S0167-7012(99)00016-0.

Koch, A.L., 1997, Microbial physiology and ecology of slow growth: Microbiology and Molecular Biology Reviews, v. 61, p. 305–318.

Koch, A.L., 2001, Oligotrophs versus copiotrophs: BioEssays, v. 23, p. 657–661, doi:10.1002/bies.1091.

Laiz, L., Gonzalez-Delvalle, M., Hermosin, B., Ortiz-Martinez, A., and Saiz-Jimenez, C., 2003, Isolation of cave bacteria and substrate utilization at different temperatures: Geomicrobiology Journal, v. 20, p. 479–489, doi:10.1080/713851125.

Laiz, L., Groth, I., Gonzales, I., and Saiz-Jimenez, C., 1999, Microbiological study of the dripping waters in Altamira cave (Santillana del Mar, Spain): Journal of Microbiological Methods, v. 36, p. 129–139, doi:10.1016/S0167-7012(99)00018-4.

Laiz, L., Groth, I., Schumann, P., Zezza, F., Felske, A., Hermosin, B., and Saiz-Jimenez, C., 2000, Microbiology of the stalactites from Grotta dei Cervi, Porto Badisco, Italy: International Microbiology, v. 3, p. 25–30.

Le Métayer-Levrel, G., Castanier, S., Loubière, J.F., and Perthuisot, J.P., 1997, La carbonatogenèse bactérienne dans les grottes. Étude au MEB d'une héliclite de Clamouse, Hérault, France: Comptes Rendus de l'Académie des Sciences Serie IIa: Sciences de la Terre et des Planets, v. 325, p. 179–184, doi:10.1016/S1251-8050(97)88286-9.

McCrea, J.M., 1950, On the isotopic chemistry of carbonates and a palaeotemperature scale: Journal of Chemical Phyics, v. 18, p. 849–857, doi:10.1063/1.1747785.

Martino, T., Salamone, P., Zagari, M., and Urzì, C., 1992, Adesione a substrati solidi e solubilizzazione del $CaCO_3$ quale misura della capacità deteriorante di batteri isolati dal marmo Pentelico, in Italian Society of General Microbiology and Microbial Biotechnology (SIMGBM) XI Meeting, Gubbio; p. 249–250.

Melim, L.A., Shinglman, K.M., Boston, P.J., Northup, D.E., Spilde, M.N., and Queen, J.M., 2001, Evidence for microbial involvement in pool finger precipitation, Hidden Cave, New Mexico: Geomicrobiology Journal, v. 18, p. 311–329, doi:10.1080/01490450152467813.

Miller, M.B., and Bassler, B.L., 2001, Quorum sensing in bacteria: Annual Review of Microbiology, v. 55, p. 165–199, doi:10.1146/annurev.micro.55.1.165.

NORMAL Commission, 1990, NORMAL 9/88 recommendations. Microflora Autotrofa ed Eterotrofa: Tecniche di Isolamento in Coltura: Rome, Consiglio Nazionale Ricerche, Istituto Centrale Restauro, 26 p.

Northup, D.E., Dahm, C.N., Melim, L.A., Spilde, M.N., Crossey, L.J., Lavoie, K.H., Mallory, L.M., Boston, P.J., Cunningham, K.I., and Barns, S.M., 2000, Evidence for geomicrobiological interactions in Guadalupe caves: Journal of Cave and Karst Studies, v. 62, p. 80–90.

O'Neil, J.R., Clayton, R.N., and Mayeda, T.K., 1969, Oxygen isotope fractionation in divalent metal carbonates: Journal of Chemical Physics, v. 51, p. 5547–5558, doi:10.1063/1.1671982.

Poluzzi, A., and Minguzzi, V., 1998, Un caso di biocostruzione in un ambiente di grotta. L'area carsica delle Vigne di Verzino: Memorie dell'Istituto Italiano di Speleologia, ser. 2, v. 10, p. 93–100.

Riding, R., 2000, Microbial carbonates: the geological record of calcified bacterial-algal mats and biofilms: Sedimentology, v. 47, no. suppl. S1, p. 179–214, doi:10.1046/j.1365-3091.2000.00003.x.

Rivadeneyra, M.A., Delgado, G., Ramos-Cormenzana, A., and Delgado, R., 1998, Biomineralisation of carbonates by Halomonas eurihalina in solid and liquid media with different salinities: crystal formation sequence: Research in Microbiology, v. 149, p. 277–287.

Simkiss, K., and Wilbur, K.M., 1989, Biomineralization: Cell Biology and Mineral Deposition, San Diego, Academic Press, 337 p.

Turi, B., 1986, Stable isotope geochemistry in travertines, in Fritz, P., and Frontes, J.C., eds., Handbook of Environmental Isotope Geochemistry 2: The Terrestrial Environment: Elsevier, Amsterdam, p. 207–235.

THE PREHISTORIC CAVE ART AND ARCHAEOLOGY OF DUNBAR CAVE, MONTGOMERY COUNTY, TENNESSEE

JAN F. SIMEK[1]*, SARAH A. BLANKENSHIP[1], ALAN CRESSLER[2], JOSEPH C. DOUGLAS[3], AMY WALLACE[4], DANIEL WEINAND[1], AND HEATHER WELBORN[1]

Abstract: Dunbar Cave in Montgomery County, Tennessee has been used by people in a great variety of ways. This paper reports on prehistoric uses of the cave, which were quite varied. The vestibule of the cave, which is today protected by a concrete slab installed during the cave's days as an historic tourist showplace, saw extensive and very long term occupation. Diagnostic artifacts span the period from Late Paleo-Indian (ca.10,000-years ago) to the Mississippian, and include Archaic (10,000 to 3,000-years ago) and Woodland (3,000–1,000-years ago) cultural materials. These include a paleoindian Beaver Lake Point, Kirk cluster points, Little River types, Ledbetter types, numerous straight-stemmed point types, Hamilton and Madison projectile points. Woodland period ceramics comprise various limestone tempered forms, all in low quantities, and cord-marked limestone tempered wares in the uppermost Woodland layers. Shell-tempered ceramics bear witness to a rich Mississippian presence at the top of the deposit. Given this chronological span, the Dunbar Cave sequence is as complete as any in eastern North America. However, problems with previous excavation strategies make much of the existing archaeological record difficult to interpret. We present a new series of radiocarbon age determinations that show both the great time depth of the vestibule deposits and the problems with their integrity. There was also extensive prehistoric use of Dunbar Cave's dark zone, including mineral extraction, and ritual interment of the dead. Most importantly, thirty-five petroglyphs and pictographs were made on the cave walls, most probably during the Mississippian period. These include geometric shapes, abstract compositions, and human figures including a mythological hero warrior known from other examples of Mississippian iconography. Dunbar may also have seen ritual visitation very early, i.e., during the Archaic period (ca. 5,000-years ago), entailing the placement of offerings in the cave's interior waters.

INTRODUCTION

Over the past twenty years, archaeologists from the University of Tennessee and elsewhere, along with devoted avocational cavers, have worked to expand our knowledge of prehistoric cave art in the Appalachian Plateau uplands of southeastern North America (Simek and Cressler, 2005). First identified by archaeologists in 1980 (Faulkner et al., 1984), this cave art represents a widespread, complex, and longstanding aspect of indigenous prehistoric culture, one with local origins and development and one intrinsically linked to the evolution of prehistoric southeastern religious iconography (Faulkner and Simek, 1996). Although we have now examined more than one thousand southeastern caves in hopes of finding prehistoric art, there are more than nine thousand caves in Tennessee alone, with thousands more in Alabama, Georgia, and the upper south (Simek, 2010). There is a great deal of survey work still before us, and there will certainly be more cave-art sites discovered in the future. In this paper we will discuss the fiftieth cave in the catalog, Dunbar Cave (40MT43) in Montgomery County, Tennessee (Fig. 1).

As far as we can determine, dark-zone cave art (that is, decoration in the areas of caves beyond the reach of external light) was actually known among a small group of cavers in the Southeast from the 1950's. Engravings that were thought by those cavers who saw them to be prehistoric were identified at the mouth of 12th Unnamed Cave in Tennessee. The site remained unknown to archaeologists until Charles Faulkner of the University of Tennessee was taken there in the 1980s in conjunction with his work at Mud Glyph Cave (Faulkner, 1988). Mud Glyph Cave itself was discovered in 1979 when a recreational caver explored a narrow subterranean stream passage and saw images incised into the wet clay lining the stream banks (Faulkner et al., 1984; Faulkner, 1986). The caver alerted an archaeologist friend who told Faulkner about these images. Upon seeing the site, Faulkner quickly recognized that the art was prehistoric, and in 1980, he initiated a documentation project. Mud Glyph Cave art was seen as resembling that found on Mississippian period ceremonial objects, and therefore, linked to the wider

* Corresponding Author: jsimek@utk.edu
[1] Department of Anthropology, University of Tennessee, Knoxville, TN 37996-0720
[2] United States Geological Survey, Atlanta
[3] Volunteer State Community College, Gallatin, TN 37066
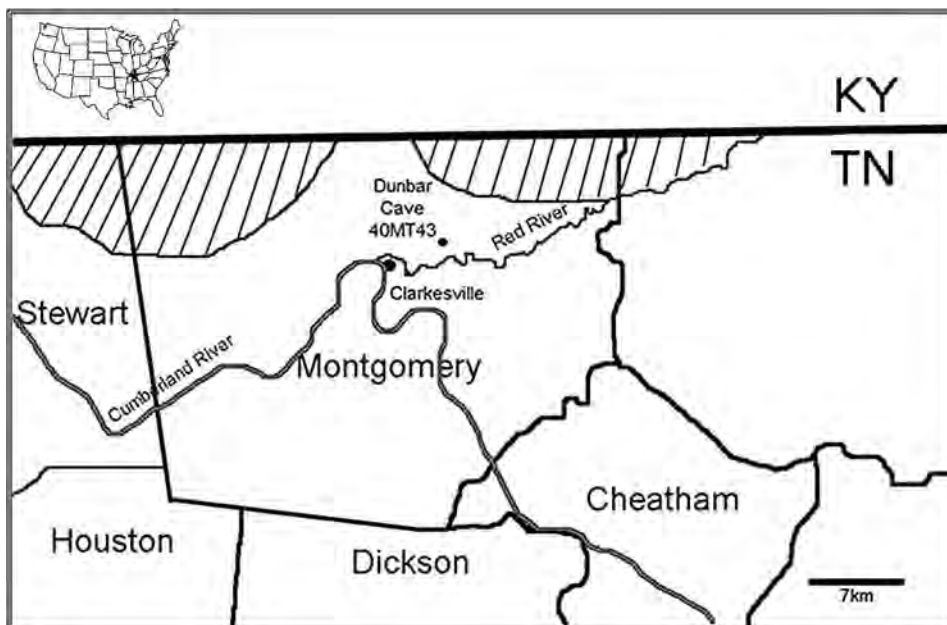[4] Dunbar Cave State Natural Area, Clarksville, TN 37043

Figure 1. Map showing the location of Dunbar Cave, Tennessee.

Mississippian iconography, dating to after AD 1000 and labeled as the Southeast Ceremonial Complex (SECC) (Waring and Holder, 1945). Other sites quickly began to come to light. By 1988, Faulkner documented seven cave-art sites, including Mud Glyph and 12th Unnamed caves (Faulkner, 1988).

Since the discovery of Mud Glyph Cave, dark zone art has been recorded in sixty-nine other caves in Tennessee, Alabama, Florida, Georgia, Kentucky, Virginia, and West Virginia. There are also a few cave-art sites in the Mississippi Valley, including Arkansas (Sabo, 2008), Missouri (Diaz-Granados and Duncan, 2000; Diaz-Granados et al., 2001), Illinois (Wagner, 1996), and Wisconsin (Boszhardt, 2003). Chronological data from these sites demonstrate a long-term regional tradition of cave art beginning some 6000 years ago (Creswell, 2007; Simek and Cressler, 2009). As Faulkner observed, some of the imagery can be understood in terms of other prehistoric iconography, i.e., SECC, but some has less obvious connection with that imagery. As we show, the cave art in Dunbar Cave is markedly SECC in its content.

The Prehistoric Cave Art of Dunbar Cave

In January 2004 a caving group including Joseph Douglas (Professor of History at Volunteer Community College in Gallatin, Tennessee, and Adjunct in the Department of Anthropology at the University of Tennessee) and cave author Larry Matthews visited Dunbar Cave State Natural Area in the company of Amy Wallace, Interpretive Specialist at the park. In an area of the cave known as the Ballroom several hundred meters into the dark zone, Douglas noticed two charcoal drawings on the

wall overlaid by nineteenth-century graffiti. (Places named in this paper can be located by reference to Walter Scheffrahn's 1978 map of Dunbar Cave based on a North Indiana Grotto survey as published in Matthews (2005, p. 27). The Ballroom, not labeled on that map, is the chamber just northeast of the Counterfeiters Room in the lower center). Douglas photographed what he saw and sent the photos to Simek at the University of Tennessee.

In February of 2005, Simek joined Douglas, John Froeschauer of the Tennessee Department of Environment and Conservation, Amy Wallace, and Alan Cressler of the U.S. Geological Survey at the site. On that visit, the two glyphs that had been discovered in January were observed and documented. In addition, a significant number of new pictographs and petroglyphs were identified in the same area of the cave and other passages. We also examined the cave floor for evidence of prehistoric occupation and found human remains in a small alcove near the cave mouth that had been noted as a looted burial area in earlier testing work by the Tennessee Division of Archaeology (Butler, 1977). We saw significant in situ deposits of burnt river cane (*Arundinaria* sp.) that were clearly ancient torch remnants, and stoke marks on the cave walls reflecting maintenance of burning torches.

Documentation has proceeded since 2005. This involves detailed photographic recording of the glyphs and mapping of the glyph distributions and the galleries in which the glyphs are found using a total-station laser transit. The survey continues in other parts of the cave, which is more than 8 miles long. Cane-torch stoke marks have been recorded at many places on the cave walls, both near and away from the glyph panels. In places where the sediment floor was not disturbed by historic digging, torch remnants

Figure 2. Burnt river cane (*Arundinaria* sp.) fragments on the sediment floor inside Dunbar Cave.

can be found (Fig. 2, Table 1). Several of these were taken as ^{14}C samples under terms of our state archaeological research permit.

A total of thirty-five individual glyphs have been recorded so far, nearly all concentrated in four panels along a west-side wall segment in the Ballroom. Two are pictographs of unidentifiable shapes incorporating disks. Three glyphs, two in the main room and one on the ceiling at the entrance to this room, are single circles. In each case, these are very faint images, and they may actually have

Table 1. Radiocarbon age determinations from Dunbar Cave (40MT43). All assays performed by Beta Analytic on burnt river cane (*Arundinaria* sp.) by Atomic Mass Spectrometry and calibrated at 2σ with INTCAL04 (Reimer et al., 2004). Location descriptions in the table follow Walter Scheffrahn's 1978 map of Dunbar Cave based on a North Indiana Grotto survey (Matthews, 2005, p. 27).

Sample Reference	Measured Age BP	^{13}C/^{12}C Ratio	Conventional Age BP	Calibrated Date	Provenience
Beta- 206332	2820 ± 40	−26.8‰	2790 ± 40	1020 to 830 BC	Collected near stoke marks between Counterfeiters Room and Ballroom
Beta- 206333	680 ± 40	−27.2‰	640 ± 40	AD 1280 to 1410	Collected from breakdown in entry to Stone Mountain Room
Beta- 225002	3750± 50	−26.3‰	3730 ± 50	2290 to 1980 BC	Collected from floor of Ballroom at base of wall between concentric circle panel and warrior anthropomorph

Figure 3. Circle glyphs from Dunbar Cave. These are complex images that include rayed circles and interior crosses. There are simple concentric circles as well in the glyph assemblage. Note "1847" scratched over the images. If this is a date engraved over the glyphs at that time, the glyphs must be older than the mid-nineteenth century.

been concentric rings that have faded beyond recognition. Nineteen individual glyphs are sets of concentric circles (Fig. 3). There is a great deal of variability in the number of circles involved in the concentric-circle images. Some images have only two rings, some have three nested together, and one complex image has four concentric circles of diminishing size. Concentric circles were produced using two techniques. Some images are drawn in black pigment (pictographs); others are engraved into the limestone of the cave wall (petroglyphs). In the main glyph gallery, seventeen of the circle glyphs are disposed in a single array of four vertical lines of images (Fig. 4). These lines include from two to six glyphs each, spaced about 25 cm apart. An arc was drawn passing over all the concentric circles in this panel, collecting them into a single composition. Circles, including concentric circles, are one of the most common design elements in prehistoric art in the southeastern US. They appear in ceramic designs and rock art outside caves, and they are also frequent in cave art assemblages. Circle motifs, however, while common during the Mississippian period, are not chronologically diagnostic in and of themselves; they can be found in art from a variety of prehistoric periods, early and late.

There are some circles in Dunbar Cave that do have chronological context, and those are the three cross-in-circle images. One, located away from the main room, is a simple image drawn in black. Even this simple version has Mississippian connotations. The other two (see Fig. 3) are the first glyphs discovered and are more complicated than simple crosses in circles. Both are concentric circle images with exterior rayed circles and crosses of different forms inside their inner rings. Also note the 1847 date scratched over the black glyphs. The left image is a denticulate circle with a straight cross in the middle. The right image differs from its companion in having a tail on the outer denticulate circle and a left-facing swastika (Brain and Phillips, 1996, p. 7) in the center. Together, they form a remarkable pair of images. The denticulate cross is found frequently in Mississippian archaeological contexts. In particular, it is characteristic of a Mississippian-period gorget style named after the Cox Mound in northeastern Alabama where it was first identified (Holmes, 1883). This gorget type is most frequent in the Cumberland River area of Middle Tennessee, however, where it is combined with images of woodpeckers into a design referred to as the Cox Style by Brain and Phillips, who suggested that it was produced by
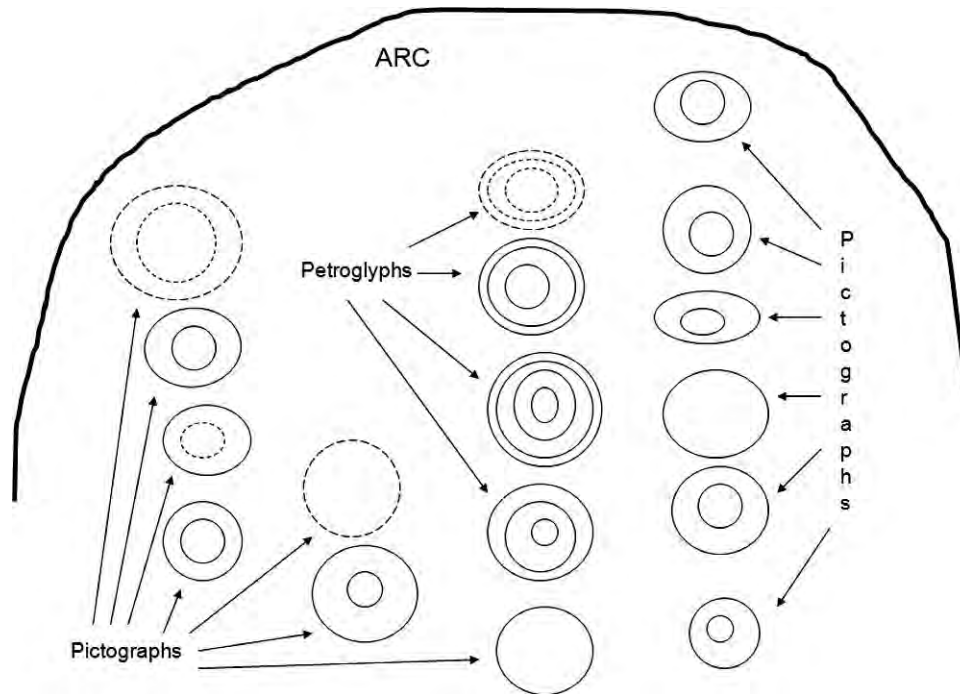
Figure 4. Sketch of concentric-circle array enclosed by a painted arc. Both pictographs and petroglyphs are included in the composition as indicated. Approximate size: 2 m wide × 1.5 m high.

craftspeople in the Cumberland region (Brain and Phillips, 1996). Dunbar Cave is within the Cumberland drainage, and the presence of these images here is strong evidence for a Mississippian origin.

The last two images, both complex anthropomorphs, also implicate Mississippian artists in the production of Dunbar Cave's artwork. One image that we originally recorded as a pair of abstract lines (Simek et al., 2007) has proved, on closer examination, to be the profile of a human face with fine features and long hair (Fig. 5). The second anthropomorph (Fig. 6a) is a reclining human-like form, clearly male, with well-defined arms and legs. Three fingers appear on the lower arm. The lower appendages (legs) thicken towards the feet, and those feet have claws, suggesting an animal element to the creature's makeup (Fig. 6b). The stippled head of this image is quite unusual. There is an axe or calumet above the head and a curving line extending out from the upper part of the head. The trunk below the arms is well defined and filled with pigment. The anthropomorph's waist and upper legs are covered with an hour-glass shaped garment, a kilt perhaps, which has several lines suggesting folds or decoration, but does not conceal the individual's phallus. All of these elements make perfect sense given what we know about prehistoric Mississippian iconography. That iconography focuses on the central tenets of Mississippian religion, namely warfare, death, and the ancestors (Hall, 1997; Muller, 1989). Mythical warriors were common and important characters in the religious narratives and thus in Mississippian art. They frequently combine human and

animal characteristics, especially avian ones (Brown, 2007). These warriors are often shown with elaborate head decoration, including weapons in the hair and curling hair locks. Kilts are also common aspects of the warrior's regalia. The Dunbar Cave anthropomorph is readily interpreted as depicting a Mississippian cosmic warrior, which fits quite well chronologically with the denticulate circles discussed earlier. Interestingly, the head of this figure, which is the image in the Ballroom farthest from the cave mouth, points down-slope toward the river that flows through the cave's interior.

All of the pictographs in Dunbar Cave are black, suggesting that charcoal was used to produce them. However, we have observed in other sites that pigments were frequently applied as paints made by mixing a chromophore (coloring agent) with binders in a liquid form to enhance adhesion and permanence (Simek et al., 2010, p. 82). To investigate the pigment technology at Dunbar Cave, we sampled a few grains of pigment from one of the glyphs, along with a few more from a nearby cane-torch stoke mark. A control sample was also obtained from bare limestone near the sampled pictograph. This strategy was designed to determine whether the pigments used in Dunbar Cave had been applied with a simple charcoal pencil, such as the end of a cane torch, or more complex liquid paint preparations were applied. Using EDS/SEM analysis of composition, we found that the pictograph pigment (Fig. 7a) differs from the bare limestone control sample (Fig. 7b) in the elevated presence of carbon, indicating that the pictographs were produced using charcoal. No other

Figure 5. Pictograph of an anthropomorph head and face in profile.

differences were observed that might reflect inclusion of a paint binder. This suggests that the pictographs were produced using raw charcoal pencils. In fact, the pictograph sample was identical to the stoke mark in composition (Fig. 7c), signifying that burnt canes were probably used to produce the pictographs.

One of the most fundamental problems for students of parietal rock art (pictographs and petroglyphs located on walls) is chronology (Leroi-Gourhan, 1971). The pictures usually lack association with sediment deposits containing temporally diagnostic materials, whether artifacts of characteristic style or items that can be dated using radiometric techniques. Unfortunately, this is true for the Dunbar Cave pictographs. As we have seen, the pictographs are made of charcoal, which is subject to aging by radiocarbon assay, but a sample from one of the pictures (taken with great care not to damage the visual image) did not contain sufficient carbon to enable a reading, even by Accelerator Mass Spectrometry. We have obtained three AMS radiocarbon age determinations from inside Dunbar Cave, all from torch fragments recovered from the cave floor (Table 1). These samples were taken from various places inside the cave, and they elucidate the complex nature of prehistoric activity within the Dunbar Cave dark zone. One

calibrated age determination (Beta206333) coincides perfectly with the time-period we would expect for the pictograph iconography: between AD 1200 and 1400. This sample was collected deep in the cave, however, the sample most distant from the glyphs. The sample closest to the glyphs, recovered directly below the circle panel (Beta 225002), has the most ancient calibrated age, about 4000 years before present, well within the Late Archaic period. The third determination (Beta206332), on a sample taken at the east edge of the Ballroom, is Woodland period, calibrated to around AD 900. Thus, while people were certainly inside the cave at the time suggested by the pictograph iconography, they were also there much earlier. In fact, this is something we find typical of caves used prehistorically in the Southeast (Simek, 2010; Simek and Cressler, 2001, 2005, 2009).

1977–78 ARCHAEOLOGICAL WORK

While the prehistoric cave art in Dunbar Cave is obviously of great anthropological interest, the archaeology of the site is also quite important. Dunbar Cave is presently owned and managed by the state of Tennessee, but that has not always been the case. Some accounts hold that the cave was mined for saltpeter in the mid-nineteenth century, and the nitrogen-rich sediment in the cave was also mined for fertilizer in the late nineteenth century. The cave then began a long history as a tourist attraction. Over time, the site was developed as a resort by several interests, including Roy Acuff after WW II, and it saw the installation of golf and swimming facilities, musical attractions befitting a site so close to Nashville, and a recreational lake (Van West, 1998; Whidby, 1999; Matthews, 2005). One effect of these rather specialized uses was the protection and eventual sealing of vestibule deposits at the mouth of the cave. First wooden and later concrete platforms were constructed on top of the sediments that filled the large rockshelter protecting the cave entrance (Butler, 1977). Thus, where so many of the great shelter sites in the eastern woodlands were looted for their artifacts, Dunbar Cave's archaeology remained intact for the most part. In 1973, the state acquired the site, and its protection was guaranteed.

When the state of Tennessee took possession of Dunbar Cave, test excavations were initiated both inside and outside the cave by the State Division of Archaeology (DOA) to determine the nature and extent of the site's archaeological record. DOA excavations were conducted on two separate occasions. Brian Butler directed a very small archaeological project in 1977 to determine whether intact archaeological deposits were present and how deeply they were buried beneath the fill (Butler, 1977). Three test pits were excavated at the entrance of the cave, after breaching the concrete dance-floor slab, and three additional pits were placed along the path just inside the cave. The three test pits outside the cave yielded charcoal, bone, shell, lithics, and pottery indicating human occupation.
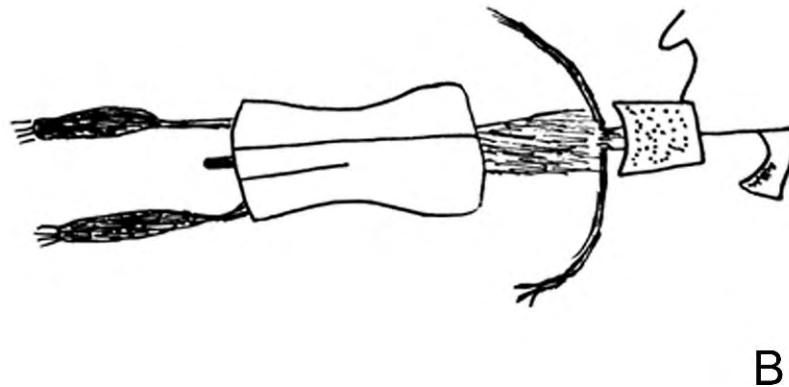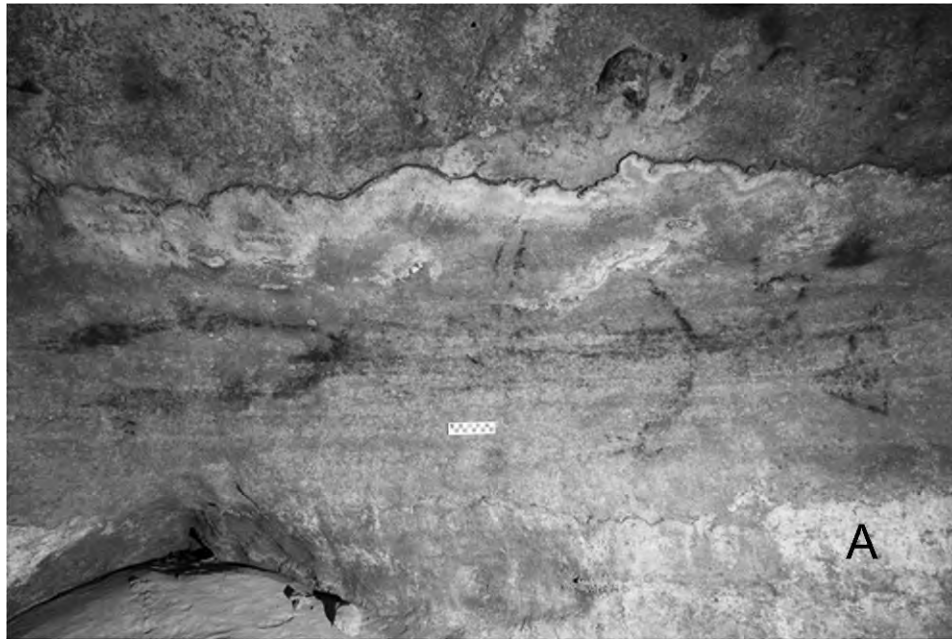
Figure 6. Pictograph of a reclining anthropomorph with animal features. A. Photograph of the pictograph. B. Sketch of the pictograph based on field observation using the red portion of the visible-light spectrum.

Those test pits within the cave interior exhibited only a minimal amount of cultural material.

In 1978, Robert Pace and Victor Hood led a larger, more involved archaeological excavation under the auspices of the DOA (Pace and Hood, 1978). For this investigation, the team dug a trench made up of eight 2 × 2 meter units running north-south at the mouth of the cave (Fig. 8). The units were excavated in arbitrary 10 cm levels starting from an established datum, with vertical control being maintained by a transit. The deposits were found to be more than 5.5 m (nearly 20 ft) deep in some areas, making this an extraordinary archaeological deposit with technical challenges for its excavators. More than sixty storage boxes of material were filled, a collection that

presently resides at the University of Tennessee. Diagnostic artifacts span the period from Late Paleo-Indian (about 10,000 years ago) to the Mississippian (to AD 1500), and they include Archaic (10,000 to 3000 years ago) and Woodland (3000 to 1000 years ago) cultural materials. Lithic artifact types in rough sequence include a Beaver Lake Point, Kirk cluster points, Little River types, Ledbetter types, numerous straight-stemmed point types, and Hamilton and Madison projectile points. Woodland ceramics comprise various limestone-tempered forms, all in low quantities, and cord-marked limestone-tempered wares in the uppermost Woodland layers. Shell-tempered ceramics bear witness to a rich Mississippian presence at the top of the deposit. Given this chronological span, the Dunbar Cave sequence is as
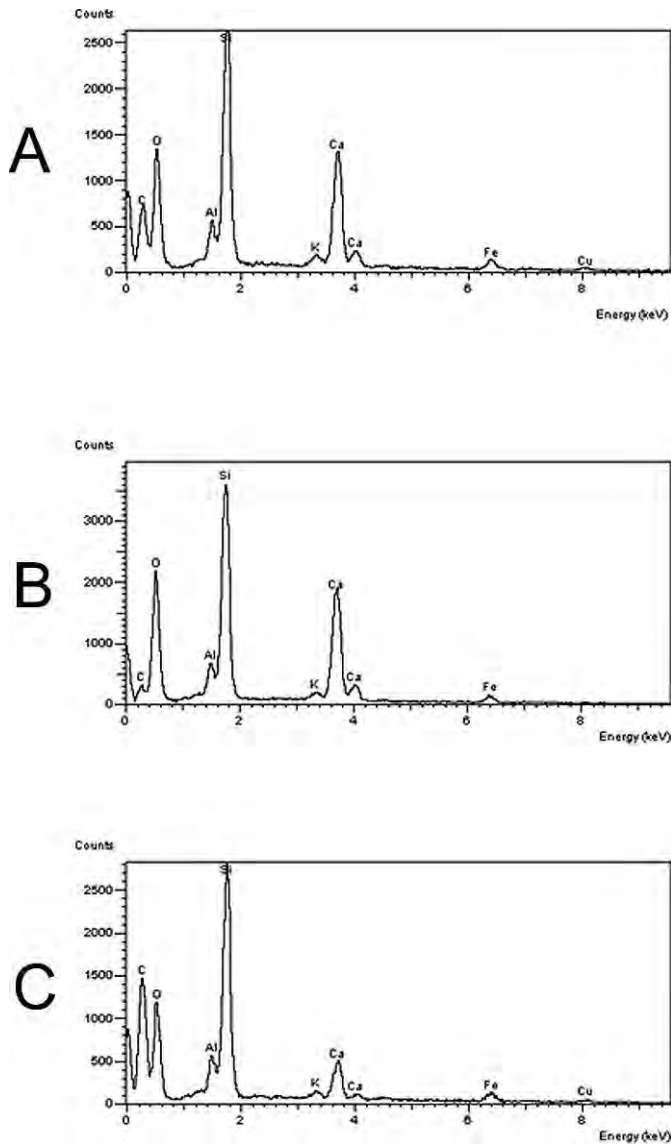
Figure 7. Element spectrographs showing results of EDS/SEM analyses of material composition. A. Analysis of pictograph pigment. B. Analysis of bare limestone wall as a control. C. Analysis of cane-torch stoke mark.

complete as any in eastern North America (Pace and Hood, 1978). However, we do not discuss the artifacts in more detail here because, as noted below, there are general problems with provenience stemming from the complex stratigraphy of the site and the way it was excavated.

Units 96N0 through 106N0 (see Fig. 8) appear to have been excavated simultaneously, while the top levels of 108N0 and 110N0 were stripped with a shovel after being identified as containing fill. Units were excavated to different depths. For example, Unit 96N0 was excavated to 2.65 m deep, where large boulders prevented any more excavation. Limestone breakdown prevented excavation deeper than 2.75 m in Unit 98N0. Unit 100N0 was excavated to a depth of 2.65 m and contained no diagnostic artifacts.
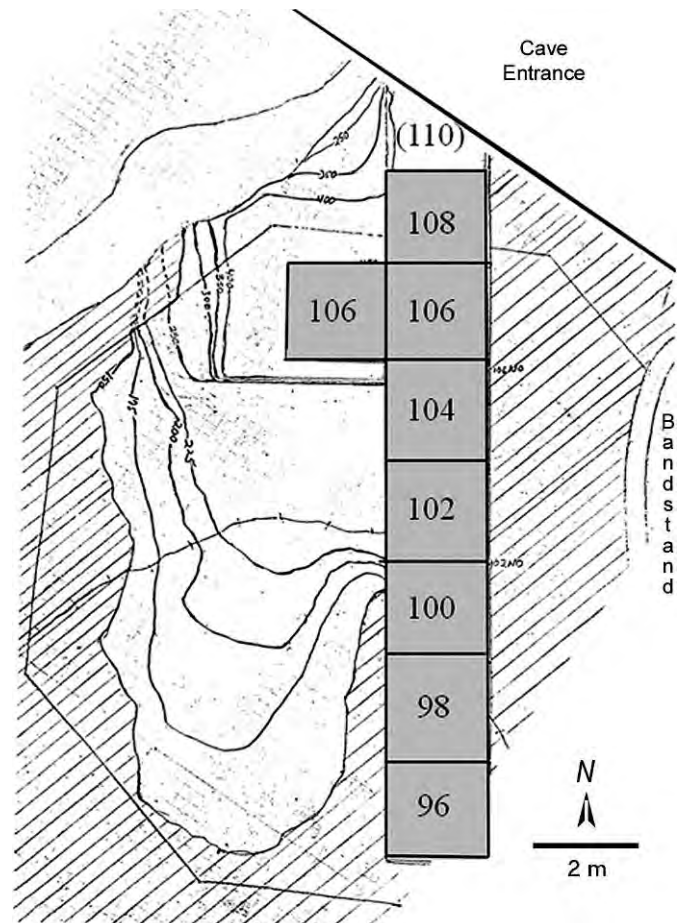
Figure 8. Plan map of 1978 vestibule excavations showing 2 × 2 m unit locations and designations, after 1978 field notes by Pace and others.

The quantity of archaeological material present in units 102N0 through 106N0 necessitated deeper excavations to document the prehistoric use of the cave in its entirety. Unit 102N0 was excavated to a depth of 4.45 m. Ceramics, lithics, and bone were recovered through the entire deposit. The artifact sequence in the square, however, is confusing. With regard to the pottery, many levels contain both limestone- and shell-tempered pottery. This is unusual because limestone pottery tends to be earlier, associated with the Woodland period, and shell temper is a later Mississippian characteristic (Lewis and Kneberg, 1995). Even more problematic are levels containing shell-tempered pottery that lie beneath levels identified as Archaic from diagnostic lithics. There would appear to be problems with the stratigraphy in this unit.

From Unit 104N0, only ten diagnostic artifacts were recovered. The unit was excavated to a depth of 3.35 m. Shell-tempered shards were found in levels 2 and 4, conveniently above limestone-tempered shards that were recovered from levels 4, 5, 8, and 17. The only diagnostic lithics were two Late Archaic stemmed points from level 8,

so this unit has probable Woodland pottery stratigraphically below Archaic projectile points. Again, stratigraphic problems are apparent.

Numerous artifacts were recovered from Unit 106N0. In the upper levels, sketches were made of the various deposits. This was to account for the lack of the sediment being screened because it was considered fill and discarded. Levels 2 through 5 were removed by shovel, as they were entirely composed of fill. Hand-excavation began only with level 15 at a depth of 2.95 m, where there was no intrusion from the red-clay fill. Excavation continued to level 31, seeking the bottom of the cultural deposits. At around 5.2 m, the decision was made to use a backhoe to facilitate digging. At 5.55 m (level 41), water began to impede the excavation. Vertical control was maintained for three more levels before it became impossible to understand the context of the artifacts. The problems with stratigraphic control observed for Unit 102NO are even more apparent when the rich assemblages from 106NO are examined. With regard to pottery, Mississippian and Woodland shards are routinely found together until level 29 (with a maximum depth of 4.45 m). Two shell-tempered shards are found below this in level 38 (5.25–5.35 m).

Because the relationship between the archaeological levels defined during excavation and the temporally diagnostic artifact types is confused, we made an effort to resolve the confusion by securing ^{14}C age determinations from several 1978 excavation units. Table 2 shows the twelve dates obtained and the measurement and provenience data associated with the samples. All analyses were carried out at the University of Tennessee Radiocarbon Laboratory. The first four determinations were made on samples from Unit 102NO. While partially conforming to what might be expected given depths below surface, the two upper dates are inverted, indicating stratigraphic mixing even at this fine scale of analysis. The second set of four determinations is from Unit 106NO. The first pair is inverted from stratigraphic expectations, while the second two, supposedly associated with bison remains, are older than their association would indicate. The last four ages are from Unit 106N2W. The first pair, in sequence within a single hearth feature (F11), is stratigraphically inverted, while the last two determinations are statistically identical even though they come from superimposed levels. Thus, new ^{14}C age determinations do not clarify the chronology. Instead, age inversion, inaccurate association, and lack of agreement between stratigraphic position and radiometric age characterize the Dunbar Cave vestibule excavation sequence.

Clearly, there are problems with the stratigraphy from the entire 1978 excavation. This might be due to one or both of two factors. It may be that the site is greatly disturbed and has lost stratigraphic integrity because of post-depositional processes affecting the sediments, something that is always possible in the complex, dynamic deposits that fill caves and rockshelters. Or, it may be that

excavation strategies failed to establish accurate provenience for the artifacts recovered from the site. We believe that the latter problem explains observed incongruities in the Dunbar Cave artifacts.

After excavation at Dunbar was completed and the deep trench at 106N expanded to two units wide to provide a profile, the drawing shown in Figure 9 was made of the deep sequence. There are complex but clear, perceptible stratigraphic layers and limits recorded by the artist. What is also apparent is that the archaeological layers are not flat and level; indeed they are mounded with sloping sides, as might be expected for a talus-slope deposit, and this character is amplified the deeper into the deposit one goes. Excavation strategy, however, was to bring all eight units to a single horizontal plane prior to excavation with absolute depth below the site datum determining the stratigraphic collection unit. According to the notebook, "Level 1 was designed to bring the entire trench to a uniform horizontal plane at the lowest point in the trench. … all other levels were uniformly 10cm in thickness." Thus, level 2 was defined as a ten-centimeter spit in each square between 1.65 and 1.75 centimeters below the surface. All levels had the same vertical depth regardless of unit or sedimentary context. In essence, the collection units were constant volumetrically but stratigraphically arbitrary. The effect of this was devastating for artifact provenience. Take, for example, a single collection spit in Unit 106NO where, according to the drawn profile, seventeen identifiable strata are mixed together into one horizontal 10 cm unit level (see Fig. 9). This example is replicated time and again across the trench. Thus, it is not surprising that artifacts from different time periods occur in nearly every level from every square. The bad news is that we cannot recover stratigraphic provenience for these materials. The good news is that the site itself probably has intact strata that can ultimately yield controlled data to new excavation.

There are some aspects of the 1978 collection that can still provide us with important information. Weinand, for example, has undertaken a study of the archaeofaunas from the 1978 Dunbar Cave excavations. The assemblage yields very few surprises. Species present include deer, small mammals, fish, turtles, and turkeys, all typical food-prey species found in southeastern archaeological sites. Two flying squirrels and a swan, more rare in archaeofaunas, have also been identified. The majority of the Dunbar Cave bones from all levels, including the deepest, are burned, indicating a human role in their accumulation. Some are fashioned into tools (awls or punches), and butchery cut-marks are evident on some remains.

The bones of three particularly interesting species were found in units 108N and 106N. One of them was identified in 1978 as one of the very few *Bison bison* bones ever identified in a Tennessee archaeological site. In fact, a total of three buffalo bones have now been identified, all from the same provenience. The bones include a metacarpal, first

Table 2. Radiocarbon age determinations from vestibule excavations at Dunbar Cave (40MT43). Samples in each unit listed in deepening stratigraphic order. All assays performed by University of Tennessee Radiocarbon Laboratory using Liquid Scintillation Counting and calibrated at 2σ with INTCAL04 (Reimer et al., 2004). Location descriptions in the table follow (Pace and Hood, 1978).

Sample Reference	Measured Age BP	Calibrated Date	Archaeological Level	Depth Below Surface, cm	Provenience
Unit 102NO					
UT 08-051	3870 ± 78	2569 to 2064 BC	5	102	Single piece of charred wood from general midden
UT 08-050	3770 ± 70	2459 to 1984 BC	10	102.52	Possibly residual feature - no depth - piece of antler in association
UT-08-048	5570 ± 107	4690 to 4174 BC	21	103.61	Concentrated scatter of wood charcoal
UT-08-043	6125 ± 141	5371 to 4718 BC	21	103.7	Charcoal scatter ~10cm in diameter N half of central portion
Unit 106NO					
UT 06-034	4300 ± 70	3309 to 2668 BC	F.5 S 1/2	103.45	Charcoal in ashy layer directly above Feature 5 - west profile
UT 06-031	3900 ± 70	2572 to 2151 BC	F.5 S 1/2	103.72	Wood charcoal directly below fired clay cap of Feature 5
UT 08-052	960 ± 81	AD 897 to 1251	⋯	⋯	Charcoal in a (hearth?) associated with the *Bison* bone
UT 08-052(2)	1000 ± 93	AD 782 to 1224	⋯	⋯	Charcoal in a (hearth?) associated with the *Bison* bone
Unit 106N2W					
UT 06-028	6740 ± 70	5752 to 5521 BC	F.11	⋯	Charred wood Level IV, Feature 11
UT 08-053	6700 ± 73	5724 to 5490 BC	F.11	⋯	Charcoal W 1/2 F.11, Lev. 7
UT 08-026	6740 ± 143	5980 to 5386 BC	37	⋯	Wood charcoal gathered from scatter throughout level
UT 08-025	6790 ± 109	5966 to 5511 BC	42	⋯	Hand sorted charcoal from concentrated scatter in NE 1/4

identified in 1978, which shows clear affinity to bison rather than cattle (Fig. 10). In addition, both a first and a second phalanx articulate with the metacarpal: MNI is therefore 1. No cut marks are present to show that Dunbar Cave inhabitants were hunting or butchering bison. The chronological position of this animal is obviously of great interest, but unfortunately, we cannot rely on stratigraphic association to provide an indication of age. Therefore a section of bone, approximately 1 cm × 3 cm, was removed from the distal, posterior medial surface. The location for bone removal was chosen to minimize damage to the bone and to avoid areas containing measurement landmarks, in case the bone is subjected to future study. The section was submitted to Beta Analytic, Inc., for AMS dating of the collagen fraction. An age determination was returned of 1455 ± 45 BP. The calibrated age of the sample indicates that the bison died between AD 1420 and 1490 (calibrated

at 2σ with INTCAL04 [Reimer et al., 2004]). This confirms a Mississippian association for the animal and represents an early date for this species in the Middle Tennessee region. This determination does not overlap with the earlier ages for supposedly associated charcoal discussed above (Table 2).

Teeth and several mandible fragments have been identified as elk (*Cervus elaphus*). These also come from Units 106N and 108N, although MNI still is 1. In contrast to the bison, the elk mandible fragments do show cut marks, suggesting human utilization of this large artiodactyl. There are also remains of the left humerus from a large black bear (*Ursus americanus*) from Unit 108N that show evidence of rodent gnawing, indicating that it was exposed for some time prior to burial. Chronological control for the elk and bear is lacking, and their ages remain to be determined.
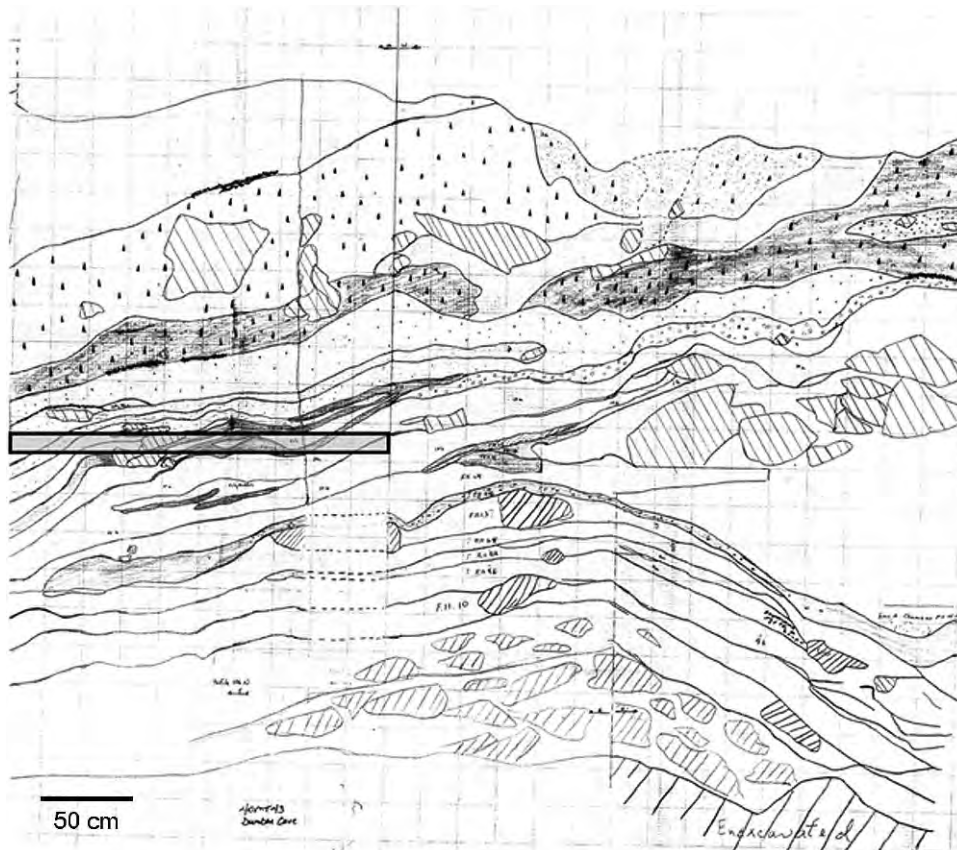
Figure 9. Profile of 1978 excavation trench at Unit 106N, after 1978 field notes by Pace and others. Shaded area shows single 2 m × 10 cm horizontal excavation spit containing seventeen strata.

Recent Archaeological Work

At the time the prehistoric art in Dunbar Cave was discovered, the cave was protected with an old gate that could easily be breeched. In July of 2006, a team of TDEC personnel and volunteers led by independent conservationist and gate-builder Kristen Bobo installed a new, more substantial, and bat-friendly gate. Once it was well-defended, the prehistoric cave art in Dunbar Cave was announced with a public ceremony at the cave. Dunbar Cave is the first Tennessee, indeed first North American, dark-zone cave-art site open to the interested public, and the cave art is part of the interpretive program offered to visitors. The bat-friendly gate has had the intended consequence of encouraging new bat habitation. Unfortunately, white nose syndrome was recognized among the Dunbar Cave bat population in March 2010, and the cave was closed to all traffic.

In May of 2007, as Dunbar Cave State Natural Area prepared interpretive exhibits, we undertook small-scale test excavations in the glyph chamber of the cave. Two 1 × 0.5 m units were excavated in the Ballroom, one near the warrior image and at the spot where a Late Archaic (i.e., Ledbetter) projectile point had been found just below the surface near the cave wall (Fig. 11a), and the other in seemingly intact deposits at the opposite wall of the chamber. These units at the edges of the room were chosen because the deposits in the center had been substantially modified by construction of a visitor pathway. Stratigraphy in the two room-edge units was essentially the same:

> Level 1 (8 to 10 cm thick): Banded dark and light fine water-laid silts, contains historic artifacts (wood, glass, nails), heavily trampled.
> Level 2 (1 to 2 cm): Solid travertine floor over entire unit composed of banded layers of calcium carbonate, archaeologically sterile.
> Level 3 (10 to 50+ cm): Homogeneous dark reddish brown sandy silt with occasional plaquettes and blocks, archaeologically sterile.

Interestingly, very few prehistoric artifacts were uncovered during these test excavations, despite the use of quarter-inch mesh to screen all sediments, but those that were found are relatively large and are made of high-quality chert. They include the stemmed point shown in Figure 11a and the biface fragment shown in Figure 11b. In every case, these artifacts were lying directly in contact with the top of Level 2, the travertine surface.

In May 2008, the state installed three interpretive panels in front of the principal glyph walls in the Ballroom, each
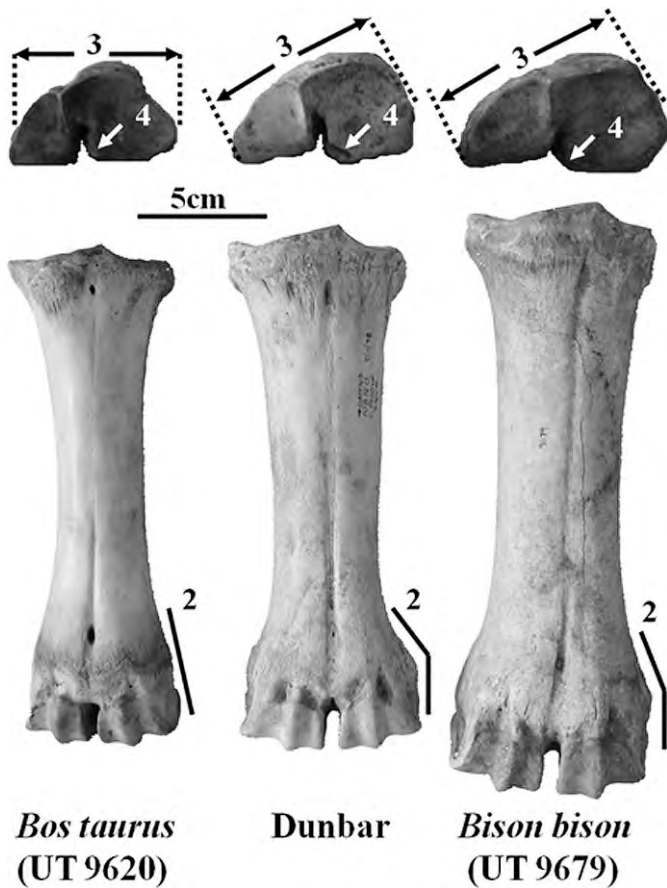
Figure 10. Comparison of Dunbar Cave bison metacarpal to modern bison and cow.

supported by two posts buried in the cave sediments. We were asked to excavate the holes for the support legs, in effect, providing six more shovel tests in the area of the main glyph concentrations. Each of these units was 20 cm square and excavated to a depth of about 50 cm where possible. In two cases, rocks were encountered at more than 30 cm below the surface. With one exception, all six shovel tests displayed the same stratigraphy as the test units described earlier, although in the northernmost test unit, closest to the warrior panel, a somewhat more complex sequence was encountered in and below Level 3. We briefly describe that profile as representative of all six 2008 units. At the top, 10 cm of banded dark and light fine water-laid sediments was encountered, Level 1 as defined in 2007. In all six units, a layer corresponding to Level 2, the travertine surface, was identified next, although in four units Level 2 was decomposed, reflected by travertine clasts and calcite sand. Level 2 varied from 1 to 3 cm in thickness. Level 3, 20 cm thick, consisted of dark, reddish-brown sandy loam with occasional lenses of silt and clay. Level 4, an 8 cm layer of plaquettes rich in calcite, and Level 5, light-colored, cross-bedded silts and sands, descends 50 cm from the base of Level 4. Only two artifacts were encountered during excavation of the six postholes: a white historic

ceramic shard at the top of Level 1, and a large chert core (Fig. 11c) lying on the travertine surface at the contact between Levels 1 and 2.

Even the limited information these excavations provide concerning prehistoric use of the interior of Dunbar Cave is intriguing. It seems that there was, at some time in the past, a travertine surface that extended across the Ballroom not unlike those present today in other parts of the cave, including the nearby Counterfeiter's Room. That surface, as elsewhere, probably held water and may have been composed of gours or other water-related speleothems. All of the excavated prehistoric artifacts are Late Archaic in aspect and lay directly on the surface of that submerged floor. Recall also that the single ^{14}C age determination from this room is Late Archaic. We speculate that these artifacts were intentionally deposited, "offered" into the waters of the Ballroom some 4000 years ago by Archaic period visitors, long before the artwork was added to the walls. Such practices are well known in Mesoamerica, where rituals and offerings were commonly made in caves, as has been demonstrated both ethnographically and archaeologically (see papers in Brady and Prufer, 2005). Such a practice would explain at least some evidence for Archaic cave use in the Southeast as well (Simek and Cressler, 2009; Simek et al., 1998; Crothers et al., 2002).

Conclusions

Dunbar Cave is a remarkable prehistoric site, not just for Tennessee but for the entire Eastern Woodlands. Human use of the cave interior spans at least 4000 years. People were interred in the cave, cave minerals may have been procured, and the cave interior was extensively explored. A prehistoric sanctuary was created during the Mississippian period (around AD 1300) with dark zone, parietal cave art depicting various iconographic images, including heroic characters from cosmological narratives. It is even possible that Archaic visitors (about 2000 BC) expressed their reverence for the underworld by leaving large, finely-worked stone tools in pools in the cave interior. Outside the cave, the vestibule rockshelter was periodically occupied beginning late in the Pleistocene and continuing through all Holocene prehistoric phases in the Southeast, with both hunting and agricultural peoples repeatedly visiting the site to hunt its surrounds, to obtain stone for their tools, to bury their dead, and to carry out religious rituals.

Archaeological work at Dunbar Cave will continue, and there are a number of aspects yet to be examined. For example, a visit to the hilltop crowning Dunbar Cave in 2007 revealed that in many places the rocky outcrops have been excavated, and in those areas large and fine-grained chert nodules were apparent, some tested with hammer-stone blows. The staff of Dunbar Cave was aware of some of these, but in a short period of time we identified at least a half-dozen major chert quarry sites outside the cave.
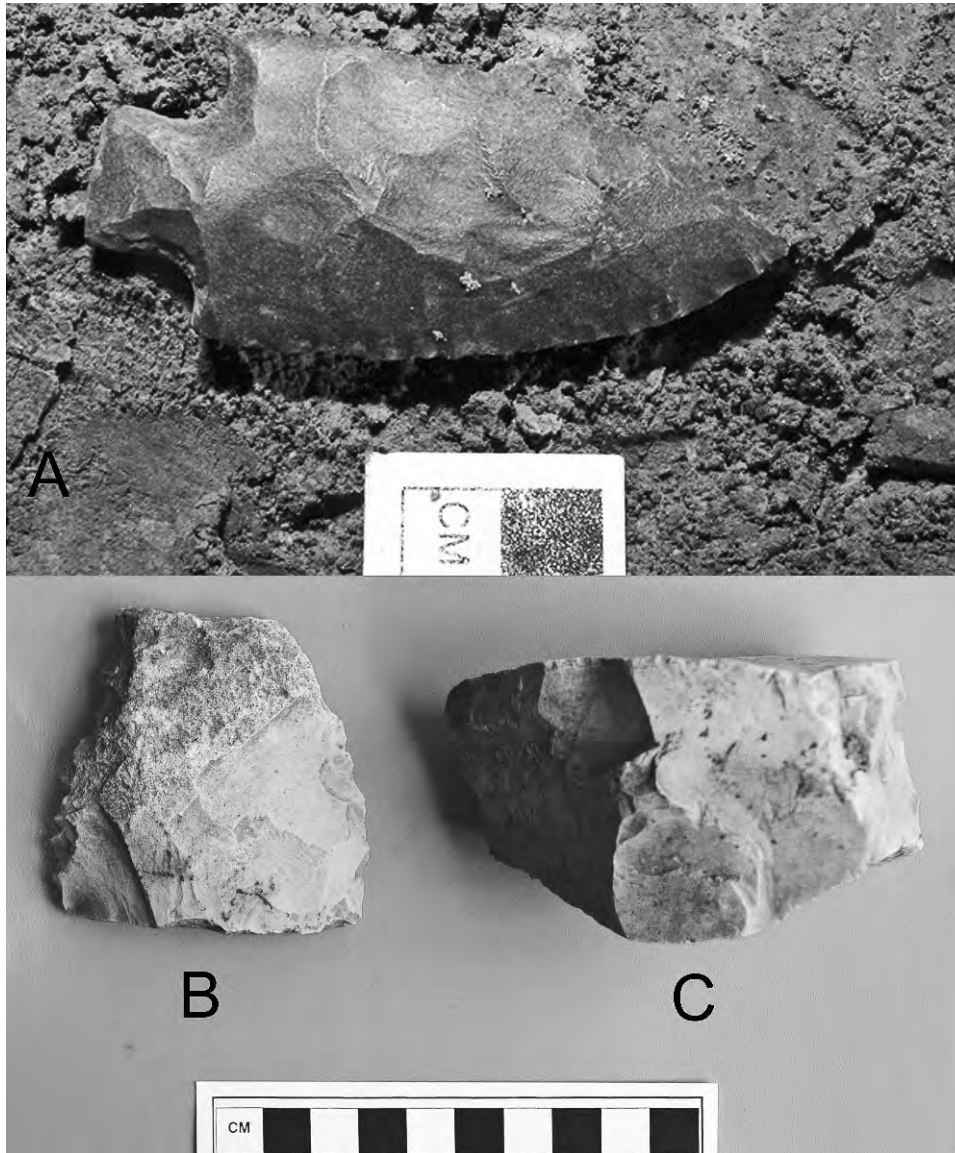
Figure 11. Artifacts recovered on the surface of buried speleothem floor in the Ballroom of Dunbar Cave. A. Late Archaic (Ledbetter type) projectile point. B. Biface fragment found in test excavation. C. Core fragment found in posthole excavation.

Some of these are quite extensive, and in some places numerous chert nodules derived from the outcrops are piled in association with knapping debris. The vicinity of Dunbar Cave was probably a significant prehistoric chert mine located near the renowned Dover, Tennessee, chert quarries. In 2006, we visited a part of the cave interior we had never seen and observed several localities where gypsum crusts had been battered from the cave walls and removed. A hammerstone lay on the floor at the base of one of these walls. It may be that prehistoric miners were active both inside and outside Dunbar Cave, as they were in several Tennessee sites. We have yet to undertake intensive work on these discoveries.

There is, thus, a great deal of research yet to do at Dunbar Cave. The cave has more than eight miles of mapped passages, but we have visited less than a quarter of that length. There is an internal archaeological survey to carry out, seeking and documenting art and other activities like mining and burial that might have taken place in the cave's recesses. Chert mining outside the cave should also be examined in detail, and the considerable remaining vestibule sediments warrant further investigation. Dunbar Cave is a remarkable archaeological resource. It deserves and will receive the attention required by its complex, multifaceted and long-term prehistoric use.

REFERENCES

Boszhardt, R.F., 2003, Deep Cave Rock Art in the Upper Mississippi Valley: St. Paul, MI, Prairie Smoke Press, 94 p.

Brady, J.E., and Prufer, K.M., 2005, In the Maw of the Earth Monster: Studies of Mesoamerican Ritual Cave Use: Austin, University of Texas Press, 448 p.

Brain, J.P., and Phillips, P., 1996, Shell Gorgets: Styles of the Late Prehistoric and Protohistoric Southeast: Cambridge, Massachusetts, Peabody Museum Press, 542 p.

Brown, J.A., 2007, On the identity of the birdman within Mississippian period art and iconography, in Reilly III, F.K., and Garber, J.F., eds., Ancient Objects and Sacred Realms: Interpretation of Mississippian Iconography: Austin, University of Texas Press, p. 56–106.

Butler, B.M., 1977, A preliminary archaeological assessment of Dunbar Cave (40MT43): Nashville, Division of Archaeology, Tennessee Department of Conservation.

Creswell, B.A., 2007, Phase I Archaeological Survey of Caves and Rockshelters within the Proposed Corridor of the Knoxville Parkway (SR475) in Anderson, Knox, and Loudon Counties, Tennessee: Knoxville, University of Tennessee Archaeological Research Laboratories.

Crothers, G., Faulkner, C.H., Simek, J.F., Watson, P.J., and Willey, P., 2002, Woodland period cave use in the eastern woodlands, in Anderson, D.G., and Mainfort, R.C., Jr., eds., The Woodland Southeast: Tuscaloosa, University of Alabama Press, p. 502–524.

Diaz-Granados, C., and Duncan, J.R., 2000, The Petroglyphs and Pictographs of Missouri: Tuscaloosa, University of Alabama Press, 280 p.

Diaz-Granádos, C., Rowe, M.W., Hyman, M., Duncan, J.R., and Southon, J.R., 2001, AMS radiocarbon dates for charcoal from three Missouri pictographs and their associated iconography: American Antiquity, v. 66, p. 481–492.

Faulkner, C.H., ed., 1986, The Prehistoric Native American Art of Mud Glyph Cave: Knoxville, University of Tennessee Press, 124 p.

Faulkner, C.H., 1988, A study of seven southeastern glyph caves: North American Archaeologist, v. 9, no. 3, p. 223–246.

Faulkner, C.H., Deane, B., and Earnest, H.H., Jr., 1984, A Mississippian period ritual cave in Tennessee: American Antiquity, v. 49, no. 2, p. 350–361.

Faulkner, C.H., and Simek, J.F., 1996, Mud glyphs: Recently discovered cave art in eastern North America: International Newsletter on Rock Art, v. 15, p. 8–13.

Hall, R.L., 1997, An Archaeology of the Soul: North American Indian Belief and Ritual: Champaign, University of Illinois Press, 222 p.

Holmes, W.H., 1883, Art in shell of the ancient Americans, in 2nd Annual Report of the Bureau of American Ethnology, 1879–80: Washington, D.C., Government Printing Office, p. 179–305.

Leroi-Gourhan, A., 1971, Préhistoire de l'Art Occidental, second edition: Paris, Mazenod, 499 p.

Lewis, T.M.N., and Lewis, M.D.K., 1995, The Prehistory of the Chickamauga Basin in Tennessee: Knoxville, University of Tennessee Press, two vols., 683 p.

Matthews, L.E., 2005, Dunbar Cave: The Showplace of the South: Huntsville, Alabama, National Speleological Society, 145 p.

Muller, J., 1989, The southern cult, in Galloway, P.K., ed., The Southeastern Ceremonial Complex: Artifacts and Analysis: Lincoln, University of Nebraska Press, p. 11–26.

Pace, R.A., and Hood, V.P., 1978, Archaeological Investigations at Dunbar Cave: A Stratified Rockshelter: Nashville, Division of Archaeology, Tennessee Department of Conservation.

Reimer, P.J., et al., 2004, IntCal04 terrestrial radiocarbon age calibration, 0–26 cal kyr BP: Radiocarbon, v. 46, no. 3, p. 1029–1058.

Sabo III, G., 2008, Rock art and the study of ancient religions in southeastern North America, in Fogelin, L., ed., Religion, Archaeology, and the Material World: Carbondale, Center for Archaeological Investigations, Southern Illinois University, occasional paper 36, p. 279–296.

Simek, J.F., 2010, Afterword: Onward into the darkness (still following the light of Pat Watson's lamp, of course), in Dye, D., ed., Cave Archaeology in the Eastern Woodlands: Essays in Honor of Patty Jo Watson: Knoxville, University of Tennessee Press, p. 261–270.

Simek, J.F., Blankenship, S., Herrmann, N., Sherwood, S.C., and Cressler, A., 2010, New cave and rock art sites in Tennessee: 2007, in Baumann, T., and Groover, M., eds., Pottery, Passages, Postholes, and Porcelain: Essays in Honor of Charles H. Faulkner: Knoxville, McClung Museum, Report of Investigations series, University of Tennessee, p. 71–88.

Simek, J.F., and Cressler, A., 2001, Issues in the study of prehistoric southeastern cave art: Midcontinental Journal of Archaeology, v. 26, no. 2, p. 233–250.

Simek, J.F., and Cressler, A., 2005, Images in darkness: Prehistoric cave art in southeastern North America, in Loendorf, L., Chippendale, C., and Whitley, D., eds., Discovering North American Rock Art: Tucson, University of Arizona Press, p. 93–113.

Simek, J.F., and Cressler, A., 2009, Prehistoric cave art in southeastern North America, in White, W.B., ed., Proceedings of the 15th International Congress of Speleology: Huntsville, Alabama, National Speleological Society, p. 135–139.

Simek, J.F., Douglas, J.C., and Wallace, A., 2007, Ancient cave art at Dunbar Cave State Natural Area: Tennessee Conservationist, v. 23, no. 5, p. 24–26.

Simek, J.F., Franklin, J.D., and Sherwood, S.C., 1998, The context of early southeastern prehistoric cave art: A report on the archaeology of 3rd Unnamed Cave: American Antiquity, v. 63, no. 4, p. 663–675.

Van West, C., 1998, Dunbar Cave State Natural Area, in Van West, C., ed., Tennessee Encyclopedia of History and Culture: Nashville, Tennessee, Rutledge Hill Press, 266 p.

Wagner, M.J., 1996, Written in stone: An overview of the rock art of Illinois, in Faulkner, C.H., ed., Rock Art of the Eastern Woodlands: San Miguel, California, American Rock Art Research Association occasional paper 2, p. 47–79.

Waring, A.J., Jr., and Holder, P., 1945, A prehistoric ceremonial complex in the southeastern United States: American Anthropologist, v. 47, no. 1, p. 1–34, doi:10.1525/aa.1945.47.1.02a00020.

Whidby, J., 1999, Idaho Springs and Dunbar Cave Resort: The showplace of the south: Journal of the Cumberland Spelean Association, v. 6, no. 1, p. 7–12.

CANDIDATE CAVE ENTRANCES ON MARS

Glen E. Cushing

U.S. Geological Survey, Astrogeology Science Center, 2255 N. Gemini Dr., Flagstaff, AZ 86001, USA, gcushing@usgs.gov

Abstract: This paper presents newly discovered candidate cave entrances into Martian near-surface lava tubes, volcano-tectonic fracture systems, and pit craters and describes their characteristics and exploration possibilities. These candidates are all collapse features that occur either intermittently along laterally continuous trench-like depressions or in the floors of sheer-walled atypical pit craters. As viewed from orbit, locations of most candidates are visibly consistent with known terrestrial features such as tube-fed lava flows, volcano-tectonic fractures, and pit craters, each of which forms by mechanisms that can produce caves. Although we cannot determine subsurface extents of the Martian features discussed here, some may continue unimpeded for many kilometers if terrestrial examples are indeed analogous. The features presented here were identified in images acquired by the Mars Odyssey's Thermal Emission Imaging System visible-wavelength camera, and by the Mars Reconnaissance Orbiter's Context Camera. Select candidates have since been targeted by the High-Resolution Imaging Science Experiment. Martian caves are promising potential sites for future human habitation and astrobiology investigations; understanding their characteristics is critical for long-term mission planning and for developing the necessary exploration technologies.

Introduction

Since Oberbeck et al. (1969) first proposed that some lunar rilles might be collapsed lava tubes, the existence, characteristics, and potential utility of extraterrestrial cave systems have been extensively discussed, particularly for the Moon and Mars (e.g., Horz, 1985; Boston et al., 2003). Considering that basaltic volcanism is generally analogous between the Earth and Mars (e.g., Glaze et al., 2005), volcanic caves are believed to be fairly common on Mars (Cruikshank and Wood, 1972; Horz, 1985), but until recently, technical limitations, such as the spatial resolution, areal coverage, and viewing perspective of orbiting instruments have hindered their detection. Bleacher et al. (2007a, 2007b) identified numerous tube-fed lava-flow systems on the flanks of Olympus Mons and elsewhere in the Tharsis region of Mars and inferred some collapsed lava-tube sections to be skylights. However, they also suggested that the host lava tubes had completely collapsed and did not elaborate upon the possibility of intact cave systems. This paper presents new observations of candidate entrances into near-surface lava tubes and volcano-tectonic caves; morphological characteristics are examined and compared with terrestrial counterparts, and implications about formation mechanisms and exploration possibilities are discussed.

Caves are important to the future of Mars exploration because they are believed to provide shelter from a range of harsh surface conditions, maintaining near-pristine surfaces and relatively stable microclimates. Mars's thin atmosphere and negligible magnetic field do not effectively absorb, deflect, or moderate numerous hazards, including micrometeoroid impacts, dust storms, extreme temperature variations, and high fluxes of UV, alpha particles, and cosmic rays (e.g., Mazur et al., 1978; De Angeles et al., 2002; Boston et al., 2004; Cushing et al., 2007). Because organic materials cannot continuously withstand such hazards, caves may be among the few human-accessible locations that preserve evidence of whether microbial life ever existed on Mars. Caves may also become valuable resources for human explorers, who would otherwise have to transport their own shelters or construct them in place (e.g., Horz, 1985; Coombs and Hawke, 1992; Boston et al., 2003). Additionally, exploring and characterizing Mars's volcanic caves should enable us to constrain theories about lava-flow thermodynamics and hydrodynamics under Mars's gravity and atmospheric conditions. Volcanic and other types of caves may also protect mineral formations that either do not form or become buried or altered under surface conditions (Hill and Forti, 1997).

We surveyed all released images from Mars Odyssey's Thermal Emission Imaging System (THEMIS) and Mars Reconnaissance Orbiter's Context Camera (CTX) covering the flank flows and lava plains to the north of Arsia Mons (235° to 243° E, −8° to 2° N, Fig. 1) because this is where the first cave-entrance candidates were identified (Cushing and Titus, 2010). Entrances into two distinctly different cave types exist in this region: near-surface lava-tube caves that form as singular, horizontal, curvilinear tunnels and volcano-tectonic caves that may extend downward into subsurface fractures. Although we cannot determine how far any of the Martian caves continue beneath the surface, it is likely that that many could be extensive if our comparisons with terrestrial examples are appropriate, because terrestrial volcanic caves can be tens of kilometers in length and hundreds of meters deep. Numerous smaller cave entrances appear to exist throughout the sample region, but these cases are not discussed here because they are too
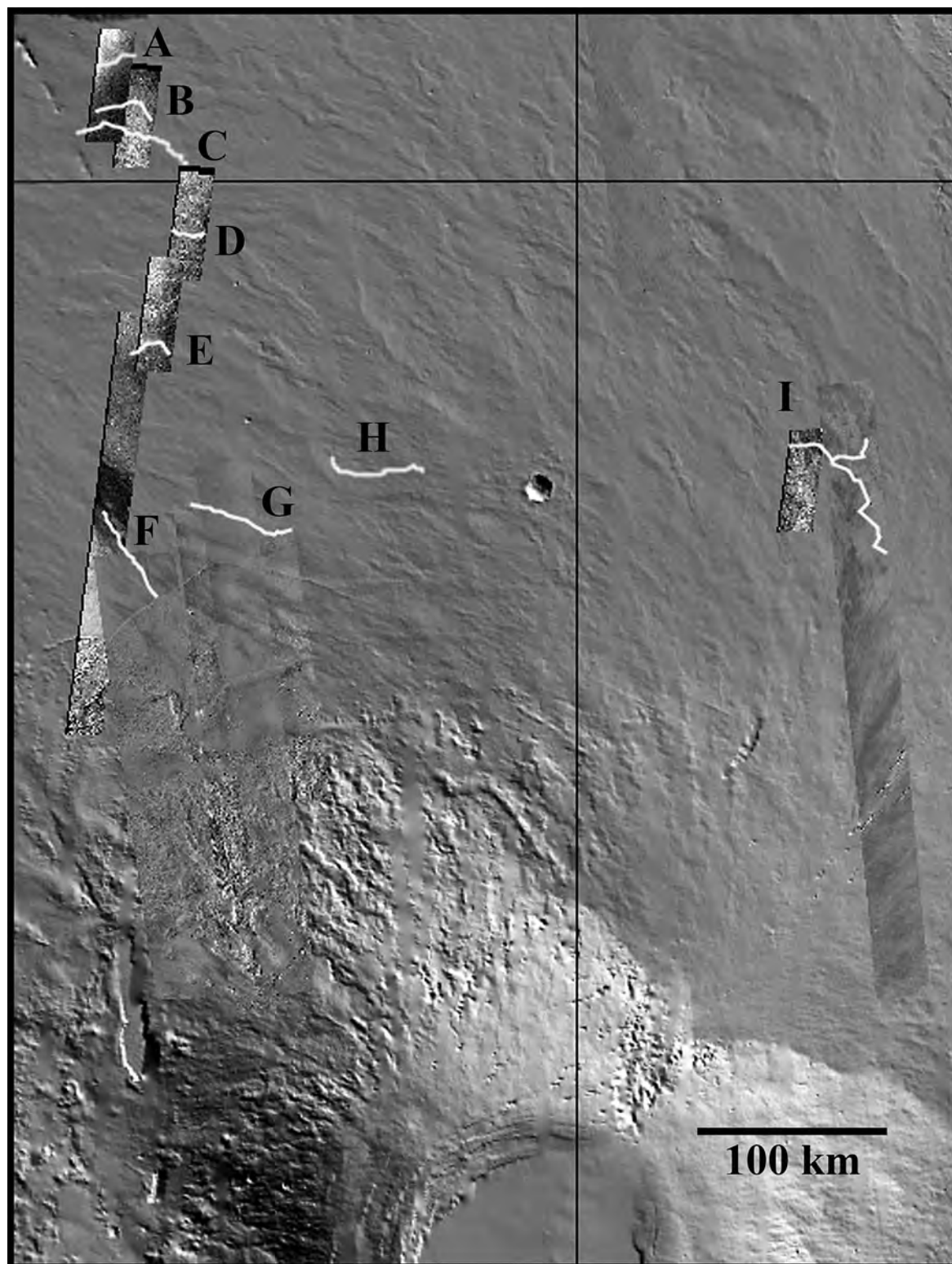
Figure 1. Context camera image showing the rift zone and lava plains north of Arsia Mons with the distribution of skylight-bearing tube-fed lava flows (A–H) and the volcano-tectonic fracture system (I) listed in Table 1 (Image: MOLA 128 pixel-per-degree shaded relief from JMARS (Christensen et al., 2007)).
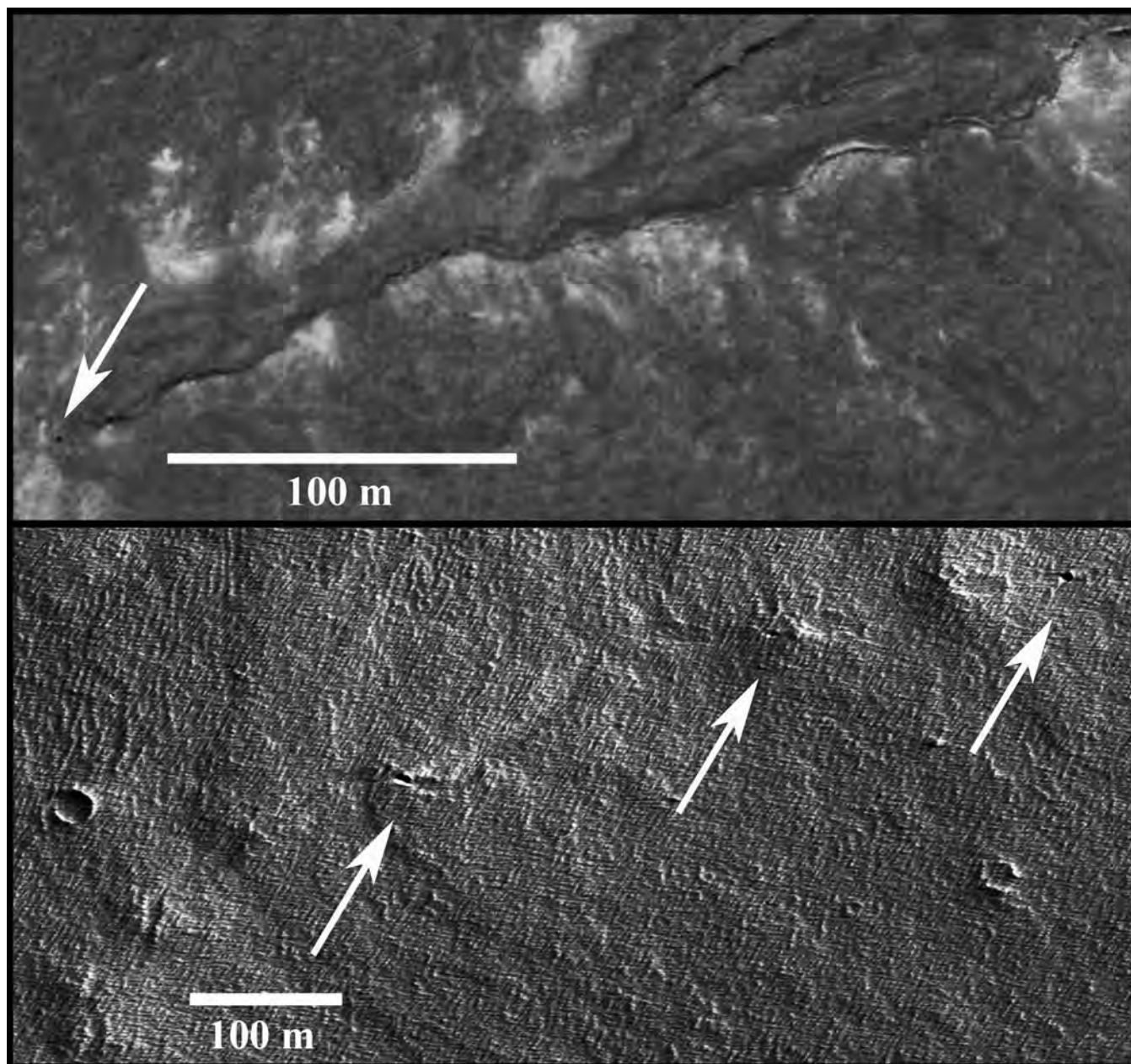
Figure 2. Comparison of inflated tube-fed lava flows (and their associated surface expressions). Top image shows an unnamed flow in Kīlauea volcano's eastern rift zone. Bottom image shows a proposed Martian tube-fed flow in the rift apron north of Arsia Mons (CTX: B02_010398_1751). Arrows indicate locations of candidate skylight entrances.

small and poorly resolved to be positively identified at this time.

SOURCE DATA

THEMIS consists of two cameras that record visible and thermal-infrared wavelengths. The visible-wavelength camera observes the Martian surface at 18 or 36 m/pixel in five discrete bands that cover the visible to near-IR spectrum between ~0.4 and ~0.9 μm (Christensen et al., 2004). In this study, we use only band-3 data (~0.654 ±

0.053 μm) because it is acquired in most observations and provides the highest signal-to-noise ratio. At ~100 m/pixel, THEMIS thermal-infrared data are too coarse to detect the features presented here. CTX detects a broad band of visible wavelengths (~0.5–0.8 μm) at ~6 m/pixel (Malin et al., 2007), allowing more precise measurements to be taken and enabling features that are small or ambiguous in THEMIS data to be more clearly identified. As of June 2010, CTX coverage did not include much of the region north of Arsia Mons, where THEMIS identified many of the tube-fed flows and fractures discussed here. THEMIS

and CTX datasets are appropriate to conduct survey-type searches for cave entrances because each observation covers hundreds of square kilometes, and they cumulatively cover the majority of Mars's total surface area. The Mars Reconnaissance Orbiter's High-Resolution Imaging Science Experiment (HiRISE) is a visible-wavelength camera that observes at ultra-fine resolution down to ~0.25 m/pixel, giving pixels about 1/5000 the size of a THEMIS pixel (McEwen et al., 2007) that allows precise measurements to be taken and fine-scale morphologies and surface textures to be evaluated. Because the MRO performs routine roll maneuvers about its direction of motion, HiRISE and CTX can observe objects from an off-nadir perspective. This is useful in determining whether a vertical wall or an overhanging rim is present around the skylights. Because HiRISE will cover only a small portion of Mars during its lifetime (~1% during its initial two-year primary science phase (McEwen et al., 2007), its targets are carefully chosen and limited to specific and scientifically relevant locations, usually based on THEMIS or CTX observations.

LAVA-TUBE CAVES

Lava tubes are insulated subsurface conduits that allow, or once allowed, flowing lava to maintain high temperatures, and thus low viscosity, as it travels from a source vent to distant flow margins (e.g., Wentworth and Mac-Donald, 1953; Greeley, 1971a, 1971b, 1972; Keszthelyi, 1995; Sakimoto et al., 1997). These are common structures in basaltic pāhoehoe–type lava flows and facilitate the spread of evolved mafic lava flows by enabling large volumes to be transported over long distances (Wentworth and MacDonald, 1953; Keszthelyi and Self, 1998). If the flow of lava through an established tube becomes either diminished or diverted, then the tube may drain and leave an empty, intact, and structurally competent tunnel. Surface entrances (skylights) may exist where portions of lava-tube ceilings either never completely formed or have collapsed. Occurring frequently in terrestrial basaltic volcanism, lava tubes are expected to be common in Mars's volcanic regions as well (e.g., Horz, 1985; Keszthelyi, 1995; Sakimoto et al., 1997).

On Mars, numerous sinuous and linear depressions in volcanic regions appear similar to orbital views of inflated tube-fed lava flows on Earth (Fig. 2). These depressions are channel-like in appearance and follow single, sinuous paths that extend along the crests of 10 to 20 m topographic rises with laterally spreading flanks that often form chains of either tumuli or vent structures. This morphology is a telltale indicator of a tube-fed system emplaced by inflation, which can be a dominant pāhoehoe mechanism across low slopes (Kauahikaua, et al., 2003). Inflated tube-fed lava flows often develop downward-propagating cracks (running along the direction of flow, Fig. 2) that form when the cooled and hardened lava-tube ceiling is raised

due to internal pressure from subsequent magma-injection episodes (e.g., Self et al., 1998; Kauahikaua, et al., 2003, Glaze et al., 2005). However, some of the tubes presented here have sections where the axial trench does not sit atop a topographic rise, but instead cuts downward into the surface and shows no evidence of inflation (e.g., Fig. 3). These apparently non-inflated lava-tube sections may have initially began as channelized flows that eventually crusted over to form insulated conduits (e.g., Wentworth and MacDonald, 1953; Greeley, 1971a, 1971b). Lava tubes that neither begin as open channels nor become inflated by internal pressures may exhibit little or no visible surface expression, and often can only be identified by the presence of skylight entrances (e.g., Daga et al., 1988; Greeley, 1972; Calvari and Pinkerton, 1999; Miyamoto et al., 2005). Although the surface grooves described here are sometimes thought to be completely collapsed lava tubes, it is important to emphasize that these features are more likely to be either dilational fractures from inflation or the upper surfaces of former channelized flows. They do not necessarily indicate the diameter of an underlying evacuated tube, that internal collapse has occurred, or even that the tube system ever drained to form an empty tunnel. Here we suggest that the presence of skylight entrances into these trenches indicates that draining did indeed occur at those locations and that lava tubes are likely to remain at least partially intact beneath the surface (Figs. 3 and 4 top).

Keszthelyi (1995) and Sakimoto et al. (1997) modeled the thermodynamics of lava-tube formation to determine how tube lengths and diameters on various planetary bodies would be related to properties such as lava viscosity, effusion rates, regional slopes, gravity, and atmosphere. The tube-fed flows on Mars observed to contain skylights show surface expressions up to 71 km long, which is considerably shorter than the maximum modeled lengths of up to 1000 km, so these tubes, whose source vents are not seen in the vicinity, could extend much farther upslope.

The proposed lava-tube skylights discussed here occur within several tube-fed flows (Table 1). These entrances are less than 60 m across, at least 10 to 30 m deep, and do not extend laterally beyond the channels or trenches that contain them. In some cases where inflation effects are not apparent, the skylights occur in relatively flat surfaces where they have caused wind-streak patterns to form (Fig. 4, top) and appear to be at least partially filled with in-blown dust.

To be classified as a candidate lava-tube skylight in this paper, a feature must have at least one pixel that is darker than the shadows cast by nearby surface features such as crater rims, exist within a sinuous trench that runs axially along a tube-fed lava flow, be substantially deeper than its host trench, and not have characteristics normally associated with impact craters such as raised rims or ejecta patterns. Bleacher et al. (2007a) observed lava-tube skylights in THEMIS image V11326014, but these are unlikely cave-entrance candidates because they are not as dark as nearby shadowed regions and are no deeper than their host trench.
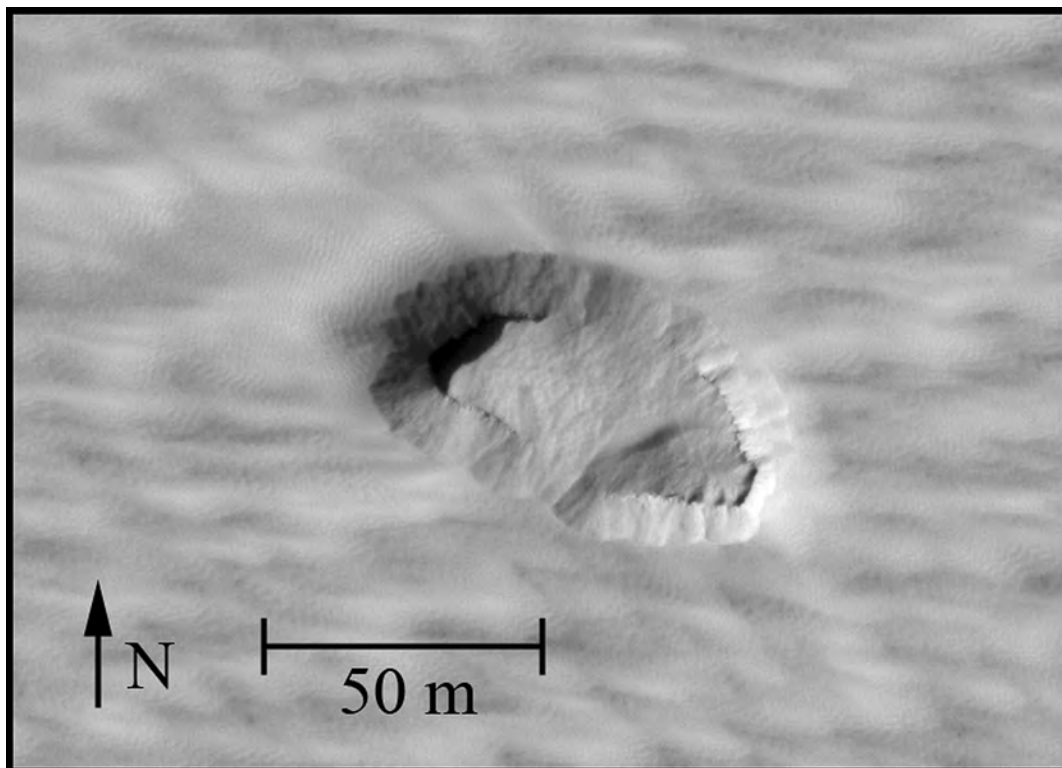
Figure 3. HiRISE ESP_016767_1785 (along flow F in Figure 1). Collapsed lava-tube section that's been partially filled by windblown dust. Cave entrance might be accessible by a vehicle.

Volcano-Tectonic Caves

The other type of linear surface depression observed to contain cave entrances is located at the distal edge of the Arsia Mons northwest-flank vent flows, approximately midway between Arsia Mons and Pavonis Mons and ~200 km east of the aforementioned tube-fed flows (I in Fig. 1). This structure shows evidence of both volcanic and tectonic mechanisms and is clearly different from the trenches associated with tube-fed lava flows in several ways. It is substantially wider than the fractures found along the crests of tube-fed flows and is composed of 10 to 20 km linear or curvilinear, rather than sinuous, segments that cut across numerous lava flows and conjoin at sharp angles, usually between 95 and 110° (Figs. 5, 6, and 7). Collectively, the connected fractures extend more than 100 km. This structure does not contain tumuli, outflow vents, or topographic high points, but instead has graben-like depressions with broad, flat floors and no apparent vertical offset between opposing walls. A regional dust mantle up to several meters thick masks any parallel normal faults that could indicate whether a graben-type collapse occurred. The lengths, segmentation, location, and orientation of these fractures, which are between Arsia Mons and Pavonis Mons and aligned with the Tharsis-ridge volcanic system, suggest they may have formed through deep tectonic processes associated with the Tharsis regional uplift (Banerdt et al., 1992; Phillips et al., 1990). Dilational tectonic fractures of this magnitude could extend downward as far as 5 km beneath the surface (Ferrill et al., 2003), where they were likely intruded and widened by magma, thus inducing formation of the observed grabens and cave entrances. As with the lava-tube skylights, the volcano-tectonic cave entrances are no wider than the fractures in which they formed. However, unlike lava-tube caves, which tend to be sinuous, remain relatively near the upper surface, and follow regional slopes, volcano-tectonic caves could extend deep into their host fractures and branch into complicated subsurface networks (Coons, 2010).

Visible evidence that low-viscosity materials flowed out of this fracture network can be seen in the form of occasional rim levees and a substantial outflow feature with distinctly fluvial-like streamlined braids where a large volume of fluid laterally breached the fracture walls in the down-slope direction (Fig. 7). If this fluid was lava, then its viscosity must have been exceptionally low to form such a fluvial pattern. Jaeger et al. (2010) rigorously examined a similar example in Athabasca Vallis, where fluvial-like features were carved by mafic or ultra-mafic flood basalts with viscosities possibly as low as 10 Pa·s. On the other hand, the streamlined islands in this outflow feature may have formed from an outbreak of liquid water, as the Tharsis region contains multiple examples of fluvial-type
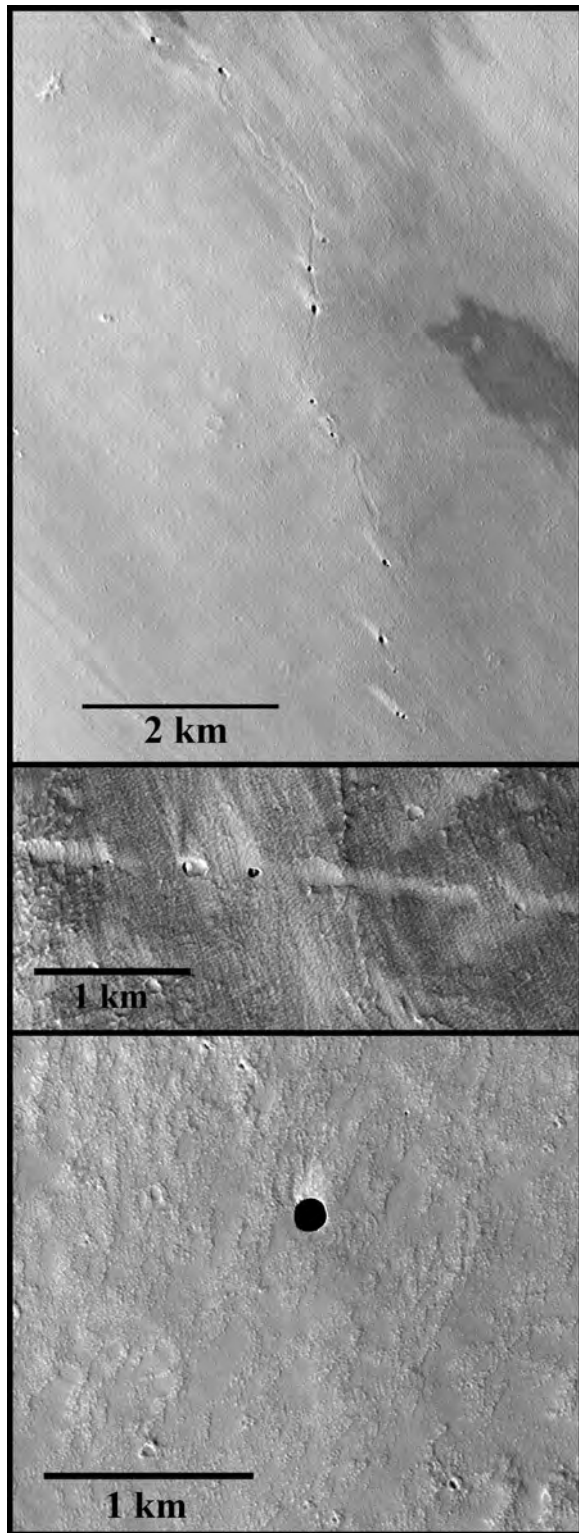
Figure 4. Three different cave entrance candidate types on Mars. Top image shows a lava-tube rille with multiple skylight entrances (CTX: P17_007774_1757); the center image is a volcano-tectonic fracture with a skylight entrance (HiRISE: ESP_014380_1775, detail in Figure 8); and the bottom image is an atypical pit crater with a diameter of

channels (Mouginis-Mark, 1990; Mouginis-Mark and Christensen, 2005), and water-ice clouds form above Arsia Mons nearly every day of the year (Noe Dobrea and Bell, 2005; Benson et al., 2006).

An appropriate terrestrial comparison to this Martian volcano-tectonic fracture system may be the Great Crack (Fig. 6, top) in Kīlauea volcano's southwest rift zone. The Great Crack is a linear series of fractures, grabens, and pit-crater chains that extend from Kīlauea's caldera to the ocean. This structure formed when upwelling magma intruded into a dike-induced fracture during the 1823 Kīlauea flow event, thus widening the fracture and forming a dike that transported material more than 35 km from the source. Normal faulting and stoping above this dike caused a series pit craters and grabens to form (Okubo and Martel, 1998), along with a number of deep and extensive caves, some of which have been explored to depths exceeding 180 m (Coons, 2010). Although the Great Crack is likely a non-tectonic feature caused by forced magmatic intrusion, while the Martian cracks were likely widened when magma flowed into pre-existing tectonic fractures, these mechanisms both involve interactions between fractures and magma and may have created similar opportunities for magma to drain and produce comparable surface expressions such as pits and fracture caves at the sub-kilometer scale.

Figure 8 shows the only currently released HiRISE observation of a volcano-tectonic fracture skylight where an overhanging, dust-mantled rim and an interior mound that is either dust or dust-covered are clearly resolved. Specifics of this skylight are discussed in the measurements section.

ATYPICAL PIT CRATERS

A different type of cave entrance is described by Cushing et al. (2007), who discuss a number of steep-walled depressions that appear to be special cases of common pit craters (Fig. 4, bottom). Atypical Pit Craters (APC) are not associated with surface grooves and are nearly always circular, with diameters of ~80 to 300 m. HiRISE shows that some APCs are deep, sheer-walled cylindrical structures with no apparent subsurface extent, while others extend laterally beneath overhanging rims for unknown distances (Cushing et al., 2008). Figure 9 shows an APC where a candidate cave entrance can be seen in its floor; the image has been contrast-enhanced to display the instrument's low-radiance limit. Figure 10 shows what appears to be a common pit crater with a central skylight entrance into which surface materials likely continue to drain. This example is possibly unique on Mars, and it

←

~165 m, a depth >245 m, and an overhanging rim of unknown extent (HiRISE: PSP_003647_1745).

Table 1. Physical characteristics of skylight-hosting lava tubes (A–H) and volcano-tectonic fractures (I) shown in Figure 1. THEMIS IDs begin with a V, CTX IDs begin with a P or a B.

Feature	Primary Image ID[a]	Image Scale (m/pixel)	Incidence Angle (deg)	Number of Skylights	Minimum Depth (m)	Longitude Range (E)	Latitude Range (N)	Total Length (km)[a]	Elevation Range (m)	Ave. Slope (deg)
(A)	V12611008	17.9	79.90	4	~10	235.9 to 236.4	0.91 to 0.92	>35	4164 to 4284	0.12
(B)	V18439013	17.7	66.72	4	~18	236.0 to 236.4	0.51 to 0.63	32.5	4114 to 4247	0.23
(C)	V18439013	17.7	66.72	9	~24	235.8 to 236.8	0.05 to 0.44	71.0	4020 to 4335	0.25
	V12611008	17.9	79.90							
(D)	V05272018	17.7	76.60	5	~10	236.5 to 236.8	−0.47 to 0.43	>19	4293 to 4347	0.46
(E)	V11988001	17.6	78.89	4	~12	236.3 to 236.5	−1.46 to −1.38	>15	4258 to 4339	0.31
(F)	V27837001	35.3	79.60	32	~23	235.9 to 236.4	−3.59 to −2.86	47.0	4457 to 4739	0.34
	P20_008763_1749	5.3	57.21							
	B05_011532_1750	5.3	57.27							
(G)	B02_010398_1751	5.28	57.89	5	~19	236.7 to 237.5	−3.00 to −2.77	>55	4655 to 5176	0.54
	B01_010187_1759	5.32	57.77							
(H)	P09_004346_1757	5.35	46.80	1	~15	237.8 to 238.3	−2.73 to −2.44	>35	5086 to 5358	0.45
(I)	V16468001	17.6	70.41	9	>35	241.7 to 242.6	−3.19 to −2.24	>100	7480 to 6990	0.28
	P17_007774_1757	5.39	49.74							

[a] Calculated along the entire observed length.

could represent an intermediate, possibly ongoing formation stage of either an APC, if ceiling collapse progresses outward, or a common pit crater, if draining surface materials eventually fill the skylight. Haruyama et al. (2009) recently discovered a lunar feature in an ancient lava channel that looks identical to Martian APCs and suggest it may be a skylight entrance into a deep lava tube. Table 2 shows a comparison of the three different cave-entrance types.

MEASUREMENTS

The Mars Orbiter Laser Altimeter on the Mars Global Surveyor measured surface elevations across Mars (Zuber et al., 1992) with a vertical resolution of ~1 m, and we used a dataset binned to a spatial resolution (equatorial) of approximately 256 pixels per degree, or ~230 m. We used the Java Mission-planning and Analysis for Remote Sensing (JMARS) tool (Christensen et al., 2007) to register MOLA with visible observations and determine the elevation profile for each feature containing at least one candidate skylight entrance. All the observed tube-fed flows run continuously down-slope at shallow angles averaging ~0.5° or less, and the volcano-tectonic fractures average ~0.3° down-slope with occasional minor rises (Fig. 11; Table 1).

In THEMIS observations, most of the skylight entrances are on the scale of only a few pixels or less, so accurate dimensions with reasonable error estimates cannot be determined from the spatial extent of pixels alone. Horizontal dimensions of the skylights were calculated by fitting an ellipse to the dark pixels corresponding to each feature, assuming that pixels outside of the ellipse match the median pixel value of the scene while those inside of the ellipse match either the minimum pixel in the scene or zero DN (Digital Number value). The scene was reconstructed assuming sub-pixel mixing between the inside and outside of the ellipse, and the estimated DN for each pixel was weighted by the area of the ellipse contained within that pixel. The location, major and minor axes, and rotation of the major axis were varied until the root-mean-square difference between the actual scene (at the median-value threshold) and the reconstructed scene was minimized (Fig. 12).

To estimate the depth (d) of a floor beneath a skylight entrance in THEMIS images, we assumed a nadir viewing perspective and divided the length (D_s) of the interior shadow cast by the rim in the direction of illumination by the tangent of the observed solar incidence angle (i). In most cases, the lava-tube floors are sufficiently deep, i is sufficiently large, and the full diameter along the line of illumination (D_i) is sufficiently small that the shadowed/sunlit boundary cannot be seen (so $D_s = D_i$), and only a minimum value for depth can be obtained. Assuming that lava-tube floors maintain essentially constant depths beneath the surface, the largest skylights indicate that interior floors run at least 15 to 30 m below the surface.
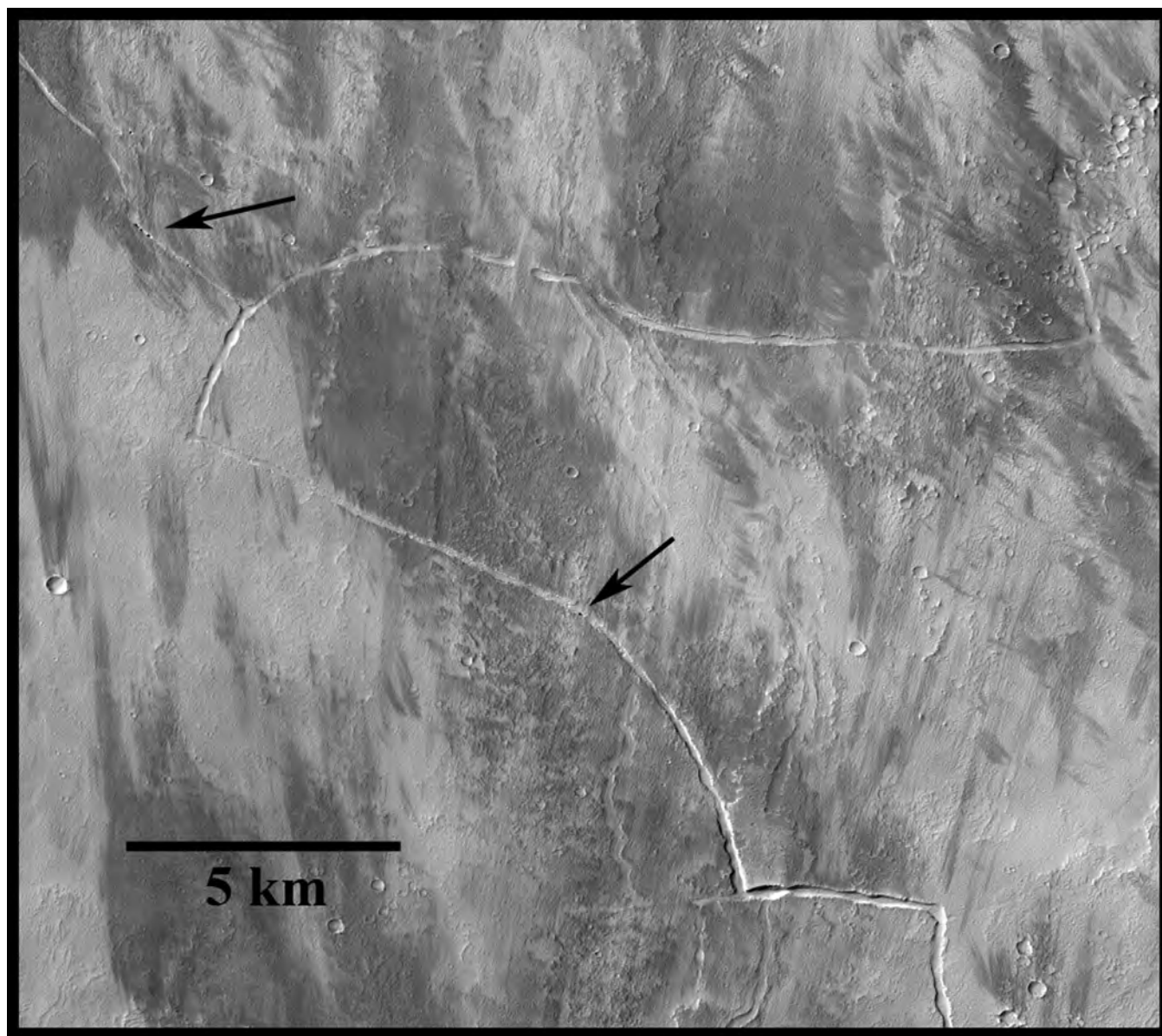
Figure 5. A small portion of the proposed volcano-tectonic fracture network, shown here to illustrate its fracture-like appearance from orbit (CTX: P17_007774_1757). The entire network spans >100 km. Figure 6 shows part of this feature compared with a terrestrial analog, Figure 7 shows evidence that low-viscosity fluid flowed through the network, and Figure 8 details one of its skylight entrances. North is upward; arrows indicate candidate skylight entrances.

HiRISE has observed one fracture-cave skylight thus far, looking slightly off nadir at an angle of 6.8° (see Fig. 8). This image shows a large central mound, not apparent in THEMIS observations, that appears to be composed of either dust or dust-covered rubble. The major and minor axes of this feature are ~68 m and ~48 m, respectively, which are within the error bounds of our ellipse fitted to the THEMIS data. Based on the solar incidence of 35°, we can determine that the depth at the edge of the shadow is approximately 37 m. Accordingly, if slopes of the central mound are at the angle of repose (~30 to 40°), then the peak of the mound is approximately 19 to 25 m beneath the surface level, and the non-illuminated area directly below the western rim is at least 49 to 55 m deep if the mound slopes consistently downward to that point. The entrance ledge appears to completely encircle the pit and slopes inward from the surface so that the dust/rock interface can be discerned. Assuming these materials lie at the angle of repose, the upper overhanging ledge is approximately 5.5 m to 8.5 m thick, with the uppermost 3 or 4 m being composed of dust mantling 2.5 m to 4.5 m of bedrock.
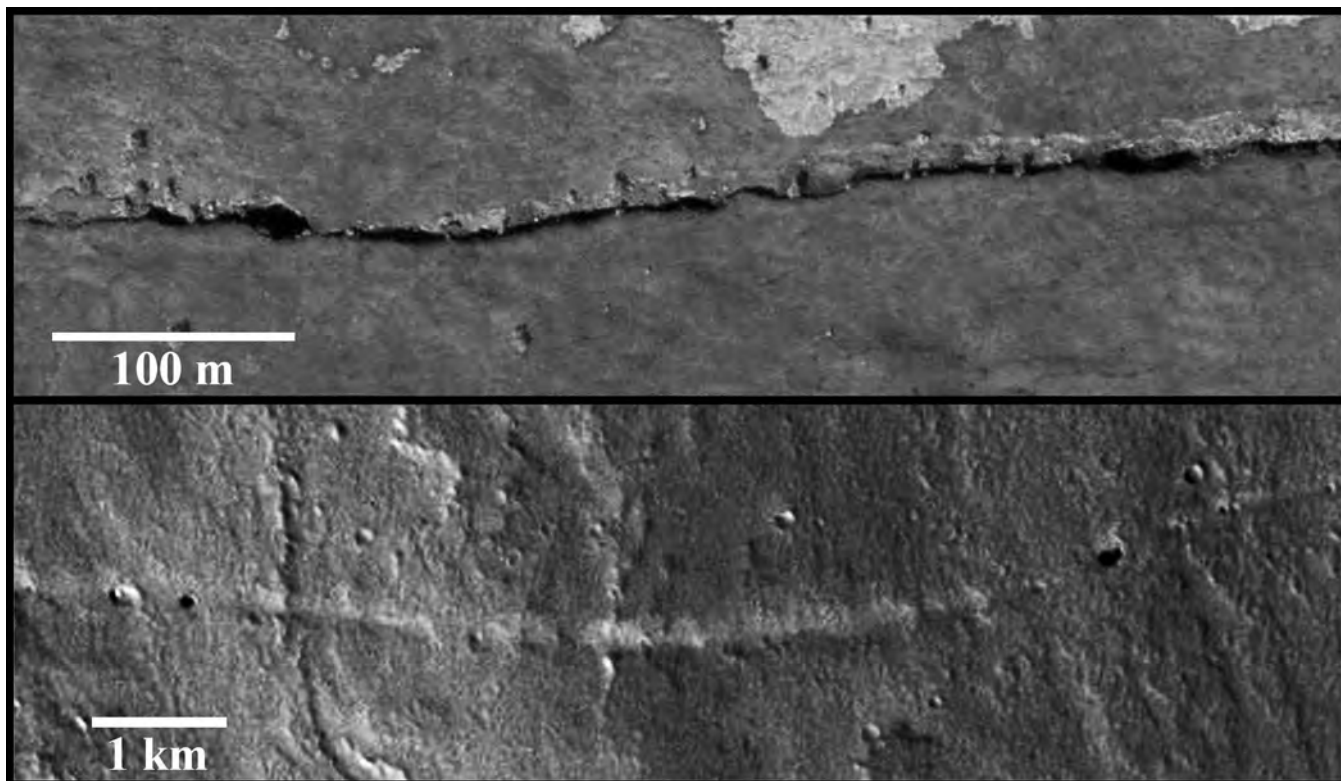
Figure 6. Volcano-tectonic fracture systems on Earth and Mars. Top image shows a portion of the Great Crack in Kīlauea volcano's southwest rift zone. Bottom image shows a portion of a proposed Martian volcano-tectonic fracture network located north of Arsia Mons (THEMIS V16468001).
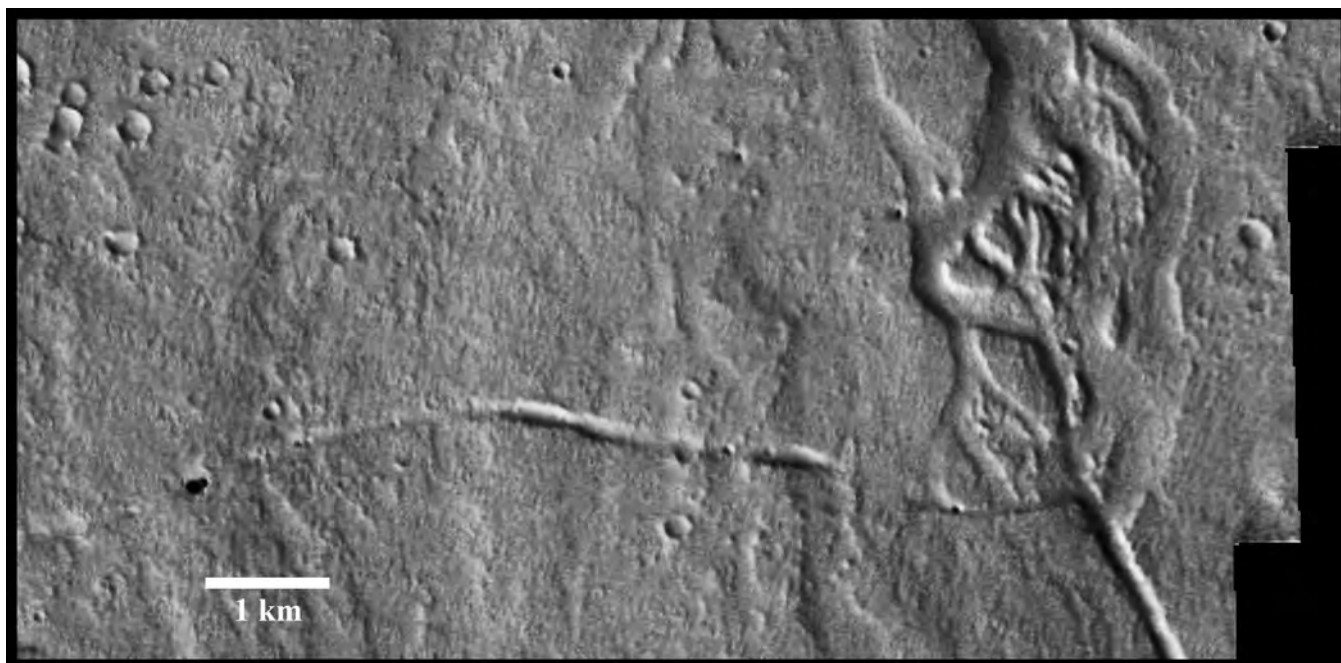
Figure 7. Evidence that low-viscosity fluid flowed through pre-existing tectonic fractures. Detail of feature I in Figure 1; at the right, fluid laterally breached its containment and flowed across the surface, creating a fluvial-like pattern (THEMIS V16468001).
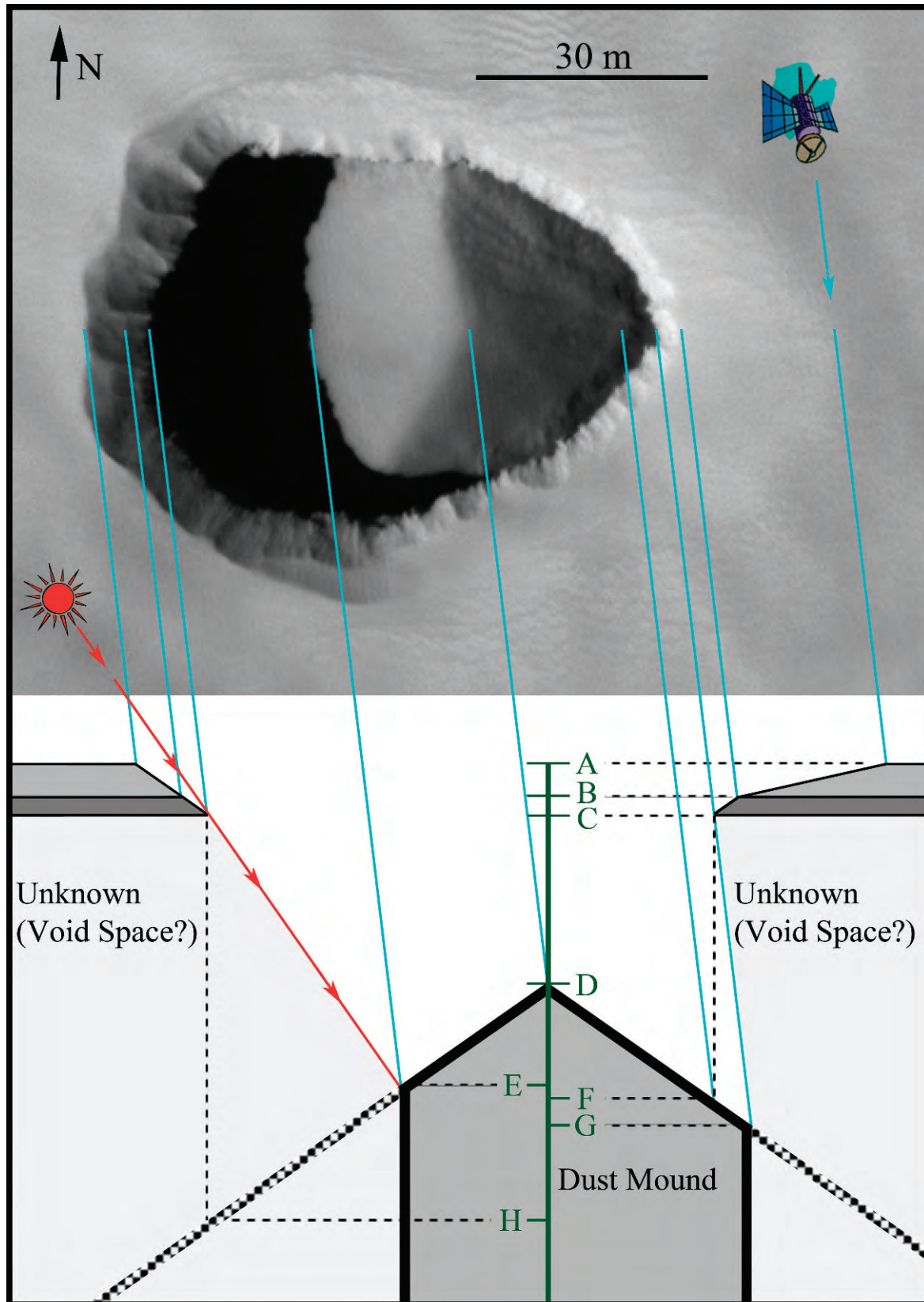
Figure 8. Detail of skylight in HiRISE: ESP_014380_1775 (also shown in the bottom of Fig. 4). Solar incidence angle = 35°, viewing angle = 6.8° from vertical. Diameter = ~68 m (measured from interior rim edges). North is upward. Approximate depths: A–B ≈ 4 m (dust layer); B–C ≈ 3 m (bedrock overhang); A–D ≈ 22 m (depth to top of mound); A–E ≈ 37 m (depth to
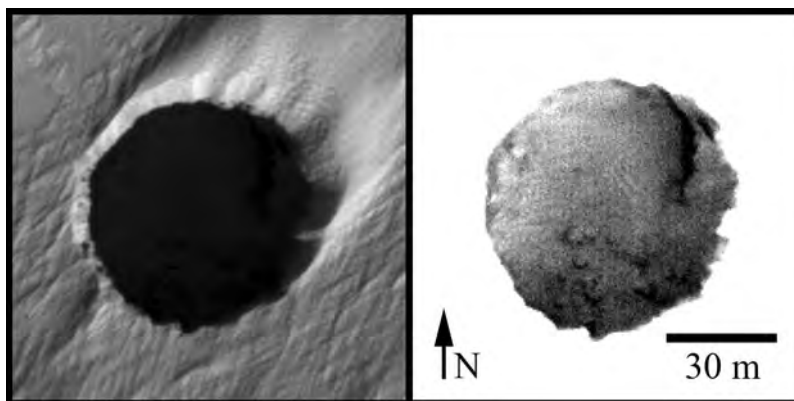
Figure 9. HiRISE image ESP_016622_1660. Right panel shows same image as left, but with contrast stretched to display the instrument's low-end radiance threshold to reveal a candidate entrance to a cave that may extend from the upper right. This pit is ~65 m across and >45 m deep.

SUMMARY AND DISCUSSION

The cave entrances and their respective host structures appear to be younger than their surroundings, not covered or crosscut by other flows or fractures, but their absolute ages cannot be determined with certainty because tube-fed flows can be much younger than the surfaces they cross. However, the entire sample region is late Amazonian in age (<500 Ma) based on crater size-frequency distributions (Plescia and Saunders, 1979; Neukum and Hiller, 1981; Werner, 2005), with some areas possibly as young as 50 Ma (Werner, 2005).

EXPLORATION

Several technologies must be advanced before robotic explorers can visit Martian caves. Precision landing techniques must be developed to place spacecraft at such small targets, and means of entering and exploring cave environments while maintaining contact with the surface must also be developed (e.g., Boston et al., 2003, 2004: Léveille and Datta, 2010). Furthermore, internationally agreed planetary protection policies forbid any visits to candidate astrobiology sites until microbial contamination issues can be addressed (COSPAR, 2008). Regardless of the challenges ahead, our identification of viable cave targets is an important step toward developing an entire new category of planetary exploration technologies.

HUMAN HABITAT POTENTIAL

From terrestrial examples, lava-tube caves, especially those with long, unbroken extents and flat, relatively smooth floors, are particularly suitable to host human habitats on Mars. Additionally, lava tubes usually have sufficient lateral extent to isolate their interiors from near-entrance surface hazards. Lava-tube caves, by their nature, can protect inhabitants from all of the hazards that humans would encounter on the surface. Dust storms and micrometeoroids cannot reach cave interiors, temperature variations are minimized in cave environments (e.g., Boston et al., 2001; Wynne et al., 2008), and roof thicknesses of only 1 to 2 m can effectively shield against all types of incoming radiation (NCRP, 2001; De Angeles, 2002).

For either small exploration teams or communities of future colonists, lava tubes may be the safest and most economical option to protect humans on Mars. Transporting or constructing shelters that adequately protect human visitors on the surface of Mars may be unrealistic in terms of resource consumption, especially since features such as lava tubes that can provide much of the necessary protection may already be present.

WATER ICE

Besides providing suitable shelter, caves are potential reservoirs of stable or metastable water-ice deposits, which could be an invaluable resource. Being highly insulated environments, caves that extend at downward angles into the surface will trap and hold cold air to form isolated microclimates (e.g., Balch, 1900; Halliday, 1954, Ingham et al., 2008). If conditions are favorable, then cave ice could either condense and accumulate at rates that exceed sublimation or could remain trapped there after forming in more favorable times. Williams et al. (2010) rigorously modeled cave-ice deposition and stability for various

←

shadow edge); A–F ≈ 38 m (depth directly below east rim); A–G ≈ 40 m (maximum visible depth); A–H ≈ 52 m (depth directly below west rim assuming the mound slopes continuously downward at the angle of repose.) Values for this figure were calculated assuming an angle of repose of 35°.
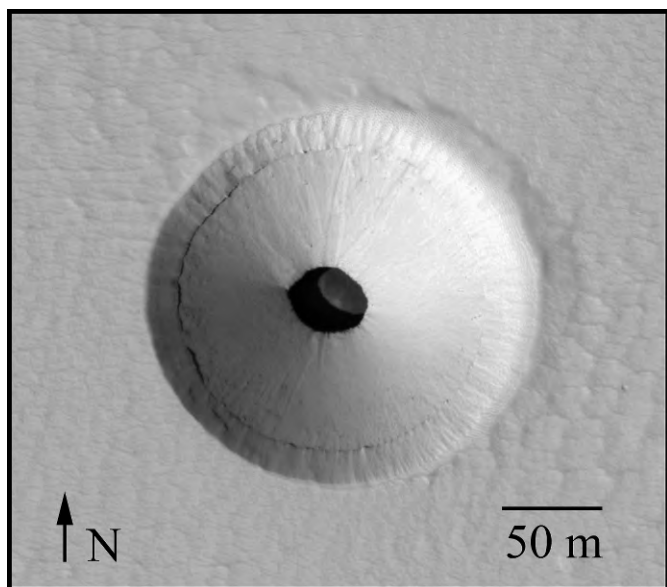
Figure 10. HiRISE image ESP_023531_1840. The main pit is ~195 m across and the central skylight is ~40 m across at the widest point. Assuming the inner slopes rest at the angle of repose (~35°), the skylight is approximately 50 m below the surface, and shadow measurements indicate a further drop of ~25 m to the center of the floor. This feature may represent an intermediate formation stage for either atypical pit craters or common volcanic pit craters.

of insulation by in-blown surface dust, cold trapping, and the absence of solar radiation. If such ancient deposits of water-ice indeed still exist, they may preserve atmospheric samples from the past that contain valuable information about Mars's climate history (e.g., Dansgaard et al., 1993).

ASTROBIOLOGY

Nearly all known caves on Earth host communities of microorganisms and caves are among the most likely places to find evidence of past or present microbial life on Mars. However, the examples presented here are unlikely prospects for astrobiology due to their location. The Tharsis Montes volcanic region is among the youngest surfaces on Mars and had not yet formed when conditions were conducive for the development of life as we understand it. Accordingly, older caves, perhaps formed by aqueous processes, where life might have retreated underground as the Martian surface became increasingly inhospitable are more likely to contain evidence of past or extant life (Grin et al., 1998; Cabrol et al., 2009). Nonetheless, all manner of extraterrestrial cave discoveries are valuable to the future of astrobiology because they encourage study and preparation for future cave-specific missions.

FUTURE WORK

Continuing HiRISE observations of cave entrances will provide important details such as accurate measurements and fine-scale morphologies that cannot be resolved by THEMIS or CTX. Besides allowing for highly accurate dimensional measurements, HiRISE may also allow us to constrain values for local dust-mantle thicknesses, near-entrance roof thicknesses (in off-nadir observations), and floor characteristics. Especially in lava-tube caves, characteristics of floor materials that lie directly beneath skylight entrances can indicate when the skylight formed in relation to the flow. For example, rubble piles would indicate that roof collapse occurred subsequent to flow activity, while smooth floors could suggest that the collapsed materials fell into viscous lava and either sank or were transported away. Smooth-floor lava tubes will be important targets for future cave-exploration because they are likely safer and simpler to enter, navigate, and possibly even inhabit, compared with rough-floored lava tubes, volcano-tectonic caves, or atypical pit craters.

locations on Mars, concluding that subsurface water-ice can exist for long periods across much of the planet and that conditions are particularly favorable in the Tharsis region, in which many caves are located. These caves are in advantageous locations for ice to accumulate because water-ice clouds are observed to form nearly every day of the Martian year above and around Arsia Mons (Benson et al., 2003, 2006; Maltagliati et al., 2008). Cold trapping and ice condensation is well documented for numerous terrestrial caves (e.g., Balch 1900; Halliday, 1954; Ingham et al., 2008) and occurs even in arid desert environments.

There is also strong evidence that the western flank of Arsia Mon, which is adjacent to our study area, becomes glaciated during periods of high obliquity (Head and Marchant, 2003; Shean et al., 2007), and thermal-diffusion models indicate that a subsurface ice table should still persist underneath a desiccated layer of dust (Helbert et al., 2006). If ice entered the nearby caves during these periods, then some of it may still be preserved by a combination

The structures discussed here exist within a limited area, and other examples are likely to exist in other volcanic

Table 2. Identification criteria for different cave-entrance types around Arsia Mons.

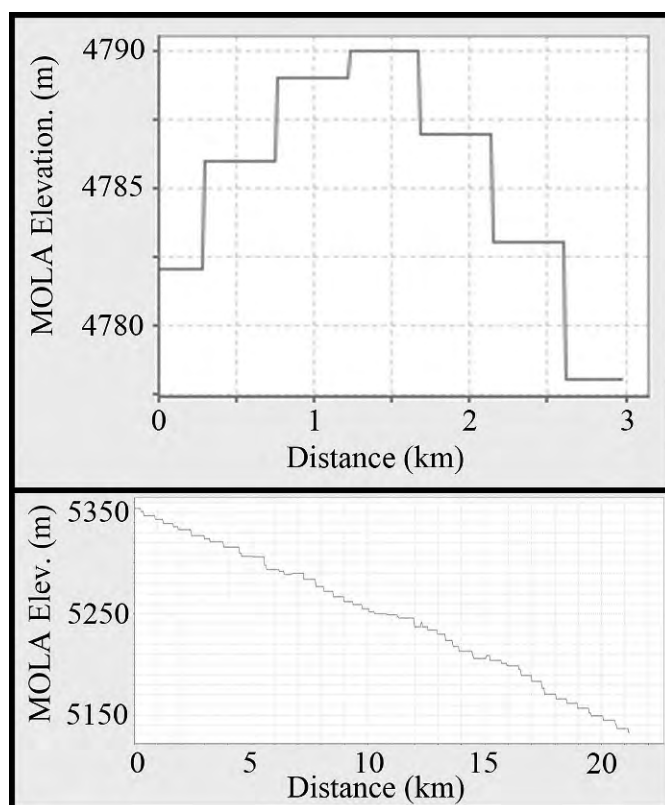| Cave-Entrance Type	Volcanic?	Tectonic?	Associated Rille?	Visible in IR?	Circular?
Lava-tube Skylight	Y	N	Y	N	Occasionally
Fracture Skylight	Y	Y	Y	N	Occasionally
Atypical Pit Craters	?	?	N	Y	Y

Figure 11. Lava-tube elevation profiles from 128 pixel per degree gridded Mars Orbiter Laser Altimeter data. Top profile runs across an inflated tube-fed flow; rilles are not resolved at this resolution. Lower profile runs along the length of a tube-fed flow, showing its continuous down-slope character.

regions across Mars. THEMIS and CTX data will be used to conduct a planet-wide survey, concentrating mostly on volcanic regions where comparable features are most likely to occur. Additional cave entrance candidates will be suggested as HiRISE targets. Caves detected in older regions, which may be more suitable astrobiology targets, will be compared with those presented here to reveal details about how these structures evolve over time due to collapse, erosion, or burial.

Future thermal-infrared observations can provide important additional information about these caves that is not available at visible wavelengths. Diurnal and annual temperature variations inside a cave can be influenced by its depth and overall subsurface extent (e.g., Ingham et al., 2008; Wynne et al., 2008), and cave internal surface temperatures tend to represent the mean annual temperature at the surface (Cropley, 1965; Pflitsch and Piasecki, 2003; Wynne et al., 2008) unless complex heat-transport mechanisms, such as seasonal ventilation due to multiple entrances, exist. For example, deep caves that trap cold air should have mean internal surface temperatures that are lower than average, while short, shallow caves can be influenced by solar insolation at their entrances and have

Figure 12. Best-fit ellipses for size for two different haze values, with surface pixels set to the median digital value of the scene.

mean temperatures that are higher than average. The caves presented here are too small to be detected in 100 m/pixel THEMIS IR data, so before their temperature variations can be analyzed, the next generation of thermal-infrared camera, which should have a resolution of 10 m/pixel or better, must be placed in orbit.

Because volcanic regions are extensive across Mars, the discovery of cave entrances within them has long been anticipated. At least three different cave-forming mechanisms appear to have operated in the flow field north of Arsia Mons: lava tubes, volcano-tectonic fractures and atypical pit craters. Specific examples can now be targeted by HiRISE and future instruments to ascertain their suitability for exploration and human habitation and to determine what capabilities must be developed to reach them.

REFERENCES

Balch, E.S., 1900, Glacières or Freezing Caverns: Philadelphia, Allen, Lane & Scott, 337 p.

Banerdt, W.B., Golombek, M.P., and Tanaka, K.L., 1992, Stress and tectonics on Mars, in Kieffer, H.H., Jakosky, B.M., Snyder, C.W., and Matthews, H., eds., Mars: Tucson, University of Arizona Press, p. 249–297.

Benson, J.L., Bonev, B.P., James, P.B., Shan, K.J., Cantor, B.A., and Caplinger, M.A., 2003, The seasonal behavior of water ice clouds in the Tharsis and Valles Marineris regions of Mars: Mars Orbiter Camera Observations: Icarus, v. 165, p. 34–52. doi: 10.1016/S0019-1035(03)00175-1.

Benson, J.L., James, P.B., Cantor, B.A., and Remigio, R., 2006, Interannual variability of water ice clouds over major Martian

volcanoes observed by MOC: Icarus, v. 184, p. 365–371. doi: 10.1016/j.icarus.2006.03.014.

Bleacher, J.E., Greeley, R., Williams, D.A., Cave, S.R., and Neukum, G., 2007a, Trends in effusive style at the Tharsis Montes, Mars, and implications for the development of the Tharsis province: Journal of Geophysical Research, v. 112, E09005. doi:10.1029/2006JE002873.

Bleacher, J.E., Greeley, R., Williams, D.A., Werner, S.C., Hauber, E., and Neukum, G., 2007b, Olympus Mons, Mars: Inferred changes in late Amazonian aged effusive activity from lava flow mapping of Mars Express High Resolution Stereo Camera data: Journal of Geophysical Research, v. 112, E04003. doi:10.1029/2006JE002826.

Boston, P.J., Spilde, M.N., Northup, D.E., Melim, L.A., Soroka, D.S., Kleina, L.G., Lavoie, K.H., Hose, L.D., Mallory, L.M., Dahm, C.N., Crossey, L.J., and Schelble, R.T., 2001, Cave biosignature suites: Microbes, minerals and Mars: Astrobiology Journal, v. 1, no. 1, p. 25–55. doi:10.1089/153110701750137413.

Boston, P.J., Frederick, R.D., Welch, S.M., Werker, J., Meyer, T.R., Sprungman, B., Hildreth-Werker, V., Thompson, S.L., and Murphy, D.L., 2003, Human utilization of subsurface extraterrestrial environments: Gravitational and Space Biology Bulletin, v. 16, no. 2, p. 121–131.

Boston, P.J., Frederick, R.D., Welch, S.M., Werker, J., Meyer, T.R., Sprungman, B., Hildreth-Werker, V., and Thompson, S.L., 2004, Extraterrestrial subsurface technology test bed: Human use and scientific value of Martian caves: American Institute of Physics Conference Proceedings, v. 699, p. 1007–1018. doi:10.1063/1.1649667.

Cabrol, N.A., Grin, E.A., and Wynne, J.J., 2009, Detection of caves and cave-bearing geology on Mars: 40th Lunar and Planetary Science Conference, Houston, Texas, Abstract No. 1040.

Calvari, S., and Pinkerton, H., 1999, Lava tube morphology on Etna and evidence for lava flow emplacement mechanisms: Journal of Volcanology and Geothermal Research, v. 90, p. 263–280. doi:10.1016/S0377-0273(99)00024-4.

Christensen, P.R., Jakosky, B.M., Kieffer, H.H., Malin, M.C., McSween, H.Y., Nealson, K., Mehall, G.L., Silverman, S.H., Ferry, S., and Caplinger, M., 2004, The Thermal Emission Imaging System (THEMIS) for the Mars 2001 Odyssey Mission: Space Science Reviews, v. 110, p. 85–130, doi: 10.1023/B:SPAC.0000021008.16305.94.

Christensen, P.R., Gorelick, N., Anwar, S., Dickenshied, S., Edwards, C., and Engle, E., 2007, New insights about Mars from the creation and analysis of Mars global datasets: American Geophysical Union Fall Meeting, San Francisco, California, Abstract No. P11E-01.

Coombs, C., and Hawke, R., 1992, A search for intact lava tubes on the Moon: Possible lunar base habitats, in Mendell, W.W., ed., The Second Conference on Lunar Bases and Space Activities of the 21st Century: NASA Conference Publication 3166, v. 1, p. 219–229.

Coons, D., 2010, Caving beneath the Great Crack of Kilauea Volcano: NSS News, v. 68, no. 12, p. 8–16.

COSPAR (Committee on Space Research, World Space Council Planetary Protection Policy), Amended 2011, http://0-science.nasa.gov.iii-server.ualr.edu/media/medialibrary/2011/02/16/Rummel_-_COSPAR_Activities_to_PPS.pdf.

Cropley, J.B., 1965, Influence of surface conditions on temperatures in large cave systems: Bulletin of the National Speleological Society, v. 27, p. 1–10.

Cruikshank, D.P., and Wood, C.A., 1972, Lunar rilles and Hawaiian volcanic features: Possible Analogues: The Moon, v. 3, no. 4, p. 412–447.

Cushing, G.E., Titus, T.N., Wynne, J.J., and Christensen, P.R., 2007, THEMIS observes possible cave skylights on Mars: Geophysical Research Letters, v. 34, L17201, doi:10.1029/2007GL030709.

Cushing, G.E., Titus, T.N., Jaeger, W.L., Kezthelyi, L.P., McEwen, A.S., and Christensen, P.R., 2008, Continuing study of anomalous pit craters in the Tharsis Region of Mars: New observations from HiRISE and THEMIS, 39th Lunar and Planetary Science Conference, Abstract No. 2447.

Cushing, G.E., and Titus, T.N., 2010, Caves on Mars: Candidate sites for astrobiological exploration: Astrobiology Science Conference 2010, Abstract No. 5414.

Daga, A.W., Towarnicki, M.A., Wendel, M.A., and Wendel, W., 1988, Evolving concepts of lunar architecture: The potential of subselene development: Abstracts of the 2nd Lunar Bases and Space Activities of the 21st Century Conference, Lunar & Planetary Institute, 67 p.

Dansgaard, W., Johnsen, S.J., Clausen, H.B., Dahl-Jensen, D., Gundestrup, N.S., Hammer, C.U., Hvidberg, C.S., Steffensen, J.P., Sveinbjörnsdottir, A.E., Jouzel, J., and G. Bond, 1993, Evidence for general instability of past climate from a 250-kyr ice-core record: Nature, v. 364, p. 218–220. doi:10.1038/364218a0.

De Angeles, G., Wilson, J.W., Clowdsley, M.S., Nealy, J.E., Humes, D.H., and Clem, J.M., 2002, Lunar Lava Tube Radiation Safety Analysis: Journal of Radiation Research, v. 43 supplement, p. S41–S45. doi:10.1269/jrr.43.S41.

Ferrill, D.A., et al., 2003, Influence of gravity on the geometry of Martian normal faults: 34th Lunar and Planetary Science Conference, Abstract. No. 2050.

Glaze, L.S., Anderson, S.W., Stofan, E.R., Baloga, S., and Smrekar, S.E., 2005, Statistical distribution of tumuli on pahoehoe flow surfaces: Analysis of examples in Hawaii and Iceland and potential applications to lava flows on Mars: Journal of Geophysical Research, v. 110, B08202. doi:10.1029/2004JB003564.

Greeley, R., 1971a, Observations of actively forming lava tubes and associated structures, Hawaii: Modern Geology, v. 2, p. 207–223.

Greeley, R., 1971b, Lava tubes and channels in the Lunar Marius Hills: Earth, Moon, and Planets, v. 3, no. 3, p. 289–314. doi:10.1007/BF00561842.

Greeley, R., 1972, Additional observations of actively forming lava tubes and associated structures, Hawaii: Modern Geology, v. 3, p. 157–160.

Grin, E.A., Cabrol, N.A., and McKay, C.P., 1998, Caves in the Martian regolith and their significance for exobiology exploration: 29th Lunar and Planetary Science Conference, Abstract No. 1012.

Halliday, W.R., 1954, Ice caves of the United States: The American Caver, Bulletin Sixteen of the National Speleological Society, v. 16, p. 3–28.

Haruyama, J., Hioki, K., Shirao, M., Morota, T., Hiesinger, H., van der Bogert, C.H., Miyamoto, H., Iwasaki, A., Yokota, Y., Ohtake, M., Matsunaga, T., Hara, S., Nakanotani, S., and Pieters, C.M., 2009, Possible lunar lava tube skylight observed by SELENE cameras: Geophysical Research Letters, v. 36, L21206. doi: 10.1029/2009GL040635.

Head, J.W., and Marchant, D.R., 2003, Cold-based mountain glaciers on Mars: Western Arsia Mons: Geology, v. 31, no. 7, p. 641–644. doi:10.1130/0091-7613(2003)031<0641:CMGOMW>2.0.CO;2.

Helbert, J., Head, J., Marchant, D., Shean, D., and Kreslavsky, M., 2006, First Prospecting for Ice in the Flank Deposit at Arsia Mons: 37th Lunar and Planetary Science Conference, Abstract No. 1371.

Hill, C.A., and Forti, P., 1997, Cave Minerals of the World, second edition: Huntsville, Alabama, National Speological Society, 463 p.

Horz, F., 1985, Lava tubes: Potential shelters for habitats, in Mendell, W.W., ed., Lunar Bases and Space Activities of the 21st Century: Houston, Lunar and Planetary Institute, p. 405–412.

Ingham, K.L., Northup, D., and Welbourn, W.C., 2008, Climate modeling for two lava tube caves at El Malpais National Monument, New Mexico USA, in Espinasa-Pereña, R., and Pint, J., eds., Proceedings of the X, XI, and XII International Symposia on Vulcanospeleology: Austin, Texas, Association for Mexican Cave Studies Bulletin 19, p. 126–131.

Jaeger, W.L., Keszthelyi, L.P., Skinner, J.A., Milazzo, M.P., McEwen, A.S., Titus, T.N., Rosiek, M.R., Galuszka, D.M., HJowington-Kraus, E., Kirk, R.L., and the HiRISE Team, 2010, Emplacement of the youngest flood lava on Mars: A short, turbulent story: Icarus, v. 205, p. 230–243. doi:10.1016/j.icarus.2009.09.011.

Kauahikaua, J., Sherrod, D.R., Cashman, K.V., Heliker, C., Hon, K., Mattox, T.N., and Johnson, J.A., 2003, Hawaiian lava-flow dynamics during the Pu'u 'Ō'ō-Kūpaianaha eruption: A tale of two decades, in Heliker, C., Swanson, D.A., Takahashi, T.J., eds., The Pu'u 'Ō'ō-Kūpaianaha Eruption of Kīlauea Volcano, Hawai'i: The First 20 Years: U.S. Geological Survey Professional Paper 1676, p. 63–87.

Keszthelyi, L., 1995, A preliminary thermal budget for lava tubes on the Earth and planets: Journal of Geophysical Research, v. 100, no. B10, p. 20411–20420. doi:10.1029/95JB01965.

Keszthelyi, L., and Self, S., 1998, Some physical requirements for the emplacement of long basaltic lava flows: Journal of Geophysical Research, v. 103, no. B11, p. 27447–27464. doi:10.1029/98JB00606.

Léveillé, R.J., and Datta, S., 2010, Lava tube caves on Mars—seeking signs of past life: Astrobiology Science Conference 2010: Evolution of Life: Surviving Catastrophes and Extremes on Earth and Beyond, Abstract No. 5344.

Malin, M.C., Bell III, J.F., Cantor, B.A., Caplinger, M.A., Calvin, W.M., Clancy, R.T., Edgett, K.S., Edwards, L., Haberle, R.M., James, P.B., Lee, S.W., Ravine, M.A., Thomas, P.C., and Wolff, M.J., 2007, Context camera investigation on board the Mars Reconnaissance Orbiter: Journal of Geophysical Research, v. 112, no. E5, E05S04. doi:10.1029/2006JE002808.

Maltagliati, L., Titov, D.V., Encrenaz, T., Melchiorri, R., Forget, F., Garcia-Comas, M., Keller, H., Langevin, Y., and Bibring, J.-P., 2008, Observations of atmospheric water vapor above the Tharsis volcanoes on Mars with the OMEGA/MEX imaging spectrometer: Icarus, v. 194, p. 53–64. doi:10.1016/j.icarus.2007.09.027.

Mazur, P., Barghoorn, E.S., Halvorson, H.O., Jukes, T.H., Kaplan, I.R., and Margulis, L., 1978, Biological implications of the Viking mission to Mars: Space Science Reviews, v. 22, p. 3–34.

McEwen, A.S., Eliason, E.M., Bergstrom, J.W., Bridges, N.T., Hansen, C.J., Delamere, W.A., Grant, J.A., Gulick, V.C., Herkenhoff, K.E., Keszthelyi, L., Kirk, R.L., Mellon, M.T., Squyres, S.W., Thomas, N., and Weitz, C.M., 2007, Mars Reconnaissance Orbiter's High Resolution Imaging Science Experiment (HiRISE): Journal of Geophysical Research, v. 112, no. E5, E05S02. doi:10.1029/2005JE002605.

Miyamoto, H., Haruyama, J., Kobayashi, T., Suzuki, K., Okada, T., Nishibori, T., Showman, A., Lorenz, R., Mogi, K., Crown, D.A., Rodriguez, J.A.P., Rokugawa, S., Tokunaga, T., and Masumoto, K., 2005, Mapping the structure and depth of lava tubes using ground penetrating radar: Geophysical Research Letters, v. 32, L21316. doi:10.1029/2005GL024159.

Mouginis-Mark, P.J., 1990, Recent water release in the Tharsis Region of Mars: Icarus, v. 84, p. 362–373. doi:10.1016/0019-1035(90)900 44-A.

Mouginis-Mark, P.J., and Christensen, P.R., 2005, New Observations of volcanic features on Mars from the THEMIS instrument: Journal of Geophysical Research, v. 110, E08007. doi:10.1029/2005 JE002421.

NCRP, 2001, Radiation Protection Guidance for Activities in Low-Earth Orbit: National Council on Radiation Protection and Measurements, NCRP Publication No. N.132.

Neukum, G., and Hiller, K., 1981, Martian Ages: Journal of Geophysical Research, v. 86, no. B4, p. 3097–3121. doi:10.1029/JB086iB04p03097.

Noe Dobrea, E.Z., and Bell III, J.F., 2005, TES spectroscopic identification of a region of persistent water ice on the flanks of Arsia Mons Volcano, Mars: Journal of Geophysical Research, v. 110, E05002. doi:10.1029/2003JE002221.

Oberbeck, V.R., Quaide, W.L., and Greeley, R., 1969, On the origin of Lunar sinuous rilles: Modern Geology, v. 1, p. 75–80.

Okubo, C.H., and Martel, S.J., 1998, Pit crater formation on Kilauea volcano, Hawaii: Journal of Volcanology and Geothermal Research, v. 86, p. 1–18. doi:10.1016/S0377-0273(98)00070-5.

Pflitsch, A., and Piasecki, J., 2003, Detection of an airflow system in Niedzwiedzia (Bear) Cave, Kletno, Poland: Journal of Cave and Karst Studies, v. 65, p. 160–173.

Phillips, R.J., Sleep, N.H., and Barendt, W.B., 1990, Permanent uplift in magmatic systems with application to the Tharsis Region of Mars: Journal of Geophysical Research, v. 95, no. B4, p. 5089–5100. doi:10.1029/JB095iB04p05089.

Plescia, J.B., and Saunders, R.S., 1979, Styles of faulting and tectonics of the Tharsis region: 10th Lunar and Planetary Science Conference, Abstract, p. 986–988.

Sakimoto, S.E.H., Crisp, J., and Baloga, S.M., 1997, Eruption constraints on tube-fed planetary lava flows: Journal of Geophysical Research, v. 102, no. E3, p. 6597–6613. doi:10.1029/97JE00069.

Self, S., Keszthelyi, L.P., and Thordarson, T., 1998, The importance of pāhoehoe: Annual Review of Earth and Planetary Sciences, v. 26, p. 81–110.

Shean, D.E., Head, J.W. III, Fastook, J.L., and Marchant, D.R., 2007, Recent glaciation at high elevations on Arsia Mons, Mars: Implications for the formation and evolution of large tropical mountain glaciers: Journal of Geophysical Research, v. 112, E03004. doi: 10.1029/2006JE002761.

Wentworth, C.K., and Macdonald, G.A., 1953, Structures and Forms of Basaltic Rocks in Hawaii: Washington D.C., Government Printing Office, U.S. Geological Survey Bulletin 994, 98 p.

Werner, S.C., 2005, Major aspects of the chronostratigraphy and geologic evolutionary history of Mars [Ph.D. dissertation]: Berlin, Frie University, http://www.diss.fu-berlin.de/2006/33/index.html, 74 p.

Williams, K.E., McKay, C.P., Toon, O.B., and Head, J.W., 2010, Do ice caves exist on Mars?: Icarus, v. 209, p. 358–368. doi:10.1016/j.icarus. 2010.03.039.

Wynne, J.J., Titus, T.N., and Chong Diaz, G., 2008, On developing thermal cave detection techniques for Earth, the Moon and Mars: Earth and Planetary Science Letters, v. 272, p. 240–250. doi:10.1016/ j.epsl.2008.04.037.

Zuber, M.T., Smith, D.E., Solomon, S.C., Muhleman, D.O., Head, J.W., Garvin, J.B., Alshire, J.B., and Bufton, J.L., 1992, The Mars Observer laser altimeter investigation: Journal of Geophysical Research, v. 97, no. E5, p. 7781–7797. doi:10.1029/92JE00 341.

THE FIRST SUBTERRANEAN FRESHWATER PLANARIANS FROM NORTH AFRICA, WITH AN ANALYSIS OF ADENODACTYL STRUCTURE IN THE GENUS *DENDROCOELUM* (PLATYHELMINTHES, TRICLADIDA, DENDROCOELIDAE)

Abdul Halim Harrath[1,2*], Ronald Sluys[3], Adnen Ghlala[4], and Saleh Alwasel[1]

Abstract: The paper describes the first species of freshwater planarians collected from subterranean localities in northern Africa, represented by three new species of *Dendrocoelum* Örsted, 1844 from Tunisian springs. Each of the new species possesses a well-developed adenodactyl, resembling similar structures in other species of *Dendrocoelum*, notably those from southeastern Europe. Comparative studies revealed previously unreported details and variability in the anatomy of these structures, particularly in the composition of the musculature. An account of this variability is provided, and it is argued that the anatomical structure of adenodactyls may provide useful taxonomic information.

Introduction

The French zoologists C. Alluaud and R. Jeannel were among the first workers to research in some detail the subterranean fauna of Africa (see, Jeannel and Racovitza, 1914). Subsequently, an increasing number of groundwater species were reported from African caves (Messana, 2004). Although the continent has not been extensively explored from a biospeleological perspective, the list of African subterranean-dwelling animals is long (Messana, 2004), but has not included flatworms. The subterranean aquatic fauna of Tunisia has received scant attention, despite the presence of a large number of wells, springs, and caves, notably in the northwestern part of the country. The first study in Tunisia on the subterranean fauna resulted in the first description of a new species of Thermosbaenacea, *Thermosbaena mirabilis* Monod, 1924 from Africa (Seurat 1921, 1934). During the past decade, only a few explorations of subterranean habitats in Tunisia have been undertaken, resulting in the finding of new records and new species of gastropods and crustaceans (Juberthie et al., 2001; Ghlala et al., 2009). However, subterranean flatworms have not been previously reported from North Africa. In the present paper, we describe three new species of dendrocoelid freshwater flatworms from Tunisia, representing the first planarians to be reported from subterranean localities in North Africa.

The freshwater planarian family Dendrocoelidae basically has a Holarctic distribution, albeit that there are major areas within this biogeographic region from which specimens have not yet been reported (Ball and Reynoldson, 1981, Fig. 7). The Dendrocoelidae are especially diverse in the lakes Ohrid and Baikal and in the area of the Carpathian Mountains. From Lake Baikal, especially, numerous morphologically complex genera and species have been reported (Porfirjeva, 1977). The Holarctic range of the Dendrocoelidae includes the northwestern section of North Africa, based on the records of *Dendrocoelum vaillanti* De Beauchamp, 1955 from the Grande Kabylie Mountains in Algeria and *Acromyadenium moroccanum* De Beauchamp, 1931 from Bekrit in the Atlas Mountains of Morocco (Sluys, 2007, and references therein). Both species were collected from epigean habitats, in contrast to the species described in the present paper. In addition to these records of *D. vaillanti* and *A. moroccanum*, De Beauchamp (1954) mentioned finding two immature, eyeless dendrocoelids in the Grande Atlas Mountains in Morocco and an equally immature, ocellated specimen in Aïn Draham in Tunisia.

All three of the new species described in the present paper possess a particular cone-shaped structure in their copulatory apparatus that is also present in many other dendrocoelids, a musculo-glandular organ or adenodactyl. Our comparative studies on other species of the genus *Dendrocoelum* Örsted, 1844 revealed previously unreported details and variability in the anatomy of these structures, particularly in the composition of the musculature. In this paper, we provide a first account of these anatomical details and their variability and argue that the anatomical structure of adenodactyls may provide useful taxonomic information.

* Corresponding author: halim.harrath@laposte.net
[1] Zoology Department, College of Science, King Saud University, PO Box 2455, Riyadh 11451, Saudi Arabia
[2] Research Unit Animal Reproduction and Developmental Biology, Department of Biology, Faculty of Sciences of Tunis, 2092 Manar II, Tunisia
[3] Institute for Biodiversity and Ecosystem Dynamics & Netherlands Centre for Biodiversity Naturalis, University of Amsterdam (section ZMA), P. O. Box 94766, 1090 GT Amsterdam, The Netherlands
[4] Unité de Recherche de Biologie Animale et Systématique Evolutive, Faculté des Sciences de Tunis, 2092 Manar II, Tunisia
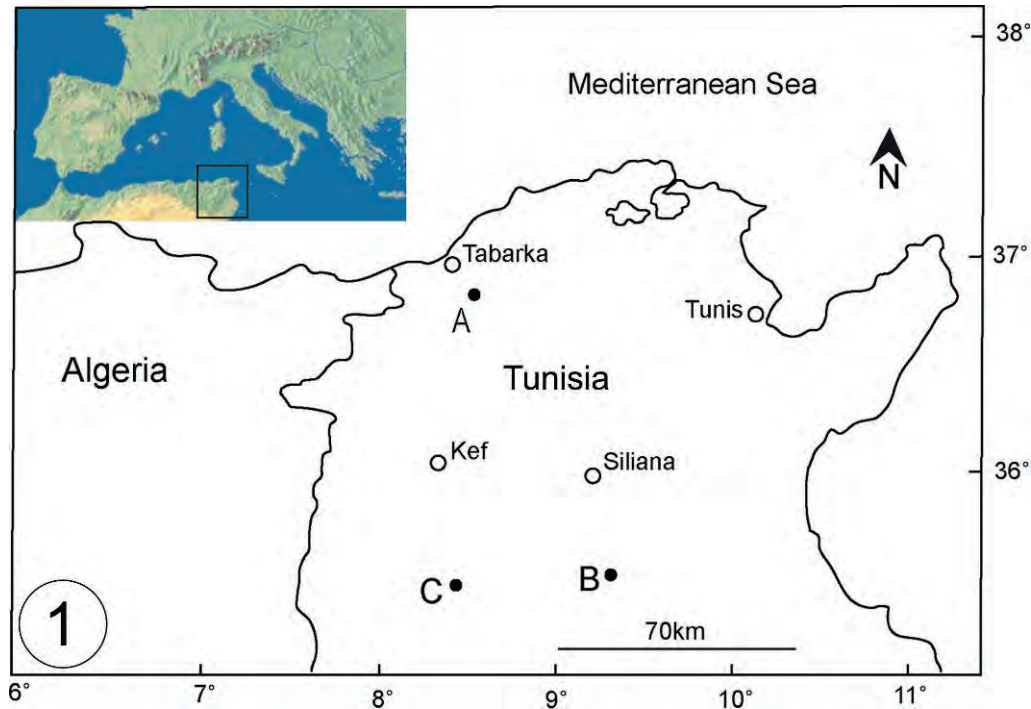
Figure 1. Sampling localities: A, Ain Sobah (Jendouba); B, Ain Dar Forn (Siliana); C, Ain El Ajmi (Kef).

Material and Methods

Flatworms were collected from three different natural springs in Tunisia. Each spring feeds an artificial reservoir of about 1 m³ from which water flows through a small channel. When the reservoir is completely closed by an iron door on its top, it is not accessible, and penetration of daylight is obstructed. Subterranean species randomly migrate to the reservoir, where, apparently, they find a favorable environment to live, because the current in the channel keeps surface species away. Specimens were collected by sweeping a net several times through the reservoir. If the iron door was closed, and thus the reservoir was not accessible, the outflow of the channel was blocked for at least 5 minutes with a piece of cloth. After removal of the cloth, the flood pulse was channeled through a net to capture the flatworm specimens. Sampled specimens were transported to the laboratory, where they were photographed, fixed in Steinmann's or Bouin's fluid, and preserved in 70% alcohol. Histological sections were made at intervals of 7 μm and stained in Mallory-Cason. Drawings of the copulatory apparatus were first made with the help of a camera lucida attached to a compound microscope, then digitized, and, subsequently, finalized with Adobe Illustrator CS and Snag It. The material examined is deposited in the Zoological Museum of the University of Amsterdam (ZMA).

Systematic Account

Order **Tricladida** Lang, 1884
Family **Dendrocoelidae** Hallez, 1892

Genus *Dendrocoelum* Örsted, 1844
***Dendrocoelum constrictum* Harrath and Sluys, sp. nov.**
(Figs. 2, 6, and 7)

Material examined. Holotype: ZMA V.Pl.6884.1, Ain Sobah spring located in the northwest of Tunisia, on the route linking Tabarka to Tunis, approximately 20 km from the sea, December 2008, coll. H. Harrath & A. Ghlala, sagittal sections on 10 slides.

Paratypes: V.Pl. 6884.2, ibid., sagittal sections on 14 slides, V.Pl. 6884.3, sagittal sections on eleven slides, V.Pl. 6884.4, horizontal sections on 6 slides.

Etymology. The specific epithet is derived from the Latin adjective *constrictus* and alludes to the constriction or diaphragm through which the seminal vesicle communicates with the penial lumen.

Habitat. Specimens were collected from Ain Sobah spring (36°87′20″ N, 8°55′01″ E), situated in a wet zone in northwestern Tunisia. This locality is close to the road from Tunis to Tabarka and located at about 10 km from the latter (Fig. 1, locality A). The worms were frequently found attached to green algae; associated fauna consisted of isopods and gastropods.

Diagnosis. *D. constrictum* is characterized by an unpigmented body; presence of rather small eyes; a common vas deferens opening into a seminal vesicle, which opens at the tip of a conical papilla projecting into the anterior section
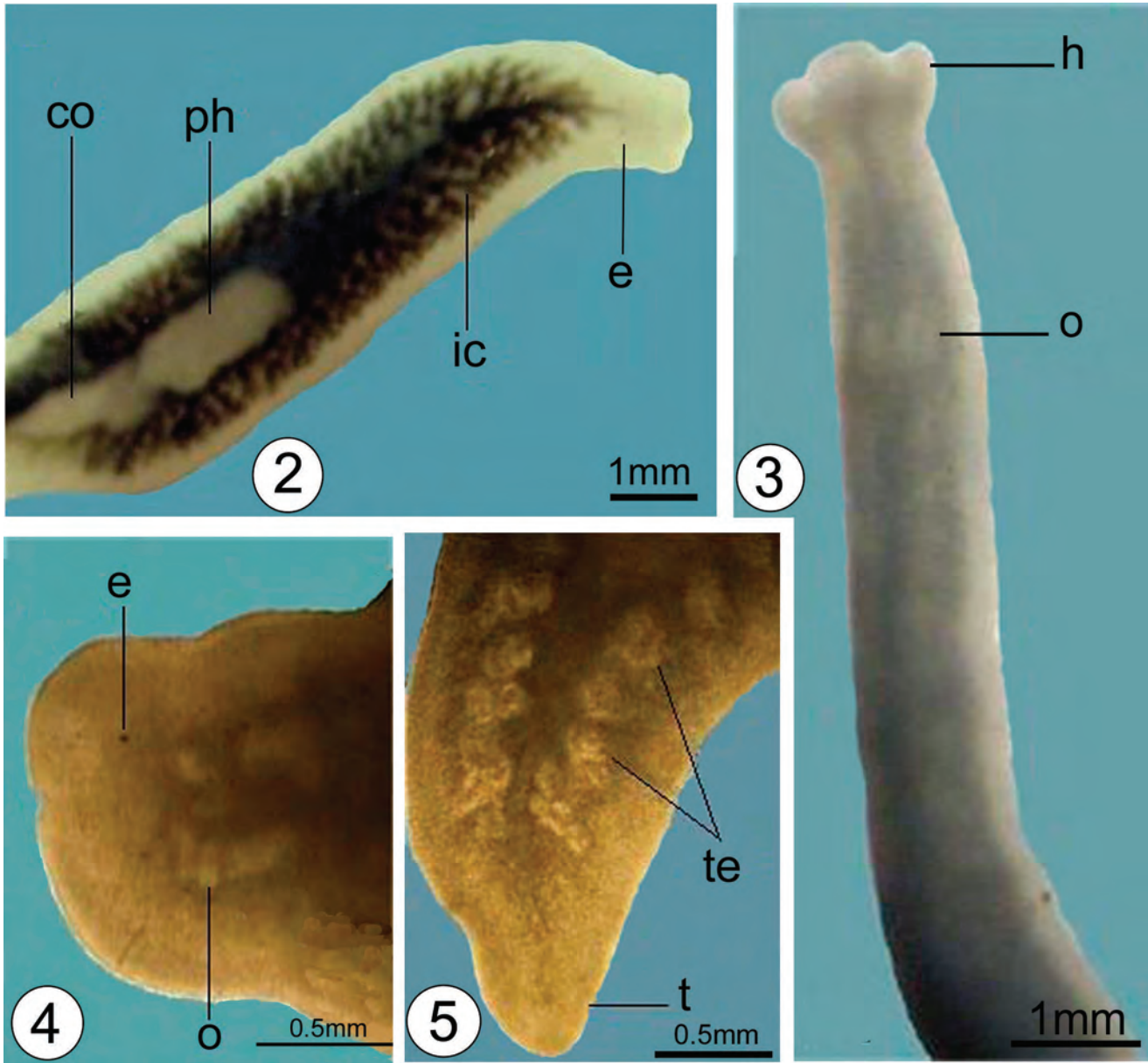
Figures 2–5. 2. *Dendrocoelum constrictum*, **external features of a live specimen. 3.** *Dendrocoelum duplum*, **external features of a live specimen. 4.** *Dendrocoelum amplum*, **head of a live specimen. 5.** *D. amplum*, **posterior end of a live specimen. See caption to Figures 6–11 for key.**

of the spacious penial lumen, thus forming a kind of diaphragm; principally dorsal testes, but with also a few ventral follicles; an adenodactyl only slightly smaller than the penis papilla.

Description. Mature specimens in fully stretched state are up to 12 mm long and 2 mm wide (Fig. 2). The body is principally unpigmented, but appears beige, red, black or slightly green, depending on the intestinal contents. The rectangular head has rather small eyes that are placed relatively far from the anterior end of the specimen. Although eyes are always present, they are not always clearly visible in live specimens. An adhesive organ was not evident in live or preserved specimens. Histological sections revealed the presence of only a very poorly developed, non-cupshaped adhesive organ.

The unpigmented pharynx is positioned entirely in the posterior half of the animal. The muscular system of the internal zone is formed by intermingled circular and longitudinal fibers, which conforms with characteristic pharynx of the family Dendrocoelidae (Sluys and Kawakatsu, 2006, and references therein).

The testes are situated on either side of the body; they are essentially dorsal in position, but with a few, distinctly

ventral follicles. The testes extend from the level of the ovaries to almost the posterior end of the body. The hemispherical penis bulb consists of intermingled longitudinal and circular muscle fibers (Fig. 6). The more or less conical penis papilla is covered with a moderately thick, nucleated epithelium that is underlain with a layer of circular muscle, followed by a thin layer of longitudinal fibers. The two vasa deferentia run ventrally, but at the level of the copulatory bursa, they curve to the dorsal side and separately enter the penis bulb, after which the ducts unite to form a common vas deferens that opens into a seminal vesicle. The latter opens at the tip of the papilla, which projects into the voluminous proximal section of the penial lumen, thus forming a kind of diaphragm. This wide cavity is lined with a thick, nucleated epithelium.

The adenodactyl (Fig. 7) is slightly smaller than the penis and situated to the right of the latter. It has a spherical and very muscular bulb, with intermingled longitudinal and circular muscle fibers and an elongated papilla. The adenodactyl contains a rather long tubular lumen. Throughout the parenchyma of the papilla extends a layer of fine circular muscle fibers that stains bright blue. Ectally to this zone of circular muscles runs a layer of longitudinal muscle fibers. Entally to the bright blue zone of circular muscles there is also a thin layer of longitudinal fibers.

The ovaries are situated at about one third of the distance between the brain and the root of the pharynx and occupy the entire dorso-ventral diameter of the body. The oviducts arise from the postero-dorsal wall of the ovaries and run ventrally caudad to the level of the copulatory apparatus. They unite to form a common oviduct just behind the copulatory apparatus. This common oviduct receives the secretion of shell glands and opens into the posterior part of the common atrium.

The copulatory bursa is a large sac that occupies almost the entire dorsal-ventral diameter of the body and is situated directly behind the pharynx. The bursa is covered by a thin layer of longitudinal muscles and in mature specimens has a large cavity containing remnants of a spermatophore. The bursal canal arises from the postero-dorsal wall of the bursa and runs latero-dorsally to the male atrium and the penis bulb. It is lined with a thick, nucleated epithelium and is surrounded by two layers of longitudinal muscles. At its distal part, just above the common atrium, the bursal canal widens considerably and is covered with a layer of subepidermal circular muscles, followed by a layer of longitudinal fibers.

Discussion. There are only four other species of *Dendrocoelum* for which a common vas deferens has been reported: *D. puteale* Kenk, 1930, *D. kenki* De Beauchamp, 1937, *D. jablanicense* (Stanković and Komárek, 1927), and *D. botosaneanui* Del Papa, 1965. Therefore, we will restrict our comparative discussion to these four species. In

contrast to *D. constrictum*, the sperm ducts fuse outside of the penis bulb in *D. botosaneanui*, *D. puteale*, and *D. kenki* (De Beauchamp, 1932, 1937; Del Papa, 1965). It is only in *D. jablanicense* that the sperm ducts first enter the penis bulb and then fuse to form a common vas deferens (Kenk, 1978), as is the case with *D. constrictum*. However, in *D. jablanicense* the testes are ventral, contrasting with the dorsally placed follicles in *D. constrictum*. In *D. botosaneanui* and *D. puteale* the testes are situated centrally and dorsally in the body, respectively, whereas in *D. kenki* they have a ventral position.

Apart from the point of fusion of the vasa deferentia and the position of the testes, there are a few other details of the copulatory apparatus worth mentioning in which *D. constrictum* either differs from or agrees with the four other species of *Dendrocoelum* mentioned above. *D. constrictum* resembles *D. jablanicense*, *D. kenki*, and *D. puteale* in that they all lack a flagellum in the penis papilla, whereas *D. botosaneanui* does have a flagellum. In *D. constrictum*, *D. jablanicense*, and *D. kenki* the adenodactyl is situated on the right side of the midline of the body, whereas in *D. puteale* it is located on the left side; the precise situation in *D. botosaneanui* is not clear from its description. In both *D. constrictum* and *D. botosaneanui* the adenodactyl is somewhat smaller than the penis, whereas in *D. jablanicense* and *D. puteale* the adenodactyl is bigger than the male organ; in *D. kenki* the adenodactyl and the penis are about the same size.

Both *D. constrictum* and *D. jablanicense* possess eyes, whereas these are absent in *D. botosaneanui*, *D. kenki*, and *D. puteale*.

A characteristic feature of *D. constrictum* is that the seminal vesicle opens at the tip of a conical papilla projecting into the proximal, anterior section of the lumen of the penis papilla. A similar projection is also present in *D. kenki* and *D. racovitzai* De Beauchamp, 1949, but on the basis of other features *D. constrictum* cannot be equated with either of these two species.

Dendrocoelum duplum Harrath and Sluys, sp. nov.
(Figs. 3, 8, and 9)

Material examined. Holotype: ZMA V.Pl. 6885.1, Ain El Ajmi spring, located in the northwest of Tunisia, at 12 km from Dahmani village, December 2008, coll. H. Harrath and A. Ghlala, sagittal sections on 12 slides.

Paratypes: V.Pl. 6885.2, ibid., sagittal sections on 8 slides.

Etymology. The specific epithet is derived from the Latin adjective *duplus*, double, and refers to the presence of two constrictions or diaphragms in the male duct running through the penial papilla.

Habitat. The material examined was collected from Ain El Ajmi spring (Fig. 1, locality C) (35°51′03″ N, 8°47′52″ E).
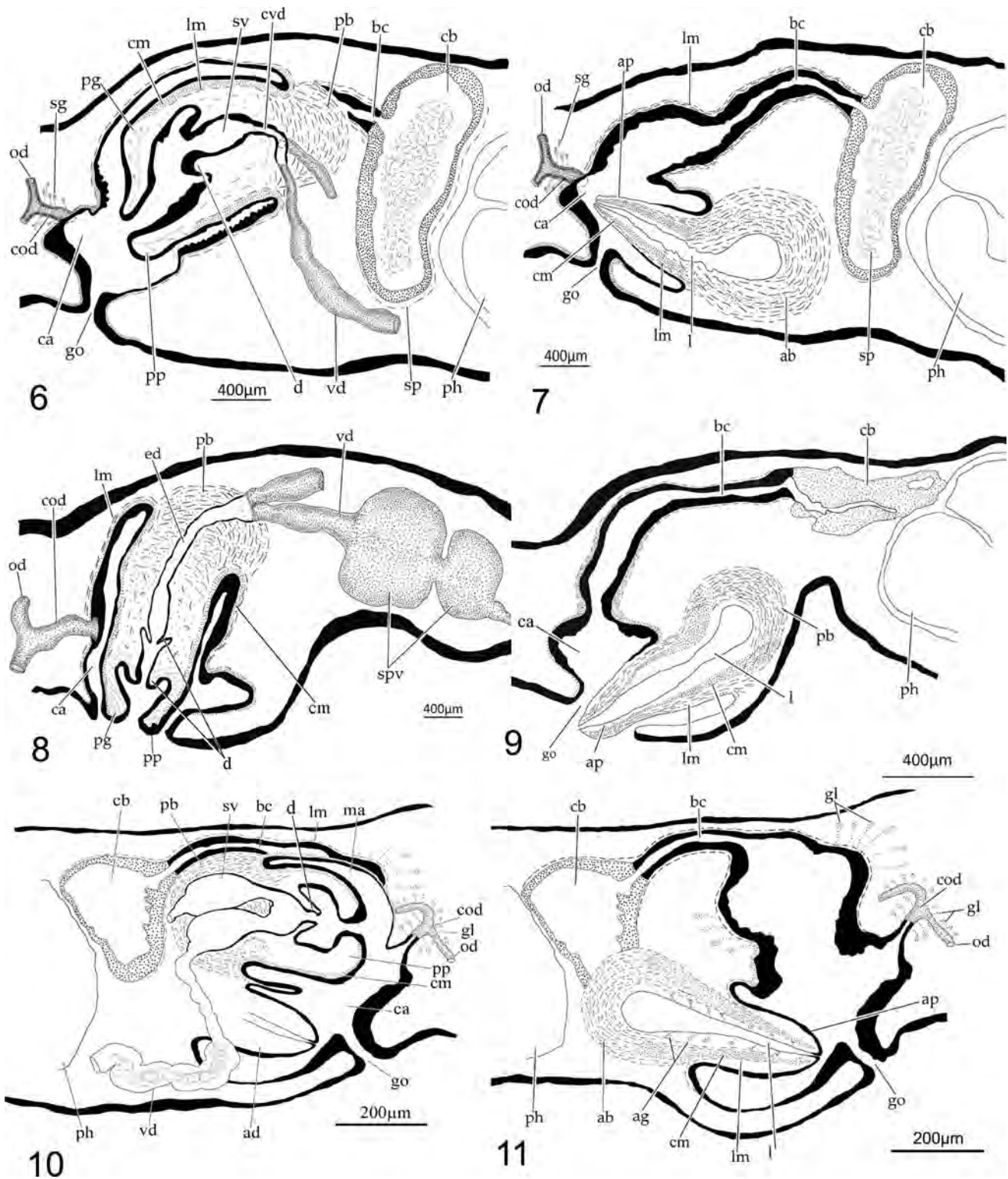
Figures 6–11. 6. *Dendrocoelum constrictum.* ZMA V.Pl. 6884.1, sagittal reconstruction of the copulatory apparatus at the level of the penis (anterior to the right). 7. *D. constrictum.* ZMA V.Pl. 6884.1, sagittal reconstruction of the copulatory apparatus at the level of the adenodactyl (anterior to the right). 8. *Dendrocoelum duplum.* ZMA V.Pl. 6885.1, sagittal reconstruction of the copulatory apparatus at the level of the penis (anterior to the right). 9. *D. duplum.* ZMA V.Pl. 6885.1, sagittal reconstruction of the copulatory apparatus at the level of the adenodactyl (anterior to the right). 10. *Dendrocoelum amplum.* ZMA V.Pl. 6886.1, sagittal reconstruction of the copulatory apparatus at the level of the penis (anterior to the left). 11. *D. amplum.* ZMA V.Pl. 6886.1, sagittal reconstruction of the copulatory apparatus at the level of the adenodactyl (anterior

This locality is not very far from the Roman ruins of El Medeina and located about 12 km from the town of Dahmani. Accompanying fauna: a large number of isopods.

Diagnosis. *D. duplum* is characterized by an unpigmented body; the presence of broad auricular lobes; testes that are located dorsally as well as ventrally; an almost vertically oriented penis papilla; a diaphragm in the distal section of the ejaculatory duct; an ejaculatory duct that opens at the tip of a blunt papilla, projecting into the penial lumen, thus forming a kind of second diaphragm; an adenodactyl papilla that is considerably smaller than the penis papilla.

Description. Living animals up to 14 mm long and 1.4 mm wide. Dorsal surface white. Head of freely moving animals with a truncated anterior margin and a distinct, broadly rounded auricular lobe on either side; eyes absent (Fig. 3). An adhesive organ was not evident in live or preserved specimens.

Testes are situated dorsally, as well as ventrally, extending throughout the body from directly behind the ovaries to almost the tail end. There are only a few (3 to 4) testes in the prepharyngeal part of the body, with the majority of the follicles being located in the postpharyngeal part. The penis is provided with a relatively small hemispherical muscular bulb and an elongated, more or less vertically oriented cylindrical papilla (Fig. 8). The papilla is covered with a flat, nucleated epithelium that is underlain by a layer of circular muscle fibers and a very thin layer of longitudinal muscle fibers. The two vasa deferentia run ventrally, and when they arrive at the level of the copulatory bursa, they widen to form two very large spermidual vesicles. After having narrowed and penetrated the penis bulb, the sperm ducts immediately unite to form a common intrabulbar vas deferens that extends as the ejaculatory duct (Fig. 8). Through a diaphragm this ejaculatory duct communicates with a distal, narrow section of the penis lumen that opens at the tip of a blunt papilla and projects into the proximal part of the lumen of the penis papilla, forming a kind a second diaphragm. This penis lumen receives the abundant secretion of erythrophilic penis glands.

The adenodactyl (Fig. 9), situated ventrally to the left of the penis, is a little larger than the penis and is provided with a conical papilla and a spherical, well-developed bulb. This adenodactyl is provided with a distinctly light-blue-staining zone of circular muscles that runs through the mesenchyme from the bulb to the tip of the papilla. Ectally to this blue zone of circular muscles runs a layer of red-staining longitudinal muscles. A thin layer of erythrophilic longitudinal muscles is also present entally to the blue zone of fine circular muscle fibers. No glands were observed to discharge into the large lumen of the adenodactyl.

The two ovaries are situated just above the ventral nerve cord about one quarter of the distance between the brain and the root of the pharynx. They are relatively large and can be observed in a living mature specimen as two whitish spots. The two oviducts unite to form a relatively long common oviduct that opens into the common atrium. The copulatory bursa is a small sac, situated dorsally and directly behind the pharyngeal pouch. From the bursa runs the bursal canal, which narrows at its proximal section and is only surrounded by a thin layer of longitudinal muscles. Thereafter the duct widens, and at its vertically, dorso-ventrally running section, it is surrounded by a thick, subepithelial layer of circular muscles, followed by a thin layer of longitudinal muscles; this section of the canal opens into the dorsal part of the common atrium.

Discussion. Most species of *Dendrocoelum* have a more or less developed auricular lobe on either side of the head. But the broad lobes of *D. duplum* have not been described for any other species. Only the auricular lobes of *D. adenodactylosum* (Stanković and Komárek, 1927) approach the condition of *D. duplum* (Kenk, 1978, Fig. 5).

With respect to the communication of the vasa deferentia with the penis, four conditions can be distinguished within the genus *Dendrocoelum*: (1) In the majority of the species, the vasa deferentia separately penetrate the penis bulb and subsequently open into an intrabulbar seminal vesicle. (2) In a smaller number of species, the sperm ducts open into the somewhat expanded proximal portion of the ejaculatory duct. (3) In a number of species, the vasa deferentia open separately into a much more distal section of the ejaculatory duct. (4) In only five species, the vasa deferentia fuse to form an intra- (condition 4a) or extrabulbar (condition 4b) common vas deferens. For these conditions, see discussion above on *D. constrictum*; the difference between condition (4a) and condition (2) resides in the fact that in the former the proximal section of the ejaculatory duct is hardly or not at all expanded. Conditions (2) and (4a) also hold true for *D. duplum*.

←

to the right). Abbreviations used in the figures: ab: adenodactyl bulb; ad: adenodactyl; ap: adenodactyl papilla; bc: bursal canal; ca:common atrium; cb:copulatory bursa; cm: circular muscles; co: copulatory apparatus; cod: common oviduct; cvd: common vas deferens; d: diaphragm; e: eye; ed: ejaculatory duct; gl: glands; go: gonopore; h: head; ic: intestinal caecum; l: lumen; lm: longitudinal muscles; ma: male atrium; o: ovary; od: oviduct; pb: penis bulb; pg: penis glands; ph: pharynx; pp: penis papilla; sg: shell glands; sp: spermatophore; spv: spermidual vesicle; sv: seminal vesicle; t: tail; vd: vas deferens; te: testes.

Among the species for which conditions (2) or (4a) are applicable, the gross morphology of the copulatory apparatus of *D. duplum* resembles that of *D. banaticum* Codreanu and Balcesco, 1967, *D. cavaticum* (Fries, 1874), *D. chappuisi* De Beauchamp, 1932, *D. coiffaiti* De Beauchamp, 1956, *D. maculatum* (Stanković and Komárek, 1927), *D. polymorphum* Codreanu and Balcesco, 1967, *D. stenophallus* Codreanu and Balcesco, 1967, *D. tuzetae* Gourbault, 1965, and *D. vaillanti* De Beauchamp, 1955. However, in all of these species, the vasa deferentia separately traverse the penis a considerable distance before communicating with the ejaculatory duct, whereas in *D. duplum,* the sperm ducts join immediately after they have penetrated the dorsal part of the penis bulb. Furthermore, none of these species show the double valve or diaphragm system of *D. duplum.*

Eyes are absent in *D. duplum*, *D. banaticum*, *D. chappuisi*, *D. polymorphum*, *D. stenophallus*, and *D. tuzetae*, whereas they are present in *D. cavaticum*, *D. coiffaiti*, *D. maculatum*, and *D. vaillanti*.

Dendrocoelum amplum Harrath and Sluys, sp. nov.
(Figs. 4, 5, 10, and 11)

Material examined. Holotype: ZMA V.Pl. 6886.1, Ain Dar Forn spring, near Bargou village, located in the governorate of Siliana, December 2008, coll. H. Harrath and A. Ghlala, sagittal sections on 10 slides.

Etymology. The specific epithet is derived from the Latin adjective *amplus*, spacious, and alludes to the distinct widening of the bursal canal before it opens into the atrium.

Habitat. Animals were collected from Dar Forn spring in the Bargou Mountains (35°58′52.75″ N, 9°30′43.32″ E), at approximately 1 km north of the road from Siliana to Ousletia (Fig. 1, locality B). Associated fauna: chiefly isopods.

Diagnosis. *D. amplum* is characterized by a white body; the presence of two small eyes; large testes, situated both dorsally and ventrally; two intrabulbar seminal vesicles, each receiving the openings of a vas deferens; a common intrabulbar seminal vesicle that opens via a diaphragm into the spacious penial cavity; a bursal canal that forms a considerable expansion at the vaginal region; an adenodactyl that is smaller than the penis.

Description. Living specimen up to 8 mm long and 1.6 mm wide. Dorsal surface dirty white. Head slightly rounded, with two small eyes situated at equal distance from each other and from the margins of the head (Fig. 4). The anterior end of the animal is provided with an adhesive organ, consisting of a considerable invagination that is lined with an infranucleated epidermis, penetrated by erythrophilic glands.

The numerous, large testes are situated dorsally, as well as ventrally, beginning at the level of the ovaries and extending to almost the tail end (Fig. 5). The subspherical penis bulb is muscular and houses two large seminal vesicles that are situated close to each other and filled with sperm in the holotype specimen (Fig. 10). Each seminal vesicle receives at its anterior section the opening of a sperm duct and, subsequently, opens into a smaller common vesicle. The latter is separated by a large diaphragm from a voluminous penial cavity. This wide cavity is lined with a thick, nucleated epithelium. The papilla is covered with a thick, nucleated epithelium, which is underlain by a layer of circular muscle fibers.

The adenodactyl, located to the left of the penis, is smaller than the latter and is provided with a wide lumen that receives the secretion of glands (Fig. 11). In the muscular hemispherical bulb this lumen expands to form a cavity of regular outline that is surrounded by intermingled layers of longitudinal and circular muscle fibers. The adenodactyl lumen follows a central course through the conical papilla and opens terminally. A layer of fine circular muscle fibers that stains bright blue extends throughout the parenchyma of the papilla. Ectally and entally to this zone of circular muscles runs a layer of longitudinal muscle fibers.

The two spherical ovaries, about 0.22 mm in diameter, are situated very close to the brain (Fig. 4). The oviducts arise from the postero-ventral side of the ovaries and run ventrally to the level of the copulatory apparatus, where they curve dorsally and unite to form a common oviduct, which opens into the female atrium. The common oviduct, as well as the distal sections of the oviducts, receives the secretion of shell glands. The bursal canal is lined with a thick epithelium and surrounded by a thin layer of longitudinal muscle fibers. The canal runs dorsally to the copulatory apparatus to communicate with a sac-shaped copulatory bursa, situated close to the posterior wall of the pharyngeal pouch and lined with a tall epithelium. The bursal canal expands considerably in diameter at the vaginal area, where it receives the secretion of well-developed shell glands and subsequently opens into the female atrium via a slight constriction.

Discussion. Several species of *Dendrocoelum* are similar to *D. amplum* in possessing eyes, a vasa deferentia expanded to form large, introbulbar seminal vesicles, or the presence of a distinct widening of the bursal canal. They are similar to the conditions found in *D. amplum* are the following: *D. adenodactylosum* (Stanković and Komárek, 1927), *D. maculatum* (Stanković and Komárek, 1927), *D. jablanicense* (Stanković and Komárek, 1927), *D. lacustre* (Stanković, 1938), *D. plesiophthalmum* De Beauchamp, 1937.

In both *D. adenodactylosum* and *D. maculatum* the adenodactyl is very large (Kenk, 1978), as compared with the size of the penis, thus contrasting with the condition in *D. amplum*, in which the adenodactyl and penis are of

about the same length. *D. maculatum* shares with *D. amplum* the presence of both dorsal and ventral testes, albeit that the follicles are comparatively small in the former and large in the latter.

In *D. jablanicense,* the bursal canal may communicate with the common atrium through one or two openings (Kenk, 1978). However, in this species the vasa deferentia fuse to form a short, intrabulbar common vas deferens, which opens into a seminal vesicle. This situation is strongly different from the course of the vasa deferentia in *D. amplum.*

Although *D. lacustre* does possess a widened bursal canal near the point of communication with the atrium, it lacks the expanded, intrabulbar seminal vesicles that are characteristic for *D. amplum.*

Judging from the drawing of the copulatory apparatus published by De Beauchamp (1937, Fig. 3), *D. plesiophtalmum* does possess the widened section in the posterior part of the bursal canal, but lacks the widened, intrabulbar portions of the vasa deferentia. The long, conical and pointed penis papilla of *D. plesiophthalmum* is rather different from the stubby papilla of *D. amplum.* Unfortunately, the precise morphology and course of the ejaculatory duct through the penis papilla is unknown for *D. plesiophthalmum.*

ANATOMY OF ADENODACTYLS IN *DENDROCOELUM*

The presence and precise location of a musculoglandular organ or adenodactyl in the copulatory complex of dendrocoelid planarians has gained some taxonomic importance. For example, the genus *Dendrocoelopsis* Kenk, 1930 is characterized by the fact, among others, that it lacks an adenodactyl, while several subgenera of *Dendrocoelum* have been proposed based partly on the shape, size, and location of the adenodactyl (Gourbault, 1972). On the level of species, the size of the adenodactyl in comparison with the penis papilla, and vice versa, forms a useful taxonomic character.

Adenodactyls or comparative structures have been reported for a considerable number of planarians, including land, freshwater, and marine species. Morphological differences suggest that these organs are not homologous and evolved independently in various groups of species (Sluys and Rohde, 1991, and references therein). Adenodactyls occur in several dendrocoelid genera: *Dendrocoelum*, *Caspioplana* Zabusova, 1951, *Baikalobia* Kenk, 1930, *Polycladodes* Steinmann, 1910, and *Acromyadenium* De Beauchamp, 1931. Our analysis is restricted to the genus *Dendrocoelum*, thus likely involving homologous adenodactyls.

Within *Dendrocoelum*, adenodactyls are cone-shaped structures with a distinct bulb and papilla, provided with a well-developed lumen that receives the abundant secretion of many glands. The precise location, orientation, and shape of the adenodactyl vary between species and form

important taxonomic characters that have been taken into consideration by the classical studies on these animals. However, the same studies consistently fail to document the precise arrangement of the musculature of the adenodactyls (e.g., Stanković and Komárek, 1927; De Beauchamp, 1932; Kenk, 1978), thus apparently echoing Von Graff's (1912–17: 3112) statement that in freshwater planarians all adenodactyls are histologically alike.

However, in the present study and other joint projects, it was noticed that particularly the *Dendrocoelum* species from the Lake Ohrid region have a histologically characteristic type of adenodactyl. The most striking feature of these adenodactyls is the presence of a zone of fine circular muscle fibers that runs through the mesenchyme of the papilla and stains bright blue when stained with a trichrome stain such as Mallory-Cason. This blue zone runs through the papilla and extends onto the bulb of the adenodactyl. Ectally and entally to this blue zone of circular muscles run layers of longitudinal fibers, which stain red, as do all other muscle fibers in the animal. Especially in *Dendrocoelum adenodactylosum* this situation can be observed clearly because of the very large size of the adenodactyl (Fig. 12). We observed the same adenodactyl histology in *Dendrocoelum maculatum* (Stanković and Komárek, 1927) (Fig. 13) and expect the blue zone of fine circular muscles to be present in the adenodactyl of many other species from the Balkan region. We will call this the Balkan type of adenodactyl, albeit that its occurrence is not restricted to this geographic region. For example, it is also present in the widely distributed *Dendrocoelum lacteum* (Müller, 1774) (Fig. 14). The Balkan type of adenodactyl is also present in the three new Tunisian species described above and in some species from Sardinia (Stocchino et al., in prep.). It is true that in trichrome stains, muscle fibers always stain either blueish or reddish, even in the same preparation. However, the difference with these species of *Dendrocoelum* is that there is such a clear difference in staining properties of the blue zone of circular muscles of the adenodactyl and the musculature of the rest of the body. For example, in a series of sections of *Dendrocoelum amplum* from Tunisia that generally show poor affinity for the aniline blue (Wasserblau) component of the Mallory-Cason stain, the fine circular muscle zone of the adenodactyl, nevertheless, stains bright light blue. The chemical reason why this particular zone of muscles stains so much differently remains an enigma. Reexamination of the material of *D. spatiosum* Vila-Farré and Sluys, 2011 from northeastern Spain revealed that the thick circular zone of mesenchymal muscles is also present in the adenodactyl of this species, although its differential staining is much less explicit than in the other species mentioned.

The Balkan type of adenodactyl is absent in species such as *Dendrocoelum nausicaae* Schmidt, 1861 and *D. beauchampi* Del Papa, 1952. In such species the mesenchymal musculature of the adenodactyl consists predominantly of
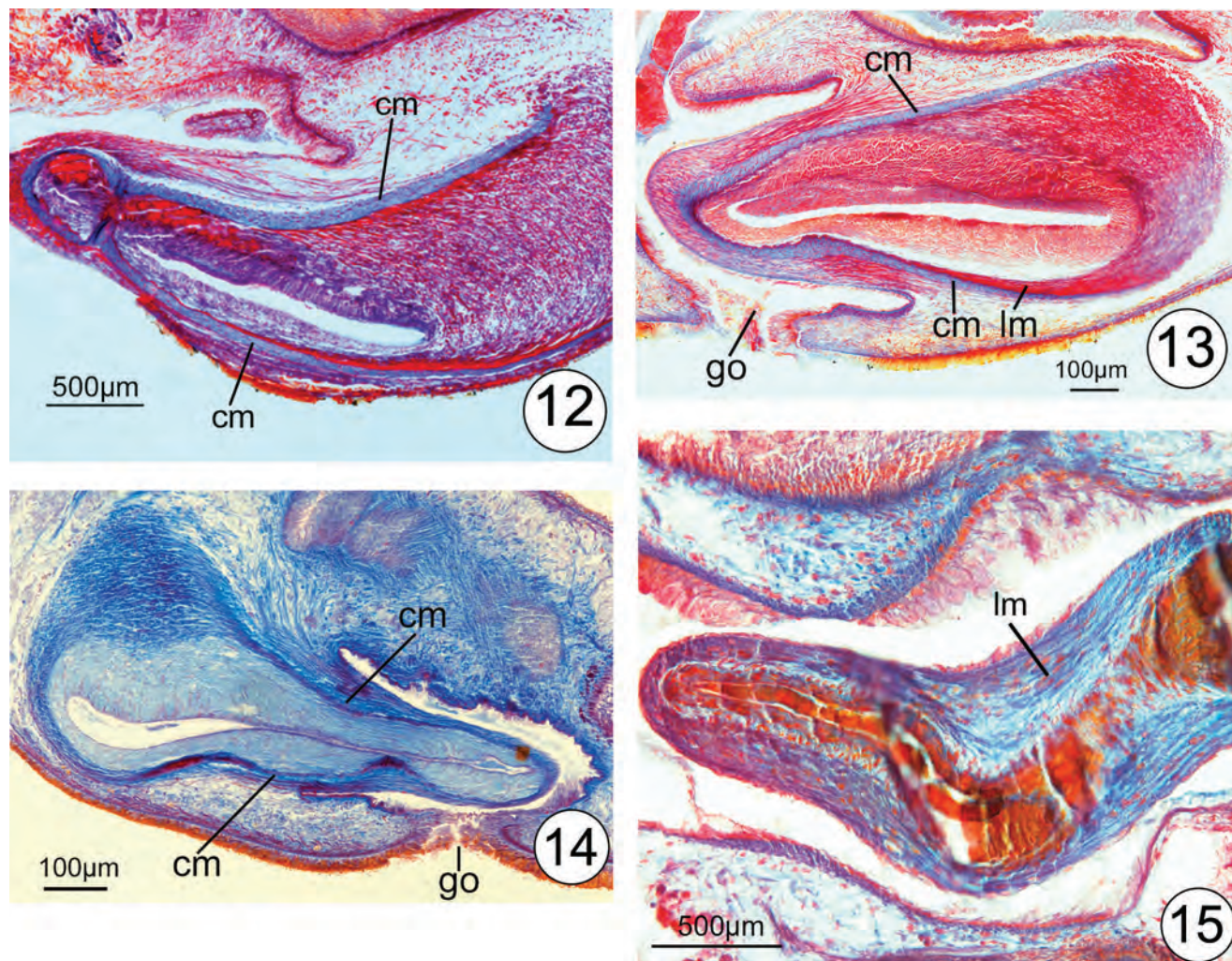
Figures 12–15. 12. *Dendrocoelum adenodactylosum* from near Resen (Crusje), Macedonia. Photomicrograph of adenodactyl, showing the conspicuous, blue-staining zone of circular muscle. 13. *Dendrocoelum maculatum* from Bej-Bunar stream near Ohrid, Macedonia. Photomicrograph of adenodactyl, showing the conspicuous, blue-staining zone of circular muscle. 14. *Dendrocoelum lacteum* from the Ebro delta, Spain. Photomicrograph of adenodactyl, showing the conspicuous, blue-staining zone of circular muscle. 15. *Dendrocoelum nausicaae* from Corfu, Greece. Photomicrograph of adenodactyl. See caption to Figures 6–11 for key.

longitudinal muscles, with only a thin layer of circular muscles directly underneath the lining epithelium of the lumen of the adenodactyl that stains no differently from the other muscle fibers, as is the case in *D. nausicaae* (Fig. 15). In *D. beauchampi,* the mesenchymal musculature of the adenodactyl papilla is poorly developed, merely consisting of some circular fibers (Sluys and Benazzi 1992).

Evidently, the precise taxonomic distribution of the Balkan type of adenodactyl needs to be studied and evaluated in more detail in future studies. However, in our opinion present evidence already suggests that presence of this structure signals a closely related group of *Dendrocoelum* species, which shows a geographically interesting distribution that currently comprises northern Europe, southeastern Europe, Sardinia, northwestern Africa and, most likely, also northeastern Spain.

REFERENCES

Ball, I.R., and Reynoldson, T.B., 1981, British Planarians: Cambridge, Cambridge University Press, 141 p.

De Beauchamp, P., 1932, Biospeologica LVI, Turbellariés, Hirudinées, Branchiobdellidés, Deuxième Série: Archives de Zoologie Expérimentale et Générale, v. 73, p. 113–380.

De Beauchamp, P., 1937, Turbellariés triclades de Yougoslavie récoltés par MM. Remy et Hubault: Bulletin de la Société Zoologique de France, v. 62, p. 351–365.

De Beauchamp, P., 1954, Nouvelles diagnoses de triclades obscuricoles VIII-IX: Bulletin de la Société Zoologique de France, v. 79, p. 418–427.

Del Papa, R., 1965, Descrizione di Dendrocoelum (Eudendrocoelum) botosaneanii n. sp. delle grotte del Banato (Romania): Monitore Zoologico Italiano, v. 73, p. 156–162.

Ghlala, A., Della Valle, D., and Messana, G., 2009, First record of the genus Typhlocirolana Racovitza, 1905 (Isopoda: Cirolanidae) from Tunisia and description of a new species from the National Park of Ichkeul: Zootaxa, no. 2176, p. 57–64.

Gourbault, N., 1972, Recherches sur les Triclades paludicoles hypogés: Mémoires du Muséum National d'Histoire Naturelle, nouvelle série (Série A), Zoologie 73, 249 p.

Jeannel, R., and Racovitza, E., 1914, Biospeologica XXXIII: Enumération des grottes visitées 1911–1913: Archives de Zoologie Expérimentale et Générale, v. 53, p. 325–558.

Juberthie, C., Decu, V., Aellen, V., and Strinati, P., 2001, Tunisie, in Juberthie, C., and Decu, V., eds., Encyclopaedia Biospeologica, Tome III: Bucarest, Société Internationale de Biospéologie, p. 1719–1728.

Kenk, R., 1978, The planarians (Turbellaria: Tricladida Paludicola) of Lake Ohrid in Macedonia: Smithsonian Contributions to Zoology, no. 280, 56 p.

Messana, G., 2004, Africa Biospeleology, in Gunn, J., ed., Encyclopedia of Caves and Karst Science: New York and London, Fitzroy Dearborn, p. 24–25.

Porfirjeva, N.A., 1977, Planarii Ozera Baikal: Novosibirsk, Nauka Publishing, 206 p. [in Russian]

Seurat, L.G., 1921, Faune des eaux continentales de la Berbérie: Alger, Publications de la Faculté des Sciences, Travaux du Laboratoire de Zoologie appliquée, 66 p.

Seurat, L.G., 1934, Faune aquatique du sud et de l'extrême sud de la Tunisie: Annales des Sciences Naturelles, Zoologie, v. 17, p. 441–450.

Sluys, R., 2007, Annotations on freshwater planarians (Platyhelminthes Tricladida Dugesiidae) from the Afrotropical Region: Tropical Zoology, v. 20, p. 229–257.

Sluys, R., and Benazzi, M., 1992, A new finding of a subterranean dendrocoelid flatworm from Italy (Platyhelminthes, Tricladida, Paludicola): Stygologia, v. 7, p. 213–217.

Sluys, R., and Kawakatsu, M., 2006, Towards a phylogenetic classification of dendrocoelid freshwater planarians (Platyhelminthes): a morphological and eclectic approach: Journal of Zoological Systematics and Evolutionary Research, v. 44, p. 274–284. doi: 10.1111/j.1439-0469.2006.00371.x.

Sluys, R., and Rohde, K., 1991, A new species of freshwater triclad (Platyhelminthes: Tricladida) from Australia: Zoological Journal of the Linnean Society, v. 102, p. 153–162. doi: 10.1111/j.1096-3642.1991.tb00286.x.

Stanković, S., and Komárek, J., 1927, Die Süßwasser-Tricladen des Westbalkans und die zoogeographischen Probleme dieser Gegend: Zoologische Jahrbücher Abteilung für Systematik, Ökologie und Geographie der Tiere, v. 53, p. 591–674.

Stocchino, G.A., Sluys, R., Manconi, R., Casale, A., Marcia, P., Grafitti, G., Cadeddu, B., Corso, C., and Pala, M., (in prep.), Triclads from Sardinian groundwaters.

Vila-Farré, M., Sluys, R., Almagro, Í., Handberg-Thorsager, M., and Romero, R., 2011, Freshwater planarians (Platyhelminthes, Tricladida) from the Iberian Peninsula and Greece: diversity and notes on ecology: Zootaxa, no. 2779, p. 1–38.

Von Graff, L., 1912–17, Tricladida, in Dr. H.G. Bronn's Klassen und Ordnungen des Tier-Reichs, Bd. IV Vermes, Abt. IC: Turbellaria, II Abt.: Tricladida: Leipzig, C. F. Winter, p. 2601–3369.

MICRO-CHARCOAL ABUNDANCES IN STREAM SEDIMENTS FROM BUCKEYE CREEK CAVE, WEST VIRGINIA, USA

GREGORY S. SPRINGER[1*], L. NIVANTHI MIHINDUKULASOORIYA[2], D. MATTHEW WHITE[3], AND HAROLD D. ROWE[4]

Abstract: We compare micro-charcoal abundances in laminated cave-stream sediments to the presences of Native Americans and later settlers in the same watershed. Samples were obtained from a core taken from a 2.5 m high point bar located 1 km inside of Buckeye Creek Cave, West Virginia. Thirty-three subsamples were treated with hydrogen peroxide to bleach or whiten non-charcoal organic matter. In the absence of opaque mineral grains, this technique creates a large visual contrast between dark charcoal grains and other substances. The subsamples were photographed using a microscope-mounted camera, and pixels darker than 99/255 (grayscale) were used to calculate charcoal concentrations. The record spans the last 6,000 years, and four of the five highest charcoal concentrations are from the last 2,000 years. The highest concentration is from AD 1093, and the second-highest concentration is from the nineteenth century. Post-Colonial settlers began making extensive use of the watershed sometime in the eighteenth century and may, therefore, be responsible for the second-highest charcoal concentration. However, archaeologists independently concluded that Native Americans made peak use of the watershed between AD 1000 and 1200, which coincides with the highest charcoal concentration in the record. Native Americans are known to have extensively used fire, so there is good circumstantial evidence tying high concentrations in the last 2,000 years to human activities. Our method is suitable for use elsewhere, and we present a detailed statistical analysis of our data as a guide toward interpreting charcoal concentrations in karst and non-karst deposits.

INTRODUCTION

Clastic cave sediments preserve records of geomorphic processes, climate, and land uses as fluctuations in geochemistry, mineralogy, or organic matter (Springer, 2005). The latter includes charcoal, the abundance of which is an especially valuable proxy for land use. However, sedimentary-charcoal abundances are little studied in true caves, as opposed to rock shelters. Charcoal abundances are widely measured in lacustrine sediments, and lake-based studies often focus on reconstructing detailed fire histories and identifying peak times of charcoal deposition (Higuera et al., 2007). These have many applications within climate, forest succession, and archaeological studies (Conedera et al., 2009; Théry-Parisot et al., 2010). Conceptually, high charcoal abundances may represent periods of frequent fires or greater fire severities, but mixing and storage during transport through stream networks creates a persistent background signal, while the mechanisms of transport and the distances over which charcoal is transported significantly affect particle size and abundance in sedimentary deposits (Conedera et al., 2009; Higuera et al., 2007). These limitations explain why much attention is given to peaks in charcoal abundance data. Nonetheless, the fluvial processes that effectively filter and smooth charcoal abundances are presumably true of both surface and subsurface streams and charcoal abundances in clastic cave sediments may be valuable for understanding a variety of natural and anthropogenic processes (Carcaillet et al., 2007).

As part of a geoarchaeological study, we sought to efficiently measure a statistically meaningful number of charcoal abundances in clastic cave sediments ($n \geq 30$) by refining an existing charcoal separation method (Rhodes, 1998). We examined fine-grained sediments containing only micro-charcoal fragments less than 1 mm in diameter and not readily visible to the unaided eye. After separating or distinguishing charcoal from unconsolidated sediments and other detritus, the necessary data are obtained by counting charcoal grains or measuring charcoal-grain surface areas or volumes (Ali et al., 2009). The separation and quantification procedures can be very time consuming and impacts the number and spacing of samples and their temporal resolution (Rhodes, 1998). These issues can limit

* Corresponding Author
[1] Department of Geological Sciences, Ohio University, Athens, OH 45701 springeg@ohio.edu
[2] Department of Geology, Kent State University, Kent, OH 45701 lnivanthi@yahoo.com
[3] ExxonMobil, 800 Bell Street, Room 2897D, Houston, TX 77002 david.m.white@exxonmobil.com
[4] Department of Earth and Environmental Sciences, The University of Texas at Arlington, Arlington, TX 76019 hrowe@uta.edu
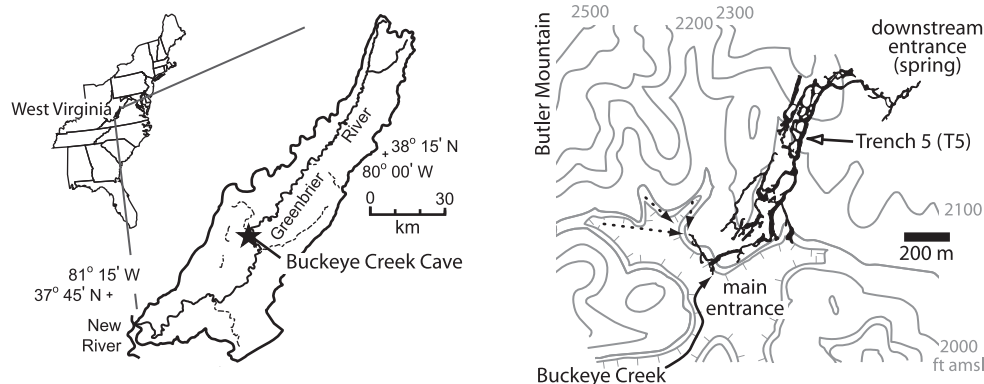
Figure 1. Buckeye Creek is located in southeastern West Virginia (left panel) and enters the cave after flowing across an active floodplain within a large karst depression (right panel). A plan view of the cave is superimposed on basin topography at right, and the location of our sediment trench is indicated. Adapted from Dasher and Balfour (1994) and Springer et al. (2010).

a researcher's ability to distinguish between charcoal-abundance values of anthropogenic and non-anthropogenic origins. Therefore, we used digital processing to generate data more efficiently and in sufficient numbers for statistical analysis. We describe our laboratory method and provide statistical analysis of our results. The reliability of the latter is tested by briefly comparing micro-charcoal abundances to independent geological (Springer et al., 2008) and archaeological data (McBride and Sherwood, 2006; Springer et al., 2010). In doing so, we assumed that charcoal abundances reflect some aspect of fire frequencies or severities (Higuera et al., 2007; Conedera et al., 2009; Théry-Parisot et al., 2010), but do not interpret our record as a detailed fire history. Instead, we focus on peak abundances and whether these peaks are correlated with human activities in the source watershed. Our micro-charcoal technique should be of value to others and has many potential applications in cave and karst studies.

Study Area

We report data collected from a point bar deposited by a stream in Buckeye Creek Cave, which drains a topographically enclosed, 14 km^2 watershed in southeastern West Virginia, USA (Fig. 1). Buckeye Creek flows through a 2 km long passage averaging 10 m wide and 4 m high (Dasher and Balfour, 1994; Springer, 2004). Silt banks are found on one or both sides of the stream for much of its underground course. The fine-grained sediments are derived from a karst watershed draining Mississippian-age sandstones, siltstones, and shales of Butler Mountain. Surface streams carry siliciclastic detritus to the base of Butler Mountain, where streams sink into their beds or swallet holes in limestone-floored valleys (Springer et al., 2003).

Methods

We dug a trench in the face of a 2.6 m high point bar, 1 km downstream of the cave entrance in a 20 m wide by 7 m high passage. Deposition continues atop the point bar, although the stream has meandered against the bar to create a cutbank. The sediments lack interior scour surfaces, hard-grounds, and other indications of erosion or periods of non-deposition. Therefore, we assume deposition has been essentially continuous since the sediments began accumulating. The sediments were described and sampled in the field, but we also cored the face of the trench by pushing PVC sleeves into the sediments. The sleeves are made from PVC tubes with square cross sections, measuring 10.2 cm on a side (4 inches square), cut lengthwise to yield a square-cornered trough. Core lengths were typically ~50 cm, and the sleeves overlapped to create a continuous sample of the sediments. The open sides of sleeves were pressed into sediment before being cut out of the trench wall, wrapped in protective materials, and carried out of the cave. This allowed us to perform detailed subsampling and laboratory analyses in a controlled environment.

The cores were sampled at selected depths for charcoal analysis using a method described by Rhodes (1998). Subsamples weighing 2 g were removed from sediment cores and dried for two days, rehydrated with dilute potassium hydroxide (KOH), decanted, and treated with 20 ml of 5% hydrogen peroxide (H_2O_2). The peroxide treatment bleaches all organic matter except charcoal, which remains dark and contrasts markedly with the bleached organics and light-colored and translucent sediment grains. We used the contrast created by the H_2O_2 treatment to estimate charcoal concentrations using a digital technique. The prepared samples were placed in petri dishes and photographed using digital photomicroscopy. Individual images were converted to grayscale, and all pixels below a grayscale threshold of 99/255 were counted using ImageJ software (http://rsbweb.nih.gov/ij/) (Fig. 2). The use of pixel-counting greatly speeds estimation of charcoal concentrations, but it over-counts charcoal abundances because some dark objects are probably not charcoal. However, we visually scanned all dishes during
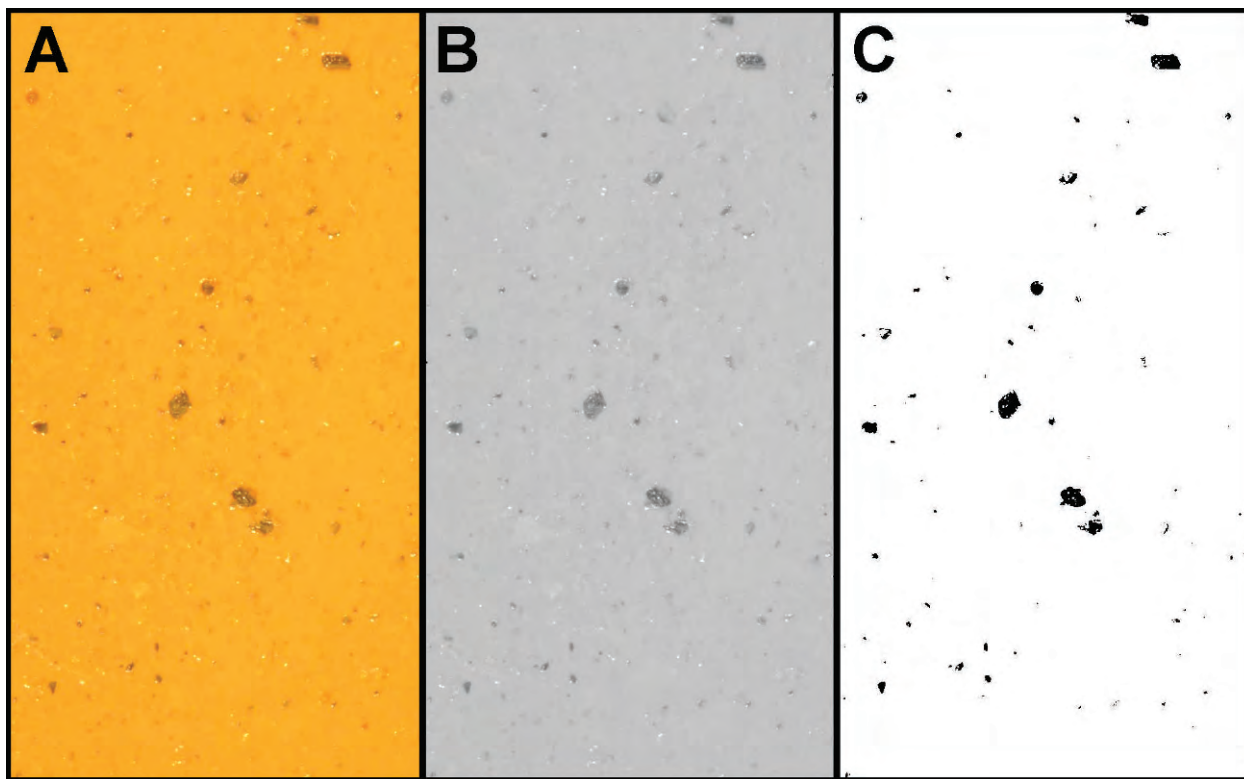
Figure 2. Charcoal concentrations were measured by photographing prepared sediment samples (A), converting the images to grayscale (B), and counting all pixels below a grayscale threshold of 99/255 (C). The darkest pixels were assumed to be charcoal because extensive pretreatment with H_2O_2 bleached all other organic matter and no dark mineral grains were observed during photographing.

photomicroscopy and did not observe any dark mineral grains, probably because the silts and sands are greater than 99% quartz, as measured using X-ray diffraction. However, to control for contamination from dark, non-charcoal particles, we averaged the results of multiple images taken from different areas within individual petri dishes.

MICRO-CHARCOAL RESULTS AND STATISTICS

A total of 33 samples were analyzed for micro-charcoal concentrations. The first sample was taken 1 cm below the top of the deposit (core), and additional samples were taken every 2 cm to a depth of 27 cm (total $n = 14$). Thereafter, samples were collected every 3 to 4 cm to a depth of 98 cm ($n = 19$). Ages were assigned to each sample using an age-depth model built from seven radiocarbon dates. The model and its uncertainties are discussed in Springer et al. (2010), and the basal sediments are ~6,500 years old. Charcoal concentrations range over an order of magnitude (0.22 to 2.15 mm^2 cm^{-2}). Overall, values are highest in the late Holocene, but there is considerable variability during this time (Fig. 3). Overall, concentrations are strongly skewed to the left and failed a Shapiro-Wilk test for normality ($p = 0.007$). Using the

same test and a base-ten log transformation, the values are lognormally distributed ($p = 0.995$) and their cumulative frequencies fall on a nearly straight line when plotted using a probability scale (Fig. 4). Nonetheless, the lowest and five highest points do not fall on the line. Following the methods of Sinclair (1974) and Reimann et al. (2005), we did not perform outlier tests, but calculated thresholds above which data points are anomalous and deserving further analysis.

Threshold values can be chosen in a variety of ways. Conventional methods include using the value corresponding to the mean ±2 standard deviations (mean ±2 sdev), median ±2 median absolute deviation (MAD), and the box-plot method (Reimann et al., 2005). According to mean ±2 sdev method, values outside upper and lower thresholds are considered possible outliers worthy of further attention. However, this method identifies only 5% of actual extreme values (Reimann et al., 2005), and in our case, is exceeded only by the AD 1093 value (Fig. 4). The box-plot method was performed using Systat's SigmaPlot and identified the AD 1889, AD 1093, and AD 24 values as outliers (Fig. 4 inset). The MAD method usually resulted in a lower threshold level than the box-plot or mean ±2 sdev methods, and its threshold was lower than the four largest charcoal concentrations (Fig. 4).
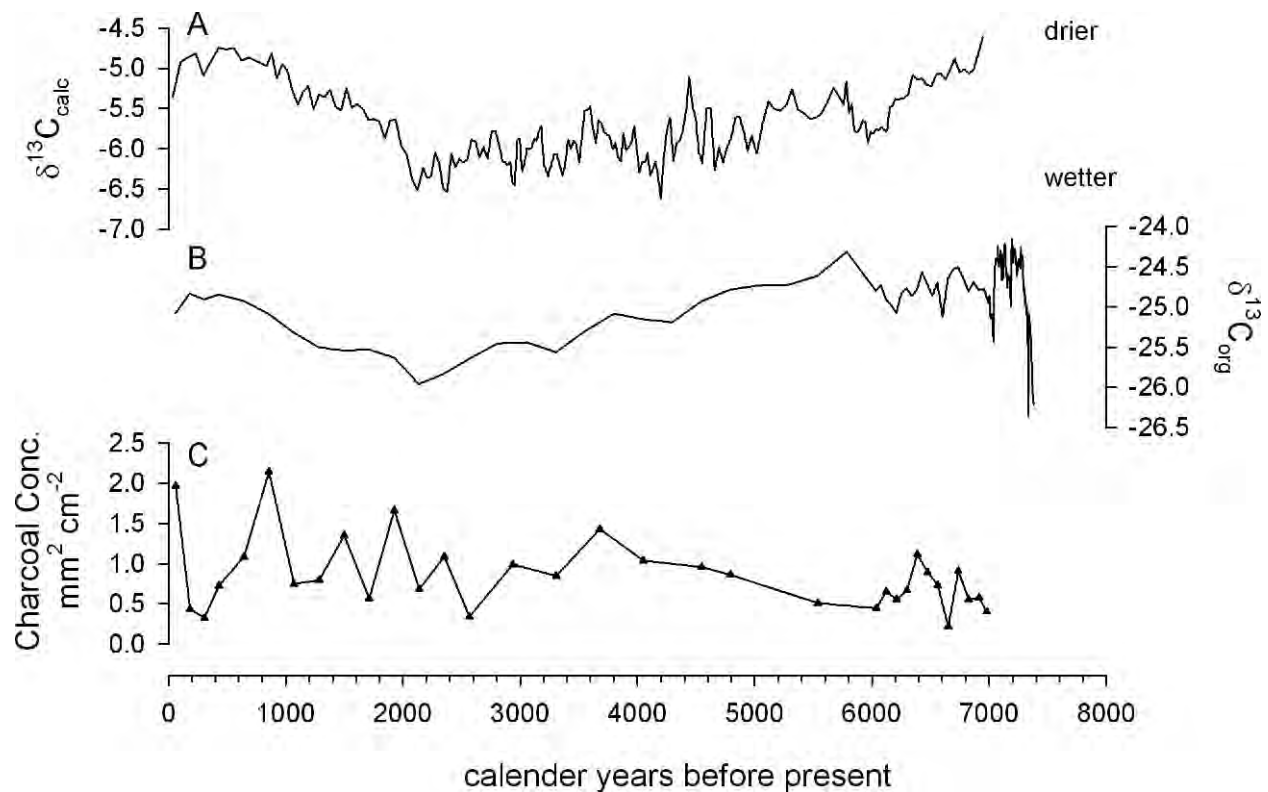
Figure 3. (A) A stable isotopic ($^{13}C_{calc}$) paleoclimatic record obtained from a stalagmite records long-term changes in the soils and ecosystem above Buckeye Creek Cave (Springer et al., 2008). Moisture levels increased from the mid to late Holocene, but $^{13}C_{calc}$ values increased abruptly ~100 BC This coincides with use of Unnamed Cave #14 (UC14) by Native Americans, and values peak approximately when Native Americans were making their most extensive use of UC14 (Maslowski, 2006). Other regional paleoclimatic records do not record drying after 2,100 years BP (Springer et al., 2009; 2010), but the anomalous $^{13}C_{calc}$ record is corroborated by stable isotopic analysis of organic material ($^{13}C_{org}$) in the Trench Five sediments (B). (C) Fire activity was high during the Late Holocene and peaks near the times of peak $^{13}C_{calc}$ and $^{13}C_{org}$ values, coinciding with peak Native American use of the watershed, as inferred from the UC14 record (McBride and Sherwood, 2006).

However, these methods do not take into account the possibility that the anomalous values are derived from a different population than the background population of points falling on an approximately straight line in Figure 4. If two populations have been sampled, the mean and standard deviation of the pooled data may not be statistically meaningful. As a consequence, the strict application of threshold values yields questionable results (cf. Reimann et al., 2005).

There are alternatives to using thresholds of purely quantitative derivation. Among these, the most popular remains subjective interpretation of non-linearity in cumulative probability plots, whereby the point of maximum curvature is interpreted as the threshold separating different populations (Sinclair, 1974; Reimann et al., 2005). Points beyond the curvature threshold should be subjected to additional investigation, because Monte Carlo simulations indicate this method yields too many outliers (Reimann et al., 2005). When plotted as cumulative probabilities (Fig. 4), the five highest concentrations do not fall on a trend line drawn through intermediate

charcoal concentration values and five samples qualify as being anomalous: AD 1889, AD 1093, AD 452, AD 24, and 1730 BC.

DISCUSSION

The last 2,000 years includes four of the five highest micro-charcoal concentrations and all statistical methods identified the AD 1093 event as an anomalous value. The charcoal is derived from a very small watershed (14 km²), which is ideal because large watersheds allow too much particle mixing and smoothing of peak fire events (Carcaillet et al., 2007). Variability in locally generated charcoal deposits usually reflects an event-dominated record, with major fire episodes recorded as spikes in charcoal abundances (Clark et al., 1996; Marlon et al., 2006; Carcaillet et al., 2007). Alternatively, variability can reflect one or more flaws in sampling or measurement methodologies. On this matter, we note that White (2007) contains a lower resolution micro-charcoal record made using the same techniques. His record also shows high late
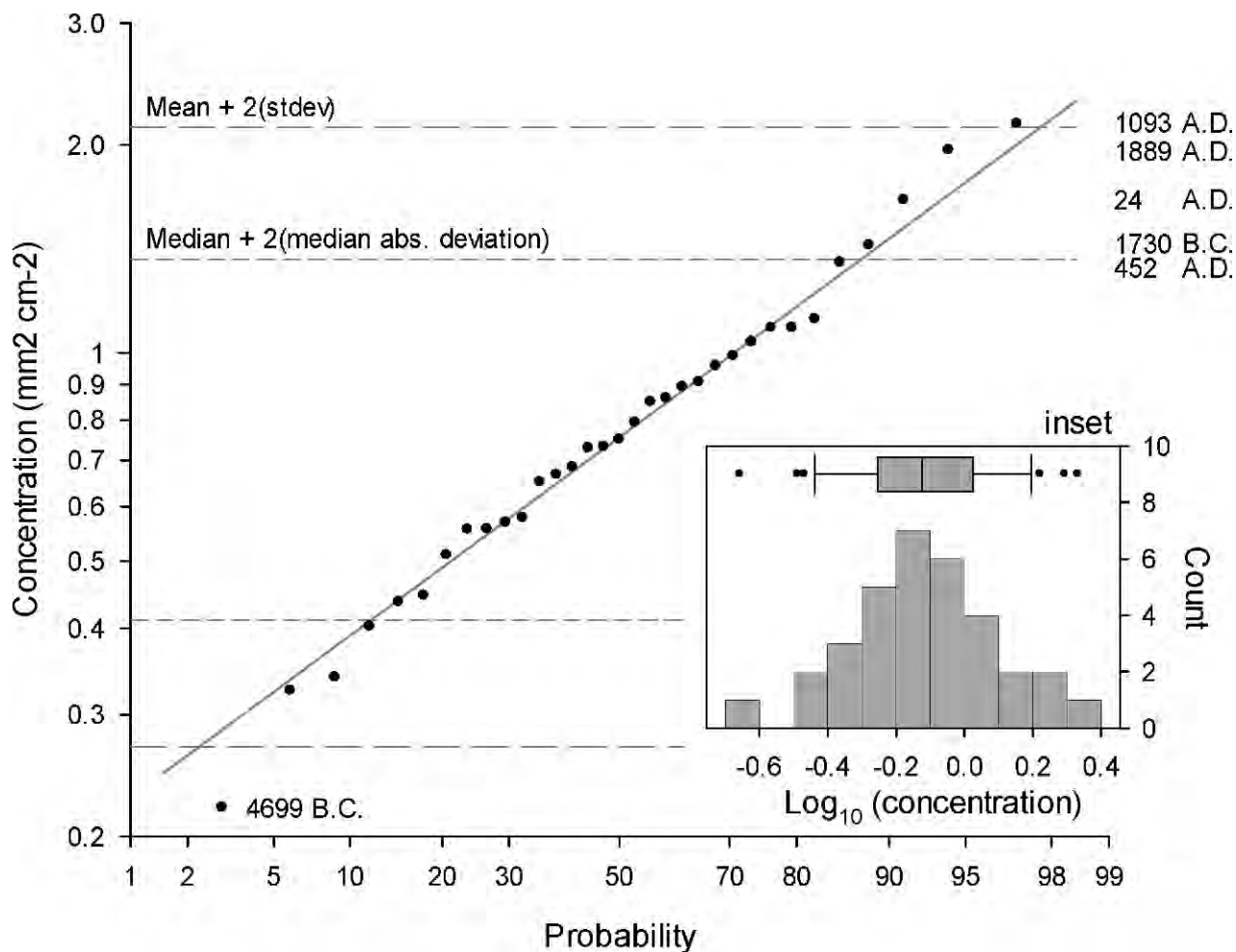
Figure 4. Charcoal concentrations display a log-normal distribution (inset). The cumulative distribution function of charcoal concentrations is plotted, and five anomalously high concentrations are labeled. Thresholds calculated to identify anomalous values are shown as dashed lines and within the box plot (inset) as black circles. Details discussed in the text.

Holocene charcoal abundances relative to mid-Holocene values. Nonetheless, the highest concentrations are above several thresholds (Fig. 4) and, therefore, worth additional consideration. So, we compare their timings to an independent archaeological investigation conducted in Unnamed Cave #14 (UC14) adjacent to Buckeye Creek Cave (Fig. 5). (The common name and entrance location of UC14 are on file with the State of West Virginia Division of Culture and History, but are withheld to protect enclosed cultural remains.) The comparison is a test of whether humans could be responsible for the high charcoal concentrations.

UC14 consists of a 30 m by 46 m entrance room and more than 100 m of interior passages. The entrance room is more than 3 m high and hospitable for human habitation, with a flat floor and daytime illumination from a southeast-facing entrance. Drs. Kim McBride and Sarah Sherwood of the Kentucky Archaeological Survey and Dickinson College in Pennsylvania, respectively, led the project and co-edited a volume composed of chapters dedicated to stone implements and debitage, pottery sherds, petroglyphs, hearths, and foodstuffs (McBride and Sherwood, 2006). The report is on file with the West Virginia Cave Conservancy (http://www.wvcc.net/).

Cultural remains were assigned ages by comparing their morphologies to published, well-dated cultural materials from other regional excavations (Fig. 5) (Maslowski, 2006; McBride, 2006; Simek and Cressler, 2006). Collectively, the cultural remains reveal that UC14 was utilized in one or more ways from the Late Archaic through the Late Prehistoric (5,000 to 250 calendar years BP), at least occasionally. The three most culturally distinctive artifact classes are projectile points, pottery, and petroglyphs. All three types of remains are represented between AD 1000 and 1200 (750 and 550 years BP; black in Fig. 5). Maslowski (2006) inferred that peak Native American utilization of UC14 occurred during that time period. This is circumstantial evidence that Native Americans are responsible for fires that produced several of the highest charcoal concentrations.

Figure 5. The gray regions represent cultural ages assigned to projectile points (McBride, 2006), pottery (Maslowski, 2006), and petroglyphs (Simek and Cressler, 2006) found i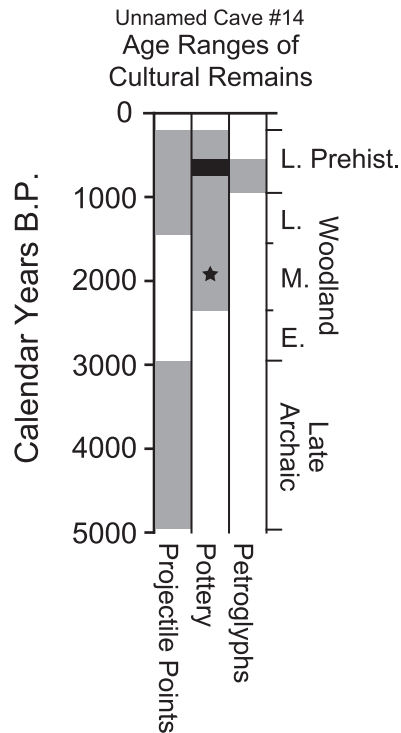n Unnamed Cave #14. The black bar in the pottery column denotes the age range of distinctive Page Cord ceramics (Maslowski, 2006). The black star is a radiocarbon date obtained from pottery fragments (McBride and Sherwood, 2006).

However, the second highest value is found at 1 cm depth in Trench Five. The corresponding date, AD 1889, is after Europeans began making substantial changes to Greenbrier County ecosystems (Hale, 1886). Knowing that settlers and their descendants performed extensive land clearance (Hale, 1886), it seems highly probable that the second-highest peak reflects human activities. A fifth point, 1730 BC, also lies above the trend line, but only a few Archaic artifacts were found in UC14, and the significance of the high micro-charcoal abundance value is unclear.

Conclusions

Four of the five highest micro-charcoal abundances in Buckeye Creek Cave sediments were generated at times when humans were making significant use of the Buckeye Creek watershed. Native Americans are known to have managed forests using fire, and subsequent settlers used fire to clear land, so there is strong circumstantial evidence that humans are responsible for high charcoal concentrations created during the late Holocene (Springer et al., 2010). Archaeological studies often make use of clastic sediments in rock shelters (Springer, 2005), but cave

interior deposits are rarely used as we have done. Micro-charcoal may represent a valuable resource because it accumulates in laminated sediments with simple origins, and very small samples are sufficient for analysis. Non-cave records may be unavailable in many settings, so agreement between our micro-charcoal results and human activities give confidence that micro-charcoal in cave sediments can be useful for reconstructing land uses and ecological regimes. We recommend micro-charcoal data be subjected to statistical analysis, because high concentrations are not uniquely associated with any particular source (Conedera et al., 2009). We also believe threshold-based approaches used in geochemical studies are appropriate for micro-charcoal studies (Sinclair, 1974; Reimann et al., 2005), but recommend generating as many data points as is practical.

References

Ali, A.A., Higuera, P.E., Bergeron, Y., and Carcaillet, C., 2009, Comparing fire-history interpretations based on area, number and estimated volume of macroscopic charcoal in lake sediments: Quaternary Research, v. 72, no. 3, p. 462–468. doi: 10.1016/j.yqres.2009.07.002.

Carcaillet, C., Perroux, A., Genries, A., and Perrette, Y., 2007, Sedimentary charcoal pattern in a karstic underground lake, Vercors massif, French Alps: implications for palaeo-fire history: The Holocene, v. 17, no. 6, p. 845–850. doi: 10.1177/0959683607080524.

Clark, J., Royall, P., and Chumbley, C., 1996, The role of fire during climate change in an eastern deciduous forest at Devil's Bathtub, New York: Ecology, v. 77, no. 7, p. 2148–2166. doi: 10.2307/2265709.

Conedera, M., Tinner, W., Neff, C., Meurer, M., Dickens, A.F., and Krebs, P., 2009, Reconstructing past fire regimes: methods, applications, and relevance to fire management and conservation: Quaternary Science Reviews, v. 28, no. 5–6, p. 555–576. doi: 10.1016/j.quascirev.2008.11.005.

Dasher, G., and Balfour, W., eds., 1994, The Caves and Karst of the Buckeye Creek Basin: Barracksville, West Virginia, West Virginia Speleological Survey bulletin 12, 326 p.

Hale, J., 1886, Trans-Allegheny Pioneers: Historical Sketches of the First White Settlements West of the Alleghenies 1748 and After: Cincinnati, Ohio, Graphic Press, 330 p.

Higuera, P.E., Peters, M.E., Brubaker, L.B., and Gavin, D.G., 2007, Understanding the origin and analysis of sediment-charcoal records with a simulation model: Quaternary Science Reviews, v. 26, no. 13–14, p. 1790–1809. doi: 10.1016/j.quascirev.2007.03.010.

Marlon, J., Bartlein, P.J., and Whitlock, C., 2006, Fire-fuel-climate linkages in the northwestern USA during the Holocene: The Holocene, v. 16, no. 8, p. 1059–1071. doi: 10.1177/0959683606069396.

Maslowski, R., 2006, Ceramic analysis, in McBride, K., and Sherwood, S., eds., Report of Archaeological Investigations at [Unnamed Cave #14], West Virginia: Lexington, Kentucky, Kentucky Archaeological Survey, p. 7.1–7.10.

McBride, J., 2006, Analysis of stone tools, in McBride, K., and Sherwood, S., eds., Report of Archaeological Investigations at [Unnamed Cave #14], West Virginia: Lexington, Kentucky, Kentucky Archaeological Survey, p. 8.1–8.9.

McBride, K., and Sherwood, S., eds., 2006, Report of Archaeological Investigations at [Unnamed Cave #14], West Virginia: Lexington, Kentucky, Kentucky Archaeological Survey.

Reimann, C., Filzmoser, P., and Garrett, R.G., 2005, Background and threshold: critical comparison of methods of determination: Science of The Total Environment, v. 346, no. 1–3, p. 1–16. doi: 10.1016/j.scitotenv.2004.11.023.

Rhodes, A.N., 1998, A method for the preparation and quantification of microscopic charcoal from terrestrial and lacustrine sediment cores: The Holocene, v. 8, no. 1, p. 113–117. doi: 110.1177/095968369800800114.

Simek, J., and Cressler, A., 2006, Prehistoric cave art in [Unnamed Cave #14], West Virginia, *in* McBride, K., and Sherwood, S., eds., Report of Archaeological Investigations at [Unnamed Cave #14], West Virginia: Lexington, Kentucky, Kentucky Archaeological Survey, p. 3.1–3.13.

Sinclair, A., 1974, Selection of threshold values in geochemical data using probability graphs: Journal of Geochemical Exploration, v. 3, no. 2, p. 129–149. doi: 10.1016/0375-6742(74)90030-2.

Springer, G.S., 2004, A pipe-based, first approach to modeling closed conduit flow in caves: Journal of Hydrology, v. 289, no. 1–4, p. 178–189. doi: 10.1016/j.jhydrol.2003.11.020.

Springer, G.S., 2005, Clastic sediments in caves, *in* Culver, D., and White, W., eds., Encyclopedia of Caves: Amsterdam, Boston, Academic Press, p. 102–108.

Springer, G., Rowe, H., Hardt, B., Edwards, R.L., and Cheng, H., 2008, Solar forcing of Holocene droughts in a stalagmite record from West Virginia in east-central North America: Geophysical Research Letters, v. 35, L17703 p. doi: 10.1029/2008GL034971.

Springer, G.S., Rowe, H., Hardt, B., Cocina, F.G., Edwards, R.L., and Cheng, H., 2009, Climate driven changes in river channel morphology and base level during the Holocene and Late Pleistocene of Southeastern West Virginia: Journal of Cave and Karst Studies, v. 71, no. 2, p. 121–129.

Springer, G.S., White, D.M., Rowe, H.D., Hardt, B., Mihindukulasoor-iya, L.N., Cheng, H., and Edwards, R.L., 2010, Multiproxy evidence from caves of Native Americans altering the overlying landscape during the late Holocene of east-central North America: The Holocene, v. 20, no. 2, p. 275–283. doi: 10.1177/0959683609350395.

Springer, G.S., Wohl, E.E., Foster, J.A., and Boyer, D.G., 2003, Testing for reach-scale adjustments of hydraulic variables to soluble and insoluble strata: Buckeye Creek and Greenbrier River, West Virginia: Geomorphology, v. 56, no. 1–2, p. 201–217. doi: 10.1016/S0169-555X(03)00079-5.

Théry-Parisot, I., Chabal, L., and Chrzavzez, J., 2010, Anthracology and taphonomy, from wood gathering to charcoal analysis. A review of the taphonomic processes modifying charcoal assemblages, in archaeological contexts: Palaeogeography, Palaeoclimatology, Palaeoecology, v. 291, no. 1–2, p. 142–153. doi: 10.1016/j.palaeo.2009.09.016.

White, D.M., 2007, Reconstruction and Analysis of Native American land use during the late Holocene [M.S. Thesis]: Athens, Ohio, Ohio University. 164 p.

RESPONSE OF THE KARST PHREATIC ZONE TO FLOOD EVENTS IN A MAJOR RIVER (BOHEMIAN KARST, CZECH REPUBLIC) AND ITS IMPLICATION FOR CAVE GENESIS

Helena Vysoká[1*], Jiří Bruthans[1,2], Karel Žák[3], and Jiří Mls[1]

Abstract: Hydraulic and hydrochemical relationships between a medium gradient river and a karst aquifer were studied by water level and temperature logging combined with water geochemistry and $\delta^{13}C$. The cave lakes are separated from the river by a floodplain up to 150 m wide formed by a gravel and sand layer up to 13 m thick covered with fine-grained floodplain sediments. During minor discharge peaks (water level in the river < 1.5 m above the normal river stage), a water level oscillation in the cave lakes situated 40 to 190 m away from river is induced by the river level oscillation, but the river water does not enter any of the lakes. The groundwater chemistry in the cave lakes differs from that of the river water. Low bicarbonate content and high $\delta^{13}C$ values indicate that some of cave lakes' waters have undergone CO_2 degassing and calcite precipitation. During a major flood (recurrence interval > 100 years, level rising 7 m above the normal stage), the river water rapidly flooded the caves through openings in the river canyon (flood-flow injection), while those connected to the river via alluvium only were flooded by an elevated groundwater stage, and the resulting water level rise was only about 50 percent of the river level increase. A simple hydraulic model was successfully used to simulate and explain the water table oscillations in the cave lakes. Flood-flow injection has recently been substantially reduced by low-permeability, fine-grained late Holocene fluvial sediments that cap coarse gravels in the river floodplain. Fast speleogenesis by flood injection would be expected in periods when the river canyon was bare or filled by gravel alone (glacial periods, transition to Holocene). Ice jams causing local increases in the river level are recognized as one of factors that can be important in speleogenesis.

INTRODUCTION

Generally, direct invasion of river floodwaters into the karst environment enables fast development of caves (Palmer, 1991), since water in rivers originating outside of the karst area can be undersaturated with respect to calcium carbonate, and the mixing of river water and the usual karst $Ca-HCO_3^-$ waters is another factor enhancing corrosion of the limestone (Klimchouk et al., 2000). During the last few decades, injection of river floodwaters into karst porosity began to be considered as an important speleogenetic process (Palmer, 1991).

Choquette and Pray (1970) subdivided the evolution of carbonate rocks into three time or porosity stages reflecting the rock cycle. Deposition and early exposure are eogenetic; deep burial is mesogenetic; postburial exposure and erosion are telogenetic. Because karstification results from processes near the surface, karst can be subdivided into two main types, eogenetic and telogenetic (Vacher and Mylroie, 2002). Telogenetic aquifers differ from eogenetic aquifers not only in their much lower primary porosity and matrix permeability (Florea and Vacher, 2006), but also in the steeper inclination of their water table level (e.g., Bailly-Comte et al., 2010). Hydraulic and hydrochemical relationships between rivers and eogenetic karst aquifers were studied by Katz et al. (1998), Martin and Dean (2001), Opsahl et al. (2007) and others.

In telogenetic karst aquifers, the overwhelming majority of studies concerning the relationship between allogenic streams and karst aquifers are focused on partly or fully sinking streams (e.g. Bailly-Comte et al., 2009; Doctor et al., 2006). There is a lack of studies concerning the effect of a river that crosses the karst area but does not lose water into the karst aquifer under normal water stages.

The hydraulic and hydrochemical relationships between major low gradient or medium gradient rivers (≤ 1 m/km in this paper) crossing telogenetic karst areas and the phreatic zone in karstified limestone around the river represent a topic that is not yet fully understood. The valley bottoms of medium and low gradient rivers are typically filled with fluvial river sediments (Anderson and Anderson, 2010) and the sediment thickness is affected by climatic changes (e.g., Springer et al., 2009). Hydraulic conductivity and water exchange between the river and the karstic phreatic zone may be affected by the sedimentary valley fill.

* Corresponding Author

[1] Faculty of Science, Charles University in Prague, Albertov 6, 128 43 Praha 2, Czech Republic. helenavysoka@hotmail.com
[2] Czech Geological Survey, Klárov 3, 11821 Praha 1, Czech Republic
[3] Institute of Geology, Academy of Sciences of the Czech Republic, v.v.i., Rozvojová 269, 165 02 Praha 6 - Lysolaje, Czech Republic

Where rivers freeze in the winter, the formation of either frazil-ice jams during river freezing or major ice jams during the spring snowmelt leads to the formation of river stretches with very steep gradients. Differences in the water level above and below the ice barrier can be as high as several meters (Matoušek, 2004). These events generate a steep hydraulic gradient between the river and the limestone aquifer.

The Bohemian Karst, located in the central part of the Czech Republic southwest of Prague, is a small karst area that is highly suitable for studying these relationships. The karst region is crosscut by a canyon of the Berounka River in a section about 8 km long. The Berounka River is a major, medium-gradient (0.79 m per km) river draining the western part of the Czech Republic. Altogether sixteen caves have been found around the river that either contain small permanent cave lakes or where water occurs periodically during river floods. This river valley suffered a major flood in August 2002 (a flood with recurrence interval of 500 to 1000 years; data from www.chmi.cz, MoE CR, 2003). Observations of the behavior of the cave lakes during this extreme event enabled us to formulate ideas about river-groundwater interaction during such major hydrological events. These observations prompted a more detailed study of the relationship between the river and the karst phreatic zone. The objective of this study is therefore to describe the hydraulic relationship between the Berounka River and nearby cave lakes during stable flow and flood events and also to describe the origin of the water in caves and its possible relationship to the river water. These data provide important information about the modern rate of speleogenetic processes.

REGIONAL SETTING

THE BOHEMIAN KARST

The Bohemian Karst is a small, isolated region with a total area of about 140 km^2 consisting of Silurian to Middle Devonian limestones that were folded and faulted during the Hercynian Orogeny. These limestones are frequently folded deep below the surface and are interbedded with non-karstic rocks (Havlíček, 1989; Chlupáč et al., 2002). The limestones are either covered by Cretaceous platform sandstones and marls or are overlain by fluvial river terraces of Tertiary and Quaternary age (Včíslová, 1980; Kovanda and Herzogová, 1986; Kukla and Ložek, 1993). The area where caves and other karst features can be directly observed is therefore much smaller than the full 140 km^2 area. While the northeastern part of the Bohemian Karst is flat, its southwestern part is hilly, with elevations between 208 and 499 m a.s.l. Deep valleys of local streams and especially of the Berounka River cut through this southwestern part. Relative elevation differences between the river valley bottom and its surrounding hills reach more than 200 m. The present day climate of the area is moderate, with mean annual precipitation of 493 mm (measured at the Beroun station, 1931–1960). The mean annual air temperature is between 8 and 9 °C.

The known caves are developed mostly in the 120 to 300 m thick Lochkovian and especially the Pragian limestone, a high-grade limestone with usually more than 95 percent CaCO$_3$ (Bruthans and Zeman, 2001, 2003). A total of 685 mostly small caves with a total length of 23.1 km have been mapped in the area as of December 31, 2010, according to the Cave Database of the Institute of Geology AS CR. Some 59 percent of them were found when exposed in limestone quarries. Three-dimensional phreatic mazes with multiple loops and irregular cross-sections predominate in the Bohemian Karst. There are also several bathyphreatic caves (Bruthans and Zeman, 2003). The known depth of loops in the bathyphreatic caves exceeds 100 m; continuations are either closed by cave sediments or too deep and narrow to be investigated by diving (Podtrat′ová Cave; Bruthans and Zeman, 2003).

The origin of the caves is not yet fully understood. Bosák et al. (1993) believed that the caves mostly originated by mixing-corrosion of river water with water from the limestone aquifer during the late Cretaceous and Paleogene, when the relief was relatively flat, with broad river valleys. Bruthans and Zeman (2001) proposed the idea of cave evolution by diffuse recharge from the Cretaceous sandstones that covered the whole region in the past and by injection of floodwaters of the Berounka River and its Tertiary precursor, the Paleo-Berounka River (Žák et al., 2001b). Some caves are clearly hydrothermal in origin (Cílek et al., 1994; Bosák, 1998); but there are no indications for hydrothermal origin in most of the caves in the area.

The main present-day regional aquifer is developed in the same lithological sequence as most of the caves (Bruthans and Zeman, 2001). Based on thermal modeling, recent groundwater circulation in the main aquifer occurs in synclines down to depths of about 600 m below the surface (Žák et al., 2001a). Sinks of surface streams, stream caves, dolines, and other surface karst features common in classical karst areas are generally absent in the Bohemian Karst (Bruthans and Zeman, 2003).

THE BEROUNKA RIVER AND ITS VALLEY

The study area (Fig. 1) surrounds an 8 km long section of the Berounka River canyon between the towns of Beroun and Karlštejn. The Berounka River is the only large stream in the area, with a catchment area of 8284.7 km^2, mean flow rate of 35.6 m^3 s^{-1}, calculated 10-year flood flow (Q$_{10}$) of 799 m^3 s^{-1}, and calculated 100-year flood flow (Q$_{100}$) of 1560 m^3 s^{-1}. During the August 2002 flood, the peak flow was 2170 m^3 s^{-1}. (All data are from the Beroun gauge, located just above the beginning of the karst canyon; data from www.chmi.cz, see also MoE CR, 2003). During normal summer water levels, the river elevation changes from 213 to 209 m a.s.l. The mean gradient of the water level of the Berounka River in the studied section is 0.64 m per km, locally varying
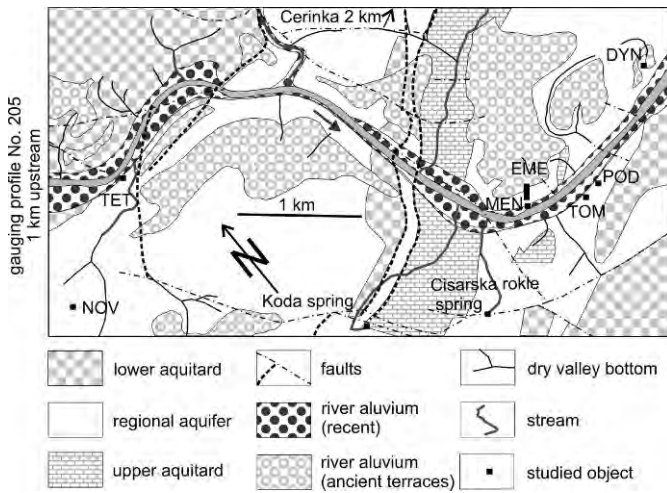
Figure 1. The study area along the Berounka River in the Bohemian Karst. The full names of the caves are given in the text. The geology is based on a 1:25,000 geological map (Havlíček, 1989).

between 0.4 and 1.1 m per km (Fig. 2). Overbank flooding begins approximately at a flow of 450 $m^3 s^{-1}$ (i.e., a water-level increase of more than 3 m). Local streams entering the Berounka River in the Bohemian Karst have catchments

up to tens of km^2. Only the larger Kačák (Loděnice) stream has a larger catchment, 271.1 km^2, and the mean flow at its confluence with the Berounka River is 0.53 $m^3 s^{-1}$. Most of the catchment area of the Kačák stream is outside of the karst area.

From written records and flood marks preserved in the river valley, it can be concluded that floods similar to the Q_{100} peak flow or higher occurred seven times during the last 500 years, in 1598, 1655, 1675, 1769, 1784, 1872, and 2002 (Elleder, 2004; Žák and Elleder, 2007). The highest flood ever recorded occurred on May 25, 1872, when the maximum water level in the village of Srbsko, in the middle of the studied river section, was 7.7 m above the usual level there, 0.47 m higher than during the 2002 flood (Žák and Elleder, 2007).

The August 2002 flood affected most of the Czech Republic. The Berounka River water level rose as a result of heavy rains that occurred August 6–13 in southwestern Bohemia. River peak at the Beroun gauge occurred at midnight on August 13, with peak flow of 2170 $m^3 s^{-1}$ (www.chmi.cz). The mean river slope during the flood was similar to that of the normal water stage, 0.66 m and 0.64 m per km, respectively (data from Žák and Elleder, 2007; see Fig. 2). Local variations in the gradient were smaller during the flood compared to normal flow.

Figure 2. Profile of the Berounka River (Žák and Elleder, 2007). Triangles represent the elevations of the cave lakes. The lower line and solid triangles are for normal flow (100 cm on the Beroun gauge), and the upper line and open triangles are for the peak of the 2002 flood. The gradients (‰ or m per km) are indicated for local stretches of the river.

Table 1. Parameters of the cave lakes.

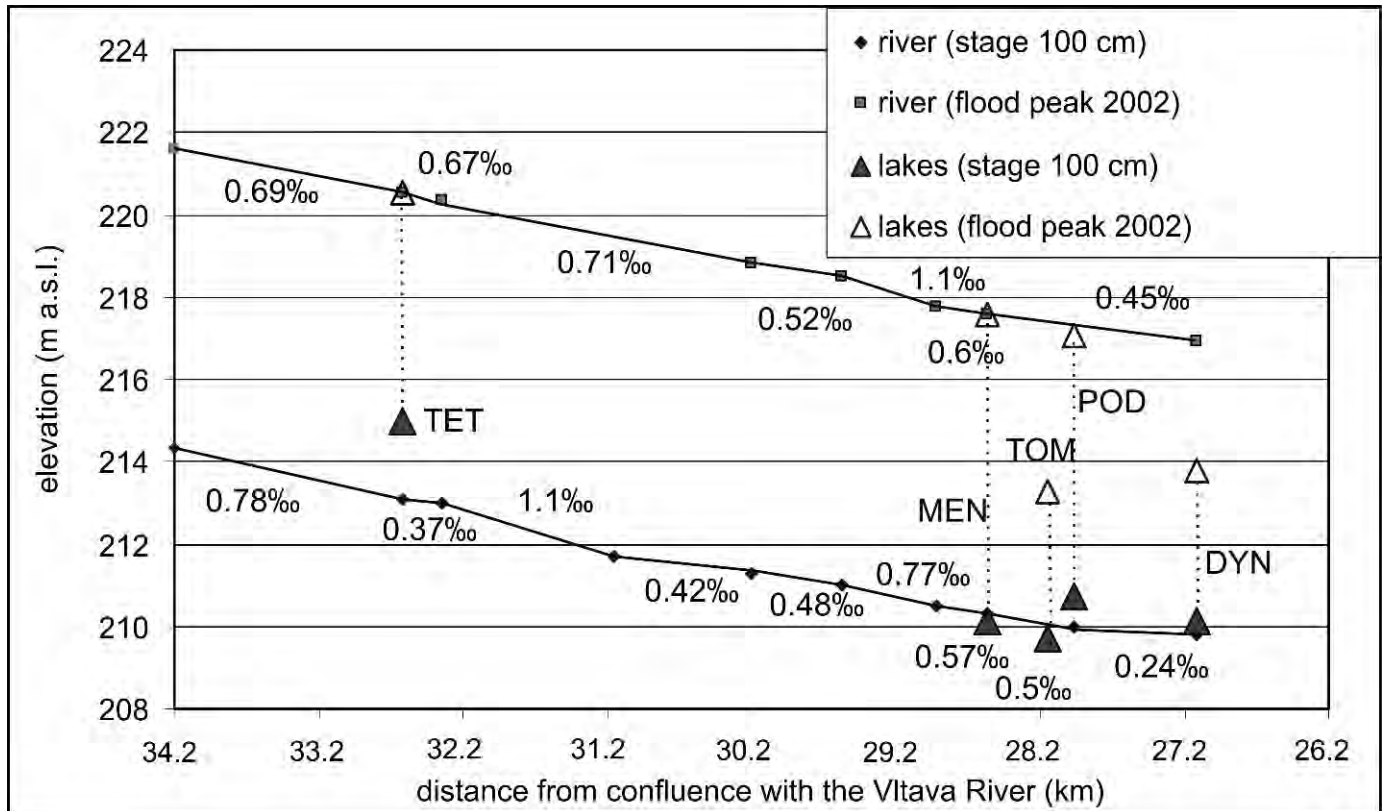| Cave	Abbreviation	Cave length (m)	Cave lake above the Berounka river (m)	Lake depth (m)	Lake surface (m^2)	Distance from river[a] (m)	Distance from river[b] (m)	Landuse above cave
Podtratova	POD	180	±0.3	67	18	55	20	unused; bushes
Tomaskova	TOM	80	±0.3	2	5	170	120	abandoned quarry; bushes
Dynamitka	DYN	180	±0.3	1.5	12	190	140	abandoned quarry; forest
Menglerova/ Emental	MEN/EME	15/1884	±0.3	6	14/50	40	0	unused; bushes-agricultural land
Tetinska	TET	8.5	+1.9	0,5	0–8	50	0	unused; bushes - buildings
Nova	NOV	156	+70	0–15	0–75	1200	1200	abandoned quarry; bushes

[a] Nominal stage.
[b] Flood culmination 2002.

The evolution of the studied section of the Berounka River valley during the Tertiary and Quaternary was quite complex. Starting in the Oligocene and early Miocene, the paleo-Berounka River formed a wide valley with bottom located about 70 m above the present riverbed (Kukla and Ložek, 1993; Žák et al., 2001b). The same wide valley was used again during the early Pleistocene. During the Pleistocene, after 780 ka BP, as indicated by paleomagnetic and paleontological studies (Horáček and Ložek, 1988; Kočí, 1991; Kovanda, 1991), the Berounka River started to cut a narrow canyon, in which individual river terraces, corresponding to middle Pleistocene climatic changes, are preserved locally. The area of the Bohemian Karst was never glaciated during the Quaternary. During the last glacial period (Weichselian), the deepest level of the river bottom was several meters below the present bed. During the late Weichselian or early Holocene, the bottom of the valley was filled in with gravel and sand, forming a flat floodplain. These coarse-grained alluvial sediments are 8.0 to 13.5 m thick, based on borehole data (Včíslová, 1980), and are usually covered by a 0.5 to 2.5 m thick layer of late Holocene fine-grained fluvial sediments (Žák et al., 2010).

The hydraulic conductivity of the coarse alluvium ranges between 10^{-4} and 10^{-2} m s^{-1}, based on pumping tests conducted over the area (Včíslová, 1980). The vertical hydraulic conductivity of the late Holocene fine-grained fluvial cover of the floodplain varies between 10^{-5} and 10^{-4} m s^{-1}, based on field infiltration tests. The hydraulic conductivity of the limestone aquifer (mainly fracture and karstic porosity) is between 10^{-8} and 10^{-4} m s^{-1}, based on pumping tests in the area (Včíslová, 1980). The storativity of the limestone aquifer, derived from integration of the spring yield together with monitoring of the water level recession at the boreholes, is 3 to 7‰ (Bruthans and Zeman, 2000).

STUDIED CAVES

Six caves that contain small lakes and are located on both sides of the river were chosen for regular monitoring (Table 1, Fig. 1). Five of them are situated relatively close to the Berounka River: Menglerova Cave (abbreviated MEN), which is connected with the Ementál Cave (EME) by an open conduit (sump), Dynamitka Cave (DYN), Podtraťová Cave (POD), Tomáškova Chasm (TOM), and Tetínský Vývěr Cave (TET). These caves occur between 40 and 190 m from the river channel. The Nová na Damilu Cave (NOV), situated approximately 1 km away from the river at a much higher elevation, with no river influence but with highly variable water level, was also included. Since the studied caves are located within the steep slopes of the canyon, the unsaturated zone above the cave lakes is several tens of meters thick. Under normal flow conditions, the river channel is not directly connected with any of studied cave lakes. The alluvial sediments block direct, rapid infiltration of river water into the limestone aquifer. Under the flood regime, the water level in the river reaches solutional openings in the limestone sides of the canyon
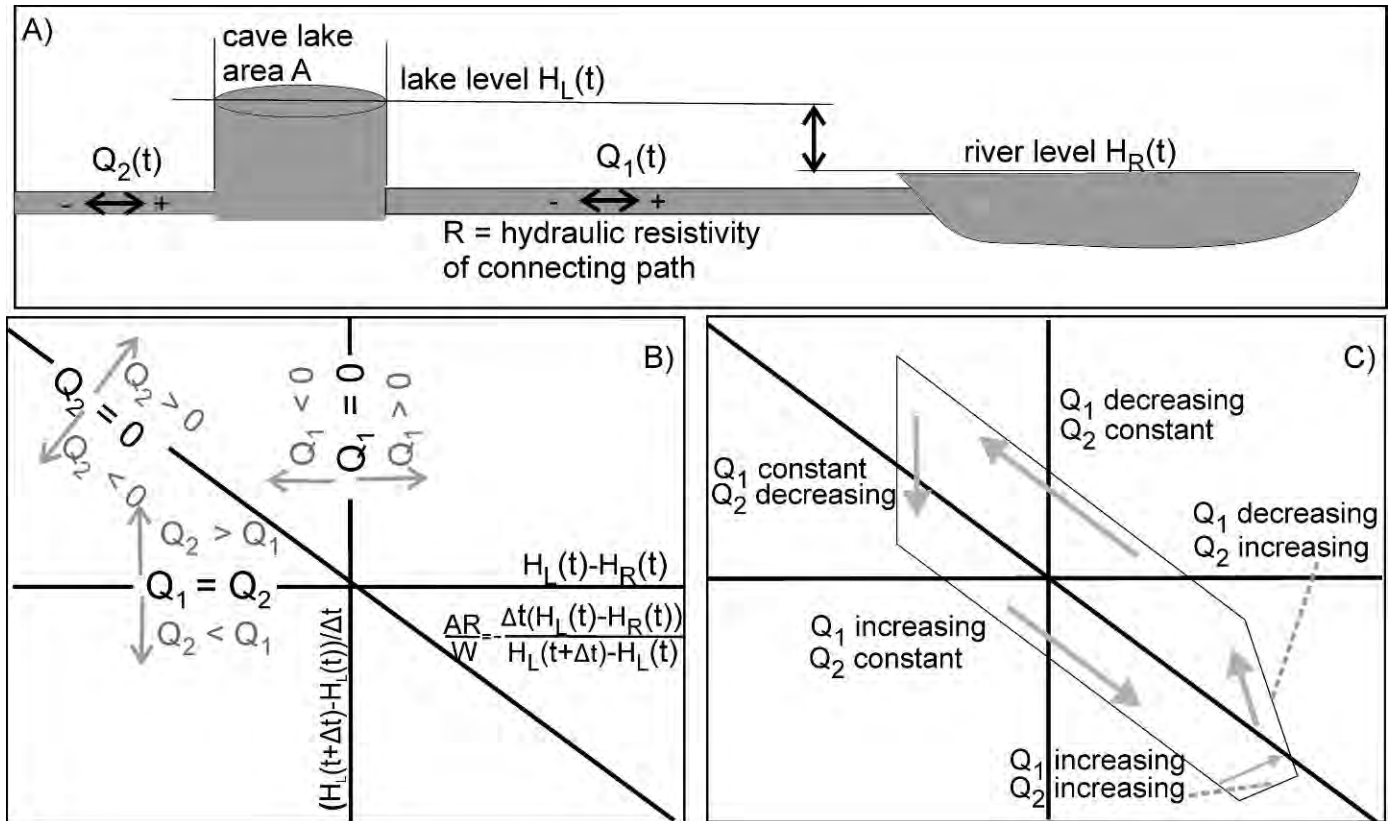
Figure 3. The model of the hydraulic relationship between the river and a cave lake. See Equations 3–6. A. The geometry of the model. B. Relationship of Q_1 and Q_2 to the axes in Figure 6. C. An example of a possible time evolution of Q_1 and Q_2.

(mostly the entrances of the caves). In the MEN-EME cave system, sedimentary evidence shows that floodwaters can rapidly reach even very distant parts of the cave, and is a perfect example of a flood-flow labyrinth (sensu Palmer, 1991).

Quarries close to the studied caves have quarry bottoms above the highest groundwater level and the highest floods. Quarry debris does not block the artificial entrances anywhere. Above the active phreatic and epiphreatic zones, the studied caves have dry, now inactive sections that extend up to several tens of meters above the groundwater level. These dry sections were locally partly quarried out, but did not impact on deeper cave sections. Therefore, the influence of quarrying on the hydraulic regime of studied caves can be considered to be negligible.

METHODS

The maximum water level of the August 2002 flood in the valley and in the caves was marked for later measurements. After the flood, plastic water-gauging laths were placed and fixed by screws in the six caves, as well as on the bank of the Berounka River close to the caves. The altitudes and positions of the laths outside the caves and cave entrances were measured by a total station with precision of ±5 mm (Sokkia and Topcon). The peak water

levels of the 2002 flood at several profiles within the studied valley and the elevations of historical flood marks were measured in the same way. The data of Žák and Elleder (2007) were used for comparison. The elevations of the laths inside caves were measured by a precise inclinometer and a laser rangefinder (Disto Lite 5, Leica Co.).

Three cave lakes (in MEN, DYN, and POD Caves) were equipped with pressure and temperature sensors (Lucas) connected with data loggers and automatically measuring the water level and temperature every 30 minutes with an accuracy of ±1 cm and ±0.03 °C, respectively (LGR, Geomon Co.). The submerged pressure sensors are connected to the atmosphere by a capillary tubes to compensate for air pressure changes.

The conductivity, temperature, and pH were measured in the cave lakes and river water using portable devices (Cond 340i, pH 330i, WTW Co.) on a monthly basis. The cave lakes and the Berounka River were sampled monthly for chloride, a conservative tracer. Samples for major chemical analysis were taken during high flow (April 2003) and low flow (September 2003). Samples for ^{13}C and major chemistry were taken in October 2007.

Water chemistry was analyzed by FAAS, HPLC, and titration in the laboratories of the Czech Geological Survey. Samples for chloride content were analyzed by argentometric titration. Samples for the ^{13}C determination

of HCO_3^- were collected in vapor-tight containers with zero headspace, and the bicarbonate was immediately precipitated as $BaCO_3$ in the laboratory. For the isotope measurement, the $BaCO_3$ was converted to CO_2 by the usual reaction with 100% H_3PO_4. The ^{13}C measurements were performed on a Finnigan Mat 251 Mass Spectrometer in the laboratories of the Czech Geological Survey with an analytical error of $\pm0.1‰$. The results are expressed in the usual delta notation against the international PDB standard.

The saturation indexes with respect to calcite were calculated from the chemical analyses data and field pH measurements using the PHREEQC 2.14 code (Parkhust and Appelo, 1999).

Communication between the river and the limestone caves through the alluvium was modeled as nonstationary 1D flow in a vertical plane normal to the river flow and assumed an unconfined aquifer. The model was governed by the nonlinear parabolic partial differential equation

$$S\frac{\partial u}{\partial t} = \frac{\partial}{\partial x}\left(Ku\frac{\partial u}{\partial x}\right), \quad (1)$$

where x is the distance from the river, t is time and u is the hydraulic head. The model contains two parameters, hydraulic conductivity K and the storativity S of the aquifer. The Rothe method was applied to discretize the problem in time, and the Galerkin method with finite elements was utilized when solving the resulting elliptic boundary value problem. The output data are the hydraulic head u and discharge q given by

$$q = -Ku\frac{\partial u}{\partial x}. \quad (2)$$

The model and the measured data sets were used to solve the inverse problem of determining the model parameters at the three locations. The first results made it obvious that the connecting paths between the river and cave lakes are under confined aquifer conditions. This allowed the authors to introduce transmissivity T and to simplify the model in the linear form

$$S\frac{\partial u}{\partial t} = T\frac{\partial^2 u}{\partial x^2} \quad (3)$$

Equation (3) was used to simulate the hydraulic head propagation between the river and the cave lakes. The low values of the storativity made it possible to assume $S = 0$ and to further simplify the model, illustrated in Figure 3, to

$$Q_1(t) = W\frac{H_L(t) - H_R(t)}{R}, \quad (4)$$

$$H_L(t) = H_L(t-\Delta t) + \Delta t\frac{Q_2(t-\Delta t) - Q_1(t-\Delta t)}{A}, \quad (5)$$

or more simply

$$Q_2(t) = A\frac{H_L(t+\Delta t) - H_L(t)}{\Delta t} + Q_1(t), \quad (6)$$

where

$$R = \frac{L}{T}. \quad (7)$$

$H_R(t)$ is the river level, $H_L(t)$ is the lake level, $Q_1(t)$ is the flow between the cave lake and the river, $Q_2(t)$ is the flow between the cave lake and the limestone aquifer. W is the width of the aquifer parallel to the river (m), A is the area of the cave lake (including unknown cave lakes in the vicinity of the cave), R is the hydraulic resistivity of the connecting path between the river and the cave lake, T is the transmissivity of the flowpath ($m^2\,s^{-1}$), and L is the distance between the cave lake and the river along the flowpath. R and A are considered to be constant in time, which may be a considerable simplification of reality (see below in the discussion of the simulation). $Q_1(t)$, $Q_2(t)$, R, and A are unknown, but plotting the measured values of $H_L(t+\Delta t)$ $- H_L(t)/\Delta t$ and $H_L(t) - H_R(t)$ for each cave lake in Figure 3 enables us to directly determine if $Q_1(t)$ and $Q_2(t)$ are positive or negative and which one is increasing or decreasing at a given time in the course of the flood.

RESULTS AND DISCUSSION

RELATIONSHIP BETWEEN THE WATER LEVEL IN THE RIVER AND IN THE CAVE LAKES

At steady state, the water levels in the cave lakes are at the same elevation as the water level at the closest point in the river within a measurement error of ±0.3 m. The only exceptions are the TET Cave, with an average water level of +1.9 m above the river, and the NOV Cave, which is about 1 km away from the river.

A total of twelve water level peaks with amplitudes of up to 1.5 m were documented between January and July 2004 (Fig. 4). The water oscillations in all the caves were very similar (the Pearson correlation coefficient among the cave lakes was between 0.977 and 0.990). The river water did not directly enter the caves during the period of automatic logging. The river and the cave lakes were thus hydraulically connected only via the saturated zone of the Quaternary gravels in the river alluvium.

The Beroun gauging station used for monitoring the water level in the river is situated 5.5 to 7.0 km upstream from cave lakes POD, DYN and MEN included in Figure 4. Propagation of the flood peaks down the Berounka River occurred at average speeds of 3.5 to 7.0 km h^{-1}, based on nine flow peaks in 2004. The delay between gauging station and the river in front of caves is thus in order of 1 to 2 hours, which can be neglected since individual peaks last tens of hours and more. There was a high correlation between the levels of the river and of the
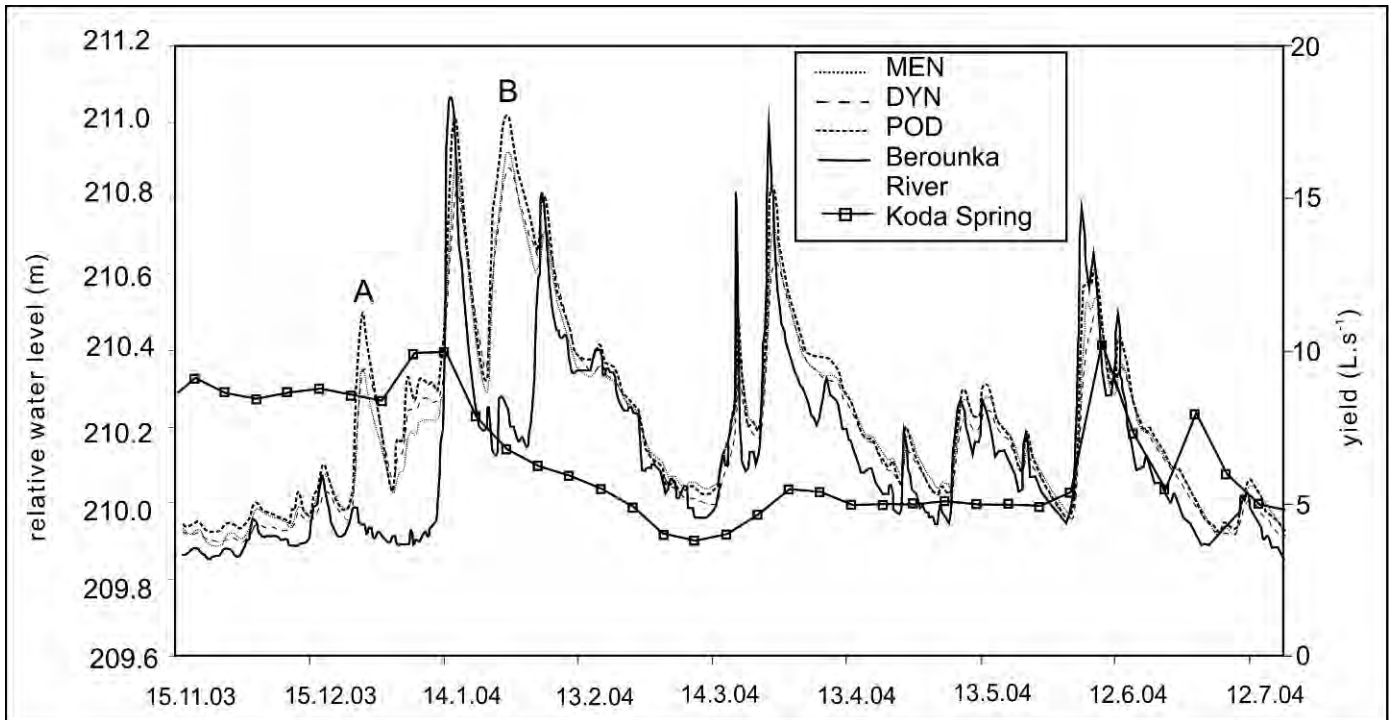
Figure 4. Water level in the river at the Beroun gauge and water levels in some cave lakes. The yield of the Koda Spring (Fig. 1; right axis) is shown for comparison. Note that the vertical position of a lake trace may be off by up to 0.3 m. Peaks A and B are due to winter ice jams downstream from the caves that affected the river near the caves but did not affect the river at the gauge. The time scale is day.month.year after 2000.
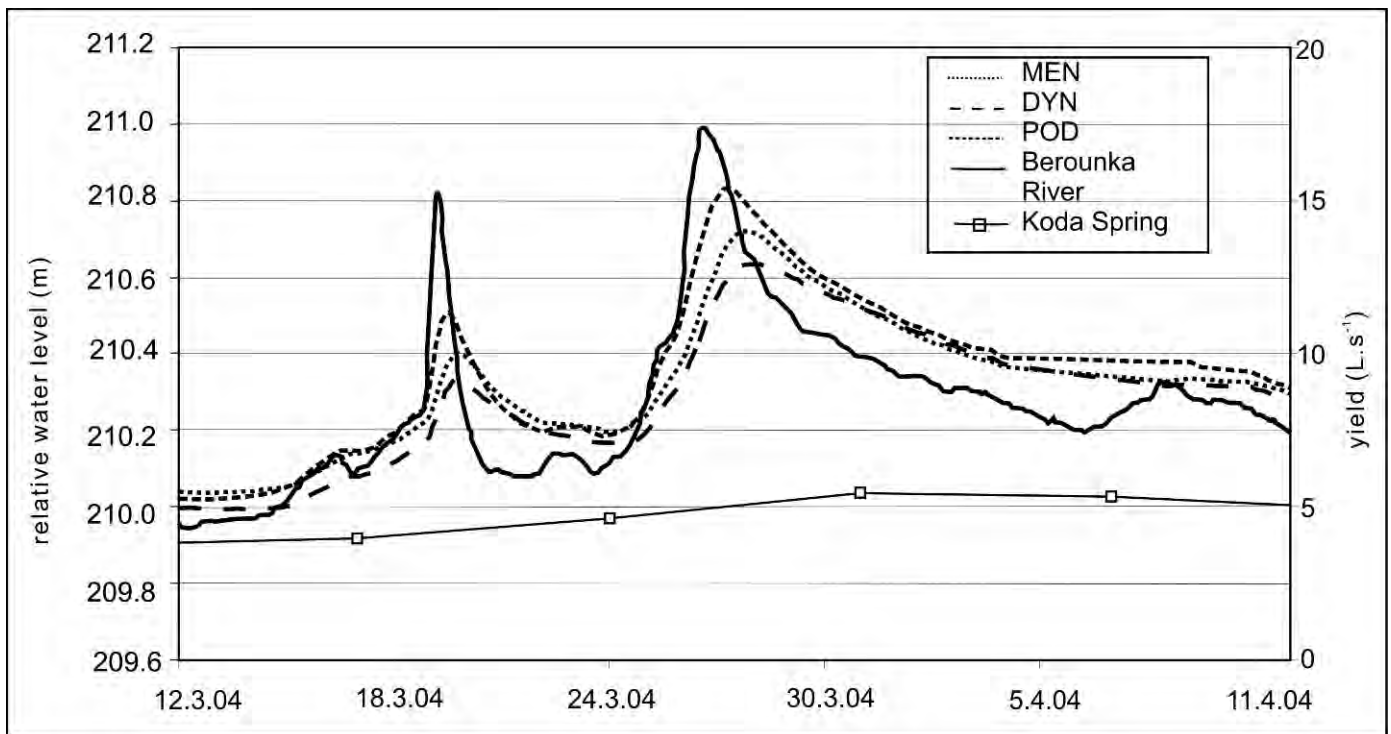
Figure 5. Detail from Figure 4 of March and early April 2004. See the caption for Figure 4 for explanation.

cave lakes. Once the river level started to rise, the lake levels rose as well, but slightly more slowly. During all the events, the fastest reaction was observed in the POD Cave, and the slowest and least prominent increase was in the DYN Cave (Fig. 5). This probably reflects the longer distance between the river and the DYN Cave (Table 1). The cave lake levels were mostly still rising when the river level started to fall. Lake levels started to decline when the river level became lower than the lake levels (Fig. 5). The lake levels' decline was very slow, taking several weeks to several months to return to the river level. Short periods with the river level above that of the cave lakes, compared to relatively long periods of the opposite relationship show that river water tends to flow into the limestone aquifer only during flood peaks. During most of time, water drains from the limestone aquifer into the river.

During the winter, two water level peaks were observed in the cave lakes that were not connected to peaks in the river level (periods designated A and B in Fig. 4). Nothing similar to these peaks was observed in the water levels of local wells or springs or in stream discharges. These oscillations of the cave lakes water levels were clearly caused by a slush-ice barrier formation on the Berounka River above the town of Karlštejn, immediately below the studied river section. Ice jams form repeatedly at this site, since the floating slush ice accumulates here at the upper edge of already fully frozen, almost stagnant water above the Karlštejn weir. Thanks to the modest river gradient, the back flooding affects the river level up to several kilometers above the ice jam and consequently also affects the monitored cave lakes, but it did not reach the Beroun gauging station situated several km farther upstream. The existence of the temporary ice jams was later confirmed by ice accumulations high on the banks of the river channel. Unfortunately, no large flood with water filling the whole floodplain and flowing directly into the cave openings occurred during the period of automatic monitoring of the cave lake levels.

The hydraulic relationship between the river and the cave lakes levels is presented in Figure 6. Time intervals affected by ice jams were not used in the graphs and calculations. Both the river and the lake level were measured very precisely over time (± 1 cm), but there is considerable uncertainty in the relative positions of these two datasets (± 0.3 m). Therefore, in parts A–C of Figure 6, the real position of the whole dataset may be shifted either to the left or to the right along the horizontal axis. In all the monitored caves, the temporal change in the cave level is clearly controlled by a difference between the level in the river and that in the cave. There is a linear relationship between these two parameters with coefficients of determination between 0.55 and 0.78. The individual measuring points do not follow the regression line exactly. Instead, there is some tendency for hysteresis (most pronounced in the POD Cave). Temporal tracks of points in the upper left-hand part of the graphs, corresponding to the rising limbs of cave lake

hydrographs, follow paths in a counterclockwise direction (see the arrows). The tracks can be interpreted by means of Figure 3, parts B and C, and Figure 6D. When the river level rises above the lake level ($H_L(t) - H_R(t) < 0$ and decreasing), Q_1 brings water towards the cave lake proportionally to the difference $H_L(t) - H_R(t)$. Q_2 is positive and the water table in the cave rises. When $H_L(t) - H_R(t)$ is most negative, Q_2 abruptly falls to 0 or even to negative values (see Fig. 3A for the meaning of negative and positive Q_1 and Q_2 values). Then the absolute value of Q_1 decreases proportionally to the decrease in the absolute value of $H_L(t) - H_R(t)$.

REACTION OF CAVE LAKES TO THE EXTREME FLOOD IN AUGUST 2002

The cave lakes were visited twice during this major flood event. The first visit took place on August 14 about 12 hours after the river peak, when the river level at the Beroun gauge was 710 cm, following a peak of 796 cm. The second visit was on August 16, when the river level had fallen to 400 cm on the Beroun gauge.

The main cause of the catastrophic August 2002 flood was intense precipitation, especially in the southern and southwestern parts of the Czech Republic, where the total precipitation in the period between August 6 and August 15 exceeded 300 mm in the mountain regions. Precipitation occurred in two separate periods, between August 6 and 7, and between August 11 and 13, when a larger amount fell. In the Bohemian Karst itself, the precipitation from August 6 to August 13 reached 130 to 160 mm, approximately twice the normal total precipitation for August. As a consequence, the groundwater level rose quickly, and intense drip water from the unsaturated zone was encountered in some caves during the August 14 visit.

Figure 2 shows the response of the cave lakes to this major flood. Their behavior can be split into the following groups: A) The Berounka River directly flooded the entrance passages of the TET and MEN Caves. After the river peaked, the water level in the caves rapidly decreased to the level of the bottom of the cave entrance. Then the water level in both caves decreased very slowly due to the low permeability of the sedimentary fill between the cave lakes and the river and also because of the intense inflow of groundwater from the limestone aquifer into the caves. In the TET Cave, the water table fell slowly for a period of 1.5 years; B) In the TOM and DYN Caves, situated 120 to 140 m away from the river, no traces of direct river water intrusion were found. This is based on conductivity (Fig. 7) and temperature measurements. No muddy water was observed in the cave lakes. In the TOM cave, the water level rose 3.5 m, as observed during the visit 12 hours after the peak of the flood. In the DYN cave, the water rose 3.6 m, and the water level had dropped only 0.2 m below the maximum level recorded in this cave by the August 16 visit, 60 hours after the peak; C) The water of the POD Cave lake was composed of a mixture of river water with groundwater (temperature 14.2 °C and high turbidity, but
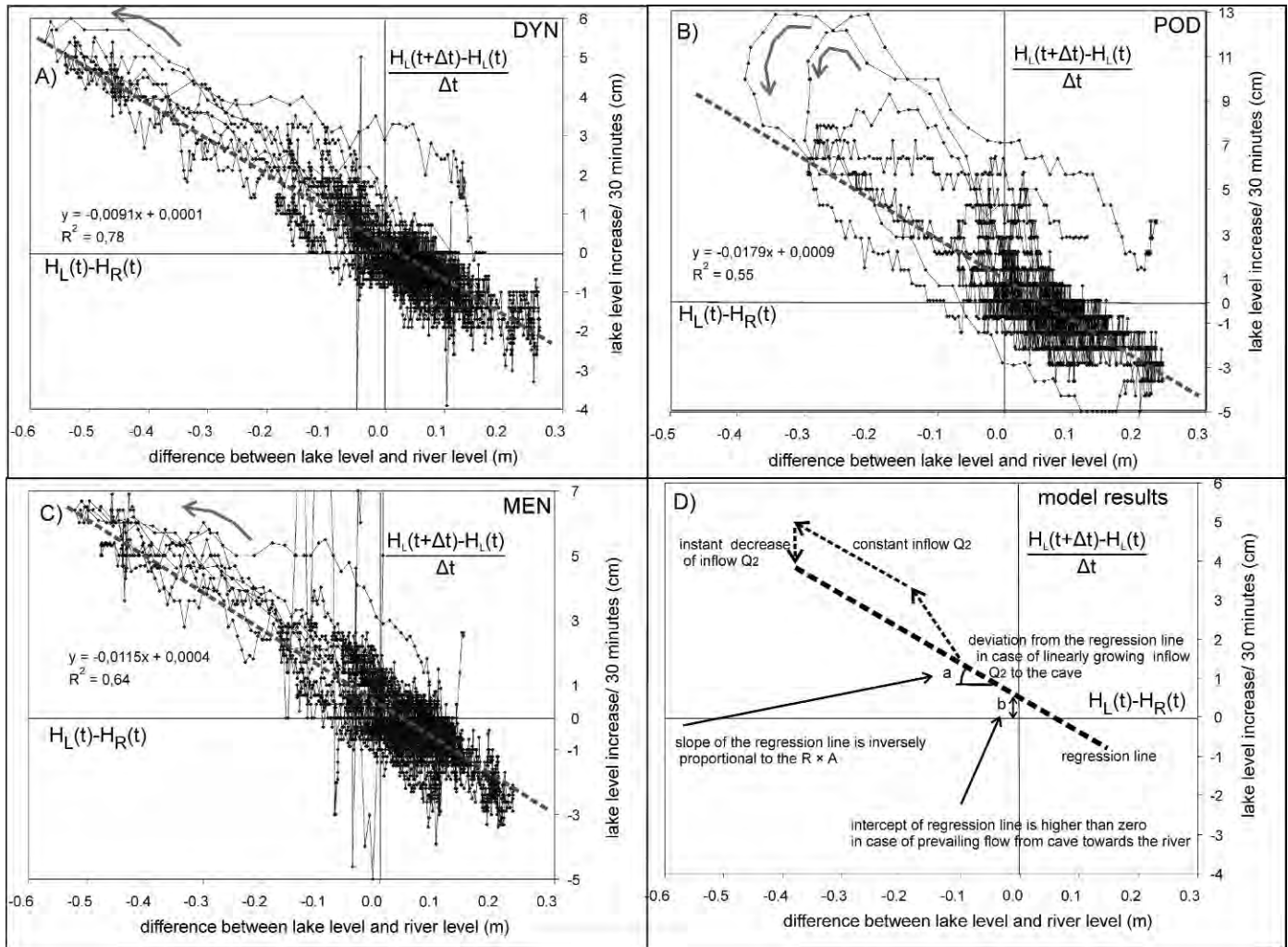
Figure 6. The relationship during the monitored period between the difference between the cave-lake and river level HL(t)–HR(t) and the change in lake level HL(t)–HL(t–1) between observations. Points are connected in time order. Bold arrows indicate trajectories during peaks of floods. Note that the positions of the data for a given cave in the horizontal direction may be consistently off by up to 0.3 m. A. DYN cave. B. POD cave. C. MEN cave. D. Illustration of the relation of these plots to the model.

higher conductivity than river water; Fig. 7). Water in the cave reached the same level as in the river. The distance of the cave lake from the river was only 20 m at the peak of the flood.

The Model of Hydraulic Head Propagation and Flow Between the River and Cave Lakes

Equation (3) governs the hydraulic-head propagation between the river and the cave lakes. Solution of the inverse problems for the transmissivity of the alluvium between 10^{-3} and 10^{-2} m^2 s^{-1} demonstrated that the storativity is $\leq 10^{-3}$ for the connecting path between the river and caves DYN, MEN, and POD. The low values of the storativity made it possible to further simplify the problem to Equations (4)–(6), which provide the model for the flow shown in Figure 3.

The relationship between the data in Figures 6A–C and this model is shown in Figure 6D. The slope indicated by angle a is inversely proportional to the product $R \times A$. The POD Cave has the highest slope and thus the lowest $R \times A$ value, while DYN has the lowest slope and thus the highest $R \times A$ value. That the intercept of the regression line is slightly greater than zero for the POD and MEN caves indicates permanent inflow into the cave lake that is drained into the river (Q_2).

The DYN Cave lake level oscillation during the 2002 flood was simulated using the slope -0.0091 of the linear regression between the difference in the DYN Cave lake and the river level and the change in the cave-lake level in 30 min time increments (Fig. 6A). The simulated level in the DYN Cave fits very well with the measured level in the cave (Fig. 8). This shows that flood water used the same path
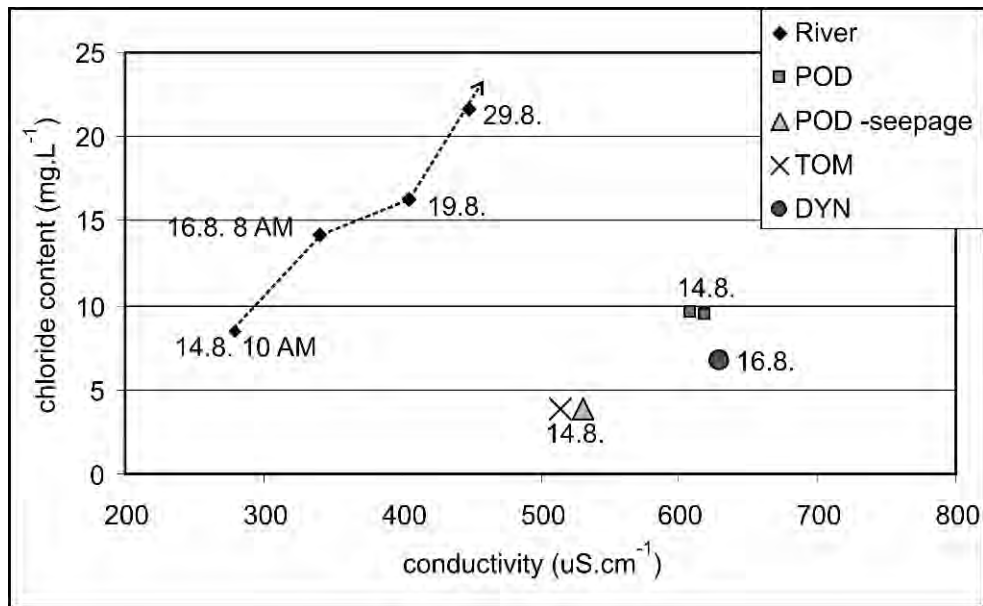
Figure 7. Conductivity and chloride contents in river water and selected cave lakes following the peak of the 2002 flood. Points are labeled by the day in August 2002.

between the river and the cave lake with the same parameters during the major flood in 2002 as during the much lower water stages when the level was logged. R × A thus remained constant even during this extreme flood. No additional conduit was activated during the flood in the DYN Cave.

The slope of the linear regression (Fig. 3 B, C, 6) can be potentially used for simulation of the lake level in other objects if tight correlation exists between $(H_L(t+\Delta t) - H_L(t))/\Delta t$ and $H_L(t) - H_R(t)$. The slope of the regression line can be used for simulation of the water table even when the relative position of the level in the river (or,
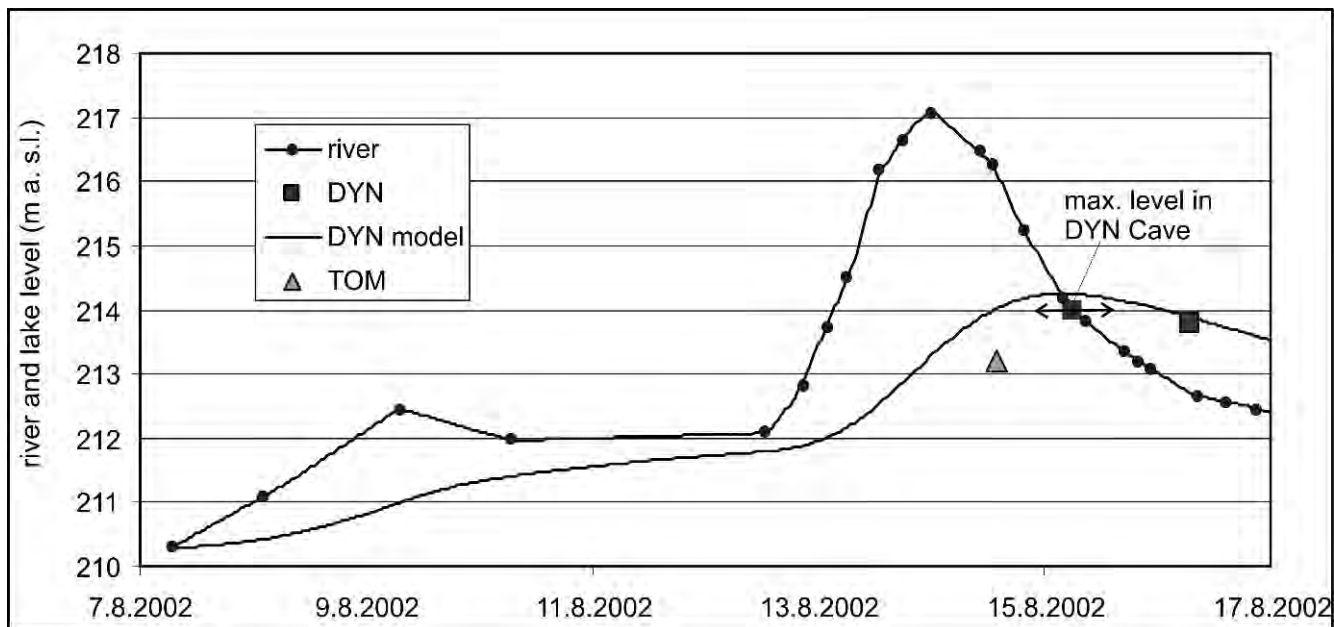
Figure 8. The flood on the Berounka River in August 2002, with some measured levels of the cave lakes. Note that the peak level of the lake in DYN is from traces left in the cave, and the timing of the peak is uncertain. The elevations of the cave lake observations relative to the river are uncertain by up to 0.3 m. The model line is a simulation based on the model described in the text and the DYN cave parameters derived from Figure 6. The horizontal axis labels are day, month, and year.
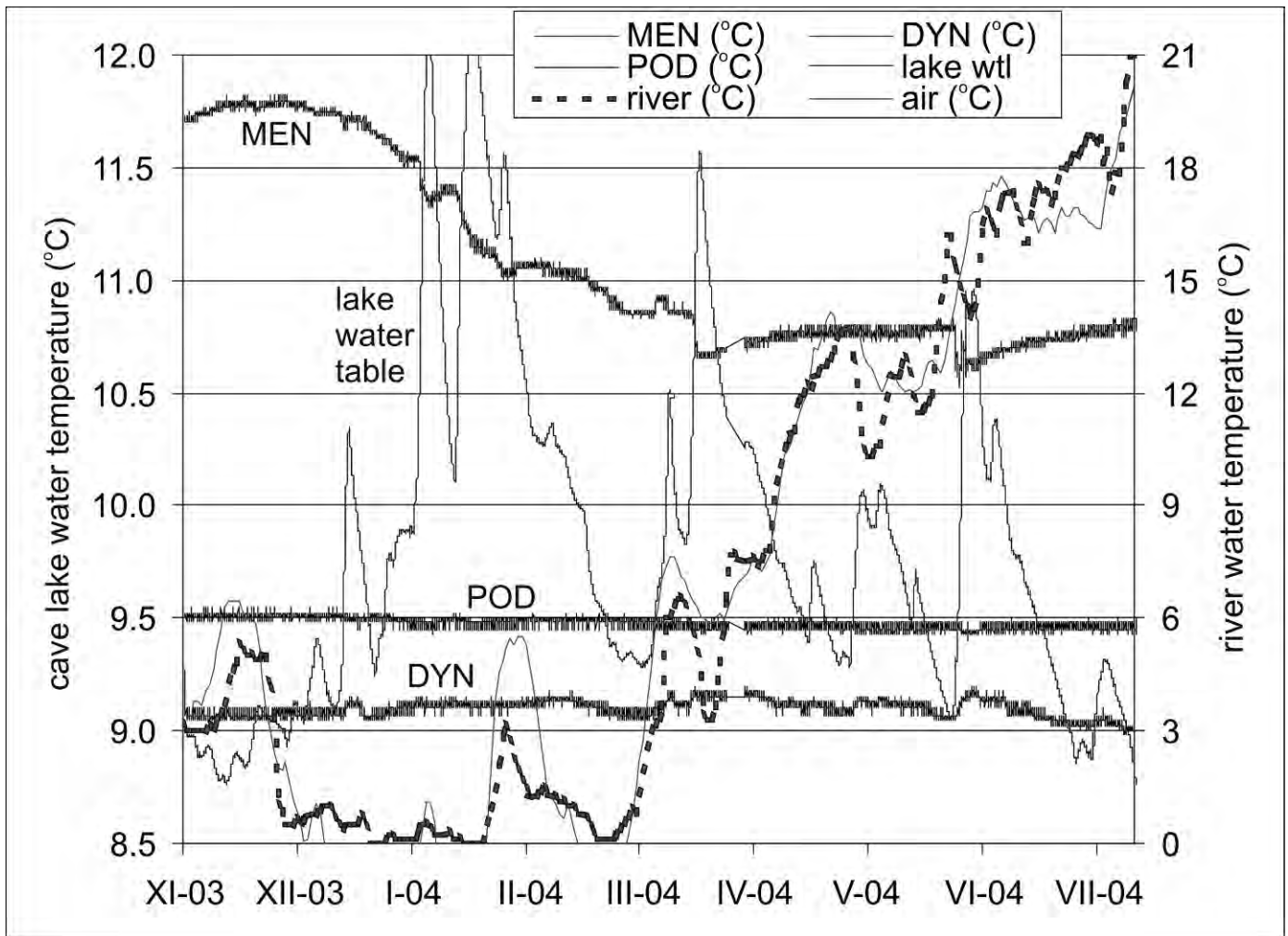
Figure 9. Measured temperatures of the cave lakes (left axis) and river and outdoor air (daily average; right axis). The water level in the POD cave lake from Figure 4 is superimposed (no scale). The horizontal scale is the month and year during the period of detailed data logging.

in general, any driving object in general) and the lake (or any dependent object such as a well) is not known exactly.

Cave Lake Water Temperature

The water temperature in the cave lakes (Fig. 9) is strongly affected by exposure of the terrain above the cave to radiation from the sun. While the TOM Cave, which is shielded from direct solar radiation by the subvertical north-facing side of the river canyon, has an annual average temperature of 8.4 °C, the MEN Cave, situated under a south-facing slope just 400 m away, has an annual average temperature of 11.1 °C.

The lake temperature in the POD Cave is stable (9.5 ± 0.06 °C), except for extreme flood events larger than those during the period of data collection. The DYN Cave exhibits a slight temperature oscillation over the range 9.0–9.3 °C, and the water temperature is directly proportional to the lake water level (r of 0.62). This can be interpreted as a rise of water with slightly higher temperature from a

deeper part of the cave lake towards the water table during a rising lake level. The TOM and NOV Cave lakes also exhibit only very limited temperature variations, based on manual measurements (less then ± 0.2 °C).

In the MEN Cave, the water temperature ranged from 10.6 to 11.7 °C. The temperature was highest in late November and lowest in June during the monitoring period, which is the opposite to the seasonal trend of the ground surface. Its temperature graph consists of a smooth sinusoidal annual oscillation with short-time deviations correlated with lake-level changes. The water temperature decreases during brief river rises even when the river water is warmer than the water of the cave lake. The MEN Cave lake's water-temperature oscillations are typical for combined heat transport (conduction together with convection), based on the study of Bundschuh (1997). Sinusoidal oscillation of the lake water temperature is generated by annual changes in the solar radiation that directly affect the soil temperature. This variation propagates with a delay, to
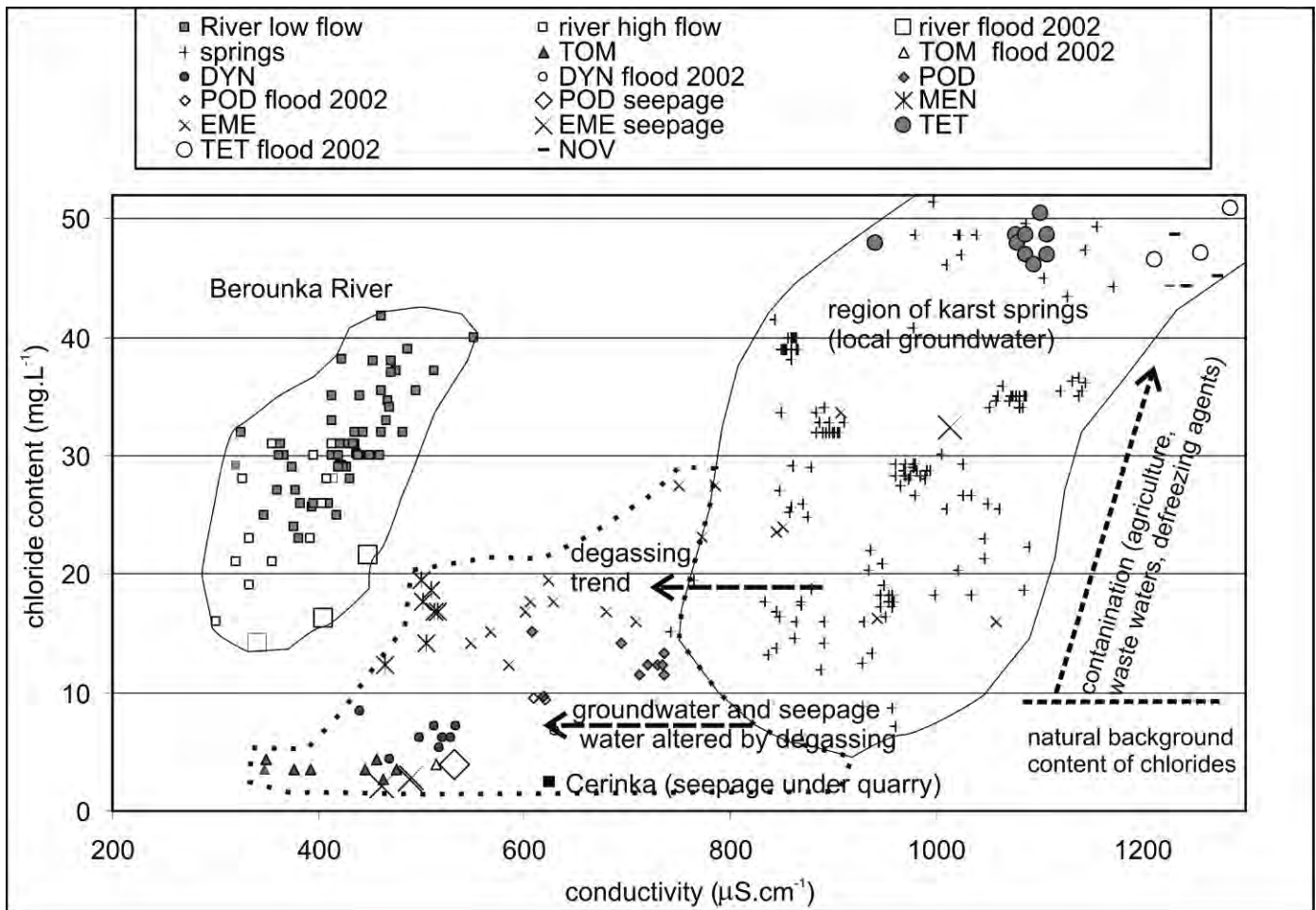
Figure 10. Plot of conductivity versus chloride content of water samples analyzed during the study. The area occupied by the river samples is clearly distinct from cave lakes, seepage, and other underground water. Degassing and calcite precipitation move underground waters horizontally to the left as shown, because chloride is conserved. The spring data (+) are from the Bohemian Karst, measured in 2000–2004. The chloride background indicated is the approximate minimum of those samples; near-surface underground water can be lower. The Cerinka quarry is 2 km north of the study area (Fig. 1).

depth by heat conduction via rocks. Short-lived peaks on the sinusoidal trend are a result of intrusion of water with lower temperature, most probably from the Quaternary gravels of the floodplain.

CHEMICAL COMPOSITION OF THE CAVE LAKE WATER AND ITS ORIGIN

The water in the caves studied can be derived from two possible sources, the Berounka River and local groundwater. About 500 pairs of conductivity and chloride-content values were measured for springs, streams, and cave lakes and pools in the Bohemian Karst in the 2000–2004 period. The water of the Berounka River has low conductivity and thus low total dissolved solids (TDS), thanks to the location of most of its catchment on silicate rocks, above the studied karst area. The chloride content of the river water is elevated, thanks to multiple sources of pollution, both urban and agricultural. The conductivity-chloride plot of the water

of the Berounka River differs from those of all the groundwater and cave lake water types of the Bohemian Karst (Fig. 10).

Springs and wells located both in the limestone and in the surrounding non-karstic rocks show considerably higher conductivity than the river water thanks to higher TDS. The chloride content varies from 6 to more than 50 mg L^{-1}, depending on the degree of pollution in the catchment of a particular spring. The cave lake of the Čeřínka Cave, situated under an open limestone quarry 3 km away from the river (Fig. 1), exhibits a chloride content as low as 2 mg L^{-1}, thanks to the very low evapotranspiration enrichment of chloride ions in water infiltrating into limestone fractures with lack of soil cover removed by quarrying. Cave lakes and pools that retain water from the unsaturated zone could be split into two groups, based on their observed chemistry.

Some of the lakes and pools fall inside the field typical for the karst springs (Fig. 10) and their chemical composition is

Figure 11. Bicarbonate and δ¹³C values for some samples analyzed in this study. Bohemian karst springs fall in the area outl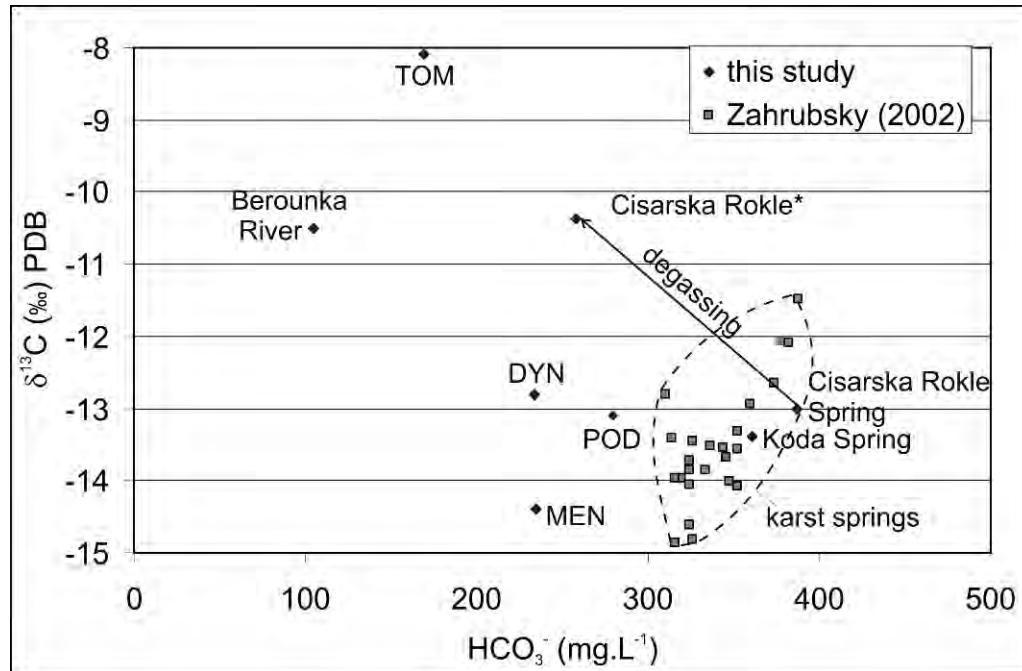ined. As an example of the effect of degassing, values for the Cisarska Rokle Spring (Fig. 1) are shown at the spring and after 1 km of flow on the surface toward the river (*).

also the same (NOV Cave, TET Cave, part of EME Cave. These lakes are recharged by local groundwater with no subsequent changes in the water chemistry.

Some lakes and pools exhibit low conductivity and low chloride content (the TOM, DYN and POD Caves and some of the EME Cave pools). On the conductivity-chloride plot, they fall neither in the field of karst springs nor in the area of Berounka River water (Fig. 10). As chloride is a conservative tracer, these waters cannot be derived from river water, which has a much higher chloride content. The calcium and alkalinity contents in some of these waters are up to two or three times lower than those of the karst springs. Other components have similar concentrations to those measured in the karst springs. These compositions can be explained by prolonged equilibration of the water with a cave atmosphere containing low CO_2 partial pressure (0.04 to 0.18 vol. % CO_2 in the studied caves).

Long-term stagnation of water in lakes and pools and high water pH are in agreement with this explanation, as are their high δ¹³C values (Fig. 11). The TOM Cave lake shows the most significant loss of calcium and bicarbonate ions by CO_2 degassing and calcite precipitation. It contains only 66–70 mg L^{-1} calcium compared to 140–200 mg L^{-1} typical for the karst springs of the area. In the TOM and POD Caves, the content of both components varies slightly over time, probably due to variations in the intensity of flow through the cave lake and mixing of stagnant lake water with water from the unsaturated or saturated zones. Generally, the lowest TDS and highest pH values were

detected during the winter of 2003–2004, after a more than year-long recession in groundwater levels. The very low chloride content in the TOM Cave shows that the cave lake is predominantly supplied from direct infiltration in the quarry above the cave.

We studied the temporal behavior of chloride to discover whether the cave lakes are partly recharged by river water (Fig 12). The figure clearly demonstrates that the temporal trends in river water and cave lakes are different. During the recession (March 2003 to October 2003), the chloride content generally rose in the river water, whereas it was quite stable in the cave lakes. It decreased slowly in the MEN Cave lake, probably as a consequence of dilution of the river water injected during the 2002 flood by local groundwater. Inflow of river water was thus not observed in any of the studied caves during low and normal water stages.

The cave lakes were slightly oversaturated with respect to calcite (SI 0.2 to 0.7). River water was undersaturated with respect to calcite during high water stages (SI −0.5) but oversaturated during low and normal water stages (SI 1.0 to 1.3).

Interaction Between the River and the Limestone Aquifer: A Model

Based on observations of the water level in wells and caves located farther away from the river, the minimum hydraulic gradient in the limestone aquifer is between 1 and 2%, and locally higher. The river slope is significantly less (0.064%, on an average, see Figure 2). Therefore the groundwater tends to
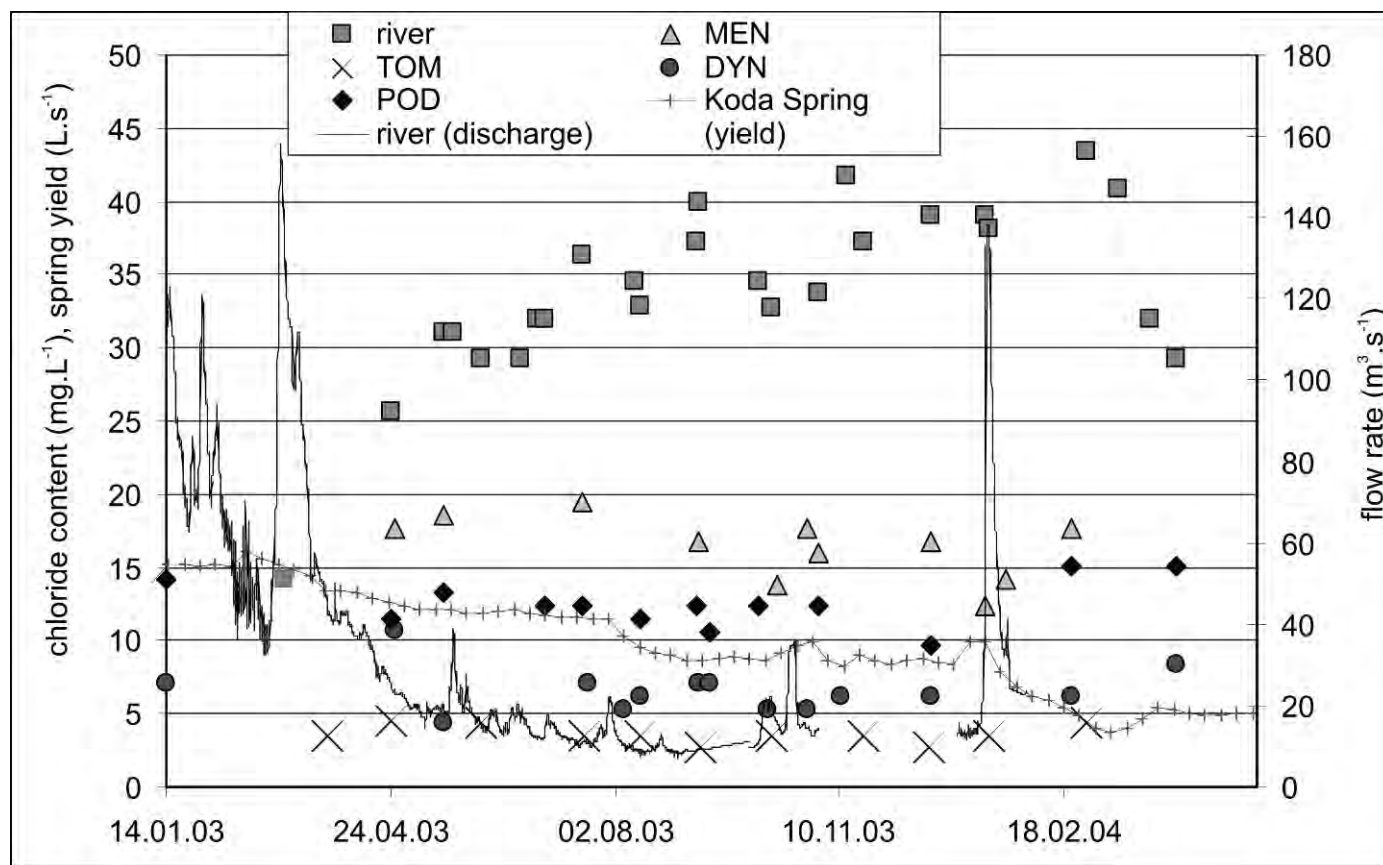
Figure 12. Chloride content in the river and monitored cave lakes. The discharge (not level) of the river at the Beroun gauge is shown for comparison, as is the yield of the Koda Spring (Fig. 1). The time scale is day.month.year after 2000. Note that the period covered is different from that of Figure 4.

discharge into the river at steady state. River water enters the limestone aquifer only temporarily, during flood events or during winter ice jams, when the high water level in the river canyon injects river water into the limestone aquifer. During major floods, the water level in the limestone aquifer is several meters below the water level in the river, thus enabling very effective injection of floodwaters into the karst porosity up to a distance of a few hundred meters away from the river (e.g., the EME Cave). After floods, water returns back to the river by the same path.

Observations of cave lakes during the August 2002 flood clearly demonstrated the importance of open cave entrances for flooding by river water. Caves with open entrances at elevations accessible to flood intrusion were extensively flooded by river water. Caves separated from the river by a Quaternary alluvium were flooded by elevated groundwater instead of river water. The water level in such caves rose to only about half of the river's peak level. River water penetrated only a few tens of meters into the limestone aquifer in these cases.

Under current conditions, massive flood-flow injection only occurs in caves, such as MEM, EME, and TET, with exposed openings below the level of river floods, which, as in 2002, can be up to 7 m above the normal river stage. In caves

separated from the river by Quaternary alluvium, flood-flow injection is strongly reduced or absent at the present time. In those caves, flood-flow injection was a very important process during some periods within the last two glacial periods, when the rocky faces of the river canyon were not covered by fine-grained sediments and river water was easily injected into fractures and cave openings. At present, the flood-flow injection is also reduced by anthropogenic factors, especially the 1 to 2 m thick late Holocene fine-grained fluvial sediments covering the floodplain surface, largely the result of enhanced erosion due to deforestation and extension of agriculture in the river catchment since the thirteenth century.

The shape of vertical section of the caves is also an important factor for the extent of river-water penetration into the limestone aquifer during a flood (Fig. 13). In highly permeable shallow cave passages, where part of the passages is situated in the epiphreatic (periodically flooded) zone, the river water can penetrate several hundred meters into the limestone aquifer, as there is enough room for incoming river water. (EME Cave is an example.) In high volume phreatic loops connected to only small spaces in the epiphreatic zone, the rising water fills less volume. Consequently, river water cannot penetrate farther into the limestone aquifer (TOM and POD caves).
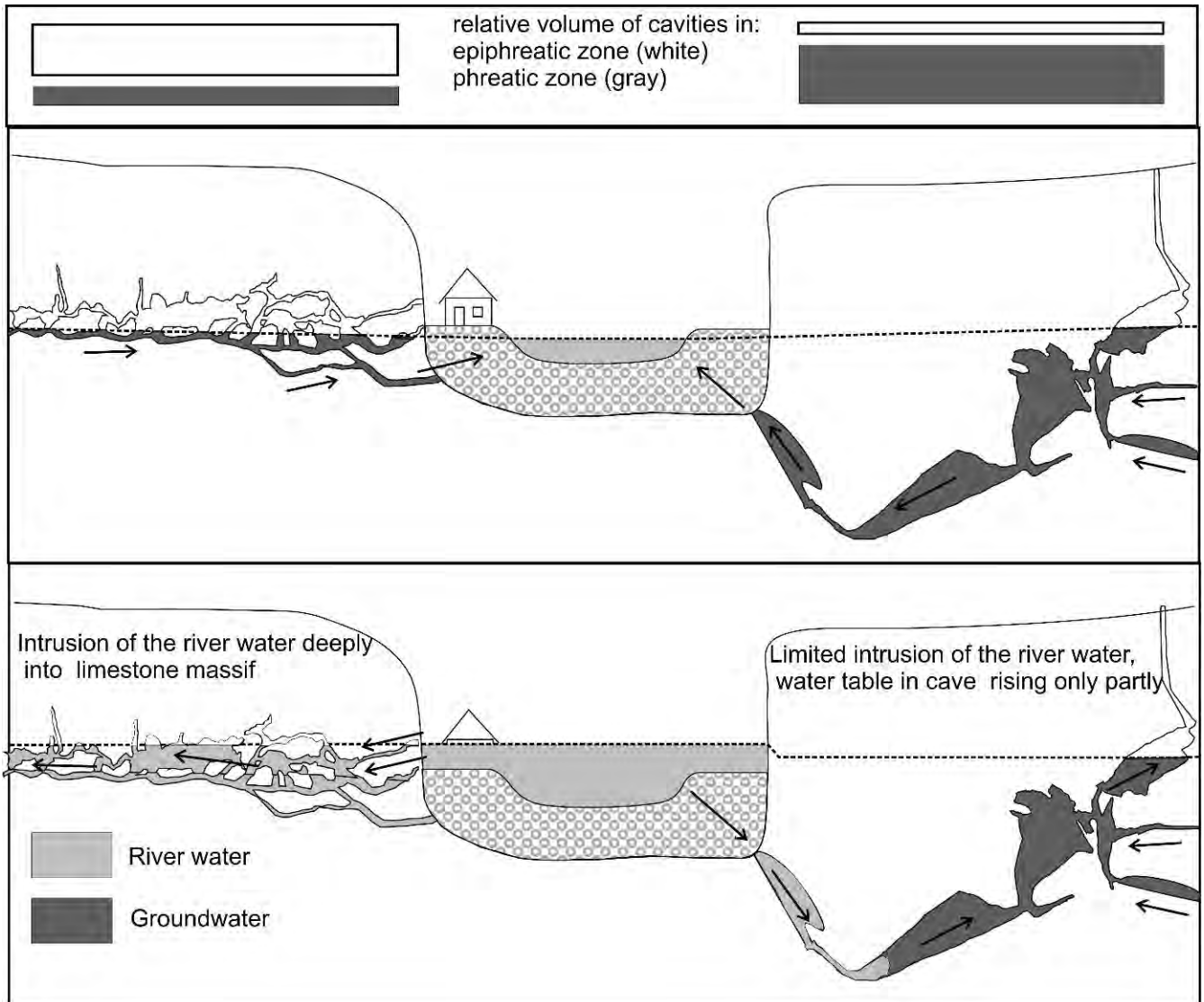
Figure 13. Conceptual models of flow between the river and limestone aquifer during, top, normal river stage and, bottom, a high flood that reaches entrances above the alluvium. The cave on the left is predominantly epiphreatic and has entrances directly accessible to floods; the cave on the right is predominantly phreatic and connects to the river only through alluvium.

One new result of this study was the observation of water level increases in the river (and in the cave lakes) related to ice jams blocking the river and thus elevating the river level during the winter. These ice jams are of two types, formed by either the accumulation of moving slush ice during the periods with the lowest temperatures or spring ice during the spring thaw. Historically, ice jams have been recorded on the Berounka River (e.g., in 1940, 1942 and 1947; Matoušek, 2004) that locally increased the water level by more than 5 m. During the summer floods, the river-water density is usually lower than that of the cave-lake water, and the river floodwaters mostly penetrate into the cave in the upper part of the water column of the flooded section. The water of winter floods can be more dense than the water of cave lakes and thus penetrates preferentially into their deepest parts.

The behavior of floodwaters derived from summer floods and winter floods related to ice jams might therefore be different in the flooded cave sections.

During the glacial periods, increases in the water level in the river caused by ice jams could have been much more frequent than in the contemporary climate. The difference in the water level above the ice jam and below it can be several meters. This can induce strong injections of river waters into the karst and even the formation of karst flow paths in the limestone massif parallel to the river.

CONCLUSIONS

Based on the results presented in this study, the following conclusions can be reached regarding the relationships

between the cave lakes and the adjacent medium-gradient Berounka River:

During minor water level peaks in the river of up to 1.5 m above normal, a water level oscillation in the karst aquifer is induced. The oscillation amplitude is slightly dampened and delayed compared to that in the river. Based on the groundwater chemistry, it can be concluded that the river water did not flow more than a few tens of meters into the karst aquifer behind the rocky slopes of the river canyon and did not reach the sampled cave lakes. Low bicarbonate contents and high $\delta^{13}C$ values indicate that some of the cave lakes' waters are stagnant and undergo CO_2 degassing accompanied by calcite precipitation.

During major river floods (recurrence interval >100 years), the river water rapidly floods the caves through openings in the sides of the river canyon, while those connected to the river only via the alluvium are flooded by the elevated groundwater level, and the increase in the water level in them is only about 50% of the increase in the river level. A simple hydraulic model was successfully used to simulate and explain the water table oscillations in the cave lakes.

Thanks to the very low gradient of the river, the river water cannot infiltrate into the limestone aquifer and flow there parallel to the course of the river. Instead, river water is injected into the aquifer only during flood events before and during the peak. Then the water drains back into the river. This process is substantially impeded by low-permeability late Holocene fine-grained fluvial sediments that cap the coarse gravels in the river floodplain.

Increases in the level of the river by ice jams were recognized as one factor that can be important in speleogenesis. Under these events, temporary flow of river water through the karst aquifer parallel to the river is possible because of the very high relief across the ice dam.

Fast speleogenesis by means of flood injection could be expected in periods when the river canyon was bare or filled by gravel alone. Such conditions characterized the last two glacial periods and transition to the Holocene in the studied river valley.

ACKNOWLEDGMENTS

REFERENCES

Anderson, R.S., and Anderson, S.P., 2010, Geomorphology: The Mechanics and Chemistry of Landscapes Cambridge University Press, 640 p.

Bailly-Comte, V., Jourde, H., and Pistre, S., 2009, Conceptualization and classification of groundwater-surface water hydrodynamic interactions in karst watersheds: case of karst watershed of the Coulazou river (Southern France): Journal of Hydrology, v. 376, p. 456–462. doi: 10.1016/j.jhydrol.2009.07.053.

Bailly-Comte, V., Martin, J.B., Jourde, H., Screaton, E.J., Pistre, S., and Langston, A., 2010, Water exchange and pressure transfer between conduits and matrix and their influence on hydrodynamics of two karst aquifers with sinking streams: Journal of Hydrology, v. 386, p. 55–56. doi: 10.1016/j.jhydrol.2010.03.005.

Bosák, P., 1998, The evolution of karst and caves in the Koněprusy region (Bohemian Karst, Czech Republic), Part II: Hydrotermal paleokarst: Acta Carsologica, v. 27, no. 2, p. 41–61.

Bosák, P., Cílek, V., and Bednářová, J., 1993, Tertiary morfogeny and karstogenesis of the Bohemian karst, Prague, The Czech Speleological Society, v. 21 (Karst sediments), p. 10–19.

Bruthans, J., and Zeman, O., 2000, New findings on hydrogeology of the Bohemian Karst: Český kras, v. 26, p. 41–49. (in Czech with English abstract).

Bruthans, J., and Zeman, O., 2001, New data on character and evolution of underground karst forms in the Bohemian Karst and other areas with diffuse recharge mode in the Czech Republic: Český Kras, v. 27, p. 21–29. (in Czech with English abstract).

Bruthans, J., and Zeman, O., 2003, Factors controlling exokarst morphology and sediment transport through caves: Comparison of carbonate and salt karst: Acta Carsologica, v. 32, no. 1, p. 83–99.

Bundschuh, J., 1997, Temporal variations of spring water temperatures in relation to the extents of heat transport modes occurring in the karstified lower Gypsum-Keuper aquifer (Karnian, southern Germany), in Proceedings of the 12th International Congress of Speleology, Conference on Limestone Hydrology and Fissured Media, 6th, Switzerland, Volume 2, p. 129–132.

Chlupáč, I., Brzobohaty, R., Kovanda, J., and Stráník, L., 2002, Geologická minulost České republiky, Prague, Academia, 436 p.

Choquette, P.W., and Pray, L.C., 1970, Geologic nomenclature and classification of porosity in sedimentary carbonates: American Association of Petroleum Geologists Bulletin, v. 5, no. 2, p. 207–250.

Cílek, V., Dobeš, P., and Žák, K., 1994, Formation conditions of calcite veins in the quarry "V Kozle (Hostim I, Alkazar)" in the Bohemian Karst: Journal of the Czech Geological Society, v. 39, no. 4, p. 313–318.

Doctor, D.H., Calvin, A.E., Petrič, M., Kogovšek, J., Urbanc, J., Lojen, S., and Stichler, W., 2006, Quantification of karst aquifer discharge components during storm events through end-member mixing analysis using natural chemistry and stable isotopes as tracers: Hydrogeology Journal, v. 14, p. 1171–1191.

Elleder, L., 2004, Floods in city of Beroun: Český kras, v. 30, p. 59–62. (in Czech with English abstract).

Florea, L.J., and Vacher, H.L., 2006, Springflow hydrographs: eogenetic vs. telogenetic karst: Ground Water, v. 44, no. 3, p. 352–361.

Havlíček, V., 1989, Geological map, Prague, Czech Geological Survey, scale 1:250,000, sheet Králův Dvůr, 12–413, 1 sheet.

Horáček, I., and Ložek, V., 1988, Palaeozoology and the Mid-European Quaternary past: scope of the approach and selected results: Rozpravy Československé akademie věd, řada matematických a přírodních věd, v. 98, no. 4, p. 1–102.

Katz, B.G., Catches, J.S., Bullen, T.D., and Michel, R.L., 1998, Changes in the isotopic and chemical composition of ground water resulting from recharge pulse from sinking stream: Journal of Hydrology, v. 211, p. 178–207.

Klimchouk, A.B., Ford, D.C., Palmer, A.N., and Dreybrodt, W., 2000, Speleogenesis, Evolution of Karst Aquifers, Huntsville, Alabama, National Speleological Society, 521 p.

Kočí, A., 1991, Palaeomagnetic investigation of the Beroun highway section: Antropozoikum, Ústřední ústav geologický, v. 20, p. 103–109.

Kovanda, J., 1991, The significance of the Lower Pleistocene sedimentary complex of the Beroun highway: Antropozoikum, Ústřední ústav geologický, v. 20, p. 129–142.

Kovanda, J., and Herzogová, J., 1986, Druhé chronologické paradoxon v Kruhovém lomu u Srbska: Český kras, v. 12, p. 59–62.

Kukla, J., and Ložek, V., 1993, Průzkum říčních teras v okolí Tetína a otázka prvního říčního paradoxon: The Czech Speleological Society, v. 21 (Karst sediments), p. 30–40.

Martin, J.B., and Dean, R.W., 2001, Exchange of water between conduit and matrix in the Floridan Aquifer: Chemical Geology, v. 179, p. 145–165. doi: 10.1016/S0009-2541(01)00320-5.

Matoušek, V., 2004, Ledový režim vodních toků: Praha, Výzkumný ústav vodohospodářský T.G.Masaryka, Práce a Studie, v. 199, p. 1–203.

MoE CR (Ministry of the Environment of the Czech Republic), 2003, Final report of the project Evaluation of catastrophic flood of August 2002 and of proposal of the Flood preventive system, Praha, MŽP ČR, unpublished report, the final version accepted by the Government of the Czech Republic on January 21, 2004. (In Czech).

Opsahl, S.P., Chapal, S.E., Hicks, D.W., and Wheeler, C.K., 2007, Evaluation of ground-water and surface-water exchanges using stream-flow difference analyses: Journal of the American Water Resources Association, v. 43, no. 5, p. 1132–1141. doi: 10.1111/j.1752-1688.2007.00093.x.

Palmer, A.N., 1991, Origin and morphology of limestone caves: Geological Society of America Bulletin, v. 103, p. 1–21. doi: 10.1130/0016-7606(1991)103<0001:OAMOLC>2.3.CO;2.

Parkhurst, D.L., and Appelo, C.A.J., 1999, User's guide to PHREEQC (Version 2) – A computer program for speciation, batch-reaction, one-dimensional transport, and inverse geochemical calculations, U.S. Geology Survey Water Resources Investigations Report 99–4259, 312 p.

Springer, G.S., Rowe, H.D., Hardt, B., Cocina, F.G., Edwards, R.L., and Cheng, H., 2009, Climate driven changes in river channel morphology and base level during the Holocene and Late Pleistocene of southeastern West Virginia: Journal of Cave and Karst Studies, v. 71, no. 2, p. 121–129.

Vacher, H.L., and Mylroie, J.L., 2002, Eogenetic karst from the perspective of an equivalent porous medium: Carbonates and Evaporites, v. 17, no. 2, p. 182–196. doi: 10.1007/BF03176484.

Včíslová, B., 1980, Silur - devon Barrandienu - II. fáze - závěrečná zpráva, Praha, Stavební geologie, 191 p.

Záhrubský, K., 2003, Možnosti využití izotopů uhlíku ^{14}C a ^{13}C v hydrogeologii Českého krasu [Ph.D. thesis]: Praha, Charles University in Prague, 136 p.

Žák, K., Cílek, V., Danielisová, A., Hlaváč, J., Kadlec, J., Kyncl, T., Pokorný, P., and Světlík, I., 2010, Holocene section in the excavation for construction of the Hýskov Hydropower Plant and its bearing to the understanding of the Berounka River floodplain evolution: Český kras, v. 36, p. 42–51. (in Czech with English abstract).

Žák, K., and Elleder, L., 2007, History of floods in the karst canyon of the Berounka River in surroundings of Srbsko village during the last two hundred years: Český kras, v. 33, p. 9–15. (in Czech with English abstract).

Žák, K., Hladíková, J., Buzek, F., Kadlecová, R., Ložek, V., Cílek, V., Kadlec, J., Žigová, A., Bruthans, J., and Šťastný, M., 2001a, Karstic spring and calcareous tufa accumulation of Holocene age in Svatý Jan pod Skalou (Bohemian Karst), Praha, Czech Geological Survey, Special Papers 13, no. 1, 135 p. (in Czech with extended English summary).

Žák, K., Táborský, Z., Lachmanová, M., and Pudilová, M., 2001b, Heavy mineral assemblages in allochthonous clastic cave sediments of the Bohemian Karst: A pilot study: Český kras, v. 27, p. 5–14. (in Czech with English abstract).

A NEW SPECIES OF NICOLETIIDAE (INSECTA: ZYGENTOMA) FROM KARTCHNER CAVERNS STATE PARK, ARIZONA

LUIS ESPINASA[1]*, ROBERT B. PAPE[2], ALANNA HENNEBERRY[1], AND CHRISTOPHER KINNEAR[1]

Abstract: *Speleonycta anachoretes*, n. sp., is described and differentiated from *S. ozarkensis*, known from caves in the Ozark Plateau. The new species was collected from Kartchner Caverns State Park in Arizona. Morphology and preliminary analyses using 16S rRNA corroborate that *Speleonycta* may be related to *Texoreddellia*, another nicoletiid genus from caves of Texas and northern Mexico. General information regarding its conservation status within the commercial cave is provided.

INTRODUCTION

While insects of the family Nicoletiidae are among the most important and common representatives of cave-adapted fauna in the neotropics (Espinasa and Giribet, 2009), they have a limited presence in caves of northern latitudes. Texas has a complex of at least six species in the genus *Texoreddellia* (Espinasa and Giribet, 2009), and specimens collected from several Ozark caves in Arkansas and Oklahoma were recently described under a new genus, *Speleonycta* (Espinasa et al., 2010).

The cave system of Kartchner Caverns is in an isolated outcrop of limestone near the base of the Whetstone Mountains southwest of Benson, Arizona (Jagnow, 1999). The Kartchner Caverns system was discovered in 1974 and was kept in nearly pristine condition (Tuffs and Tenen, 1999). In 1988 the state of Arizona purchased the cave as a state park and developed it into one of the top show caves in the US, with conservation of the resource as its top priority. As part of the pre-development studies, Welbourn (1999) conducted an inventory of the invertebrate cave fauna between 1989 and 1991. In that study, he observed three individual nicoletiids and reported them as *Nicoletia* sp., but studied them no further.

Under the auspices of Arizona State Parks, we are conducting a re-inventory of the invertebrate fauna to analyze its current status and identify changes that have occurred in the invertebrate ecology of the cave over the twenty years since the original inventory, including ten years of post-development visitation. Several nicoletiid specimens were collected, their relatively abundance was assessed, and they are described here as a new species using morphologic and DNA data. Genus assignment is also corrected, as they belong to *Speleonycta* and not to *Nicoletia*.

MATERIAL AND METHODS

Dissections of a paratype were made with the aid of a stereo microscope and mounted as fixed preparations with Cytoseal 60 solution (Richard-Allan Scientific). The remaining samples were left in vials with ethanol. Illustrations were made with the aid of a camera lucida attached to a microscope. Specimens will be deposited in a collection at the American Museum of Natural History in New York.

A DNA sample was extracted using Qiagen's DNEasy Tissue Kit by digesting a leg in lysis buffer. Amplification and sequencing of the 16S rRNA fragment was done as in Espinasa and Giribet (2009) following standard protocols and primers used in the past for nicoletiids. Chromatograms obtained from the automated sequencer were read and contigs made using the sequence-editing software Sequencher 3.0. External primers were excluded from the analyses. Sequences were aligned and neighbor-joining analysis was performed with ClustalW2.

Population density was roughly assessed by counting the number of animals observed in four days of observations divided by the area of the floor (including habitat under rocks) that was accessible for direct examination in the small, approximately 20 m long Jackrabbit Gallery.

RESULTS

Molecular data were obtained from the Kartchner Caverns nicoletiid and from *S. ozarkensis*. The 16S rRNA fragments were 496 bp long (primers excluded). Using these same sequences of 16S rRNA fragments of twenty-three species within the subfamily Cubacubaninae, Espinasa and Giribet (2009) observed that pairs of specimens within a population differ by an average of 1.8 nucleotides ($\pm$ 2.2 stdev; range 0 to 7; n = 26), by 2.3 nucleotides ($\pm$ 1.9 stdev; range 1 to 6; n = 9) in different populations of the same species, and by 54.7 nucleotides ($\pm$ 9.5 stdev; range 45 to 64; n = 3) among sister species. Nucleotide alignment of the Kartchner Caverns specimen with *S. ozarkensis* showed considerable sequence difference (65 bp, 13.1%; Table 1),

* Corresponding Author, luis.espinasa@marist.edu
[1] School of Science, Marist College, 3399 North Road, Poughkeepsie, NY 12601
[2] University of Arizona, Department of Entomology, Tucson, AZ 85721

Table 1. Alignment of the 16S rRNA fragment sequences of S*peleonycta ozarkensis* **and** *S. anachoretes* **n. sp. showed considerable sequence difference (65 bp; 13.1%).**

Species	16S rRNA Fragment Sequence	
S._ozarkensis	GGCCTTTTGTTTATATATAAGGTCTGACCTGCCCAATGAGGTTTT-AATGGCCGCGGTAT	59
S._anachoretes	GGCTTTTTGTAAGTATATAAGGTCTAGCCTGCCCAATGAGATTTTTAATGGCCGCGGTAT	60
	*** ****** *********** ************* **** **************	
S._ozarkensis	TTTGACCGTGCAAAGGTAGCATAATCATTAGTCTTTTAATTGGGGGCTGGTATGAACGGT	119
S._anachoretes	TTTGACCGTGCAAAGGTAGCATAATCATTAGTCTTTTAATTGAGGGCTGGTATGAATGGC	120
	*** ************* **	
S._ozarkensis	TGGACGAGGGGAAAGCTGTCTCGTAAAGTATGGTACGTAATTTTACTTTTAAGTGAAAAG	179
S._anachoretes	TGGACGAGGTGAAAGCTGTCTCGTAAGATATGGTACATAATTTTACTTTTGAGTGAAAAG	180
	********* **************** ******* ************* ********	
S._ozarkensis	GCTTAAATGGATGTGGGGGACGATAAGACCCTATAGATCTTAACAGTCTGGTTTGTTATA	239
S._anachoretes	GCTTAAATAGGTGTGAGGGACGATAAGACCCTATAGATCTTTACA-TTTAGTATGCATTC	239
	******** * **** ********************** *** * * ** ** *	
S._ozarkensis	AGTGAGGTTTGTAACR-ATAAGGGTTGTTTTGTTGGGGCGACAGGAGGATAGGTAAAACT	298
S._anachoretes	CCT----CTTGGGATGCAAGACGTTTGTTTTGTTGGGGCGACAGAAGAATATATTCAACT	295
	* *** * * * * ******************* ** *** * ****	
S._ozarkensis	CTTCTTATTTAAGGTTATTTTTATTGATATATTTGTGATCCATTGTTGGTGATTGTAAGA	358
S._anachoretes	TTTTCT-TTTAGGGTTATT--TATTGATATGTTTTTGATCCATTTGTGGTGATTATAAGA	352
	** * **** ******* ********* ** ******** ******* ******	
S._ozarkensis	CTAAGTTACCTTAGGGATAACAGCGTAATCTTTCTTGAGAGTTCATATCGACAGGAAGGG	418
S._anachoretes	CTAAGTTACCTTAGGGATAACAGCGTAATCTTTCTTAAGAGTTCATATCGACAGGAGGGG	412
	************************************ ******************* ***	
S._ozarkensis	TTGCGACCTCGATGTTGGATTAAGGATT-CACTATGGTGTAGCAGTTATAGAAGGAGGGT	477
S._anachoretes	TTGCGACCTCGATGTTGGATTAAGGTTTTCTCTATGGTGTAGCAGTTATAGAAGGAGGGT	472
	************************* ** * **************************	
S._ozarkensis	CTGTTCGACCCTTAAATCCTTACA 501	
S._anachoretes	CTGTTCGACCCTTAAATCCTTACA 496	
	************************	

supporting the hypothesis that they belong to separate species. A neighbor-joining tree showed the new species and *S. ozarkensis* clustered together. Both species of *Speleonycta* are then shown to be within a monophyletic group with *Texoreddellia,* at the exclusion of other genera of the Cubacubaninae and in agreement with previous histone sequence data of *S. ozarkensis* (Espinasa et al., 2010). Nevertheless, these results should be considered as preliminary. Establishing the phylogeny of the group and assessing whether *Speleonycta* and *Texoreddellia* should be placed in a new subfamily are the aim of current research using data from additional molecular markers.

NEW SPECIES: *Speleonycta anachoretes* Espinasa, Pape, Henneberry, and Kinnear (Figs. 1, 2A–J, 3A–F)
Material
Holotype male, body 12.7 mm, tarsus 3rd leg 1.4 mm. Paratypes: Males 7.5, 6.5, and 6.2 mm; Females 15, 11, and 10.5 mm; Juvenile 5 mm. Kartchner Caverns, Kartchner Caverns State Park, Cochise County, Arizona. 31°50′16″N 110°21′05″W. 3/14-18/10, 1/9/10 and 11/27/09.

Other locality
Speleonycta sp. - Arkenstone Cave, Colossal Cave Mountain Park. Pima County, Arizona. 32°02′N 110°35′W. Male 9.4 mm; Female 9.9 mm.

Description
Maximum body length of samples 15 mm. Maximum conserved length of antennae and caudal appendages 15 mm and 12 mm respectively. When complete, their length is only slightly longer than body. General color light yellow to white. Body proportions as in Figure 1.
Head with macrochaetae and microchaetae as shown in Figure 2A, with about seven macrochaetae on border of insertion of antennae. Pedicellus of male shorter than first

Figure 1. *Speleonycta anachoretes* **n. sp. Live specimen from Kartchner Caverns.**

article and with clusters of unicellular glands. Four ventral clusters are bordered with a not very conspicuous row of microchaetae forming a U (Fig. 2B) and, on outer border, a blade-like cusp not very sclerotized and with more unicellular glands at its base (Fig. 2B-C), similar to *Speleonycta ozarkensis.* Basal articles of antennae of female simple.

Mouthpart appendages short, especially when compared with other cave nicoletiid species. Labial palp as in Figure 2D, apical article distinctly longer than wide and longer than the penultimate article. Penultimate article with a not very distinct bulge containing two macrochaetae. Labium and first article of the labial palp with macrochaetae. Maxilla as shown in Figure 2E. Last article only slightly longer than penultimate in large individuals, but in small ones it can be 1.5×. Apex of galea with two conules, one longer than wide and the other slightly wider than long (Fig. 2F). Two teeth on lacinia. Mandible chaetotaxy as in Figure 2G, with five or six macrochaetae. Pro-, meso-, and metanota with several macrochaetae on postero-lateral margins, apart from several setae of varied sizes (Fig. 2H). Legs long, hind tibia about 5× longer than wide and slightly shorter than tarsus (Fig. 2I). Juveniles with thinner legs. On largest male (12.7 mm), tibia of second leg without the large bulge or modified macrochaetae found in *S. ozarkensis.* Female legs also simple. Claws short and with a hairy appearance similar to *S. ozarkensis.*

Abdominal terga as in Figure 3A, with multiple macrochaetae of varied sizes on their edges and 1 + 1

distinct macrochaetae within the surface of the terga. *Speleonycta ozarkensis* also has these distinct macrochaetae, but they were not mentioned or represented in the original description. Abdominal sterna as in Figures 2J and 3B. Urosterna I entire and II–VII subdivided into two coxites and one sternite. Urosterna VIII and IX of male entire. Urosternum III and IV of adult male apparently without modifications. Posterior margin of urosternum VIII of male straight, without emarginations or projections in between the stylets of this segment (Figs. 3B and 3G). Urosternum IX of male as in Figures 3B (Kartchner specimen) and 3G (Arkenstone specimen). Point of insertion of paramera in urosternum IX slightly below level of base of the stylets of this segment. Base of internal faces of coxal processes with one slightly sclerotized macrochaeta (Figs. 3B and 3G). Penis and paramera as in Figures 3B and 3G. Paramera very stout, with a distal semi-eversible vesicle and with long specialized macrochaetae, somewhat similar to *S. ozarkensis.* Paramera attain about half the length of stylets IX.

Stylets IX stout and without small teeth on robust terminal spine. Stylets IX larger than others, without sensory cones, but with some sclerotized macrochaetae of varied sizes (Fig. 3G), ventrally with about five macrochaetae (Fig. 3B). Other stylets have a terminal spine with small teeth and with about four macrochaetae (Fig. 3B). Urotergite X protruding, shallowly emarginate in both sexes, posterior angles with several macrochaetae and a few relatively strong setae (Fig. 3D). Length of
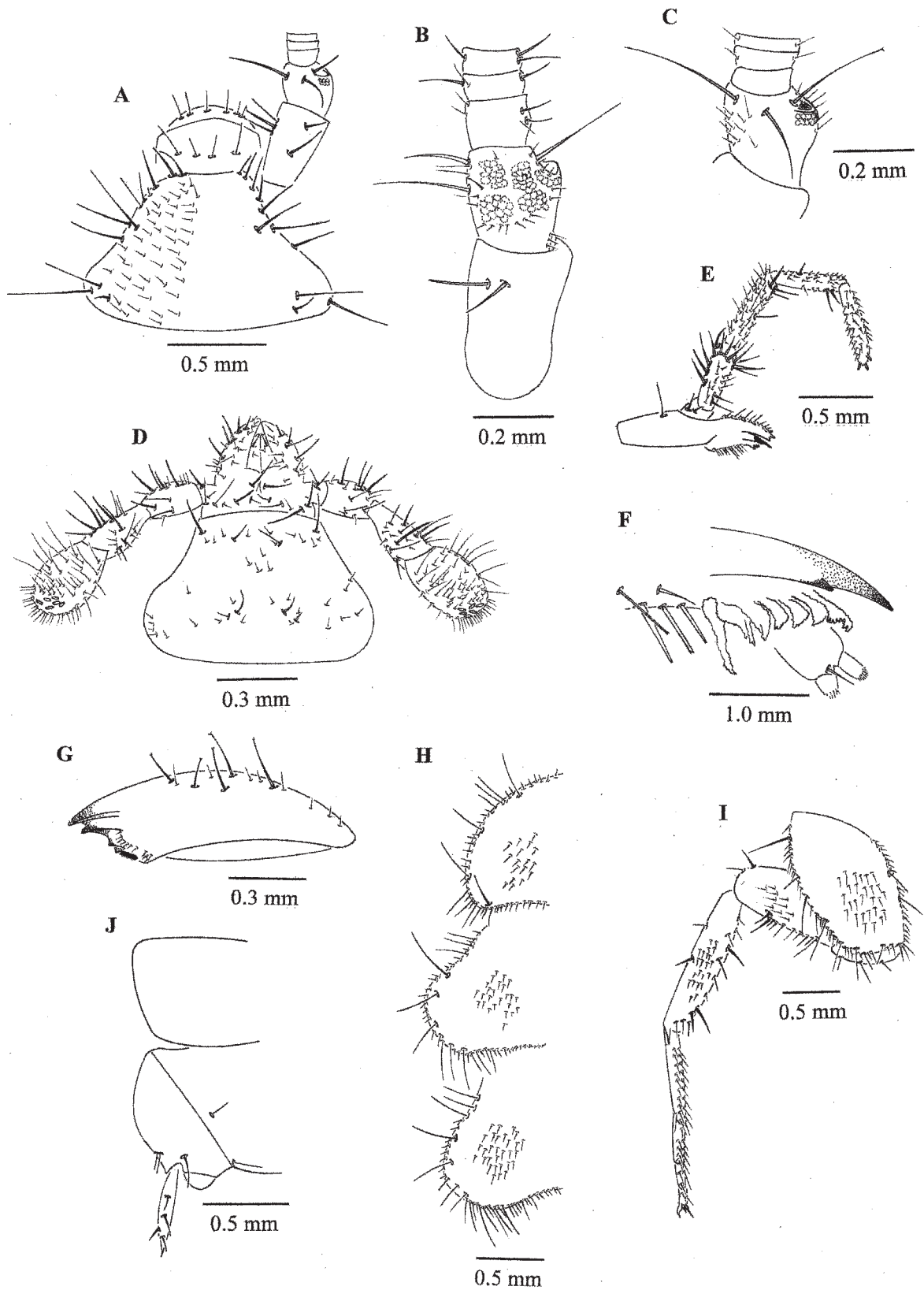
Figure 2. *Speleonycta anachoretes* **n. sp. Male holotype from Kartchner Caverns. A, head and antennae; B, basal portion of antennae, ventral view; C, pedicellus, dorsal view; D, labium; E, maxilla; F, apex of maxilla; G, mandible; H, thoracic nota; I, hind leg; J, urosterna I and II.**
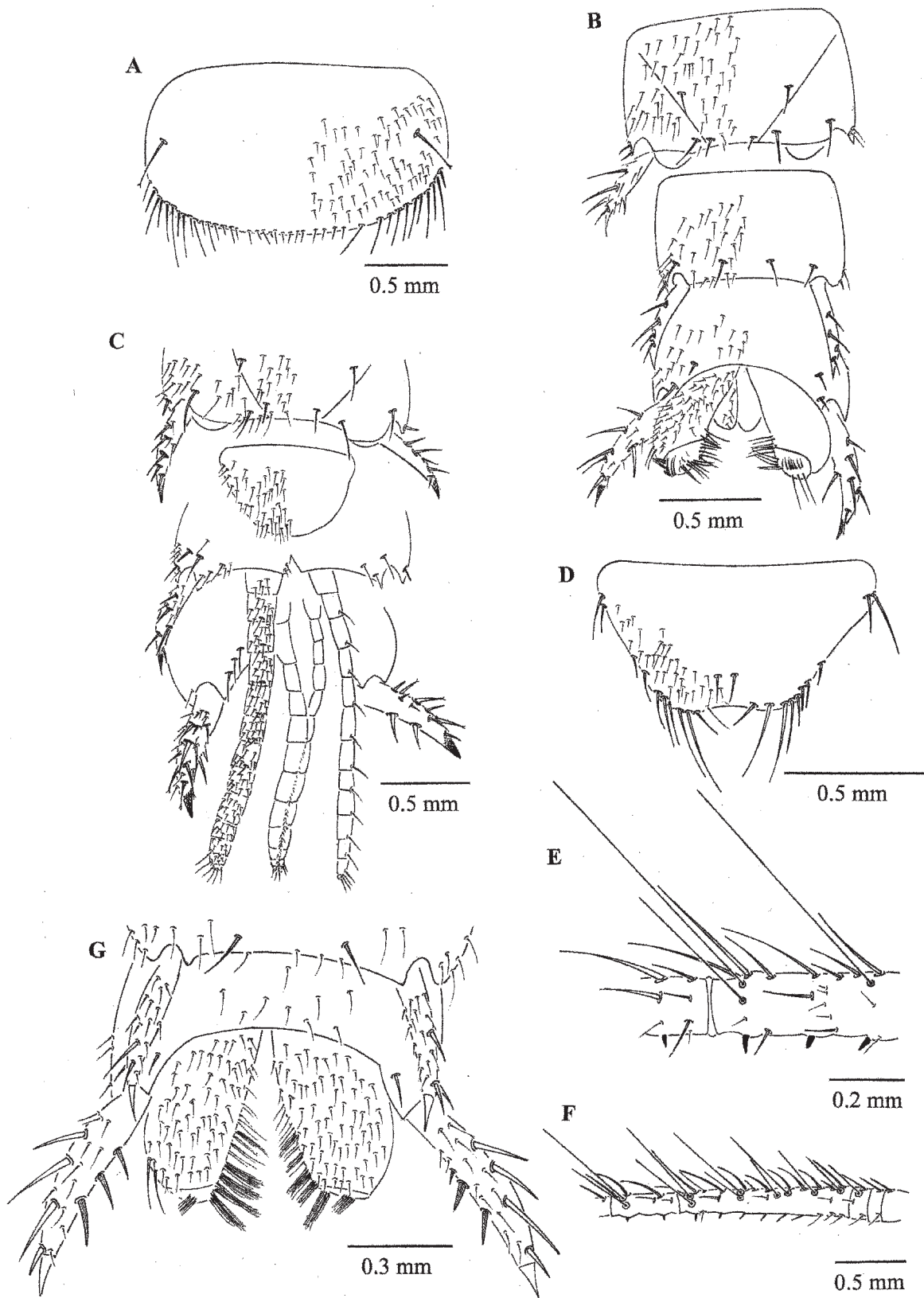
Figure 3. *Speleonycta anachoretes* n. sp. A–B, D–F, male holotype from Kartchner Caverns; C, female paratype from Kartchner Caverns; G, male *Speleonycta* sp. from Arkenstone Cave. Note that parts B and G are shown at different scales; the size of specimens from both localities are actually similar. A, uroterguite III; B, genital area of male; C, genital area of female; D, urotergite X; E, spines on cercus; F, cercus; G, paramera and stylets IX.

inner macrochaetae about equal to the distance between them.

Cerci of adult male straight, basally with two or three annuli slightly wider than long, followed by a very long annulus and many subequal annuli. The very long annuli and the first of the subequal annuli with small sensory pegs. Pegs start as sclerotized chaetae and progressively become thicker (Figs. 3E-F). Cerci with long trichobothria (Fig. 3E). Appendix dorsalis without sensory pegs. Female cercus and appendix dorsalis simple.

Subgenital plate of female rounded to sub-parabolic (Fig. 3C). In the largest adult female (15 mm) and in females measuring 10.5 and 9.9 mm long the ovipositor surpasses apex of stylets IX by half the length of stylets (Fig. 3C), but in the 11 mm female it surpasses by a full length of the stylets. Gonapophyses with about 13 annuli.

Postembryonic Development

Males 12.7, 9.4, and 7.5 mm long had pedicellus with unicellular glands and the distinct blade-like cusp, paramera attaining about half the length of stylets IX, and small spines on cerci. Pedicellus of males 6.5 and 6.2 mm long had a few unicellular glands and the blade-like cusp was just beginning to form. The paramera attain one third the length of stylets IX and no spines on cerci.

Length of ovipositor in the four females of 15, 11, 10.5, and 9.9 mm long varied between surpassing the stylets IX by half to one times the length of the stylets, and gonapophysis had about 13 annuli. In the juvenile female (5 mm), the ovipositor is just barely beginning to form.

Etymology

The species name *anachoretes* is Greek, meaning "one that retired from the world" (a hermit or recluse), in allusion to living a rather isolated existence without much competition from other species. The species inhabits nutrient-poor environments in caves where few other species can survive. An adjective.

Remarks

Speleonycta anachoretes has the diagnostic characters of the genus: no scales, urosternum VIII of male flat posteriorly, without emarginations or projections in between the stylets of this segment, and paramera with very long and specialized chaetae and a distal semi-eversible vesicle.

Speleonycta anachoretes shares with *S. ozarkensis*, the only other described species in the genus, the distinctive blade-like cusp with unicellular glands on the pedicellus of adult males, abdominal terga with 1 + 1 distinct macrochaetae within the surface of the terga, and stylets IX stout with a robust terminal spine. The two species can be easily differentiated by the ovipositor of females. In *S. anachoretes*, females up to 15 mm long have a short ovipositor that surpasses stylets IX by half to one times the length of the stylets and have about 13 annuli on the gonapophyses. In

the largest described female of *S. ozarkensis*, despite being smaller (12 mm), the ovipositor is longer (2× the length of stylets) and gonapophysis is more subdivided (15 to 16 annuli). Males of *S. anachoretes* also have proportionally smaller paramera; the paramera of males 7.5 to 12.7 mm long attain about half the length of stylets IX, while in *S. ozarkensis*, males 11 mm long have distinctly longer paramera that attain the apex of the stylets.

Speleonycta anachoretes can furthermore be differentiated from *S. ozarkensis* by its proportionally shorter last article of the maxillary palps in large individuals (slightly longer than penultimate article versus 1.5× in S. ozarkensis), less macrochaetae on mandibles (5 to 6 versus 7), and longer legs (hind tibia about 5× longer than wide versus 3.5×). Finally, the tibia of the second leg in the male holotype of *S. ozarkensis* is very stout (2× longer than wide) and has a large bulge with 3 distinctly long, sclerotized, and curved macrochaetae. These modifications are apparently absent in the new species.

Discussion

Currently, observations of *S. anachoretes* have been mostly confined to the easternmost passages of Kartchner Caverns. Welbourn (1999) found them near the entrance of the Red River Passage. We found them primarily in the Jackrabbit Gallery and in the vicinity of the Tarantula Room. These three sites are in the same general area and adjoin the Big Room, one of the two large sections shown to tourists at Kartchner Caverns. A single specimen observed in the interior of the Big Room may represent a vagrant animal. Two specimens have also been found in the Granite Dells section of the cave. This area is approximately 275 m west of the Tarantula Room and is not directly connected by humanly accessible cave passage. Both areas are equally close (approximately 15 m) to the surface of the hill containing the cave and near areas where there is an interface of epigean and hypogean environments. So far, the nicoletiids at Kartchner Caverns appear to inhabit the periphery of the cave and have not been found deep in the interior. This is in sharp contrast with the long-term observation data of a population of *Speleonycta* occupying Arkenstone Cave, located in the Rincon Mountains, 36 km northwest of Kartchner Caverns. There, the animals occur only in the deeper reaches of the cave. Regardless of their apparent habitat differences, the Arkenstone specimens do not appear to be more troglomorphic than those at Kartchner. For example, the length of the legs is the same (hind tibia about 5× longer than wide and slightly shorter than the tarsus) at both localities.

Despite their proximity, both caves are in isolated karst areas with no possible connection between the caves. Due to the spatial separation of the populations and since both appear to be cave adapted, one might expect them to be different species. However, similar situations exist with other cave-inhabiting invertebrates in southern Arizona,

where species occur in caves in widely separated, isolated karst areas with no underground connection. An example is *Sitalcina peacheyi* (Opiliones: Laniatores), a troglophilic harvestman, which is recorded from the Baboquivari, Santa Rita, and Rincon Mountains (Ubick and Briggs, 2008). Additionally, our examination of the only two available specimens from Arkenstone Cave revealed no distinctive morphological characteristic that would readily separate the populations as distinct species. It remains to be determined whether the Arkenstone population is a distinct species or not.

Regional desertification (drying and warming) of the northern Chihuahuan and Sonoran deserts began at the end of the Wisconsin glacial episode about 11 ka, and reached its current condition about 4 ka (Van Devender, 1990). Conceivably, a single widely-occurring nicoletiid species may have been present in the region prior to desertification, when the climate was wetter and cooler. The species would likely have occupied both epigean (surface) and hypogean (subsoil and cave) habitats, with gene flow between populations during those times. Desertification likely resulted in extirpation of the epigean populations. The cave populations would have been isolated by intervening inhospitable hot, dry terrain, preventing gene flow between any remaining populations. Extant cave populations in the region today may thus represent relictual populations of the historic species. Obtaining fresh samples from Arkenstone Cave to sequence their DNA could help resolve whether both populations represent a single species or two troglobitic sister species, and if the latter is the case, the timing of their separation.

Speleonycta anachoretes is currently the largest troglobite documented from Kartchner Caverns and arguably one of the most interesting. It is a prime example of an organism displaying traits of cave adaptation: blind, albino, with long appendages and sensory structures. Its distinctive morphology can make it alluring not only to scientists, but also to the general public who come to visit Kartchner Caverns. At the same time, it highlights their fragility and the need for their conservation.

Our observations indicate that the nicoletiids appear to inhabit a core area around the Jackrabbit Gallery that is located about 15 meters from the developed tourist trail. Very rough estimates indicate that this small gallery could support a population of around one hundred nicoletiids, since there were about two individuals per square meter in this area. One of the nicoletiids was caught less than one meter from a large spotlight that fully illuminated the area. The presence of light does not appear to disturb the animals.

What is the size of the nicoletiid population at Kartchner Caverns? This is an extremely difficult question to answer with the data currently available, and only a very vague estimate can be provided at this time. The Jackrabbit Gallery represents less than one percent of the total mapped length of the cave, and this area is estimated to harbor up to a hundred individuals. Furthermore, there are many areas within the cave that are, due to their small size, inaccessible to man, but which are accessible to nicoletiids. These areas are not represented by the mapped portion of the cave, and because they are inaccessible to humans, their extent can only be surmised. Even if other areas of the cave have much lower densities of nicoletiids than the Jackrabbit Gallery, it is probably safe to assume that the total population for the cave is at least in the hundreds.

The commercial development of Kartchner Caverns for tourism does not appear to have adversely affected the nicoletiid population. They appear to cope well with the conditions of illumination and limited human use of their habitat. In the center of Jackrabbit Gallery there is an environmental monitoring station, one of a series of such stations placed throughout the cave that are used by park rangers to check cave microclimatic conditions on a regular basis. Despite routine visits by the park staff to this area over the years, the species has persisted. Additionally, the development of the cave included the boring of a horizontal access tunnel (Tarantula Tunnel) within what we now consider to be the core habitat area of the species in the cave. Furthermore, a vertical shaft (Jackrabbit Shaft) was drilled down from the surface to provide an escape route for construction personnel and for the moving of materials into the cave prior to completion of the tunnel access. This shaft is right in the heart of the nicoletiid habitat, and over the years of cave construction caused extensive human traffic and movement of equipment and supplies through the area. Nevertheless, the gross numbers of animals observed in our study are within an order of magnitude of those observed in Welbourn's study twenty years ago. If anything, we are finding more animals now.

But the cautionary principle has to be used when considering conservation issues for the species in the cave. Neither Welbourn's nor our study has been designed to provide a quantitatively accurate assessment of the health of the population, nor can we confidently state whether the population has decreased or increased since the commercial development of the cave.

References

Espinasa, L., Furst, S., Allen, T., and Slay, M.E., 2010, A new genus of the subfamily Cubacubaninae (Insecta: Zygentoma: Nicoletiidae) from caves in south-central and southwestern USA: Journal of Cave and Karst Studies, v. 72, no. 3, p. 161–168, doi: 10.4311/jcks2009lsc0097.

Espinasa, L., and Giribet, G., 2009, Living in the dark—species delimitation based on combined molecular and morphological evidence in the nicoletiid genus *Texoreddellia* Wygodzinsky, 1973 (Hexapoda: Zygentoma: Nicoletiidae) in Texas and Mexico, *in* Cokendolpher, J.C., and Reddell, J.R., eds., Studies on the Cave and endogean Fauna of North America, Part V: Austin, Texas Memorial Museum Speleological Monograph 7, p. 87–110.

Jagnow, D.H., 1999, Geology of Kartchner Caverns, Arizona: Journal of Cave and Karst Studies, v. 61, no. 2, p. 49–58.

Tufts, R., and Tenen, G., 1999, Discovery and history of Kartchner Caverns, Arizona: Journal of Cave and Karst Studies, v. 61, no. 2, p. 44–48.

Ubick, D., and Briggs, T.S., 2008, The harvestman family Phalangodidae. 6. Revision of the *Sitalcina* Complex (Opiliones: Laniatores): Proceedings of the California Academy of Sciences, ser. 4, v. 59, no. 1, p. 1–108.

Van Devender, T.R., 1990, Late Quaternary vegetation and climate of the Chihuahuan Desert, United States and Mexico, *in* Betancourt, J.L., Van Devender, T.R., and Martin, P.S., eds., Packrat Middens: The Last 40,000 years of Biotic Change: Tucson, University of Arizona Press, 467 p.

Welbourn, W.C., 1999, Invertebrate cave fauna of Kartchner Caverns, Kartchner Caverns, Arizona: Journal of Cave and Karst Studies, v. 61, no. 2, p. 93–101.

REGIONALIZATION BASED ON WATER CHEMISTRY AND PHYSICOCHEMICAL TRAITS IN THE RING OF CENOTES, YUCATAN, MEXICO

Rosela Pérez-Ceballos[1*], Julia Pacheco-Ávila[2], Jorge I. Euán-Ávila[1], and Héctor Hernández-Arana[3]

Abstract: Assessing water quality in aquifers has become increasingly important as water demand and pollution concerns rise. In the Yucatan Peninsula, sinkholes, locally known as cenotes, are karst formations that intercept the water table. Cenotes are distributed across the peninsula, but are particularly dense and aligned along a semi-circular formation called the Ring of Cenotes. This area exhibits particular hydrogeological properties because it concentrates, channels, and discharges fresh water toward the coasts. In this study, we identify spatial and temporal variations in chemical and physical variables at twenty-two cenotes to identify groups that share similar characteristics. Water samples from each cenotes were taken at three depths (0.5, 5.5, and 10.5 m) and during three seasons (dry, rainy, and cold-fronts season). Field measurements of pH, temperature, electrical conductivity, and dissolved oxygen were taken, and the concentrations of major ions (K^+, Na^+, Mg^{2+}, Ca^{2+}, HCO_3^-, SO_4^{2-}, Cl^- and NO_3^-) were quantified. Identifying regions of the cenotes were done by applying multivariate statistical techniques (PCA, PERMANOVA, CAP). The chemical variables revealed spatial trends among the cenotes. We identified three main regions. Region 1 is associated with sea-water encroachment and high levels of sulfate that travel through preferential groundwater flowpaths from evaporites in the southern Yucatan Peninsula; Region 2 is a recharge zone, and Region 3 is characterized by sea water encroachment and by the high chemical and physical variability associated with groundwater flow from the east.

Introduction

Karst aquifers are characterized by having compact and soluble carbonate rocks in which the dissolution process (i.e., karstification) forms conduits and caverns through which groundwater flows (Antigüedad et al., 2007; Custodio and LLamas, 1983, p. 1495; Fernández et al., 2003; Moore et al., 2009). Rainfall quickly filters through karst surface features and enters the aquifer, leading to the storage of enormous quantities of water. In most karst regions, these reservoirs are vital water sources for human consumption, agriculture, livestock raising, and industry, among other uses. Karst aquifers therefore constitute a constraining input in the development of regions and even countries (Pacheco et al., 2004).

Karst systems' high permeability allows substances such as nutrients, metals, hydrocarbons, and bacteria to rapidly enter the aquifer. These substances, including contaminants, are distributed throughout the subterranean flow network, from which they are frequently discharged into the sea. Karst systems with a direct marine connection are also exposed to a serious risk of seawater encroachment as freshwater is extracted and saline water steadily advances into the system (Fernández et al., 2003).

Groundwater contains dissolved substances, largely in an ionic state. Major ions include sodium (Na^+), calcium (Ca^{2+}), magnesium (Mg^{2+}), potassium (K^+), chloride (Cl^-), sulfate (SO_4^{2-}), bicarbonate (HCO_3^-), and nitrate (NO_3^-). The concentrations of these ions can be used to understand the chemistry of groundwater and its interaction with the subterranean environment, helping to identify the possible existence of chemical processes (Custodio and Llamas, 1983, p. 1020).

The Yucatan Peninsula is a large karst zone, with the main karst characteristic being sinkholes. Sinkholes are locally known as cenotes and can be found across the peninsula, but are particularly abundant in a semi-circular formation in the north-central portion of Yucatan state. This Ring of Cenotes (RC) is the edge of the terrestrial portion of the surface expression of the Chicxulub meteorite impact crater (Penfield and Camargo, 1981; Perry et al., 1989; Hildebrand et al., 1995; Perry et al., 1995; Marín et al., 2004). The RC was proposed in 2008 as a Ramsar site for conservation and rational use (Gobierno del Estado de Yucatan, 2008).

* Corresponding Author, rosela.perezc@gmail.com
[1] Centro de Investigación y de Estudios Avanzados del Instituto Politécnico Nacional Unidad Mérida, Antigua Carreta a Progreso Km. 6, Apartado Postal 73, Cordemex, 97310, Mérida, Yucatán, México
[2] Universidad Autónoma de Yucatán Facultad de Ingeniería, Av. Industrias no Contaminantes por Periférico Norte Apartado Postal 150 Cordemex, 97310, Mérida, Yucatán, México
[3] El Colegio de la Frontera Sur, Ave. Centenario Km 5.5. Chetumal, Quintana Roo México
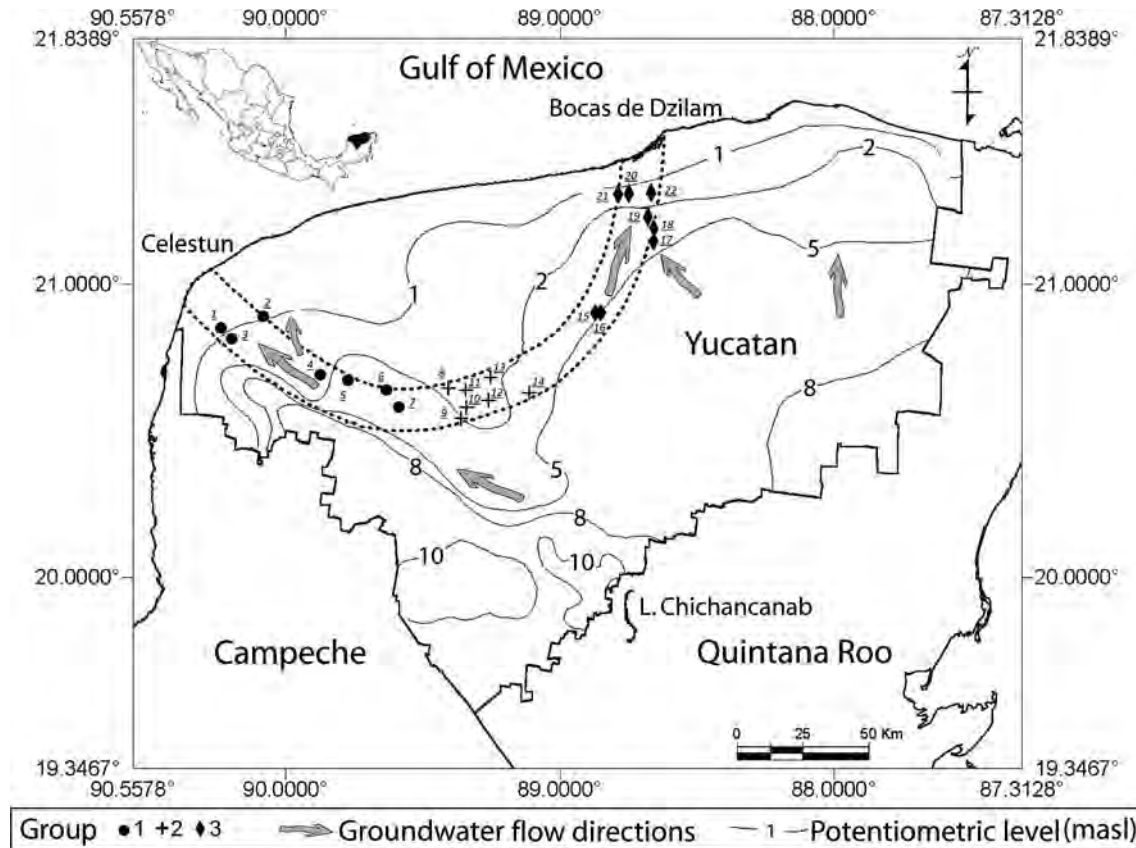
Figure 1. Study area in Yucatan state, Mexico, showing groundwater main flow directions, isopotentiometric levels (msal) and spatial distribution of the twenty-two sampled cenotes in the groups discussed in the text (adapted from SARH, 1989 and Perry et al., 2002).

The RC has been the focus of a number of hydrogeological studies. Using hydraulic gradients, Marín and Perry (1994) identified the RC as a zone of high permeability, which they linked to the Chicxulub crater. Hildebrand et al. (1995) determined the size of the crater and suggested that the formation of the RC was closely linked to a depression at the crater's edge. Steinich et al. (1996, 1997) defined the RC as a system with special hydrogeological properties, such as high permeability and subterranean-river behavior that concentrates, transports, and discharges water toward the coast near Celestún and Dzilam de Bravo. Using hydrochemical and hydrogeological data, they also determined that the zone is divided into two watersheds near its central portion. Finally, they identified groundwater flow as moving from southeast to northwest. Perry et al. (2002) reported that most groundwater of the Yucatan aquifer is in approximate chemical equilibrium with calcite and dolomite, but stated that other minerals were subsaturated. Using strontium isotopes, Perry et al. (2009) demonstrated that the water arriving at the western edge of the RC originates near Chichancanab lagoon in the southern part of the peninsula, flows through a permeable fault zone manifested on the surface by the Ticul Ridge, and finally discharges into the Celestún coastal lagoon (Fig. 1).

These studies have advanced the hydrologic and hydrochemical understanding of the Yucatan Peninsula. However, chemical data are needed from the RC in order to increase our understanding of the spatial and temporal variations in water chemical composition. The RC offers a myriad of research opportunities, because it is located in an area influenced by local factors such as human land use, as well as regional factors such as subterranean flow. The present study's objectives were to spatially and temporally quantify the physical and chemical characteristics of water in representative cenotes along the RC, to identify similarities among the cenotes based on chemical composition in order to obtain a hydrochemical regionalization of the area, and to establish characteristic values for these regions.

Study Area

The RC area covers the northwest portion of the Yucatan Peninsula (88°30′ and 90°30′ W, 20°00′ and 21°30′ N) (Steinich et al., 1996). The width of the RC is approximately 12 km, and extends from the coastal lagoon of Celestún in the west to the Bocas de Dzilam lagoon in the east, both in Yucatán state (Fig. 1).

Table 1. Names and locations of the twenty-two sampled cenotes. The distance from shoreline is along the path of flow, not the shortest line.

ID	Name	Municipality	Latitude, N (°)	Longitude, W (°)	Distance to Shoreline, km
1	Sabtún	Celestún	20.850260	90.235590	13.45
2	Xelactún	Kinchil	20.889640	90.081060	26.94
3	Chunchucmil	Celestún	20.813056	90.196667	19.29
4	Chen ha	Kopomá	20.689480	89.875890	59.72
5	Yax ha	Abalá	20.672640	89.774157	68.13
6	Kankirixche	Abalá	20.637230	89.632980	82.22
7	Sabak ja	Sacalum	20.580490	89.588200	93.10
8	Nayah	Tecoh	20.646510	89.404670	108.12
9	X-pakay	Tekit	20.539150	89.365040	115.82
10	Uitzan	Tekit	20.580690	89.342140	116.67
11	Chonquilá	Tecoh	20.637760	89.344290	118.23
12	Lum há	Tekit	20.602230	89.260180	121.69
13	Uaymil	Homún	20.681910	89.253120	106.74
14	Ixinha	Huhí	20.630350	89.110750	110.29
15	X-colac	Izamal	20.909770	88.866290	61.91
16	Hotzó	Izamal	20.904070	88.861730	62.36
17	Chen Vázquez	Buctzotz	21.148380	88.657850	41.56
18	San Pedro	Buctzotz	21.189070	88.659620	36.16
19	Itzincab	Buctzotz	21.227510	88.679290	25.95
20	Dzonot sábila	Buctzotz	21.310510	88.747790	12.98
21	X-kay	Buctzotz	21.306790	88.788100	13.14
22	Dzonot Trejo	Dzilam González	21.312060	88.667860	16.41

The calcareous plain of the peninsula is formed of Quaternary (Holocene-Pleistocene) sediments in the form of limestone rock of the Paleogene Carrillo Puerto formation. Surface topography is flat with very smooth slope (Perry et al., 1995). Solubility of limestone is produced by carbon dioxide originated in the soil-plant system infiltrated by rainfall (Gaona-Vizcayno et al., 1980). Secondary porosity, fractures, underground channels, and caverns are the main sources of the aquifer permeability (Steinich et al., 1996).

The peninsula's aquifer is unconfined, with the exception of a slight hydrogeological confinement created by a thin (0.5 to 1.4 m) caliche layer along the coastal margin (Perry et al., 1989). The static level varies from 1.0 meters above sea level (masl) at the coast to up to 10.0 masl to the south of the RC (INEGI, 2002). The potentiometric level varies from less than 1.0 masl near the coast to 5.0 masl in the southeast part of the RC (SARH, 1989).

Habitat biodiversity in the study region includes marine, coastal, and inland areas. Marine areas contain features such as the continental platform, extensive seagrass meadows, and intertidal zones. The coastal area includes mangrove wetlands, coastal dunes, and seasonally flooded forest. Inland areas are characterized by thorny dry forest, semi-evergreen tropical forest, and dry tropical forest. Soil types in the area include regosols associated with sand barrier islands and beaches, solonchaks and histosols in the

mangrove wetlands, and litosols and rendzins in the inland forests (Batllori-Sampedro et al., 2006).

Climate zones in the Yucatan include the driest of the arid and semiarid classes, and cover a spectrum from the driest of the subhumid hot to very hot classes. Three seasons occur in the region, a dry season with high temperatures and low rainfall (March to May), a rainy season with frequent rainfall (June to October), and a cold-fronts season with winter storms and occasional rainfall (November to February) (Schmitter-Soto et al., 2002).

The cenotes included in the study were open air, with the exception of two semi-open ones (see classification proposed by Duch, 1991). Cenotes in the area are used to provide water for livestock, crop irrigation, and human use.

METHODS

Based on the cenote inventory of the Yucatan State Secretariat of Ecology (SECOL, 1999), a preliminary selection of fifty-two cenotes within the RC was made. Field data on accessibility and depth were collected. From a selection of about thirty cenotes reasonably well distributed in the study area, twenty-nine were found to have a minimum water depth of 11 m. Seven proved to be inaccessible, giving a final sample of twenty-two (Fig. 1). The names of the cenotes, their municipalities, geographic coordinates, and their distances from the shoreline are given in Table 1.

Analysis	Analytical Methods
Alkalinity	Titration
Calcium	EDTA titrimetric
Magnesium	Calculation (difference between hardness and calcium as calcium carbonate)
Chloride	Argentometric
Sulfate	Turbidimetric
Sodium	Atomic absorption spectrometric
Potassium	Atomic absorption spectrometric
Nitrate	Ultraviolet spectrophotometric screening

A total of 198 water samples were collected from the twenty-two cenotes. Water samples were taken at three water depths during the three seasons, dry, rainy, and cold-fronts. In situ measurements of water temperature, pH, electrical conductivity and dissolved oxygen were obtained using a multiparameter probe (Hydrolab G-Quanta). Water samples were taken at depths of 0.5, 5.5, and 10.5 m using 1.0 L and 0.25 L plastic bottles and were kept cold during transport to the laboratory for major ion and other chemical analyses. Concentrations of major ions and alkalinity were determined in accordance with standard methods for each analyte (APHA-AWWA-WPCF, 2005) (Table 2). Quality of the results was established by analysis at least three times for each sample for titration, titrimetric, and argentometric methods, and by calibration with standards and analysis of reagent blanks for turbidimetric, atomic-absorption spectrometric, and ultraviolet spectro-photometric screening methods. Charge-balance errors

were as total cations minus total anions divided by total ions, all in meq L^{-1}, times 100 (Deutsch, 1997). A total of 87% of the samples had cation/anion balance of $\pm$ 5%, while the remaining 13% were between $\pm$ 5 and $\pm 10\%$.

To visualize and explore the spatial and temporal behavior of the chemical and physical characteristics, a set of plots were created (Figs. 2–4). In these plots the numbers on the abscissa identify the cenotes according to their location within the RC from Celestún to Dzilam de Bravo (Fig. 1). The trend lines were generated using a locally weighted regression method (LOWESS) that filters the dispersion of each variable (Di Rienzo et al., 2008).

An exploratory analysis of normality was done to decide which statistical technique to apply. The data did not fit a normal distribution, and they were consequently analyzed with a non-parametric Kruskal-Wallis test to identify any significant differences among depths and seasons. Considering the univariate exploratory graphic analysis, the limited data provided by the non-parametric univariate statistical analysis, and the depth and season data, it was decided to regionalize the cenotes using spatial structural characteristics to provide a more informative and relevant result. Three groups were proposed based on the major ion concentrations and the variability of these parameters over season and space. These groups were evaluated and tested with a sequence of multivariate analyses, Principal Component Analysis (PCA), Permutational Multivariate Analysis of Variance (PERMANOVA), and Canonical Analysis of Principal Coordinates (CAP), based on ten hydrochemical variables (conductivity, pH, K^+, Na^+, Mg^{2+}, Ca^{2+}, HCO_3^-, SO_4^{2-}, Cl^-, NO_3^-) and distance from each cenote to the shoreline along the groundwater flow.
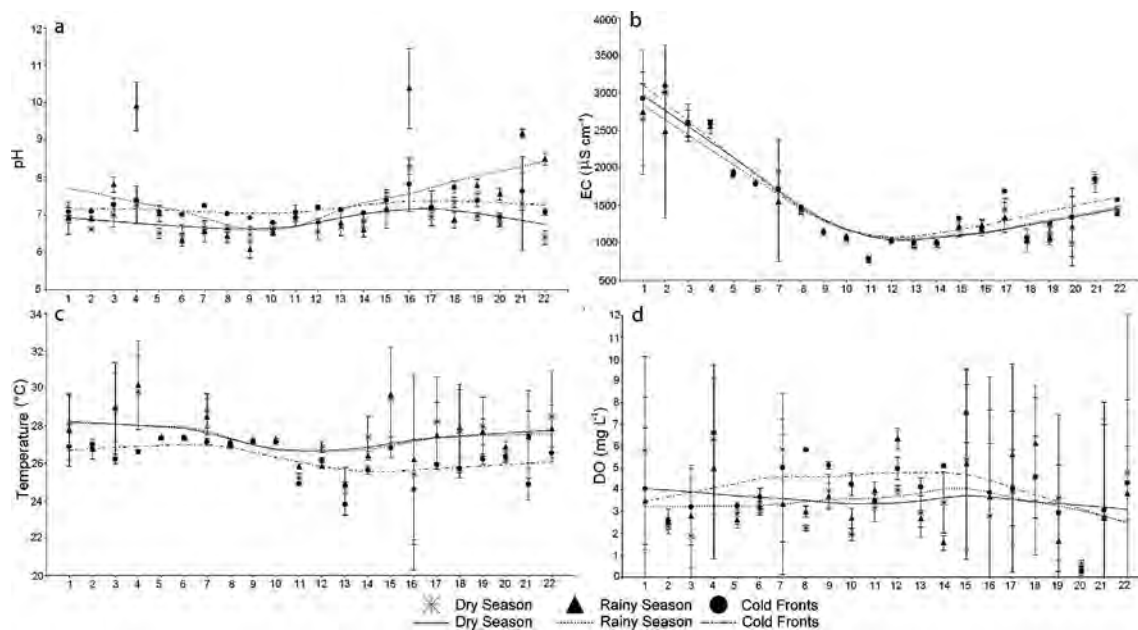
Figure 2. Spatial and temporal patterns from field variables averaged for three depths and measured at the twenty-two cenotes. EC is electrical conductivity and DO is dissolved oxygen.

Figure 3. Spatial and temporal patterns in cation concentrations averaged for three depths and measured at the twenty-two cenotes.

PCA was applied to identify structural patterns in the multivariate data matrix of eleven variables measured at the twenty-two cenotes grouped into three regions (west, center, and east) in three seasons, treating the measurements at different depths as repetitions. The PCA was based on a correlation matrix of logarithm-transformed (base 10) data normalized to eliminate the influence of differences between measurement units. This technique aims to reduce data dimensionality and to search for linear relationships among the original variables through the creation of new, independent variables that explain the maximum possible variation in the original data.

The general hypothesis of no differences between seasons and cenote groups was tested using PERMA-NOVA. This simultaneously falsifies the response of the eleven measured variables versus the factors season and

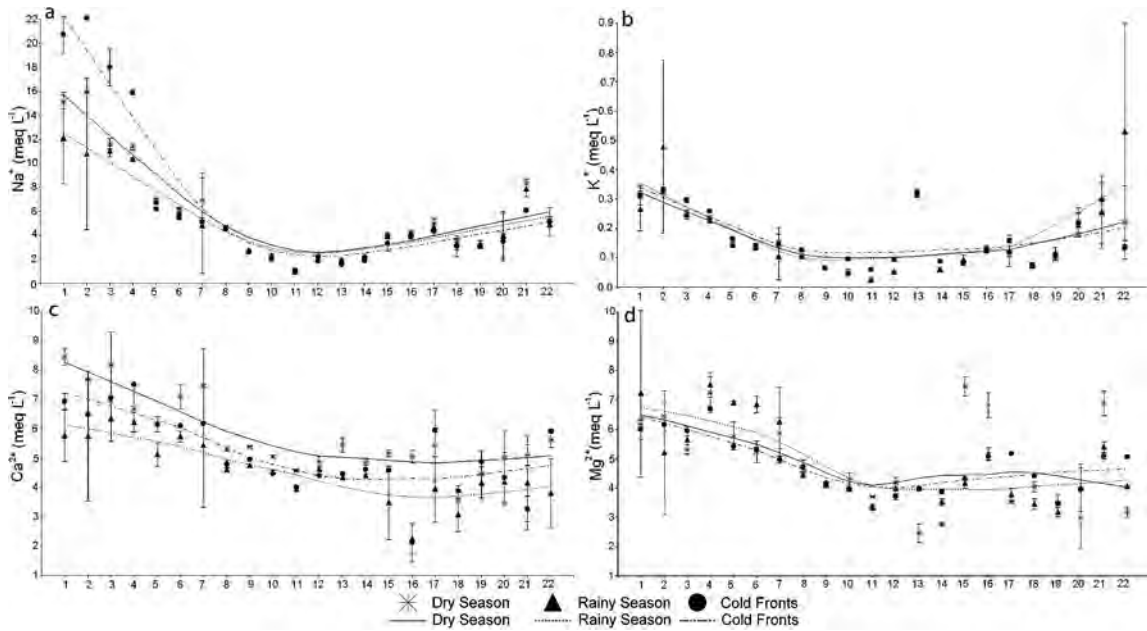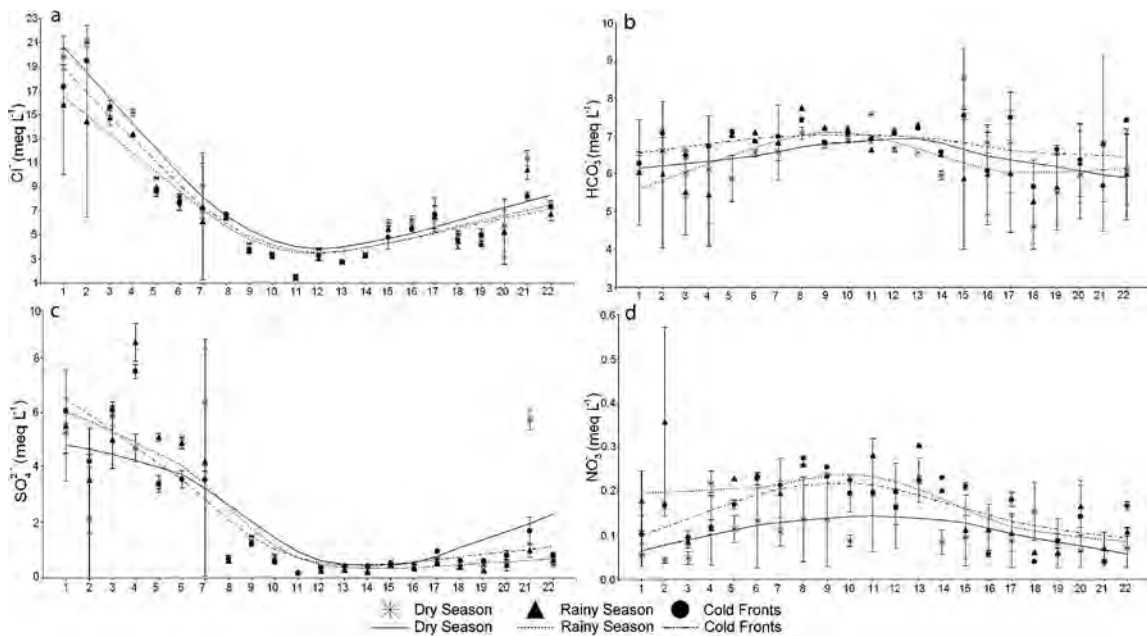**Figure 4. Spatial and temporal patterns of anion concentrations averaged for three depths and measured at the twenty-two cenotes.**

Table 3. Chemical and physical parameters of the water in the twenty-two cenotes from the Ring of Cenotes, averaged over seasons and depth, with standard deviation.

ID	pH	EC (μS cm⁻¹)	Temperature (°C)	DO (meq L⁻¹)	Na⁺ (meq L⁻¹)	K⁺ (meq L⁻¹)	Ca²⁺ (meq L⁻¹)	Mg²⁺ (meq L⁻¹)	Cl⁻ (meq L⁻¹)	HCO₃⁻ (meq L⁻¹)	NO₃⁻ (meq L⁻¹)	SO₄²⁻ (meq L⁻¹)
1	6.96	2775.56	27.60	4.45	15.97	0.30	7.04	6.46	17.66	6.20	0.08	5.66
	0.25	543.56	1.41	3.66	4.32	0.05	1.27	1.55	3.48	0.73	0.07	1.17
2	6.87	2867.78	26.83	2.48	16.27	0.38	6.63	5.93	18.29	6.56	0.16	3.33
	0.21	646.81	0.30	0.32	5.85	0.17	1.39	1.22	4.96	1.08	0.17	1.86
3	7.36	2602.22	28.02	2.63	13.53	0.26	7.18	5.62	15.32	6.01	0.04	5.71
	0.41	177.33	2.07	2.05	3.47	0.03	1.05	0.38	0.61	0.78	0.02	0.77
4	8.19	2588.88	28.85	5.97	12.52	0.24	6.81	7.14	13.93	6.09	0.12	6.97
	1.36	55.78	2.29	2.79	2.58	0.01	0.71	0.51	0.96	1.13	0.07	1.78
5	6.87	1931.11	27.36	2.92	6.63	0.15	5.81	6.03	9.07	6.67	0.14	4.02
	0.31	24.21	0.04	0.41	0.38	0.01	0.57	0.72	0.54	0.67	0.05	0.87
6	6.60	1802.22	27.34	3.33	5.82	0.14	6.31	5.79	7.94	6.83	0.17	4.56
	0.34	12.02	0.05	0.37	0.34	0.003	0.65	0.82	0.40	0.23	0.07	0.75
7	6.80	1737.56	28.15	4.74	5.57	0.13	6.34	5.69	7.47	6.80	0.14	4.74
	0.37	486.72	1.02	2.69	2.50	0.05	1.52	0.87	3.08	0.55	0.06	2.72
8	6.70	1437.11	27.00	3.69	4.60	0.11	4.90	4.60	6.59	7.42	0.19	0.70
	0.28	37.78	0.14	1.64	0.10	0.01	0.33	0.19	0.16	0.30	0.08	0.09
9	6.49	1140.78	27.18	4.27	2.65	0.07	5.02	4.11	3.90	6.94	0.17	1.35
	0.40	21.67	0.06	0.81	0.08	0.001	0.29	0.05	0.29	0.22	0.08	0.14
10	6.65	1059.22	27.17	2.97	2.20	0.07	4.68	4.07	3.35	7.04	0.14	0.70
	0.13	26.09	0.09	1.08	0.17	0.02	0.28	0.20	0.11	0.15	0.07	0.11
11	6.98	779.56	25.31	3.54	0.98	0.04	4.17	3.45	1.51	7.04	0.19	0.17
	0.16	15.33	0.43	0.52	0.07	0.02	0.31	0.19	0.12	0.43	0.08	0.04
12	6.86	1030.78	26.28	5.11	2.11	0.06	4.63	3.95	3.40	6.95	0.14	0.34
	0.30	12.60	0.48	1.09	0.23	0.02	0.23	0.25	0.35	0.24	0.05	0.07
13	6.87	981.56	24.48	3.26	1.78	0.31	4.74	3.47	2.75	7.02	0.22	0.39
	0.26	36.30	0.78	0.93	0.17	0.01	0.55	0.78	0.05	0.35	0.05	0.08
14	6.83	987.44	26.48	3.37	2.10	0.07	4.62	3.38	3.33	6.35	0.14	0.34
	0.24	25.79	0.97	1.69	0.20	0.01	0.22	0.49	0.11	0.30	0.07	0.10
15	7.22	1239.00	28.65	6.03	3.72	0.09	4.40	5.32	5.42	7.30	0.11	0.53
	0.38	104.43	2.34	3.27	0.48	0.01	0.97	1.63	0.73	1.54	0.07	0.06
16	8.83	1194.44	25.39	3.45	4.05	0.13	3.13	5.68	5.78	6.30	0.06	0.41
	1.35	72.92	3.73	3.76	0.22	0.01	1.50	0.89	0.41	0.98	0.04	0.12
17	7.11	1489.56	27.21	4.54	4.64	0.13	5.10	4.15	6.53	6.78	0.09	0.74
	0.30	199.99	1.82	3.02	0.50	0.03	1.23	0.78	0.89	1.21	0.06	0.20
18	7.31	1060.11	27.12	5.12	3.22	0.07	3.49	3.96	4.74	5.17	0.05	0.49
	0.41	94.28	1.93	2.55	0.52	0.01	0.52	0.44	0.44	0.78	0.06	0.11
19	7.38	1136.22	27.28	2.75	3.12	0.11	4.49	3.36	4.70	5.93	0.05	0.46
	0.38	110.18	1.20	2.47	0.18	0.01	0.58	0.24	0.48	0.86	0.03	0.16

Table 3. Continued.

ID	pH	EC (μS cm^{-1})	Temperature (°C)	DO (meq L^{-1})	Na$^+$ (meq L^{-1})	K$^+$ (meq L^{-1})	Ca^{2+} (meq L^{-1})	Mg^{2+} (meq L^{-1})	Cl$^-$ (meq L^{-1})	HCO$_3^-$ (meq L^{-1})	NO$_3^-$ (meq L^{-1})	SO$_4^{2-}$ (meq L^{-1})
20	7.08	1185.22	26.48	0.42	3.80	0.22	4.51	3.64	5.39	6.21	0.09	0.67
	0.38	353.21	0.37	0.21	1.61	0.04	0.82	0.90	2.02	0.94	0.07	0.22
21	8.03	1837.78	26.61	2.84	7.37	0.27	4.16	5.78	9.99	6.42	0.02	2.84
	1.11	79.97	1.93	4.00	1.07	0.08	1.16	0.86	1.49	1.31	0.02	2.25
22	7.32	1467.33	27.62	4.31	5.09	0.29	5.11	4.09	7.19	6.51	0.08	0.70
	0.93	89.98	1.64	4.33	0.66	0.27	1.16	0.82	0.47	1.03	0.05	0.16

cenote group in a multivariate analysis of variance using a two-factor (season and group) and a-posteriori structured design over the Euclidean distances, applying permutational methods.

Finally, a CAP was done to maximize separation between groups. The first objective of the CAP was to identify axes whose direction was fundamentally different from the maximum variation identified with the PCA and that maximize the separation of the groups proposed and falsified with the PERMANOVA. The second objective was to diagnose and cross-validate the a priori assignment of the cenotes to the three groups to determine which groups were more different than others. This analytical sequence helped identify similarity between the chemical characteristics of the different cenotes and then propose chemical values representative of each region.

RESULTS

Chemical and physicochemical water parameters obtained for each cenote are shown in Table 3. The upper value in each cell is the mean and the lower value is the standard deviation.

FIELD VARIABLES

Annual average pH was 7.15 ($\pm$ 0.78), with a minimum of 5.81 (cenote 9) and a maximum of 11.06 (cenote 16), both recorded in the rainy season. High pH values are likely a result of organic matter derived from cattle farming, washed by rain into the cenotes. The Kruskal-Wallis test showed significant differences ($p<0.0001$) between the medians for seasons but not for depths. Values for pH increased from the RC center (cenote 9) towards its two extremes, with the highest increase towards the east. In the center, pH values were slightly acid (5.81–6.9) (Fig. 2a).

Annual average electrical conductivity was 1560.52 μS cm^{-1} ($\pm$ 659.64), with a minimum of 763 μS cm^{-1} (recorded in cenote 11 in the center) and a maximum of 3250 μS cm^{-1} (recorded in cenote 1 in the west near the coast), both during the rainy season. Overall, EC values increased from the center outwards during all three seasons as the result of ion incorporation from water-rock interaction and sea-water encroachment. However, the increase in EC towards the west (2775 μS cm^{-1} at cenote 1) was notably higher than towards the east (1467 μS cm^{-1} at cenote 22). Both cenotes are located approximately 18 km from the coast. During the cold fronts season, EC increased at both ends of the ring, in cenotes 1 through 4 in the west and in cenotes 20 to 22 in the east (Fig. 2b). In each of the two arms of the RC (considered separately), distance from the coast was correlated with EC. Terrain slope is steeper in the east and gentle on the west, resulting in more saline intrusion in the west compared to the east.

Average annual water temperature was 27.02 °C ($\pm$ 1.74) with a minimum of 22.2 °C (cenote 16 at 10.5 m

depth) and a maximum of 32.2 °C (cenote 15 at 0.5 m depth), both recorded during the dry season. Differences were not significant among seasons and depths. Spatially, the cenotes in the RC's center exhibited less temperature variability than cenotes at its edges (Fig. 2c).

For all cenotes in the RC, annual average dissolved oxygen (DO) content was 3.73 mg L^{-1} ($\pm$ 2.57), with a minimum average of 0.96 mg L^{-1} at a depth of 10.5 m (cenote 3) and a maximum of 13.16 mg L^{-1} at 0.5 m (cenote 22). Median values for DO were significantly different among seasons (p=0.0325) and depth (p<0.0001). In general, DO decreased with depth. The DO concentration in the water column was least variable during the cold-fronts season, with the highest concentrations located at the center of the RC (Fig. 2d).

LABORATORY VARIABLES
Cations

Average annual Na^+ content was 5.81 meq L^{-1} ($\pm$ 4.84) with a minimum of 0.88 meq L^{-1} (cenote 11) in the rainy season and a maximum of 22.45 meq L^{-1} (cenote 1) in the cold fronts season. No differences were observed between seasons or depths. Concentrations tended to increase with depth, mainly during the dry and rainy seasons. Cenotes with the most constant Na^+ concentration were located in the RC's center and east. During all three seasons, concentrations increased from the center towards the extremes, with the highest increase observed over the approximately 10 km distance between cenotes 5 (6.6 meq L^{-1}) and 4 (12.5 meq L^{-1}) in the west. Na^+ concentration was directly related to electrical conductivity. Generally, the lowest concentrations were recorded during the rainy season (Fig. 3a).

Annual average K^+ levels were 0.16 meq L^{-1} ($\pm$ 0.12), with a minimum of 0.02 meq L^{-1} (cenote 11) and a maximum of 0.81 meq L^{-1} (cenote 2), both recorded during the rainy season. No differences were observed between seasons or depths. Overall K^+ levels were most variable during the rainy season and least variable during the cold fronts season. In all three seasons, K^+ concentrations decreased with depth. Concentrations were lowest in the RC's center (cenote 11) and increased towards the coasts. The one exception was cenote 13, where concentrations surpassed 0.3 meq L^{-1} in all three seasons (Fig. 3b).

For Ca^{2+}, annual average concentration was 5.15 meq L^{-1} ($\pm$ 1.40), with a minimum value of 1.67 meq L^{-1} (cenote 16) during the rainy season and a maximum of 9.17 meq L^{-1} (cenote 3) during the dry season. Differences were present between seasons (p<0.0001) and between depths (p<0.0354). The highest variability was observed during the dry season and the lowest during the cold-fronts season. Ca^{2+} concentration also increased with depth, particularly during the dry and rainy seasons and on both sides of the RC. Concentration variation with depth in the water column was least in cenotes in the center. Overall, concentrations were highest in the cenotes to the west compared to those in the center and east (Fig. 3c).

Average annual Mg^{2+} concentration was 4.80 meq L^{-1} ($\pm$ 1.40) with a minimum of 1.95 meq L^{-1} (cenote 20) during the dry season and a maximum of 8.90 meq L^{-1} (cenote 1) during the rainy season. Variability was highest during the dry season and lowest during the cold-fronts season. Most of the studied cenotes exhibited an increase in Mg^{2+} concentrations with depth, except during the cold-fronts season. No differences were observed between seasons or depths. Spatially, concentrations were highest (average 6.09 meq L^{-1}) in the west (cenotes 1 to 7) compared to all the other cenotes (average 4.2 meq L^{-1}). The lowest variability in concentrations was recorded in cenotes in the center (Fig. 3d).

Anions

Average annual Cl^- concentration was 7.46 meq L^{-1} ($\pm$ 4.9) with a minimum of 1.37 meq L^{-1} (cenote 11) during the rainy season and a maximum of 21.15 meq L^{-1} (cenote 2) during the dry season. No differences were observed between seasons or depths. During the dry and rainy seasons, concentrations increased with depth. Water-column Cl^- concentration variability with depth was highest in cenotes 1, 2 and 7, in the west. In all three seasons, Cl^- concentrations were lowest in the center (cenote 11) and increased to the west and east. The increase was greatest towards the west, with an increase from 9.07 meq L^{-1} (cenote 5) to 13.93 meq L^{-1} (cenote 4) over an approximately 10 km distance; this is similar to the behavior of electrical conductivity and sodium (Fig. 4a).

Average annual HCO_3^- concentration was 6.57 meq L^{-1} ($\pm$ 0.93) with a minimum of 3.76 meq L^{-1} (cenote 2) during the rainy season and a maximum of 9.36 meq L^{-1} (cenote 15) during the dry season. Concentrations were most variable during the rainy season and least variable in the cold-fronts season. Differences were observed among seasons (p=0.022) and among depths (p=0.0001). The lowest variability in water-column HCO_3^- concentrations was recorded in the central cenotes. Concentrations generally increased with depth. In all three seasons, concentrations were lower to the west and east compared to higher levels in the center (Fig. 4b).

Average annual SO_4^{2-} concentration was 2.08 meq L^{-1} ($\pm$ 2.36) with a minimum of 0.12 meq L^{-1} (cenote 11) during the dry season and a maximum of 9.27 meq L^{-1} (cenote 7) during the rainy season. No differences were observed between seasons or depths. Variability was lowest during the cold fronts season and highest during the rainy season. Concentration was positively related to depth. The highest water-column concentration variability was recorded in cenotes in the west. In all three seasons, SO_4^{2-} concentrations increased from the center towards the west; a notable increase was recorded over the approximately 23 km distance between cenotes 9 (1.35 meq L^{-1}) and 7 (4.74 meq L^{-1}) (Fig. 4c).

Table 4. Percentage of variation explained, plus coefficients, for the linear combination of eleven variables making up the first two principal components (PC) for the twenty-two cenotes sampled during the dry, rainy, and cold-fronts seasons.

Variable	PC1[a]	PC2[a]
pH	0.066	**0.406**
Conductivity	**0.411**	−0.094
Na^+	**0.415**	0.022
K^+	0.310	0.186
Ca^{2+}	0.258	**−0.419**
Mg^{2+}	0.324	−0.169
Cl^-	**0.416**	0.029
HCO_3^-	−0.025	**−0.518**
SO_4^{2-}	**0.371**	−0.154
NO_3^-	−0.116	−0.377
Distance to shoreline	−0.248	**−0.390**

[a] Bold numbers are coefficients for the most influential variables on each Principal Component.

Average annual NO_3^- concentration was 0.12 meq L^{-1} ($\pm$ 0.08), with a minimum of 0.009 meq L^{-1} (minimum detectable level) during the dry and cold-fronts seasons and a maximum of 0.56 meq L^{-1} (cenote 2) during the rainy season. Differences were observed between seasons ($p < 0.0001$), but not between depths. Concentrations were highly variable during all three seasons and in all the studied cenotes, although the highest overall concentrations were recorded in the rainy season. During all three seasons, NO_3^- concentrations were highest in cenotes in the center compared to those to the west and east (Fig. 4d).

REGIONALIZATION OF THE RING OF CENOTES

Three groups of cenotes were established using the ten hydrochemical variables and the distance to the shoreline along the groundwater flow directions. Group 1 includes cenotes on the RC's west side, cenotes 1 to 7. Group 2 encompasses cenotes 8 to 14 in the center, and Group 3 includes cenotes 15 to 22 on the east side (Fig. 1).

The first two principal components from the Principal Component Analysis explained 69.3% of the total variation based on the maximum variation from eleven original variables (Table 4). The first component (PC1) explained 50.1% of the variation; the maximum variation in PC1 separated Group 1 from the others as a function of increases in electrical conductivity and the Na^+, Cl^- and SO_4^{2-} ions. The second component (PC2) explained 19.2% of the variation; the maximum variation of PC2 separated Groups 2 and 3, mainly in response to the Ca^{2+}, and HCO_3^- ions and the pH and distance-to-shoreline variables. Both principal components showed high variability within Group 3 (Fig. 5).

The Permutational Multivariate Analysis of Variance quantified differences by season and group, as well as the season-group interaction factor ($S \times G$). There were clear differences due to the main-factors effect, although the
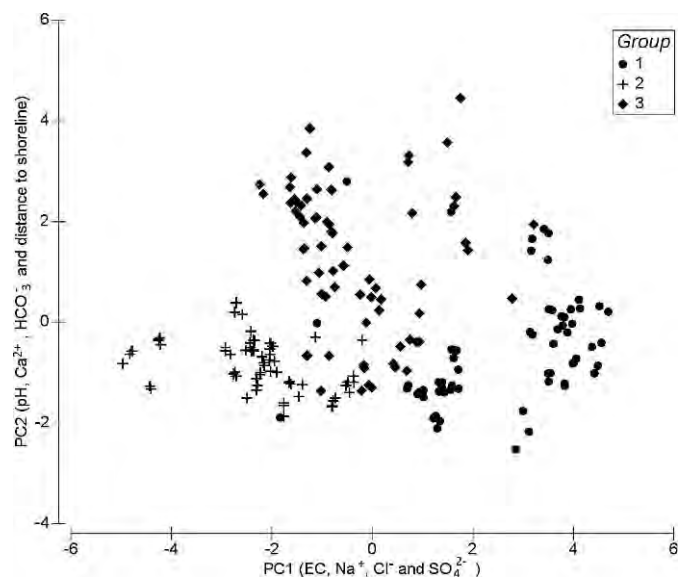

Figure 5. Multivariate ordination from Principal Components Analysis (labels on the principal axes PC1 and PC2 correspond to the most influential variables).

interaction term between main factors was also significant, meaning the effects of the main factors were not independent (Table 5).

The a posteriori paired pseudo-t test allowed us to identify the interaction source. When the ''group'' effect was fixed, the pattern of differences between seasons changed depending on the group observed, but when the ''season'' effect was fixed, the pattern of differences between groups did not change (Table 6). Therefore, the difference from the interaction term was caused by the dependence of season on the group observed ($p < 0.01$). In other words, season has an effect only on a particular group of cenotes, but the spatial pattern of group differences is consistent temporally, based on the hydrochemical characteristics (Table 6).

The Canonical Analysis of Principal Coordinates also showed the effect of the grouping of the cenotes based on the hydrochemical data (Fig. 6). Cross-validation analysis of the classification of cenotes into groups corroborated that 96.8% of the cenotes in Group 1 were correctly allocated, 100% in Group 2, and 91.7% in Group 3.

Once regionalized, the average of the hydrochemical variables values ($\pm$ standard deviation) were calculated for the three regions: Region 1, Region 2, Region 3 (Fig. 1, Table 7).

DISCUSSION

SPATIAL TRENDS

The large number of cenotes and special hydrogeological properties make the RC a unique region for the study of groundwater. The studied chemical and physical variables exhibited patterns and specific behavior along the RC.

Table 5. Permutational Multivariate Analysis of Variance results of significant differences in water properties for a structured two-factor crossed design of main factor season and group of cenotes and the interaction term season × group.

Variation Source	df[a]	SS[b]	MS[c]	p seudo-F[d]	p (perm)[e]
Season	2	80.433	40.216	6.6664	**0.0001**
Group	2	904.6	452.3	74.975	**0.0001**
Season×Group	4	40.439	10.11	1.6758	**0.0298**

[a] df = Degrees of freedom.
[b] SS = Sum of Squares.
[c] MS = Sum of Mean squares.
[d] p seudo-F = Test statistic based on distance measure.
[e] p(perm) = Probability based on permutations.
Bold figures are statistically significant to $p < 0.05$.

The variables of pH and temperature are distinctly different in the center, where pH was moderately acidic (5.81 to 6.90) and temperature remained almost constant (26.27 °C ± 1.08) during all three seasons. This suggests that this portion of the RC functions as a hydrological recharge zone that receives water mainly from direct filtration of rainfall through the permeable karst formation. This agrees with the fact that aquifer recharge zones can exhibit temperature effects that facilitate greater limestone dissolution (Custodio and Llamas, 1983, p. 1017), and the low pH values result from the direct recharge by rain water infiltration, which has a mean pH value of 6 in the groundwater of Yucatán state (Cabrera et al., 1996).

Electrical conductivity, Na^+ and Cl^- concentrations had similar spatial patterns, with considerable increases in the west. All three increased notably from cenote 4 to cenote 1. Average values at these three cenotes (EC =

2,708 μS cm^{-1}; Na^+ = 14.58 meq L^{-1}; Cl^- = 16.30 meq L^{-1}) were higher than normal freshwater values for these variables, which are EC = 100 to 2,000 μS cm^{-1} (Donado, 1999), Na^+ = 4.35 to 6.52 meq L^{-1} (Custodio and Llamas, 1976, p. 203), and Cl^- = 0.85–4.22 meq L^{-1} (Melloul and Goldenberg, 1998). The cause of these higher values, with $Cl^- > 8.5$ meq L^{-1} up to 55 km inland from the coast at cenote 4, is probably seawater encroachment (Escolero et al., 2005).

K^+ concentration tended to increase from the center towards the coast. K^+ concentrations in the aquifer are mainly due to agricultural discharge and seawater encroachment (Pacheco et al., 2001). Variability was highest during the rainy season as a result of rainfall washing contaminants into the groundwater. Most of the groundwater in Yucatán state contains K^+ levels between 1 ppm (0.0256 meq L^{-1}) and 5 ppm (0.128 meq L^{-1}), and almost always below 10 ppm (0.256 meq L^{-1}) (Cabrera, 1986). Cenote 13 had a higher K^+ concentration (0.3 meq L^{-1}) in all seasons probably due to the use of fertilizers in the

Table 6. Pair-wise comparisons for the interaction term season × group, when level of group (first column) and season (third column) is fixed (bold figures are statistically significant at $p < 0.05$).

Group 1	p (perm)	Season D	p (perm)
D-R	**0.002**	1–2	**0.001**
D-CF	**0.009**	1–3	**0.001**
R-CF	0.089	2–3	**0.001**
Group 2		Season R	
D-R	**0.010**	1–2	**0.001**
D-CF	**0.002**	1–3	**0.001**
R-CF	0.058	2–3	**0.001**
Group 3		Season CF	
D-R	**0.001**	1–2	**0.001**
D-CF	0.251	1–3	**0.001**
R-CF	**0.012**	2–3	**0.001**

D = dry, R = rainy, CF = cold-fronts season.
Numbers 1, 2 and 3 refer to cenote group.
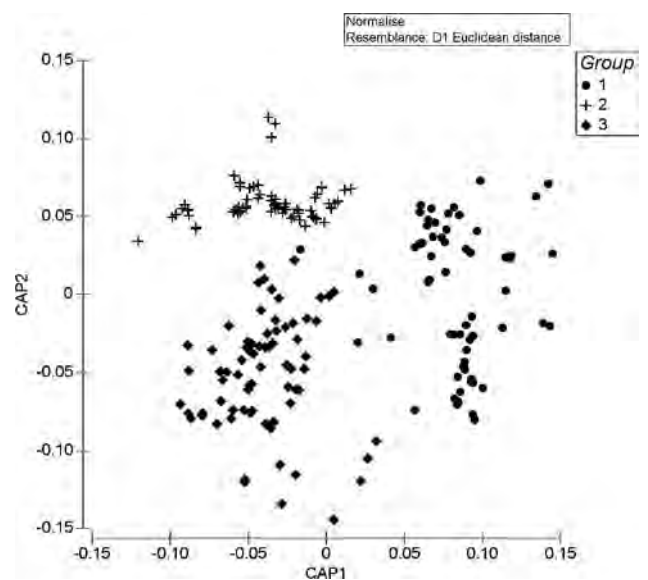Bold figures are statistically significant at $p < 0.05$.

Figure 6. Canonical Analysis of Principal Coordinates of the groups based on hydrochemical variables.

Table 7. Average values over all samples from the cenotes from each group.

Variable	Group 1 ●	Group 2 +	Group 3 ♦
pH	7.09 ± 0.75	6.77 ± 0.30	7.53 ± 0.92
Conductivity	2329 ± 577	1059 ± 188	1326 ± 287
Na^+ (meq L^{-1})	10.90 ± 5.47	2.35 ± 1.05	4.38 ± 1.50
K^+ (meq L^{-1})	0.23 ± 0.11	0.10 ± 0.09	0.16 ± 0.12
Ca^{2+} (meq L^{-1})	6.59 ± 1.12	4.68 ± 0.40	4.30 ± 1.19
Mg^{2+} (meq L^{-1})	6.09 ± 1.03	3.86 ± 0.56	4.50 ± 1.24
Cl^- (meq L^{-1})	12.81 ± 4.97	3.55 ± 1.45	6.22 ± 1.91
HCO_3^- (meq L^{-1})	6.45 ± 0.82	6.96 ± 0.41	6.33 ± 1.20
NO_3^- (meq L^{-1})	0.12 ± 0.09	0.17 ± 0.07	0.07 ± 0.06
SO_4^{2-} (meq L^{-1})	4.99 ± 1.87	0.57 ± 0.38	0.85 ± 1.08

● Group 1. Cenotes at the RC's west side.
+ Group 2. Cenotes at the center of the RC's.
♦ Group 3. Cenotes at the RC's east side.

gardens surrounding it. Likewise, in cenote 2 during the rainy season surface concentrations reached 0.81 meq L^{-1}, probably as a result of contaminants washed from a farm adjacent to the site.

Mg^{2+} concentrations were highest in cenotes 1 through 7 in the west. This ion originates from seawater and dissolution of dolomite and evaporites (Custodio and Llamas, 1983, p. 1012), suggesting that the high concentrations could be due to seawater encroachment or the presence of dolomite and low-Mg calcite (Lefticariu et al., 2006).

SO_4^{2-} behavior was similar to that of Mg^{2+}. Sulfate levels in cenote 7 (4.74 meq L^{-1}) were 3.5 times higher than in cenote 9 (1.35 meq L^{-1}). This disparity could be explained by the fact that the water in the west portion of the RC originates in the south near Chichancanab Lake, which has high SO_4^{2-} levels (52.92 meq L^{-1}) (Perry et al., 2002). Both cenotes are located in the area marking the watershed divide within the RC. This hydraulic separation of the RC was identified by Steinich et al. (1996) by using the SO_4^{2-}/Cl^- ratio, a natural tracer, in an analysis of hydrochemical and hydrogeological data to identify flow direction and the watershed divide in the southern portion of the RC. The SO_4^{2-} levels observed in the present study exhibited behavior similar to that of SO_4^{2-} in that study.

The Ca^{2+} and HCO_3^- ions form part of the carbonate system. Fully understanding their behavior requires specific analyses and calculation of saturation indices for calcite, aragonite, and dolomite to identify chemical processes. Spatial patterns for each ion were determined within the RC. The highest Ca^{2+} concentrations were in the west, and HCO_3^- had higher concentrations in the center. Finally, nitrate-ion concentrations were highest in the center. This portion of the RC is a recharge area with dissolved oxygen levels that favor oxidation of nitrogenated species, and as a result, it carries large amounts of pollutants such as NO_3^-. Overall, numerous differences were found along the RC that suggest regionalization of the aquifer in different areas.

SEASONAL TRENDS

The variables pH, temperature, dissolved oxygen, Ca^{2+}, HCO_3^-, and NO_3^- had significant statistical differences between seasons. Furthermore, electrical conductivity, temperature, dissolved oxygen, Na^+, Cl^-, and NO_3^- clearly showed differences in spatial trends values between seasons. Electrical conductivity, Na^+ and Cl^- increased at the RC's extremes (cenotes 1 to 4 in the west, cenotes 20 to 22 in the east) during the cold-fronts season due to movement of seawater into the coastal aquifer caused by sea level changes. The seawater intrusion threatens water availability for human consumption in this region (Valle-Levinson et al., 2011). Arreguín (2008) proposed that due to the characteristics of the peninsula, sea-level rise could change the interface position, causing its gradual migration inland.

During the rainy and dry seasons, temperature decreased with depth, but this did not occur during the cold-fronts season because ambient temperature is low, leading to homogeneous water column temperatures. Dissolved oxygen concentrations were higher and had less variability in the center compared to the edges during the cold-fronts season because low ambient temperature favors oxygen dissolution in the water column. Concentrations of Na^+ and Cl^- decreased at the RC's edges (cenotes 1 to 4 in the west, cenotes 20 to 22 in the east) during the rainy season due to dilution from aquifer recharge, a phenomenon also reported in groundwater (Cabrera, 1986; Cabrera et al., 2002). Nitrate concentrations increased during the rainy season as pollutants were washed into the aquifer (Pacheco and Cabrera, 1997; Pacheco et al., 2001). The chemical and physicochemical characteristics of the cenotes of the Yucatan Peninsula showed marked trends among seasons.

REGIONALIZATION OF THE RING OF CENOTES

The differences in chemical composition between water from the three groups of cenotes reflect distinct water sources. The first principal component (PC1) separated the

Group 1 of cenotes from the other two based on increased conductivity and Na^+, Cl^-, and SO_4^{2-} concentrations compared to concentrations in Groups 2 and 3. High concentrations of Na^+, Cl^-, and SO_4^{2-} at Group 1 are associated with seawater, indicating that this group is characterized by seawater encroachment that can reach 55 km inland. Furthermore, high sulfate concentrations in this group can be explained by the preferential groundwater flow rich in sulfate from evaporites in the southern Yucatan Peninsula (Perry, 2002). Positive and negative scores from the principal component two (PC2) separated Group 2 from Group 3. Group 2 consisted of cenotes located at long distances from the shoreline that were characterized by low pH values, high NO_3^-, and high Ca^{2+} and HCO_3^- concentrations. The influence of the carbonate system is showed in PC2 through Ca^{2+} and HCO_3^- ions, as well as pH values (Garrels and Christ, 1965). The low pH values in this group were likely to be a result of direct recharge from rain water, whose mean pH value in the regions is around 6 (Cabrera et al., 1996). This corroborates that Group 2, in the center of the RC, is in an aquifer recharge zone. The cenotes in Group 3 exhibited high hydrochemical variability and were consequently distributed within both principal components. The variability of this group of cenotes is likely caused by groundwater flow from the east near the cenote 17 (Fig. 1). Cenotes nearer the coast were more similar in PC1 due to concentrations of Na^+ and Cl^- similar to those of Group 1. The distances to the shoreline showed an influence on PC2, indicating that there was not a direct relationship with sea-water encroachment according to the spatial behavior of sodium and chloride ions reinforcing the differences between the cenotes from Groups 1 and 3 (Figs. 2a and 3a).

The PERMANOVA revealed the presence of an interaction between season and cenote groups. The paired tests revealed a dependence of seasons on groups but not vice versa, meaning inter-group differences were not season dependent; and therefore, regionalization is present year round. Paired tests also demonstrated that seawater encroachment in Group 1 and carbonate-system characteristics in Group 2 are identifiable in all three seasons. This is not the case in Group 3, since during the dry and cold-fronts seasons chemical processes change in response to environmental variables and the morphological and structural characteristics of each cenote. The CAP corroborated the existence of Groups 1, 2 and 3; indeed, the CAP and PCA graphic results separated the groups in similar ways. This confirms that group separation was only the product of the maximum variation in chemical and physicochemical characteristics.

Conclusions

Multivariate statistical techniques were successfully applied to regionalize into three large regions twenty-two cenotes in the RC in the Mexican state of Yucatan based on water chemistry and physicochemical characteristics. Region 1 encompasses cenotes in the RC's western portion that have Na^+, Cl^-, and K^+ concentrations mainly associated with seawater encroachment, as well as high sulfate concentrations originating in the southern Yucatan Peninsula. Region 2 includes cenotes in the RC's center with slightly acid pH values, lower electrical conductivity, and lower ion (Na^+, K^+, Mg^{2+}, Cl^-) concentrations, evidence of weak influence from seawater and suggesting that this is an aquifer recharge zone. Region 3 includes cenotes in the RC's eastern portion characterized by higher pH values, high hydrochemical variability caused by groundwater flow from the east and less seawater encroachment. The RC regions associated with water characteristics may prove helpful when making management and conservation decisions such as the restriction of human activities, the selection of waste disposal areas, and the protection of recharge areas to help move to a sustainable use of the water resources in this geographical area.

References

Antigüedad, I., Morales, T., and Uriarte, J., 2007, Los acuíferos kársticos. Caso del país Vasco: Enseñanza de las Ciencias de la Tierra, v. 5, no. 3, p. 325–332.

APHA-AWWA-WPCF, 2005, Standard Methods for the Examination of Water and Wastewater: Washington, D.C., 21 Edition, 1368 p.

Arreguín Cortés, F.I., 2008, Evaluación de los efectos del Cambio Climático Global sobre el Ciclo Hidrológico en México, in Proceedings, XX Congreso Nacional de Hidráulica: Toluca, Estado de México, Comisión Nacional del Agua, p. 1–36.

Batllori-Sampedro, E., González-Piedra, J., Díaz-Sosa, J., and Febles-Patrón, J., 2006, Caracterización hidrológica de la región costera noroccidental del estado de Yucatán, México: Investigaciones Geográficas, Boletín del Instituto de Geografía, UNAM, no. 59, p. 74–92.

Cabrera, A., 1986, Hidrogeoquímica del agua subterránea en acuíferos cársticos, [M.S. thesis]: Universidad Autónoma de Yucatán, México, 76 p.

Cabrera, A., Pacheco, J., and Cobos, G., 1996, Caracterización química de la precipitación pluvial de la ciudad de Mérida Yucatán: Boletín académico, FIUADY, no. 30, p. 13–19.

Cabrera, A., Pacheco, J., Cuevas, E., Ramírez, J., Comas, M., and Cámara, A., 2002, Hidrogeoquímica del agua que subyace a la JAPAY I, en Mérida, Yucatán, México: Ingeniería Revista Académica, v. 6, no. 3, p. 29–40.

Custodio, L., and Llamas, M., 1983, Hidrología subterránea: Barcelona, Spain, Ed. Omega, 2359 p.

Deutsch, W.J., 1997, Groundwater geochemistry, Fundamentals and Applications to Contamination: Boca Raton, Florida, CRC Press, 221 p.

Di Rienzo, J.A., Casanoves, F., Balzarini, M.G., Gonzalez, L., Tablada, M., and Robledo, C.W., 2008. InfoStat, versión 2008, Grupo InfoStat, FCA, Universidad Nacional de Córdoba, Argentina.

Donado, L., 1999, Hidrogeoquímica, Hidrogeología con Aplicaciones y Casos de Estudios Latinoamericanos: Publicado en Internet, Editado por Gonzalo Pulido Silva, PhD. Capítulo 3.

Duch, G., 1991, Fisiografía del estado de Yucatán, su relación con la agricultura: Edo. México, Universidad Autónoma de Chapingo, 229 p.

Escolero, O., Marín, L., Steinich, B., Pacheco, J., Molina, A., and Anzaldo, J., 2005, Geochemistry of the hydrogeological reserve of Mérida, Yucatán, Mexico: Geofísica Internacional, v. 44, no. 3, p. 301–314.

Fernández, R., Baquero, J.C., Lorca, D., and Verdejo, J., 2003, Acuíferos kársticos costeros, introducción a su conocimiento, in Memoria de TIAC'03 Tecnología de la Intrusión de Agua de Mar en Acuíferos Costeros: Países mediterráneos, Instituto Geológico y Minero de España y Diputación Provincial de Alicante, p. 3–30.

Gaona-Vizcayno, S., Gordillo-de Anda, T., and Villasuso-Pino, M., 1980, Cenotes, karst característico: Mecanismos de formación: UNAM, Revista Instituto de Geología, v. 4, no. 1, p. 32–36.

Garrels, R., and Christ, C., 1965, Solutions, minerals, and equilibria: New York, Harper and Row, 450 p.

Gobierno del Estado de Yucatán, 2008, Desarrollo Regional para el Crecimiento Equilibrado: Primer Informe de Gobierno de 2008, 92 p.

Hildebrand, A., Pilkington, M., Connors, M., Ortiz-Aleman, C., and Chavez, R., 1995, Size and structure of the Chicxulub crater revealed by horizontal gravity gradients and cenotes: Nature, v. 376, p. 415–417, doi:10.1038/376415a0.

Instituto Nacional de Estadística, Geografía e Informática (INEGI), 2002, Estudio Hidrológico del estado de Yucatán: Gobierno del Estado de Yucatán, México, 77 p.

Lefticariu, M., Perry, E.C., Ward, W., and Lefticariu, L., 2006, Post-Chicxulub depositional and diagenetic history of the northwestern Yucatan Peninsula, Mexico: Sedimentary Geology, v. 183, no. 1–2, p. 51–69, doi:10.1016/j.sedgeo.2005.09.008.

Marín, L., Pacheco, J., and Méndez, R., 2004, Hidrogeología de la península de Yucatán, in Jiménez, B., and Marín, L., eds., El Agua en México Vista desde la Academia: México, D.F., Academia Mexicana de Ciencias, p. 159–176.

Marín, L., and Perry, E., 1994, The hydrogeology and contamination potential of northwestern Yucatan, Mexico: Geofísica Internacional, v. 33, p. 619–623.

Melloul, A.J., and Goldenberg, L.C., 1998, Early-indicator signals of groundwater contamination: the case of seawater encroachment: Environmental Geology, v. 33, no. 4, p. 279–288, doi: 10.1007/s002540050247.

Moore, P., Martin, J., and Screaton, E., 2009, Geochemical and statistical evidence of recharge, mixing, and controls on spring discharge in an eogenetic karst aquifer: Journal of Hydrology, v. 376, p. 443–455.

Pacheco, J., and Cabrera, A., 1997, Groundwater contamination by nitrates in the Yucatan Peninsula, Mexico: Hydrogeology Journal, v. 5, no. 2, p. 47–53, doi:10.1007/s100400050113.

Pacheco, J., Cabrera, A., and Pérez, R., 2004, Diagnóstico de la calidad del agua subterránea en los sistemas municipales de abastecimiento en el Estado de Yucatán, México: Ingeniería Revista Académica, v. 8, no. 2, p. 165–179.

Pacheco, J., Marín, L., Cabrera, S., Steinich, B., and Escolero, O., 2001, Nitrate temporal and spatial pattern in 12 water-supply wells, Yucatan, Mexico: Environmental Geology, v. 40, no. 6, p. 708–715, doi:10.1007/s002540000180.

Penfield, G., and Camargo, Z., 1981, Definition of a major igneous zone in the central Yucatan platform with aeromagnetics and gravity: Society of Exploration Geophysisists, 51st Annual International meeting, Los Angeles, Abstracts, 37 p.

Perry, E., Marin, L., McClain, J., and Velázquez, G., 1995, Ring of cenotes (sinkholes) northwest yucatan, Mexico: Its hydrogeologic characteristics and possible association with the Chicxulub impact crater: Geology, v. 23, no. 1, p. 17–20, doi:10.1130/0091-7613(1995)023<0017:ROCSNY>2.3.CO;2.

Perry, E., Paytan, A., Pedersen, B., and Velazquez-Oliman, G., 2009, Groundwater geochemistry of the Yucatan Peninsula, Mexico: Constraints on stratigraphy and hydrogeology: Journal of Hydrology, v. 367, p. 27–40.

Perry, E., Swift, J., Gamboa, J., Reeve, A., Sanborn, R., Marin, L., and Villasuso, M., 1989, Geologic and environmental aspects of surface cementation, north coast, Yucatan, Mexico: Geology, v. 17, no. 9, p. 818–821, doi:10.1130/0091-7613(1989)017<0818:GAEAOS>2.3.CO;2.

Perry, E., Velazquez-Oliman, G., and Marin, L., 2002, The hydrogeo-chemistry of the karst aquifer system of the northern Yucatan Peninsula, Mexico: International Geology Review, v. 44, p. 191–221, doi:10.2747/0020-6814.44.3.191.

Secretaría de Agricultura y Recursos Hidráulicos (SARH), 1989, Sinopsis Geohidrológica del Estado de Yucatán: Subsecretaría de Infraestructura Hidráulica, Dirección General de Administración y Control de Sistemas Hidrológicos, 48 p.

Schmitter-Soto, J., Comín, F., Escobar-Briones, E., Herrera-Silveira, J., Alcocer, J., Suárez-Morales, E., Elías-Gutiérrez, M., Díaz-Arce, V., Marín, L., and Steinich, B., 2002, Hydrogeochemical and biological characteristics of cenotes in the Yucatan Peninsula (SE Mexico): Hydrobiologia, v. 467, no. 1–3, p. 215–228, doi:10.1023/A:1014923217206.

Secretaría de Ecología (SECOL), 1999, Cenotes y Grutas de Yucatán: Gobierno del Estado de Yucatán: Mérida, Yucatán, México, Ed. CEPSA, 159 p.

Steinich, B., and Marín, L., 1997, Determination of flow characteristics in the aquifer of the northwestern peninsula of Yucatan, Mexico: Journal of Hydrology, v. 191, p. 315–331.

Steinich, B., Velázquez-Olimán, G., Marín, L., and Perry, E., 1996, Determination of the ground water divide in the karst aquifer of Yucatan, Mexico, combining geochemical and hydrogeological data: Geofísica Internacional, v. 35, p. 153–159.

Valle-Levinson, A., Mariño-Tapia, I., Enriquez, C., and Waterhouse, A., 2011, Tidal variability of salinity and velocity fields related to intense point-source submarine groundwater discharges into the coastal ocean: Limnology and Oceanography, v. 56, p. 1213–1224, doi: 10.4319/lo.2011.56.4.1213.

DELINEATING PROTECTION AREAS FOR CAVES USING CONTAMINATION VULNERABILITY MAPPING TECHNIQUES: THE CASE OF HERRERÍAS CAVE, ASTURIAS, SPAIN

A.I. MARÍN[1], B. ANDREO[1], M. JIMÉNEZ-SÁNCHEZ[2], M.J. DOMÍNGUEZ-CUESTA[2], AND
M. MELÉNDEZ-ASENSIO[2,3]

Abstract: Diverse approaches are adopted for cave protection. One approach is delineating protection areas with regard to their vulnerability to contamination. This paper reports the main results obtained from the delineation of a protection zone for Herrerías Cave, declared of Cultural Interest by the Asturias Regional Government, based on assessing its vulnerability to contamination. The cave is situated in a complex karst hydrogeologic environment in which groundwater flows from southwest to northeast, following the bedrock structure. A stream flows inside the cave, emerging in a spring located to the northeast of the system. Karst recharge occurs by direct infiltration of rainfall over limestone outcrops, concentrated infiltration of surface runoff in the watershed draining the cave, and deferred infiltration of water from alluvial beds drained by influent streams. The soil and vegetation covers are natural in the majority of the test site, but land uses in the watershed, including scattered farming, stock breeding, quarrying, and tourist use, are changing the natural characteristics and increasing the cave's vulnerability to contamination. The procedure followed for delineating protection zones is based on the method COP+K that is specifically designed for vulnerability mapping of groundwater springs in carbonate aquifers. To cover the hydrological basin included in the cave's catchment area, the protection zones established includes two different areas, the hydrogeological catchment basin and adjacent land that contributes runoff. Different degrees of protection in the zones have been proposed to make human activity compatible with conservation of the cave, and our results show remarkable differences from the protection zone previously proposed for the same area.

INTRODUCTION

There is increasing public concern today regarding the protection of our natural heritage. Caves represent an outstanding, unique element in the natural landscape and are sometimes the economic driving force of regions dependent on tourism, and they may also motivate the creation of protected areas, as for example, Škocjan Caves Regional Park, Slovenia (Official Gazette of the Republic of Slovenia, 801-07/94-5/3, 1996) and Ardèche Gorge Natural Reserve, France (Statutory order n°80-27, 14 January 1980). There are different ways of extending official protection to caves. In Europe, one method is declaration as a Site of Community Interest or an Area of Special Conservation Interest. This is possible when the cave is not open to tourism and protection is necessary to maintain or restore an environment for animal or plant species of community interest that require strict protection, such as bat species listed in the Habitats Directive of the European Union, 92/43/CEE. In other cases, the cave importance may be linked to the presence of archaeological remnants, motivating its declaration as part of the national cultural heritage, or even as a World Heritage Site. For example, Altamira Cave was awarded this distinction by UNESCO (SC.85/CONF.008/09, 1985).

Conservation, evaluation, and management are frequently performed by local administrations, regional or national departments of culture, or international agencies. Thus, the United Nations has promoted different initiatives specifically focused on the protection of cultural heritage. However, these efforts are mainly aimed at restoration and conservation and rarely focus on damage prevention (Catani et al., 2002).

The underground extent of caves is usually not apparent from the surface, and this sometimes leads to damage being done unwittingly. Since caves form part of karst aquifers, the possibility of such damage is influenced by the hydrogeological characteristics of karst environments that are especially vulnerable to contamination (Zwahlen, 2004). An example is given by Slovenia, a

[1] Centre of Hydrogeology (CEHIUMA) and Department of Geology, University of Málaga, Spain aimarin@uma.es andreo@uma.es
[2] Department of Geology, University of Oviedo, Spain mjimenez@geol.uniovi.es, mjdominguez@geol.uniovi.es
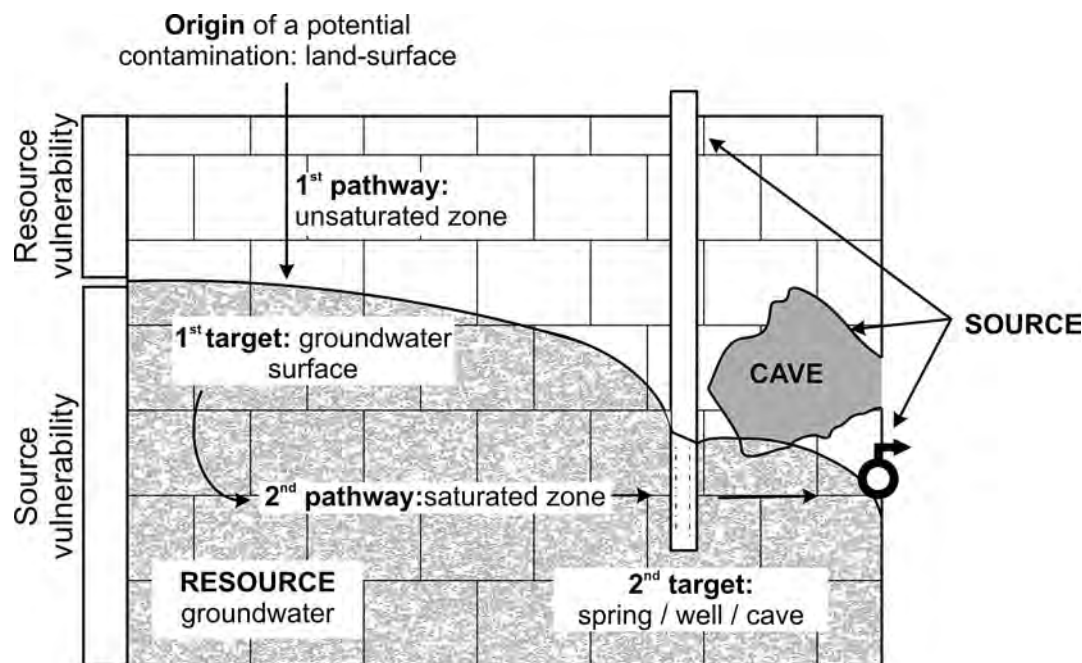[3] Spanish Geological Survey, Oviedo Office, Spain m.melendez@igme.es

Figure 1. Diagram of the origin-flow-target conceptual model, proposed in European COST Action 620 (modified from Goldscheider in Zwahlen, 2004).

country with a long tradition of karst conservation, where the first measure for cave protection dates from 1908 (Badiura and Brinšek) and in which approximately 20% of the 7405 caves recorded in the 2001 Cave Survey have been contaminated as a consequence of human activity (Kepa, 2001).

In recent years, spurred by the work of international agencies such as UNESCO, there has been an increase in legislation and practical work focusing on prevention of damage to the cultural and natural heritage. At the 32nd UNESCO Convention Concerning the Protection of the World Cultural and Natural Heritage, warnings of the risks faced regarding the conservation of caves were made: "In the context of contemporary discovery and opening of caves, complex risks have arisen related to the alteration of the physical, geological and biological conditions of conservation" and "Extremely rigorous management is required to ensure that the risks are effectively dealt with" (WHC-08/32.COM/24 Rev, 2009). Nevertheless, as yet no rules have been clearly defined in legislation regarding what kinds of measures should be taken and how protected areas should be defined to protect caves and their surroundings. In many cases, protection is limited to preventing entry into the cave, an insufficient measure that often fails (Lera, 2009). Moreover, the complexity and diversity of the karst medium hampers the design of a universal method of establishing protected areas for caves and their surroundings. Accordingly, any proposal should consider the identification and evaluation of the natural processes that involve risks to the conservation of the cave. In addition, it will be necessary to consider human

activities such as construction, livestock farming, and agriculture that could have a negative impact on the natural evolution of caves (Sánchez-Moral et al., 2002).

Evaluating the vulnerability of a cave to contamination, on the basis of the characteristics of the physical medium in which it is contained, can be used to promote land-use management that is compatible with the protection and conservation of the cave. This approach is an initial step in the delineation of protection zones for the cave and in preventing the risk of contamination. Furthermore, a good plan for the protection and conservation of a cave could include other studies, such as analysis of geological risks, particularly regarding its resistance to vibrations (Sánchez et al., 2007; Iriarte et al., 2010), the evaluation of human impact using quantitative indexes based on geomorphological features (Jiménez-Sánchez et al., 2011), and studies of the cave's environmental capacity with respect to the optimum number of visits permissible in tourist caves (Pulido-Bosch et al., 1997; Cuevas-González et al., 2010).

The concept of the contamination vulnerability of an aquifer has been defined by many investigators, among them Margat (1968) and Zaporožec (1994). The intrinsic vulnerability of an aquifer involves its sensitivity to contamination, taking into account its geological, hydrological and hydrogeological characteristics, independent of the nature of the contaminants and the contamination scenario (Zwahlen, 2004). This concept of intrinsic vulnerability, proposed in the European COST Action 620, is based on the origin-flow-target conceptual model (Fig. 1). Using this model, it is possible to distinguish between resource protection and water supply protection.
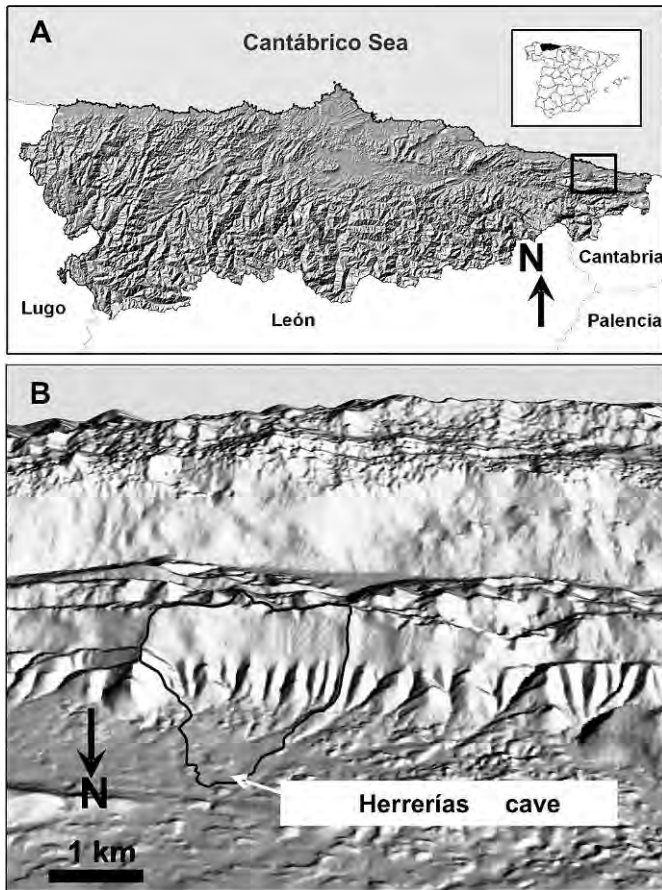
Figure 2. (A) Location of Herrerías Cave. (B) Site of cave and hydrological watershed over digital elevation model.

Considering resource protection, it is assumed that the element to be protected is the water stored in the aquifer below the piezometric surface. The flow of the polluting agent from the origin is considered to be practically vertical, passing through the soil and the unsaturated zone of the aquifer. In the case of source protection, the target of protection is the aquifer discharge point at a well or spring. Conceptually, the contaminant is assumed to be transported from the origin at the surface to the aquifer and from there to the discharge point at a spring or well. This displacement has a vertical component from the origin to the piezometric surface and a horizontal one, the latter being in the saturated zone of the aquifer.

The main aim of the present study is to adapt the groundwater-contamination vulnerability mapping method to the delineation of protection areas for caves close to the piezometric level or to a spring. The experimental site considered was the Herrerías Cave in northern Spain, for which a protection boundary has been established by the Culture and Tourism Department of the Asturias Regional Government (BOPA, 2008; BOE, 2010), permitting a comparison between this and the protection area established in present work.

THE STUDY AREA

The cave known as Herrerías, La Herrería, or El Boláu is situated in the district of Llanes in Asturias, Spain (Fig. 2). The cave contains valuable examples of prehistoric art that make it particularly interesting from a heritage point of view. The cave paintings consist of a set of grid forms composed of individual marks and parallel lines, located in the roof of the cave. The significance of the rock art, which is attributed to the Magdalenian (Jordá and Mallo, 1972), led to the cave's being declared a Good Object of Cultural Interest as a result of application of the 1985 Spanish Historical Heritage Law (BOE, 1985). The floor plan of the cave is intricate and irregular, with a horizontal extent of less than 200 m and two access points to a main gallery, the southwestern branch of which is blocked by a gate that protects the room containing the cave paintings. Land use surrounding the cave is characterized by scattered farming and stock breeding that coexist with tourist use. Also, the remnants of mining and quarrying works can be recognized in the landscape, including historic quarrying in the quaternary alluvial fans, as well as an old iron-manganese mine, located in the limestone to the west of the cave (Domínguez-Cuesta et al., 2010). The top of the karst massif in which the cave is located is presently covered by a building material dump, a potential source of cave contamination.

Herrerías Cave is located in a complex hydrogeological environment that governs its vulnerability to contamination events and thus, its need for protection. For this reason, a multidisciplinary study involving geological, geomorphological, and hydrogeological aspects have been done in a 10 km² area, including the cave's surroundings (Jiménez-Sánchez et al., 2010).

The landscape surrounding the cave contains mountainous ranges and valleys trending east-west, following the geological contacts between bedrock formations. Altitudes descend from the mountainous ranges in the south (Sierra del Cuera, 1315 meters above sea level) to the vicinity of the Cantabrian shore to the north, where remnants of karstified marine terraces can be recognized between 30 and 189 masl. The hydrographic network is superimposed on this relief, with streams mainly flowing from south to north, giving place to torrential basins and coalescing alluvial-fan deposits. Herrerias Cave is located at the bottom of one of these torrential basins, which shows a total surface of 3.37 km², a mean slope of 23° (maximum of 57°), and altitudes ranging between 34 m and 757 m (Fig. 2b).

Geologically, the study area is located in the Ponga-Cuera Unit (Marquínez, 1989). The stratigraphic sequence is composed of Barrios quartzite of the Ordovician age, the Ermita sandstone of Late Devonian age, and several Carboniferous limestone formations: the Alba, Barcaliente, and Cuera that outcrop trending east-west, showing subvertical dips (Figs. 3 and 4). The most outstanding
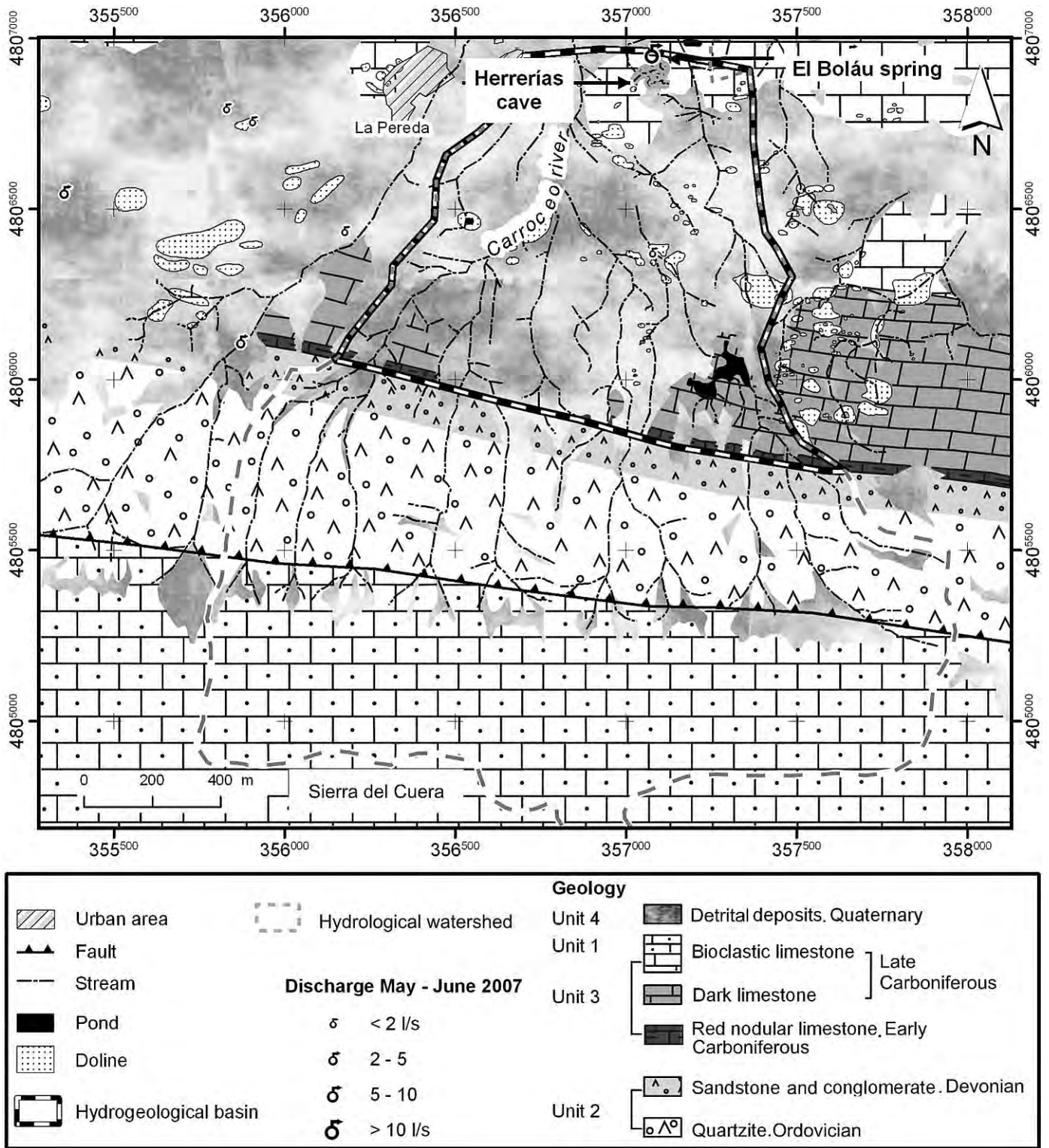
Figure 3. Geological-hydrogeological map of Herrerías Cave and its surroundings.

structure is a subvertical thrust, also trending east-west, that puts Ordovician quartzite in contact with the Cuera limestone to the south. The cave is developed in a region of Cuera limestone located in the north of the study area. The Paleozoic bedrock is covered by several Quaternary formations of alluvial, colluvial, and karstic origin.

Four hydrogeologic units can be distinguished in the study area (Figs. 3 and 4), from south to north: Unit 1
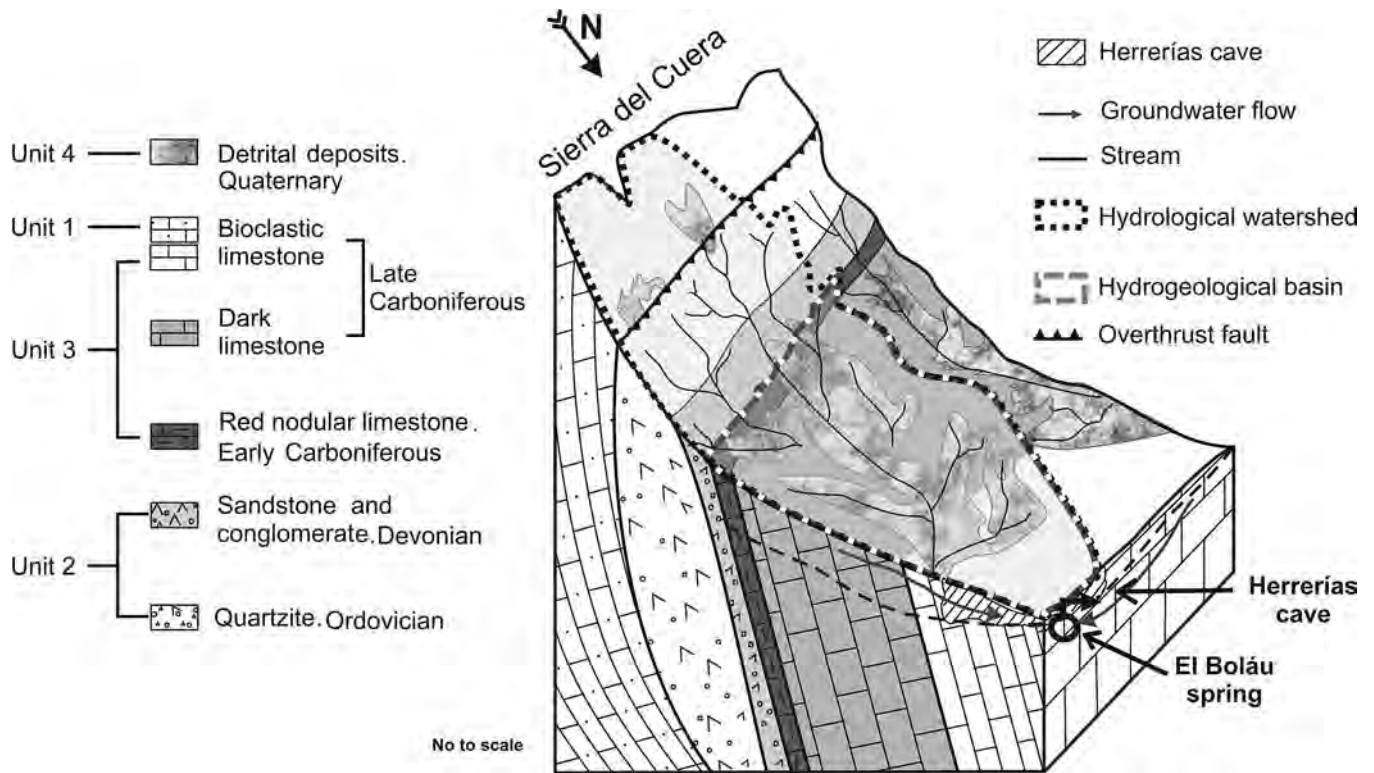
Figure 4. Geological-hydrogeological diagram of Herrerías Cave and its surroundings.

comprises the Cuera limestones; Unit 2 consists of Ordovician quartzite and Devonian sandstone and is separated of Unit 1 by a thrust fault; Unit 3 contains Carboniferous limestone of the Cuera and Barcaliente Formations. Finally, Unit 4 is characterized by Quaternary alluvial materials that lie unconformably over the bedrock formations (Jiménez-Sánchez et al., 2008a). Units 1 and 3, made up of karstifiable limestone, are carbonate aquifers; Herrerías Cave is located in Unit 3, to the north of the thrust fault (Figs. 3 and 4). The Ordovician quartzite and Devonian sandstone constitute a barrier that prevents the underground connection between the two carbonate aquifers (Ortuño et al., 2004; Fig. 4).

The Units 1 and 2 form part of the recharge area of the aquifer in which the cave is located (Unit 3), because part of the surface area drains toward this aquifer via numerous streams. Unit 3, with a groundwater flow northward, is drained by springs, including that of El Boláu, which is the resurgence of this cave. The groundwater flow into the cave takes place through multiple drip points and via a subterranean watercourse that is visible in some areas in the cave. Thus, as shown in Figures 2 and 3, in the study area the hydrological watershed and hydrogeological basin do not coincide.

From the above observations, it can be deduced that the recharge area of both El Boláu spring and Herrerías Cave, contains two different sectors. The southern sector constitutes the limestone of Unit 1 and the sandstone and quartzite of Unit 2. Surface runoff generated in this sector infiltrates into the aquifer limestones farther north in Unit 3 through the overlying Quaternary deposits of Unit 4. Therefore, the influence of the southern sector on the cave's vulnerability to contamination is related to the infiltration of surface water and potential contaminants from the hydrological watershed. The connection between certain points of this hydrographic network and the cave has been demonstrated by the injection of sodium fluoresceine into the Carroceo River (Jiménez-Sánchez et al., 2010).

The northern sector is the part of the aquifer containing the Unit 3 limestone that drains toward the El Boláu spring. Despite the lack of data on piezometric levels, it seems reasonable to believe that the El Boláu spring drains water directly infiltrating into the limestones outcrops (Unit 3), together with the infiltration water from surface runoff from the southern areas. In addition to these two components, there is recharge from the Quaternary materials of Unit 4, as also demonstrated by tracer injection in the Carroceo River (Jiménez-Sánchez et al., 2010).

Analyses of water samples collected at a drip point in the cave during the months of February–June 2007 show that the evolution of the NO_3^-, NO_2^-, TOC (total organic carbon) and Cl^- content is related to recharge episodes, but also to contamination from human activities in the area of the cave's recharge zone. Peaks of 20 mg L^{-1} and

50 mg L^{-1} of TOC, 15.63 mg L^{-1} of NO$_3^-$ and ≈17 mg L^{-1} of NO$_2^-$ have been detected in the drip water (Jiménez-Sánchez et al., 2008b).

Application of the COP+K Method

In this study, the COP+K method (Vías et al., 2006; Andreo et al., 2009) was applied. This method was originally developed to evaluate contamination vulnerability and to delineate protection areas for water supply springs or wells in carbonate (karst) aquifers. However, this method must be reinterpreted and specifically adapted to this case, considering Herrerías Cave itself is a protection target (Fig. 1), in a way analogous to that applied to water supply sources.

The COP+K method is an extension of the COP method (Vías et al., 2006), by which the contamination vulnerability of karstic aquifers can be evaluated and on the basis of this assessment, protection zones defined. This method incorporates the conceptual model and the indications set out in the framework of European COST Action 620 (Zwahlen, 2004). The COP+K method is based on estimating the surface flow recharge conditions (C factor), the protection capacity of the layers overlying the aquifer (O factor), and the precipitation (P factor), together with the participation of the saturated zone (K factor). The method is applied using cartographic overlay created with geographic information systems. The procedure, classification, and scoring of the variables used to evaluate vulnerability according to the COP+K method are shown in Fig. 5 and explained in detail by Vías et al. (2006) and Andreo et al. (2009).

In accordance with current knowledge of the hydrogeological system of Herrerías Cave and its surroundings (Jiménez-Sánchez et al., 2008a, 2008b, 2010), the protection of the cavity should consider both surface water in the hydrological watershed and groundwater in the hydrogeological basin (Figs. 3 and 4). However, application of the COP+K method is only possible in the hydrogeological basin of the Herrerías Cave, where there is a vulnerable carbonate aquifer and deposits of alluvial materials (Units 3 and 4, Fig. 2). Since Unit 2 (Ordovician quartzites and Devonian sandstones) does not constitute an aquifer, it is not possible to evaluate the thickness of the unsaturated zone (O factor) or the transit through the saturated zone of possible contaminants (K factor). Likewise, no valuation is made of the K factor (transit through the saturated zone) in Unit 1 because, as remarked above, this unit has no hydrogeological connection with the cave. The main results of our evaluation of the parameters composing the method are described below (Fig. 6).

C Factor

This factor was the most difficult one to assess, due to the double component of runoff and infiltration acting as recharge and to the non-coincidence of the hydrological and hydrogeological watersheds. The surface conditions for the concentration of water flows to recharge the aquifer (the C factor) were evaluated based on a prior classification of the study area into the two infiltration sources defined in the original method, concentrated infiltration via karstic swallow holes and direct infiltration of rainfall over outcrops in the rest of the catchment (Vías et al., 2006). However, an additional source of infiltration affects a significant sector of the study area, deferred infiltration through the beds of influent streams that was demonstrated by the use of tracers at certain points (Jiménez-Sánchez et al., 2010). Evaluation of the C factor of this new source was carried out using an adaptation of the two scenarios previously defined by Vías et al. (2006). The scores of the sv, dh, and ds subfactors were modified (see Tables XII–XIV in Fig. 5; scenario 3 of C factor), taking into account that this infiltration through the unsaturated zone is concentrated, but not as much as in sinking streams via swallow holes.

O Factor

The spatial distribution of the protection capacity of the layers overlying the aquifer in which Herrerías Cave is developed reflects the distribution of the soil that is important in protecting groundwater against contamination episodes. Above this aquifer, the soil is the only layer conferring heterogeneity to the O factor, as the lithology is similar throughout the hydrogeological basin to be delineated. The protection capacity is very low immediately surrounding of the cave because the soil is practically non-existent. The protection capacity is slightly higher in the rest of the hydrogeological basin where the soil is better developed, and it has been even considered high in the small areas where soil of a clayey texture and greater thickness has been mapped.

P Factor

This factor was evaluated using data obtained from the Parres de Llanes meteorological station, located 1.3 km northwest of the cave. The P factor is based on the quantity and intensity of precipitation events based on the daily precipitation of a historical set of wet years. The average rainfall is 1600 mm and the average number of days of rain per year is 135. This annual precipitation helps in the dilution of potential contaminant that is likely to be dominant process instead of infiltration (Vías et al. 2006). A moderate reduction in the level of protection provided by the unsaturated zone (evaluated by O factor) due to the precipitation characteristics in this area has been identified. This parameter was taken as homogeneous for the test site (Fig. 6) because of the lack of an adequate number of meteorological stations. Although this factor does not influence the distribution of vulnerability classes, it affects the indexes of vulnerability, reducing the value resulting from the C and O factors; the value of P factor is 0.7.
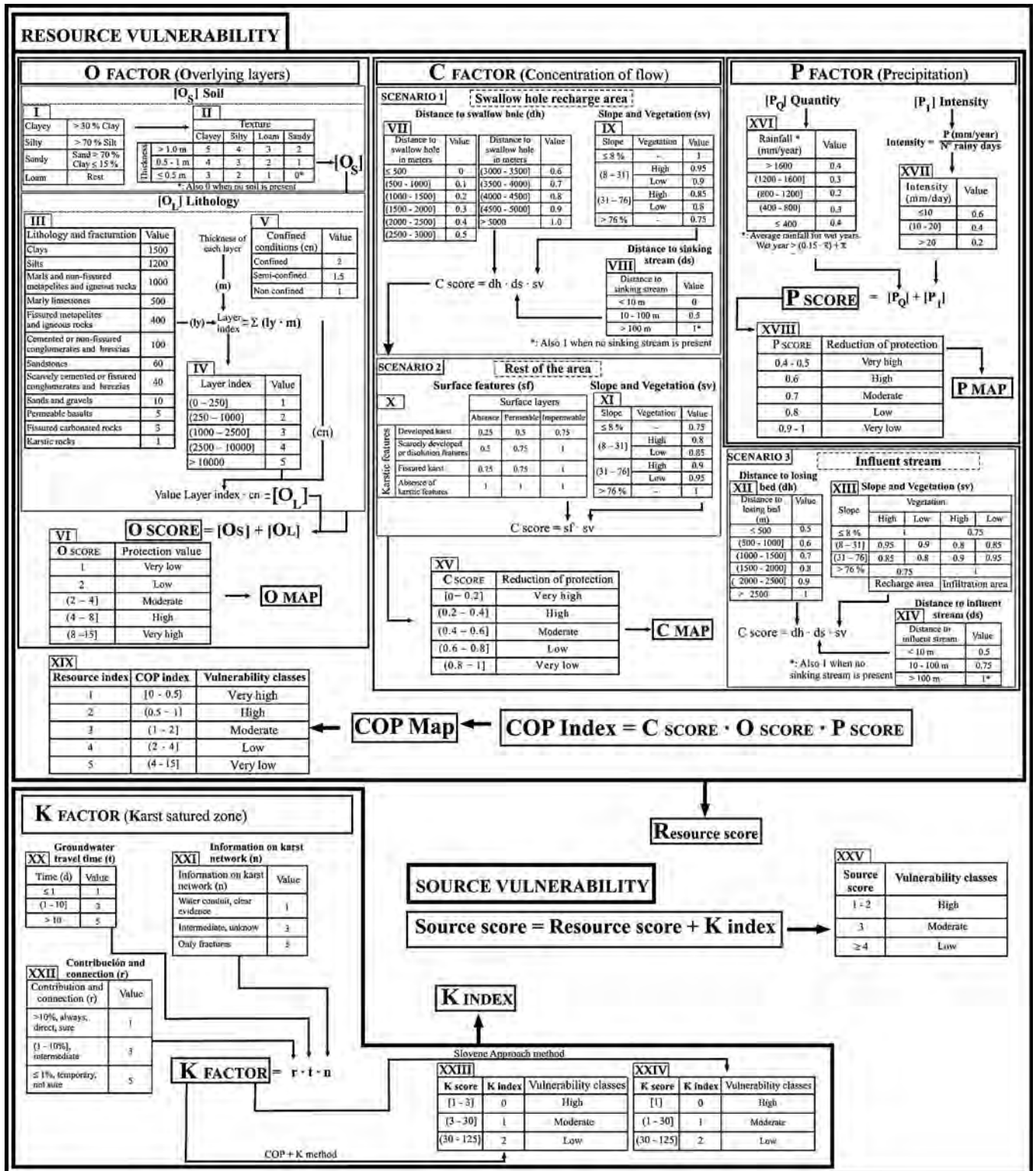
Figure 5. Diagram of the COP+K method, showing the differentiation of the C, O, P, and K factors. Modified from Vías et al. (2006).

The COP vulnerability index map (COP in Fig. 6), is the cartographic overlay of the C, O, and P factors and shows the vulnerability to contamination of the test site. The aquifer in which Herrerías Cave is located presents a contamination vulnerability level ranging from high to very high. In only a few small sectors is the vulnerability classified as moderate. The distribution of the areas where contamination vulnerability is very high is determined by
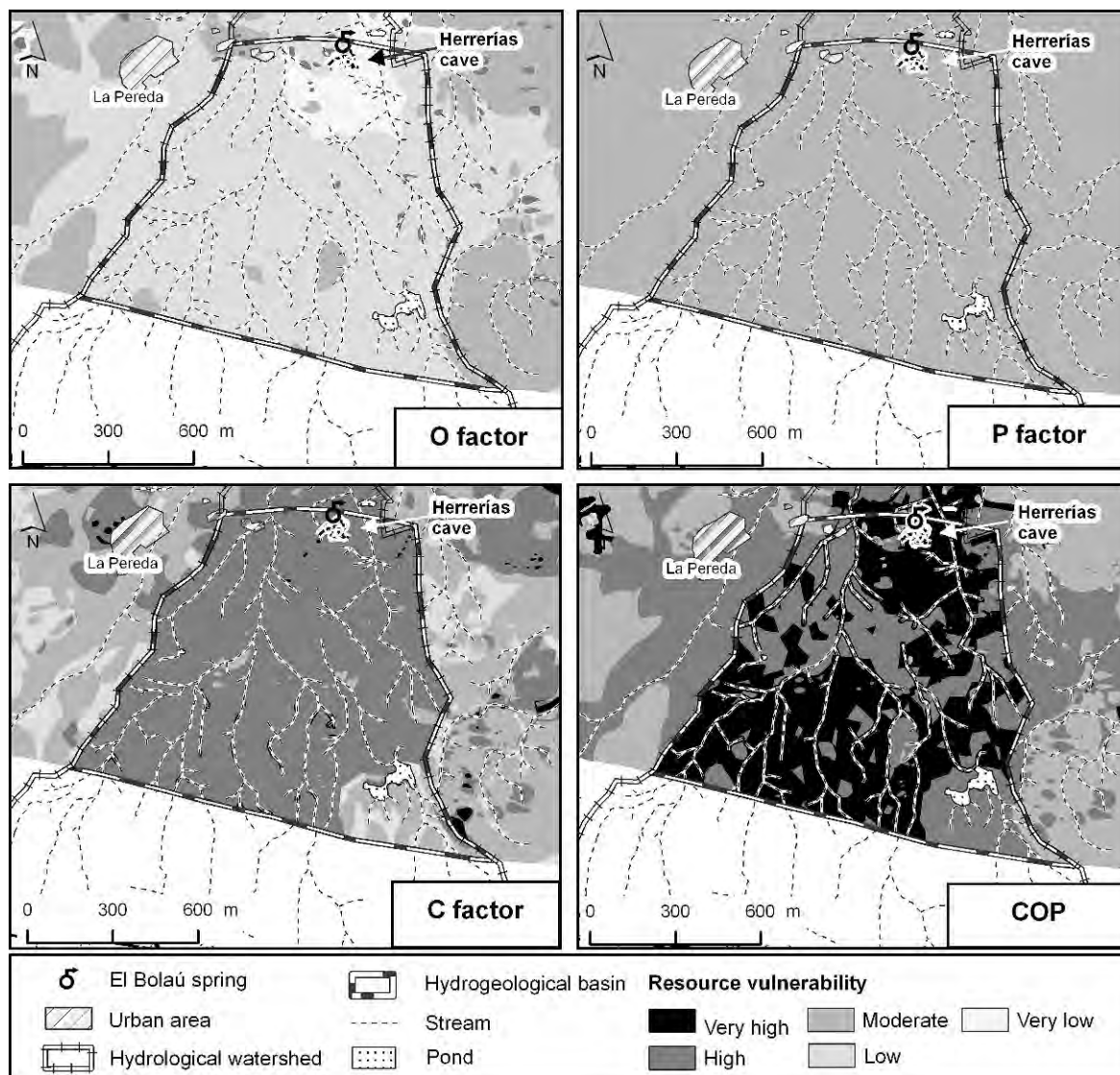
Figure 6. C, O, P, and COP maps assessing the vulnerability of the areas surrounding Herrerías Cave.

two factors: the scant protection capacity afforded by the layers overlying the aquifer (very low O factor values) and the considerable reduction of the protection capacity resulting from the concentration of surface runoff flows provoking infiltration (the C factor). Only where the slope is lower than 8% is the resource vulnerability on the hydrological watershed high instead of very high. In the COP index map in Figure 6, the watershed area fed by influent streams shows values of vulnerability higher than those obtained in similar areas out of this hydrographic basin.

K Factor

This factor was evaluated after determining the direction and velocity of groundwater flow in the study area using tracer tests and other hydrogeologic criteria. Specifically, three flow velocities were determined (Fig. 7).

Between Meandros Hall and Pinturas Hall in the cave, the approximately east to west flow velocity was 128 m h^{-1}, while between Pinturas Hall and the El Boláu spring, it ranged from 237 to 250 m h^{-1} in an approximately northeasterly direction (two tracer tests; Jiménez-Sánchez et al., 2010). The tracer tests were carried out in a small sector of the hydrogeological basin, and so their ability to represent the entire aquifer remains uncertain until additional data are acquired to improve the K factor evaluation. The difference in velocities calculated using the tracer tests has no impact on the application of the COP+K method because the entire study area has a transit time (the t subfactor in the method) of less than one day. The r subfactor considers the contribution and connection rates of different parts of the aquifer to the cave. The overall hydrogeological basin was considered directly connected to the cave.
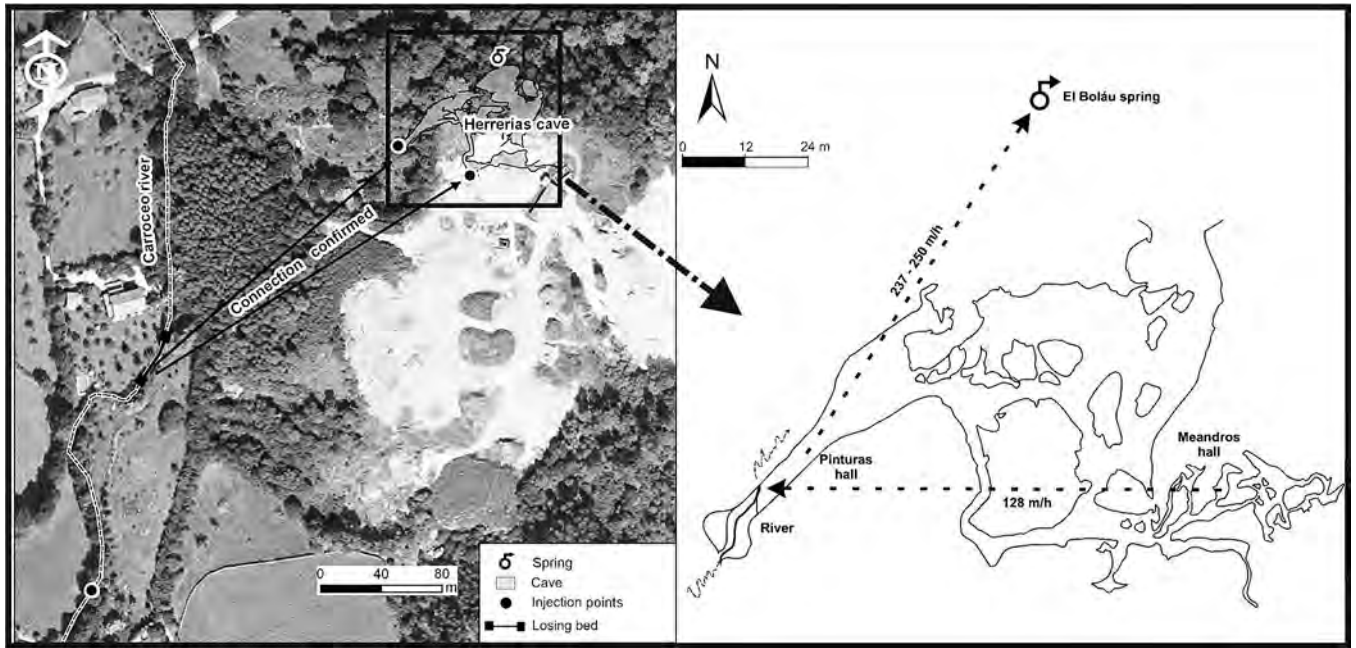
Figure 7. Sketch of the tracer tests to and within Herrerías Cave and the flow velocities deduced.

With respect to the karst network (subfactor n in the COP+K method), the cave is a conduit in which the piezometric level is visible in some sectors. However, as the cave itself is the object of protection, the water route considered is solely that from the surface to the walls and roof of the cave. Once the water or the potential contaminant reaches the cavity walls, the flow has reached the objective (Fig. 8). Water transit through the cave was not considered for the purposes of delineating the protection boundary.

The K value is the product of the three subfactors described above, the t, r, and n subfactors. K values can be subdivided into three classes, indicating different degrees of vulnerability of a water source to contamination. This enables the class boundary values to be modified in response to legislation passed to protect water supply sources (Fig. 5). For example, according to the Slovene approach (Ravbar and Goldscheider, 2007) vulnerability is high only when the K value is 1; in areas where the transit time is less than 1 day, there is clear evidence of an active karst network and the contribution rate is >10%. However, for a given source, according to the methodology proposed by Andreo et al. (2009), values of 1 to 3 indicate high vulnerability to contamination. Many carbonate
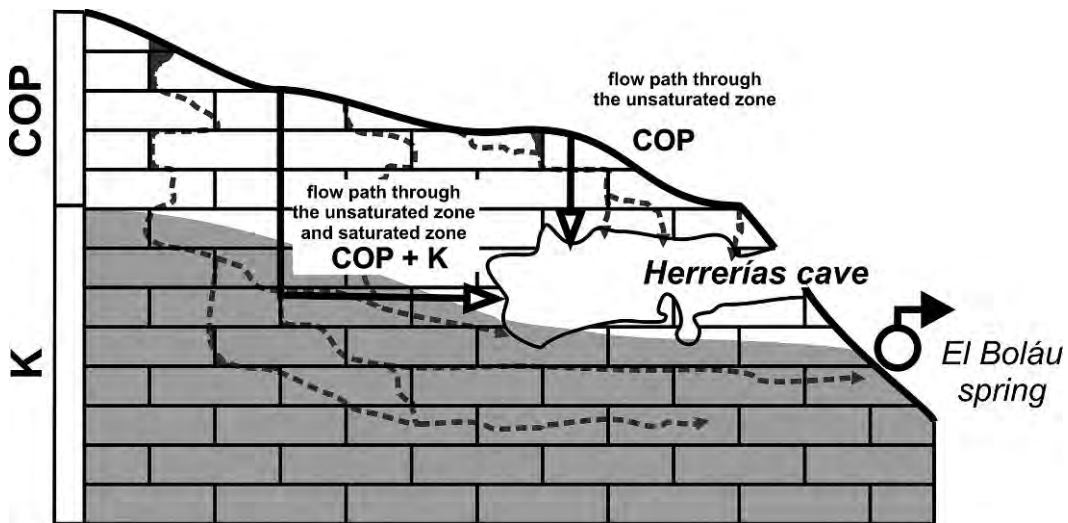

Figure 8. Conceptual diagram of the transit of possible contaminants toward Herrerías Cave.

aquifers present good permeability as a result of the development of conduits enabling rapid flow velocities and direct connections. However, these aquifers might not have been identified or explored, and so a lower subfactor n value would not be awarded. In such a case, which is very similar to the study area conditions, the K factor would represent a high level of vulnerability in accordance with the COP+K classification, and a moderate one according to the Slovene approach.

Intrinsic Source Vulnerability Map

By converting the COP and K values into their respective indices and summing them (Fig. 5), we obtain the source (the cave) contamination vulnerability map. By direct interpretation of the vulnerability classes, it is possible to find the areas that need various degrees of protection (Andreo et al., 2009). The vulnerability map for the Herrerías Cave obtained using the COP+K method, classifying the K factor according to the Slovene approach (K index = 1, Table XXIV in Fig. 5), shows a large zone classed as highly vulnerable, coinciding with the areas where the resource vulnerability is considered very high (Fig. 6). These areas are located immediately surrounding the cave and in other sectors with aquifer recharge via influent streams (Marín et al., 2010). The vulnerability is considered moderate in areas where the resource vulnerability is high (COP index = 2) due to, especially, slopes that decrease flows towards influent streams. The cave's vulnerability to contamination, evaluated using the COP+K method, with the K factor being scored using the COP+K method (K index = 0, Table XXIII in Fig. 5), is considered high in almost the entire hydrogeological basin. The vulnerability is moderate only in zones where soil and Quaternary materials offer a certain degree of protection, the zones where resource vulnerability is moderate (fig. 6). In any case, the results obtained demonstrate that Herrerías Cave shows a high level of vulnerability to contamination as a consequence of the physical characteristics and dynamics of the hydrogeological basin.

Delineation of the Protection Zone

The ultimate aim of the protection zoning is to protect the cave against possible negative impacts arising from human activity. The arrival of contaminant substances with infiltration water may provoke alterations within the cave environment. The entire area connected to the cave via flows of surface water or groundwater should be considered a possible site of contaminating activities, and therefore, should be included within the design of the protection boundary for the cave.

In the application of the COP+K method to protection zoning, the areas taken into consideration were those classed as high vulnerability, requiring maximum protection, and moderate vulnerability, requiring a moderate

degree of protection. The two maps proposed in Figure 9 illustrate the need for a protection boundary for this cave that includes the entire hydrological basin, independent of the degree of internal protection.

For comparison, Figure 9 shows the protection area published in the BOPA (2008) and BOE (2010) together with the one proposed in this study. The areas that we propose here as requiring maximum protection are larger than those defined in BOPA (2008) and BOE (2010) and include part of the watershed that feeds the influent streams. This network of influent streams on the north-facing slopes of the Sierra del Cuera merits special attention because of its hydrologic relation with the aquifer in which the cave is located. As explained above, in this area, surface runoff takes place, especially over the sandstones and quartzite of Unit 2. This surface runoff infiltrates downstream into the aquifer (Figs. 2 and 3). The maps presented in Figure 9 show that most of the river beds into which water infiltrates are located in the zone requiring maximum protection; therefore, any human use of the watershed should be controlled to avoid dumping or spills that, transported by the runoff water, could affect the cave. Accordingly, the hydrogeological basin fed by these rivers is considered part of the cave's protection zoning in a category we term watershed to control. Finally, unlike the perimeter defined in the BOPA and BOE, we do not consider it necessary to include the areas located to the north of the cave and El Boláu spring in the protection zone. The reason is that the water flow toward the north prevents any contaminant deposited in this zone from affecting the cave.

Conclusions

Protection zoning for caves is a preventive mechanism of great interest for their conservation. In the case of karst aquifers, this delineation goes beyond the simple marking out of zones requiring different degrees of protection in the immediate surroundings of the item to be protected, a spring, well, or cave. The hydrogeological characteristics of the surroundings should be considered in the process by which protection areas are defined. Therefore, in this study we adapted the COP+K method, which is specific for groundwater contamination vulnerability assessment in carbonate aquifers.

The results obtained from applying this method to the Herrerías Cave show that protection measures need to consider the entire sector of the aquifer in which the cavity is located. Such protection zoning should include the riverbeds of influent streams and the corresponding hydrographic watersheds. Independently of the classification of the K factor, which concerns the karstification of the saturated zone, the extent of the protected areas established reveals the high degree of vulnerability to contamination of Herrerías Cave and the insufficiency of the current protection area defined for it. Land-use
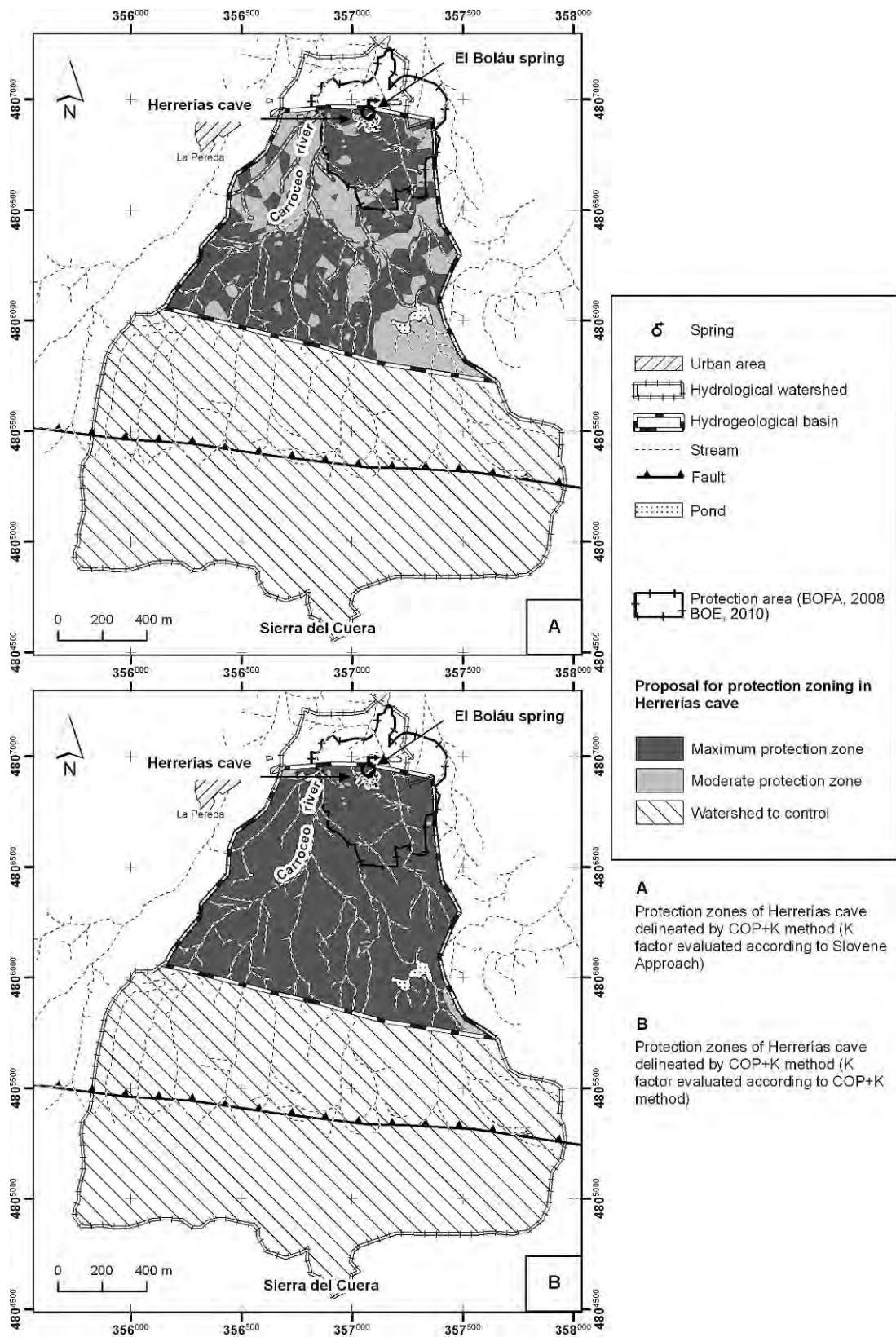
Figure 9. Protection areas proposed for Herrerías Cave on the basis of the contamination vulnerability evaluation made using the COP+K method (A) with the K factor being classified according to the Slovene approach (Ravbar and Goldscheider, 2007) and (B) with the K factor being classified using the COP+K method (Andreo et al., 2009). Also shown is the protection area recommended in BOE (2010) and BOPA (2008).

planning is required to protect the cave. Spain has no national legislation defining the activities allowed in different protected areas. However, potentially polluting land-use activities should be prohibited or restricted, especially activities creating microbial contaminants and types of polluting land-use practices that generate dangerous leachates.

Apart from the final mapping obtained of the study area, the main contribution of this study is the adaptation of the COP+K method to delineate cave protection areas, especially for caves containing groundwater flow or close to a spring. The evaluation of a cave's vulnerability to contamination, on the basis of the characteristics of the physical medium in which it is located, is a useful tool to ensure the compatibility of surface management and cave conservation. Hydrogeological studies are essential to achieve an adequate understanding of the interactions between the cave and its surroundings. The COP+K method enables us to place this knowledge on a cartographic basis, which constitutes a good initial point for delineating cave protection areas and for preventing possible contamination.

Finally, it should be noted that protection areas are not static and need to be periodically reviewed to determine whether the physical variables justifying the delineation remain unchanged. If environmental alterations are detected or if further studies produced new information about hydrogeological relationships, the proposed perimeter should be reviewed and, if necessary, modified, in accordance with the new reality.

ACKNOWLEDGMENTS

REFERENCES

Andreo, B., Ravbar, N., and Vías, J.M., 2009, Source vulnerability mapping in carbonate (karst) aquifers by extension of the COP method: Application to pilot sites: Hydrogeology Journal, v. 17, no. 3, p. 749–758, doi:10.1007/s10040-008-0391-1.

Badiura, R., and Brinšek, B., 1908. Nove jame ob Cerkniškem jezeru. – Planinski vestnik, p. 6–7, 96–99, 124–126, Ljubljana.

BOE, 1985, Ley 16/1985, de 25 de junio, del Patrimonio Histórico Español: Boletín Oficial del Estado, no. 155, p. 20342–20352.

BOE, 2010, Decreto 20/2010, de 3 de marzo, por el que se delimita el entorno de protección de la cueva de La Herrería, en La Pereda, en el concejo de Llanes: Boletín Oficial del Estado, no. 100, p. 36592–36594.

BOPA, 2008, Resolución de 27 de febrero de 2008, de la Consejería de Cultura y Turismo, por la que se aprueba el entorno de protección

provisional para la cueva de La Herrería, en la Pereda, concejo de Llanes: Boletín Oficial del Principado de Asturias, v. 74, 7147 p.

Catani, F., Fanti, R., and Moretti, S., 2002, Geomorphologic risk assessment for cultural heritage conservation, in Allison, R.J., ed., Applied Geomorphology: Theory and Practice: West Sussex, England, John Wiley & Sons, p. 317–334.

Cuevas-González, J., Fernández-Cortés, A., Muñoz-Cervera, M.C., Andreu, J.M., and Cañaveras, J.C., 2010, Influence of daily visiting regime in tourist cave at different seasons, in Andreo, B., Carrasco, F., Durán, J.J., and LaMoreaux, J.W., eds., Advances in Research in Karst Media, p. 475–481.

Domínguez-Cuesta, M.J., Jiménez-Sánchez, M., Rodríguez-Rodríguez, L., Ballesteros, D., Meléndez, M., Martos, E., and García-Sansegundo, J., 2010, Uso de la geomorfología y el SIG para caracterizar el impacto de actividades mineras en zonas kársticas: El entorno de la cueva de Las Herrerías (Asturias, España), in Berrezueta Alvarado, E., and Domínguez Cuesta, M.J., eds., Técnicas Aplicadas a la Caracterización y Aprovechamiento de Recursos Geológico-Mineros. Volumen I: Descripciones Metodológicas: Oviedo, Spain, Instituto Geológico y Minero de España, p. 80–90.

Iriarte, E., Sánchez, M.A., Foyo, A., and Tomillo, C., 2010, Geological risk assessment for cultural heritage conservation in karstic caves: Journal of Cultural Heritage, v. 11, no. 3, p. 250–258, doi:10.1016/j.culher.2009.04.006.

Jiménez-Sánchez, M., Domínguez-Cuesta, M.J., García-Sansegundo, J., Stoll, H., González- Pumariega, P., Fuente-Puente, G., Meléndez, M., Martos, E., Vadillo, I., Rodríguez-Rodríguez, L., and Aranburu, A., 2008a, Estudio preliminar de la geomorfología de la cueva de Herrerías y su entorno (Llanes, Asturias, Noroeste de España), in Benavente, J., and Gracia, F.J., eds., Trabajos de Geomorfología en España 2006–2008: Cádiz, Spain, Sociedad Española de Geomorfología and Universidad de Cádiz, p. 45–48.

Jiménez-Sánchez, M., Stoll, H., Vadillo, I., López-Chicano, M., Domínguez-Cuesta, M., Martín-Rosales, W., and Meléndez-Asensio, M., 2008b, Groundwater contamination in caves: Four case studies in Spain: International Journal of Speleology, v. 37, no. 1, p. 53–66.

Jiménez-Sánchez, M., Vadillo, I., Domínguez-Cuesta, M.J., Meléndez, M., Andreo, B., Marín, A.I., Stoll, H., Martos, E., González-Pumariega, P., Potenciano de las Heras, A., and García- Sansegundo, J., 2010, Estudio del karst en la cueva de las Herrerías y su entorno (Llanes, Asturias): Memoria final de investigación 2007–2010, Consejería de Cultura Principado de Asturias, 179 p.

Jiménez-Sánchez, M., Domínguez-Cuesta, M.J., Aranburu, A., and Martos, E., 2011, Quantitative indexes based on geomorphologic features: A tool for evaluating human impact on natural and cultural heritage in caves: Journal of Cultural Heritage, v. 12, p. 270–278, doi:10.1016/j.culher.2011.01.004.

Jordá Cerdá, F., and Mallo Viesca, M., 1972, Las pinturas de la cueva de Las Herrerías (Llanes, Asturias): Revista de la Facultad de Filología Seminario de Prehistoria y Arqueología de la Universidad de Salamanca, v. 23, p. 306–311.

Kepa, T., 2001, Karst conservation in Slovenia: Acta Carsologica, v. 30, no. 1, p. 143–164.

Lera, T., 2009, The Virginia Cave Protection Act: A review (1966–2009): Journal of Cave and Karst Studies, v. 71, no. 3, p. 204–209.

Margat, J., 1968, Vulnerabilité des nappes d'eau souterraine à la pollution: Bases de la cartographie: Orléans, France, Bureau de Recherches Géologiques et Miniéres, Document 68 SGL 198 HYD.

Marín, A.I., Andreo, B., Jiménez-Sánchez, M., Domínguez, M.J., and Meléndez, M., 2010, Delimitación del perímetro de protección de la cueva de Herrerías (Llanes, Asturias) mediante el método COP+K, in Proceedings, III Congreso Español sobre Cuevas Turísticas, CUEVATUR 2010: Cuevas: patrimonio, naturaleza, cultura, y turismo: Aracena (Huelva). Spain, p. 451–464.

Marquínez, J., 1989, Síntesis cartográfica de la Región del Cuera y de los Picos de Europa: Trabajos de Geología, v. 18, p. 137–144.

Ortuño, A., Meléndez, M., and Rodríguez, M.L., 2004, Relación entre litología y características hidroquímicas de las aguas subterráneas: Red de Control de la Calidad del Principado de Asturias: Boletín Geológico y Minero, v. 115, no. 1, p. 35–46.

Pulido-Bosch, A., Martín-Rosales, W., López-Chicano, M., Rodríguez-Navarro, C., and Vallejos, A., 1997, Human impact in a tourist karstic cave (Aracena, Spain): Environmental Geology, v. 31, no. 3–4, p. 142–149, doi:10.1007/s002540050173.

Ravbar, N., and Goldscheider, N., 2007, Proposed methodology of vulnerability and contamination risk mapping for the protection of karst aquifers in Slovenia: Acta Carsologica, v. 36, no. 3, p. 397–411.

Sánchez, M.A., Foyo, A., Tomillo, C., and Iriarte, E., 2007, Geological risk assessment of the area surrounding Altamira Cave: A proposed natural Risk Index and Safety Factor for protection of prehistoric caves: Engineering Geology, v. 94, p. 180–200, doi:10.1016/j.enggeo.2007.08.004.

Sánchez-Moral, S., Cañaveras, J.C., Soler, V., Saiz-Jiménez, C., Bedoya, J., and Lario, J., 2002, La conservación del monumento, in Lasheras, J.A., ed., Redescubrir Altamira: Madrid, Tuner Ediciones, p. 245–257.

SC.85 /CONF.008 /09, United Nations Educational, Scientific and Cultural Organization. 9th session of the Committee, Paris, France, 2–6 December 1985, 09 COM XA - Inscription: Altamira Cave (Spain), 23 p.

Vías, J.M., Andreo, B., Perles, M.J., Carrasco, F., Vadillo, I., and Jiménez, P., 2006, Proposed method for groundwater vulnerability mapping in carbonate (karstic) aquifers: the COP method: Application in two pilot sites in Southern Spain: Hydrogeology Journal, v. 14, no. 6, p. 912–925, doi:10.1007/s10040-006-0023-6.

WHC-08/32.COM/24Rev, 2009, Decisions adopted at the 32nd session of the World Heritage Committee, Convention Concerning the Protection of the World Cultural and Natural Heritage. (Quebec City, 2008): Paris, UNESCO World Heritage Centre, 230 p.

Zaporožec, A., 1994, Concept of groundwater vulnerability, in Vrba, J., and Zaporožec, A., eds., Guidebook on mapping groundwater vulnerability: Hanover, Heinz Heise, International Contributions to Hydrogeology 16, p. 3–8.

Zwahlen, F., ed., 2004, COST Action 620. Vulnerability and Risk Mapping for the Protection of Carbonate (Karstic) Aquifers: Final Report. Brussels, European Commission, Directorate-general XII Science, Research and Development, 297 p.

MICROBIOLOGICAL ACTIVITIES IN MOONMILK MONITORED USING ISOTHERMAL MICROCALORIMETRY (CAVE OF VERS CHEZ LE BRANDT, NEUCHATEL, SWITZERLAND)

OLIVIER BRAISSANT[1]*, SASKIA BINDSCHEDLER[2], ALMA U. DANIELS[1], ERIC P. VERRECCHIA[2], AND GUILLAUME CAILLEAU[2]

Abstract: Studies of the influence of microbial communities on calcium carbonate deposits mostly rely on classical or molecular microbiology, isotopic analyses, and microscopy. Using these techniques, it is difficult to infer microbial activities in such deposits. In this context, we used isothermal microcalorimetry, a sensitive and non-destructive tool, to measure microbial activities associated with moonmilk *ex-situ*. Upon the addition of diluted LB medium and other carbon sources to fresh moonmilk samples, we estimated the number of colony forming units per gram of moonmilk to be $4.8 \times 10^5 \pm 0.2 \times 10^5$. This number was close to the classical plate counts, but one cannot assume that all active cells producing metabolic heat were culturable. Using a similar approach, we estimated the overall growth rate and generation time of the microbial community associated with the moonmilk upon addition of various carbon sources. The range of apparent growth rates of the chemoheterotrophic microbial community observed was between 0.025 and 0.067 h^{-1} and generation times were between 10 and 27 hours. The highest growth rates were observed for citrate and diluted LB medium, while the highest carbon-source consumption rates were observed for low molecular weight organic acids (oxalate and acetate) and glycerol. Considering the rapid degradation of organic acids, glucose, and other carbon sources observed in the moonmilk, it is obvious that upon addition of nutrients during snow melting or rainfall these communities can have high overall activities comparable to those observed in some soils. Such communities can influence the physico-chemical conditions and participate directly or indirectly to the formation of moonmilk.

INTRODUCTION

Many biogeochemical processes involving many different microbial activities take place in caves (see Barton and Northup, 2007, and Northup and Lavoie, 2001, for reviews). Most of these microbial processes are slow due to the oligotrophic nature of cave environments (Mulec, 2008). Among the results of these processes, moonmilk is an ubiquitous cave deposit composed of various mineral components, such as needle-fiber calcite (NFC) and nanofibers. Both biotic and abiotic mechanisms have been proposed for the development of moonmilk, and multiple mechanisms are possible, but moonmilk is generally believed to be the result of microbial activity (Cañaveras et al., 2006; Mulec et al., 2002). This deposit has strong similarities with secondary calcium carbonate accumulations observed in soils that are mainly composed of NFC and nanofibres. Many papers have provided strong supporting evidence for the biogenic origin of NFC in soils (Callot et al., 1985; Phillips et al., 1987; Phillips and Self, 1987; Cailleau et al., 2009a,b; Curry et al., 2009). Moreover, recent investigations emphasize the potential implication of organic templates as a precursor to

mineralized nanofibres (Cailleau et al., 2009b; Bindschedler et al., 2010). However, the biogenic origin is still debated for both moonmilk and soil secondary calcitic deposits composed of NFC and nanofibres (Lacelle, 2010; Borsato et al., 2000; Engel and Northup, 2008). In order to investigate the biogenic origin of moonmilk, many studies have used electron microscopy, bacterial cultures, or both (Cañaveras et al., 2006; Mulec et al., 2002; Cailleau et al., 2009a,b; Bindschedler et al., 2010). Electron microscopy of natural moonmilk samples provides useful information on the spatial relationship between microorganisms and calcium carbonate needles and nanofibres, but it must be recognized that only a limited number of samples can be observed, which leads to conclusions potentially speculative. Similarly, culture-based methods provide great insight into potentially involved microbial processes. For example, culture methods were used to show the ability of soil bacteria to precipitate calcium carbonate (Boquet et al.,

* Corresponding Author: olivier.braissant@unibas.ch
[1] Laboratory of Biomechanics & Biocalorimetry, c/o Biozentrum/Pharmazentrum, University of Basel, Klingelbergstrasse 50-70, CH-4056 Basel, Switzerland
[2] Institute of Geology and Paleontology, University of Lausanne, Quartier UNIL-Dorigny, Bâtiment Anthropole, CH-1015 Lausanne, Switzerland

1973). However, a large part of the microbial population cannot be cultivated, and therefore, are not taken into account (Amman et al., 1995). Finally, nucleic acid-based studies provide insight on the microbial community, but it is often difficult to infer population sizes and specific activities from molecular data unless one uses stable isotope probing (Konhauser, 2007).

In this context, isothermal microcalorimetry can provide another valuable tool for obtaining data on microbial activities associated with moonmilk. Isothermal microcalorimetry is an efficient means of monitoring microbial activities through measurement of heat production rates. Isothermal microcalorimetry is extremely sensitive, and heat flows as low as 20 to 200 nW are sufficient to produce a reliable signal (Braissant et al., 2010; Wadsö, 2002). Assuming that a typical single bacterial cell produces about 2 pW when active (Higuera-Guisset et al., 2005; James, 1987), only 10,000 to 100,000 bacteria per sample (i.e., per 3 or 4 ml microcalorimetric ampoule) are required to produce a detectable signal in most commercial isothermal microcalorimeters. Since only heat production is measured, isothermal microcalorimetry is non-destructive and non-invasive, allowing samples to be studied *ex-situ* without disturbance other than placing them in the calorimetric vessel. Although these are still significant interactions, they can be considered minimal compared to other techniques. Due to these advantages, isothermal microcalorimetry has been widely used for soils (Rong et al., 2007; Wadsö, 2009), but it had not yet been applied to caves.

In this study, we investigated the microbial activities in moonmilk supplemented with different carbon sources. From the data, the number of active bacteria and the various substrate degradation rates are inferred. This approach provides a valuable set of data that complement previous studies on moonmilk and biomineralization.

Materials and Methods

Geological Settings

Vers chez le Brandt (46°56′16″N, 6°28′22″E) is a limestone cave (Sequanian stage) located in the Swiss Jura mountains 4 km north of the village of Les Verrières (Fig. 1A) and only 1200 meters from the French border. The cave is 63 meters deep and 336 meters long (Fig. 1B) and has been previously described (Gigon et al., 1976). The average temperature in the cave is about 10 °C (Perrin, 2003).

Sample Collection

Moonmilk samples from the location indicated in Figure 1B were collected aseptically on July 17, 2009. Although moonmilk can be found in most of the cave, this location was chosen because it is less accessible and thus less contaminated. All the material used was sterile, and samples were placed into sterile sampling bags or sterile 50 ml polypropylene tubes. Approximately 100 g of slightly wet material was collected. Samples were stored in a cooler

containing blue ice, and later at 4 °C until analysis. Samples collected for microcalorimetry were processed and incubated in the microcalorimeter within twenty hours after collection. Additional moonmilk samples were collected for microscopic observations and were stored at 4 °C for one week before preparation and observation. These samples were taken from specific moonmilk patches selected for their darker color, which we assumed to have slightly higher amounts of organic matter (authors' personal observations; no organic matter measurements were performed in this cave). Organic matter is likely brought to the cave through rock fractures (Perrin 2003). As we did not expect to find a lot of microbes in oligotrophic moonmilk deposits, so these spots with putatively more organic matter were considered to potentially have a greater number of microbes.

Microcalorimetric Analysis

Moonmilk samples were prepared as described below and introduced into the microcalorimeter (TAM 48, Waters/TA, Delaware) and kept in the equilibration position, inside the microcalorimeter but not in contact with the thermopile that is the sensing element, for 15 minutes to ensure preliminary thermal equilibration. Then, samples were lowered into the measuring position in contact with the thermopile. Sufficient thermal equilibration was achieved after 45 minutes, and heat flow measurements started approximately one hour after insertion into the microcalorimeter and lasted for about 5 days. All samples, controls, and blanks were measured in triplicate unless stated otherwise. All isothermal microcalorimetry measurements were performed at 25 °C because of the technical limitations of our microcalorimeter, which cannot be operated at cave temperatures (most calorimeters operate at room temperature or above). Therefore a temperature close to that used in many other studies was chosen (Laiz et al., 2000).

Estimation of the Number of Microbial Cells Present in the Moonmilk

Samples of moonmilk were coarsely ground and homogenized in a sterile Petri dish using a sterile scalpel blade. To estimate the number of active cells in the moonmilk, ampoules filled with 2 g of this coarsely ground moonmilk were prepared and supplemented with 800 µl of 50× diluted LB (Difco – tryptone 0.2 g L^{-1}, yeast extract 0.1 g L^{-1}, NaCl 0.1 g L^{-1}) as the carbon sources available in this medium will support growth of many chemoheterotrophic microorganisms. Following the addition of medium, the prepared ampoules were sealed and microcalorimetric measurements were performed at 25 °C as described above. In addition to the microcalorimetric measurements, plate counts were performed on 50× diluted LA medium (Difco – tryptone 0.2 g L^{-1}, yeast extract 0.1 g L^{-1}, NaCl 0.1 g L^{-1}, agar 15 g L^{-1}) and on 10× diluted R2A medium (Bacto Peptone 0.05 g L^{-1}, Bacto
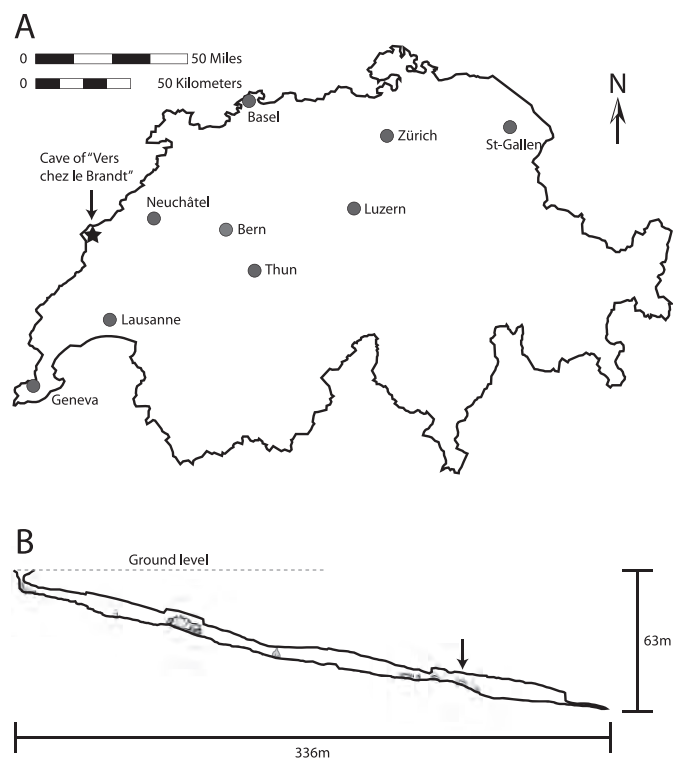
Figure 1. A. Switzerland map indicating the location of the Vers chez le Brandt cave (star) and Swiss main cities (dots). Note that the cave is located only 1200 m from the French border. B. Horizontal profile of the cave. The arrow indicates the sampling site. Grey shaded areas indicate the presence of large boulders.

yeast extract 0.05 g L^{-1}, Bacto casamino acids 0.05 g L^{-1}, glucose (Fluka) 0.05 g L^{-1}, soluble starch (Fluka) 0.05 g L^{-1}, KH$_2$PO$_4$ (Fluka) 0.03 g L^{-1}, MgSO$_4$•7H$_2$O (Fluka) 0.005 g L^{-1}, Bacto agar 15 g L^{-1}). Diluted media have previously been shown to be appropriate for plate counts of microorganisms from oligotrophic water (Kawai et al., 1999; Janssen et al., 2002; Bull, 2004; Segawa et al., 2011). All agar plates were incubated at 25 °C for the same time period as the microcalorimetric measurements (i.e., 5 days) to obtain results comparable to those obtained using microcalorimetry. Sterility controls were performed using uninoculated plates for each medium.

A similar experiment was performed to establish controls allowing quantification of the number of cells present in the moonmilk. *Bacillus subtilis* was chosen as the control because of its ability to consume a wide range of carbon sources and its structural and metabolic similarities with the actinobacteria commonly found in caves. In addition, *B. subtilis* is easier to handle, compared to filamentous actinobacteria. Ampoules were filled with 2 g of coarsely ground moonmilk and autoclaved twice at 5 to 6 hours intervals. These ampoules were inoculated with a serial dilution of a suspension of *Bacillus subtilis* (NEU 16

– Neuchâtel University culture collection) in 50× diluted LB. The *B. subtilis* suspension was prepared by centrifugation of an overnight culture grown in 10× diluted LB. The pellet was then resuspended in 50× diluted LB. This operation was repeated twice to ensure that only 50× diluted LB remained. Finally the prepared ampoules were sealed and microcalorimetric measurements were performed at 25 °C as described above. Blanks were prepared similarly, except no cells were added. Plate counts were performed on LA medium (Difco – tryptone 10.0 g L^{-1}, yeast extract 5.0 g L^{-1}, NaCl 10.0 g L^{-1}, agar 15 g L^{-1}) to estimate the number of colony forming units introduced into the ampoules.

MEASUREMENT OF MICROBIAL ACTIVITIES IN MOONMILK

Two grams of coarsely ground-up moonmilk were placed in a calorimetric ampoule and supplemented with 800 μl of chosen carbon sources. Unless stated otherwise, all the carbon sources and antibiotics were obtained from Fluka (Switzerland). The carbon sources at 0.3 mg mL^{-1} were glucose, glycerol, mannitol, Na-oxalate, Na-citrate, Na-acetate, xanthan, starch, humic acids (saturated solution), 50× diluted LB (Difco), and 50× diluted LB supplemented with a final concentration of 50 μg mL^{-1} of chloramphenicol. All carbon sources and dehydrated media were prepared in deionized water. Controls were performed using autoclaved deionized water, and blanks were performed using moonmilk autoclaved twice (25 minutes at 121 °C at 5 to 6 hours intervals) supplemented with sterile 50× diluted LB. Preliminary tests have shown that 800 μl of solution is sufficient to wet the sample homogenously without accumulation of solution at the bottom of the samples. Finally, samples were sealed and introduced in the isothermal microcalorimeter.

Apparent microbial growth rate and generation time were calculated for the different carbon sources according to the method previously described in Kimura and Takahashi (1985) and in Barros et al. (1999).

SCANNING ELECTRON MICROSCOPY (SEM)

Samples were kept at 4 °C during one week prior to SEM observations. Observations were performed using a Tescan Mira LMU scanning electron microscope. Samples were fixed with osmium tetroxide vapors, freeze-dried, and coated with gold (18 nm) and carbon (5 nm). Observations were performed at a distance of 10 mm and at 10 or 15 kV accelerating voltage, depending on charging artifacts.

RESULTS

ESTIMATION OF THE NUMBER OF MICROBIAL CELLS PRESENT IN THE MOONMILK

By using *Bacillus subtilis*, a typical soil bacterium, in autoclaved calorimetric ampoules containing sterilized moonmilk, under the experimental conditions described above, we estimated that one colony-forming unit gener-
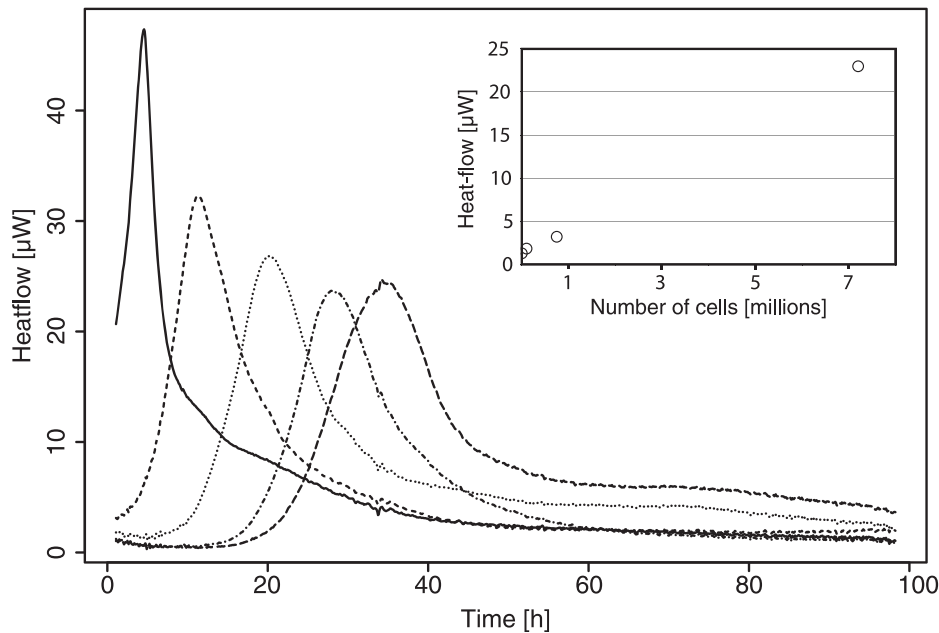
Figure 2. Heat flow pattern generated by the growth of serial 10-fold dilutions in 50× diluted LB of *Bacillus subtilis* added to sterilized moonmilk. Inside panel shows the relationship between the number of cells and the heat flow generated during the first hour, allowing an estimate of the thermal power of one colony forming unit. The curve for the most cells is the one with the left-most peak.

ated a heat flow of 3.0 pW (Fig. 2). This value is based on the first hour of recorded data. During this time, changes in heat flow were less than 5% of the initial value; therefore we made the assumption that the number of CFU did not significantly increase. It is also in accordance with the range given for bacteria by James (1987). A clear time delay until maximum activity indicated by the heat flow is visible with decreasing number of cells (Fig. 2). Similarly, a slight decrease of maximum activity with decreasing inoculum is also observed (Fig. 2). It is likely that the bacteria at lower densities did not have access to all the substrate for geometric reasons. In addition, recycling of part of the introduced biomass might explain the higher heat flow observed at high densities. Therefore, both of these factors, restrained access to carbon sources and biomass recycling, are likely to explain the observed decreasing trend. However, the total heat produced after 100 hours (i.e., the integral of the heat flow curve over 100 hours) was mostly constant, with an average of 2.2 ± 0.3 J (n = 18), showing that substrate consumption was essentially similar in all the samples.

Upon addition of 50× diluted LB medium to fresh moonmilk samples, we estimated that the amount of active chemoheterotrophic cells per gram of moonmilk from Vers chez le Brandt cave is $4.8 \times 10^5 \pm 0.2 \times 10^5$ active microbial CFU (n=5). This estimation is of course dependant on the estimation of the thermal power of one CFU.

Plate counts on 50× diluted LA and 10× diluted R2A media incubated over 5 days show counts of the same order

of magnitude ($7.7 \times 10^5 \pm 2.4 \times 10^5$ and $7.8 \times 10^5 \pm 2.9 \times 10^5$ CFU per gram of moonmilk, respectively). Although higher, these values are in the same range compared to the microcalorimetric data. It is noteworthy that the proportion of actinobacteria determined microscopically on these plates were $81\% \pm 19\%$ on 50× diluted LB and $94\% \pm 6\%$ on 10× diluted R2A. This observation is in agreement with previous report of the association of actinobacteria with moonmilk (Cañaveras et al., 2006), SEM observations, and the strong oxalate-degrading activities measured (see below).

Microbial Activities in Moonmilk

Addition of the various carbon sources resulted in an increase in heat flow, indicating an increase in microbial activity. This increase is usually observed after a lag phase up to 30 hours. After reaching a maximum, the heat flow decreases back to values close to the initial values. The resulting heat flow pattern is characterized by a single peak, usually showing a small shoulder (Fig. 3), except in the case of 50× diluted LB, where two clearly separated peaks are observed (Fig. 3A).

Strong differences are observed between heat flow patterns resulting from the addition of the various carbon sources (Fig. 3). A determination of the apparent growth rate and generation time (Table 1) clearly shows the differences in microbial stimulation generated by the different carbon sources. In the conditions of the experiment, citrate, diluted LB medium, xanthan, glucose, starch,
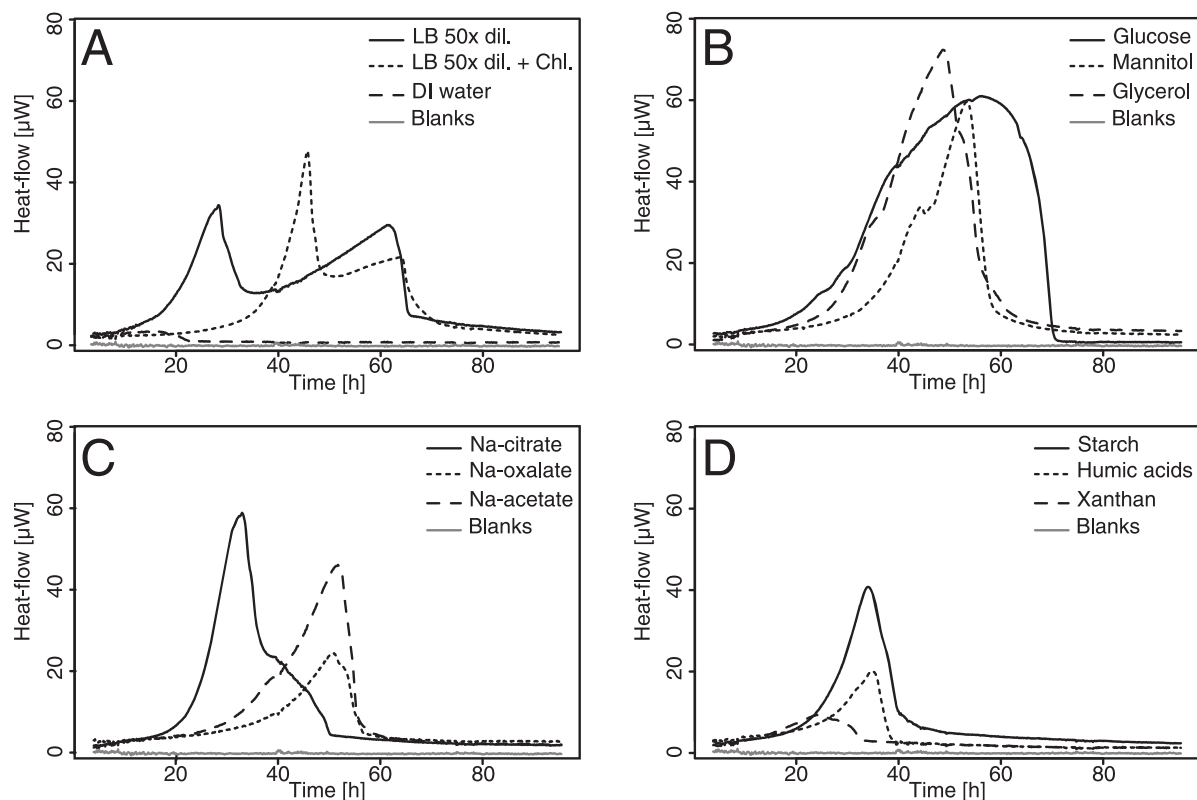
Figure 3. Representative heat flow patterns generated by the addition of various carbon sources to moonmilk. A. Moonmilk samples supplemented with 50× diluted LB medium and 50× diluted LB medium supplemented with chloramphenicol and deionized water. B. Moonmilk supplemented with glucose and poly-alcohols. C. Moonmilk supplemented with organic acids. D. Moonmilk supplemented with polymers.

and glycerol supported a higher apparent growth rate than humic acids, mannitol, acetate, and oxalate. Deionized water addition resulted in very little heat flow increase, possibly due to the dissolution of carbonate minerals or desorption processes releasing a very small amount of nutrients. A small rise in the heat flow was not observed when autoclaved moonmilk was supplemented with either diluted LB or deionized water, emphasizing the fact that it is most likely related to a biological process. On the other hand, consumption rates show a different picture. The maximum consumption rates were calculated assuming the chemical equations listed in Table 2. An obvious trend appears when plotting Gibbs free energy available versus consumption rate (Fig. 4; $r = 0.95$, $n = 6$, $p < 0.05$). The highest calculated consumption rate is given by the oxalate substrate and is in agreement with the high numbers of actinobacteria observed in the plate counts. This group of bacteria is known for its great ability to degrade oxalate (Sahin, 2003; 2004).

A much longer lag (about 20 hours longer) is observed after addition of 50× diluted LB containing chloramphenicol (Fig. 3). Nevertheless, the resulting heat flow pattern looks similar, although contracted in time. This result demonstrates that a rather large portion of the microbial community is sensitive to chloramphenicol and may show

that there is little fungal activity, because fungi should not be sensitive to such chloramphenicol concentration.

Electron Microscopy

Electron microscopy of the moonmilk samples revealed the presence of numerous morphotypes of microorganisms. Most observations show filamentous microorganisms. According to their morphology, these microorganisms could most likely be related to actinobacteria and their arthrospores (Fig. 5B, C). This is in agreement with our observations on agar plates. Other filamentous organisms, showing resemblance to hyphomicrobiaceae, are also observed (Fig. 5D). Finally, larger filaments, branched or not, are interpreted as fungi (Fig. 5E, F). Most microorganisms were observed at the surface of aggregates of intact samples of moonmilk aggregates. In contrast, observations performed on cut or coarsely ground moonmilk samples show fewer microorganisms. Considering the slow growth rate observed, even under the addition of carbon sources, and the slow appearance of colonies in the laboratory, it is likely that the bacterial morphotypes observed here belong to our sample. However, the possibility of some growth during the storage of the samples cannot be completely dismissed.

Table 1. Apparent growth rate of the microbial community when exposed to different substrates. The growth rate and generation time were determined using isothermal microcalorimetry data for the different carbon sources according to the method previously described in Kimura and Takahashi (1985) and in Barros et al. (1999).

Carbon source	Growth rate, h^{-1}	Generation time, h
Oxalate	0.0253 ± 0.0003	27.4 ± 0.3
Acetate	0.0332 ± 0.0037	21.0 ± 2.4
Glycerol	0.0456 ± 0.0041	15.3 ± 1.4
Citrate	0.0668 ± 0.0075	10.4 ± 1.2
Glucose	0.0506 ± 0.0073	13.9 ± 2.0
Mannitol	0.0336 ± 0.0009	20.7 ± 0.6
Xanthan	0.0565 ± 0.0034	12.3 ± 0.7
Starch	0.0474 ± 0.0025	14.7 ± 0.8
Humic acids	0.0369 ± 0.0008	18.8 ± 0.4
LB50x	0.0579 ± 0.0051	12.0 ± 1.1

Figure 4. Relationship between Gibbs free energy of the substrates' oxidation and their maximum consumption rate.

DISCUSSION

Our microcalorimetric data clearly show that microbial activity can easily and accurately be measured in the moonmilk samples during *ex-situ* analyses. In addition, the numbers of colony-forming units of cultivable bacteria estimated by plate counts after 5 days and by microcalorimetry are in agreement. However, the relationship between the plate count and the microcalorimetric estimates should be considered with care, since one cannot be sure that all the bacteria that produced metabolic heat upon addition of $50\times$ diluted LB are cultivable. Viable but not culturable cells might have contributed to the heat production. Indeed, after 32 days of incubation, numbers of culturable bacteria measured on the agar plates increased to 9×10^6 CFU per gram of moonmilk, and showed no further increase (data not shown). Therefore, the measured 4.8×10^5 active CFU per gram of moonmilk would represent only 5.3% of the total number of cultivable bacter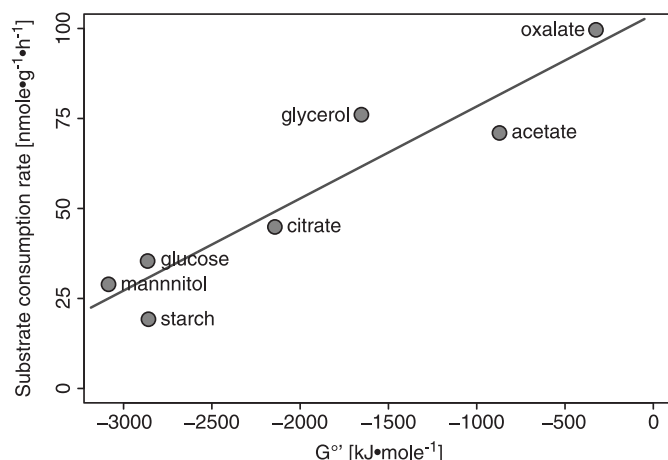ia and an even smaller fraction of the total bacteria, including those not culturable. In addition, the discrepancy between microcalorimetric estimates and plate counts at 5 and 32 days suggests that a rather large proportion of the bacteria might be dormant. This dormant fraction could be actinobacteria arthrospores (Goodfellow and Williams, 1983), but could also include dormant cells *sensu stricto* with no visible activity (Costerton et al., 1995). These dormant cells are common at very low growth rates (Pirt 1987) and may contribute to the maintenance of microbial diversity in oligotrophic environments (Jones and Lennon 2010). In oligotrophic environments such as a cave, lack of nutrients is likely to be the main cause of dormant or non-culturable states (Colwell and Grimes, 2000).

These discrepancies emphasize the limitations of isothermal microcalorimetry. Indeed microcalorimetry is a blind tool that only measures heat production rate; in this study metabolic heat production rate. To get a better picture of microbial processes in moonmilk, microcalorimetry should be coupled with other tools, allowing an estimate of the microbial population size. In addition, the composition of the community, determined by molecular

Table 2. Consumption rates of the various carbon sources calculated based on the assumption that only aerobic respiration occurred. Equations are listed with the thermodynamic parameters used to convert maximum heat flow (W or J s^{-1}) into substrate consumption rate (nmoles h^{-1} g^{-1}).

Equation	Substrate common name	$\Delta G^{0\prime}$ (KJ $mole^{-1}$)	Maximum heat flow (μW)	Substrate maximum consumption rate (nmoles h^{-1} g^{-1})[a]
$2C_2H_2O_4 + O_2 \rightarrow 4CO_2 + 2H_2O$	oxalate	-328	18 ± 2	98 ± 11
$C_2H_4O_2 + 2O_2 \rightarrow 2CO_2 + 2H_2O$	acetate	-872	34 ± 10	71 ± 21
$2C_3H_8O_3 + 7O_2 \rightarrow 6CO_2 + 8H_2O$	glycerol	-1653	70 ± 4	76 ± 5
$2C_6H_8O_7 + 9O_2 \rightarrow 12CO_2 + 8H_2O$	citrate	-2144	53 ± 1	45 ± 1
$C_6H_{12}O_6 + 6O_2 \rightarrow 6CO_2 + 6H_2O$	glucose	-2860	57 ± 1	36 ± 1
$2C_6H_{14}O_6 + 13O_2 \rightarrow 12CO_2 + 14H_2O$	mannitol	-3081	49 ± 7	29 ± 4
$(C_6H_{12}O_6)_n + 6O_2 \rightarrow 6CO_2 + 6H_2O$[b]	starch	-2860[b]	31 ± 2[b]	19 ± 2[b]

[a] Assuming that only the reaction considered takes place.
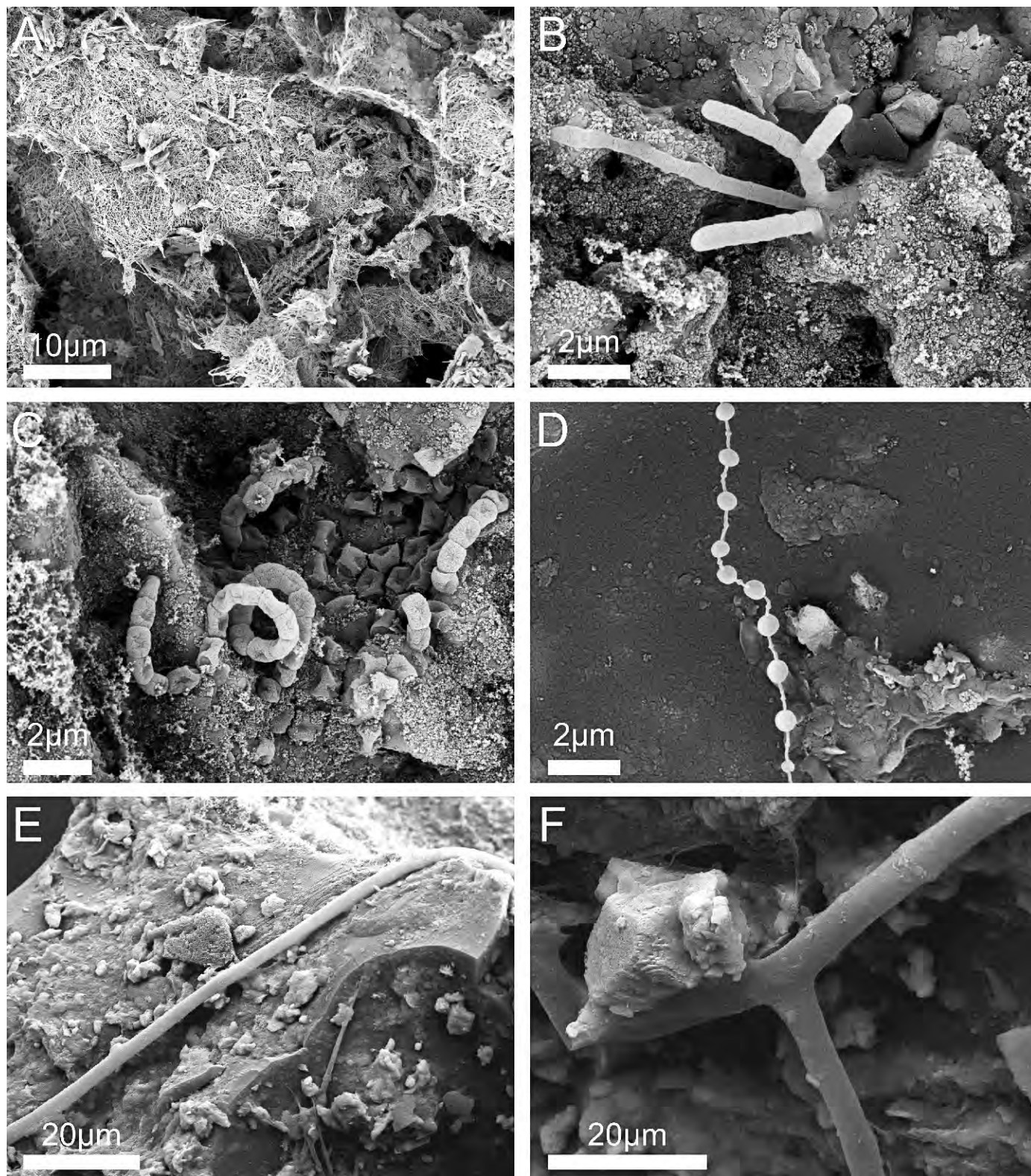[b] Converted into glucose equivalents.

Figure 5. Scanning electron micrographs of moonmilk aggregates and microorganisms found in them. A. General view of the moonmilk sample showing mostly monocrystalline and serrated-edged needle-fiber calcite. B. Growing filamentous microorganisms resembling actinobacteria. C. Chains of cells resembling actinobacteria arthrospores. Note that spores arranged in spirals are usually associated to the genus *Streptomyces* (see Holt et al., 1994). D. Chain of appendaged bacterium. E. and F. Fungal filaments.

methods, would allow relating the activities measured to the members of this community. However, in our study, the use of a specific antibiotic allows us to point to possibly important members of the moonmilk population. Upon addition of chloramphenicol, the peak of activity was strongly delayed, but not suppressed. Undoubtedly, a part of the bacterial community present was sensitive to this antibiotic. Since fungi should not be affected by such low concentrations of chloramphenicol, they might be responsible for a part of the remaining activity. Also, considering the wide occurrence of chloramphenicol resistance among actinobacteria (Shaw and Hopwood, 1976) and their high proportion in our samples, it seems that actinobacteria might be a key player in this community. Recent publications have emphasized the importance of Actinobacteria in caves. For example, Laiz et al. (2000) using both cultural and molecular methods to study the microbial community on stalactites, found that about 50% of the isolated strains were actinomycetes and that the most prominent TGGE band was most likely related to a close relative of *Nocardiopsis,* another actinobacteria. Similarly, 16% of a clone library obtained from the walls of a karstic cave in Slovenia were actinobacteria (Pašić et al., 2009), making actinobacteria the second most abundant group after gamma-proteobacteria (about 33%). Finally, combining molecular DNA and RNA based fingerprinting, targeting the total community and the metabolically active part of the community, respectively, Portillo et al. (2008, 2011) have shown that moonmilk contained a subset of the community present in the white colonization from the Altamira Cave and that actinobacteria, among others, were an important part of the metabolically active microbial population. The authors also report that about 20% of the community detected through DNA-based fingerprinting remains undetected through RNA-based fingerprinting, emphasizing that a rather large proportion of the community shows undetectable metabolic activity. Furthermore, the nanorespirometry measurements performed in the study performed by Portillo et al. (2011) indicate that once white colonizations are calcified into moonmilk, the metabolic activity decreases by about a factor of 20.

The microcalorimetric data obtained during this study also show that it is possible to further characterize the metabolically active part of the community by supplementing the moonmilk samples with different carbon sources, indicating the responses of the active part of the microbial community to specific carbon sources. Such response is expressed as the growth rate of the community in response to a carbon source or as the maximum consumption rate of this carbon source. In our study, the calculated apparent growth rates are comparable to growth rates observed in soils (Barros et al., 1995; 1999; Parinkina et al., 1973). However, we have to recognize that the temperature in the microcalorimeter was higher than the cave environment, 25 °C instead of 10 °C, which might have led to overestimating these growth rates. Nevertheless, our data show

clear differences in microbial growth rates observed upon the addition of the different carbon sources.

Similarly, substrate consumption rates of organic acids and glucose calculated in this study are within the range of those observed in forest soils (Fujii et al., 2010; van Hees et al., 2002). Both of these observations suggest that, in this cave, the microbial community can be as active as in soils. One major limitation in such a community is the substrate input that is mainly linked to the leaching of material from the soil above the cave. Such leaching can only occur during rain or storm events and spring snow melt. Therefore, the activity, in the absence of addition of substrate, is extremely low in this nutrient-deficient system (Mulec, 2008). High metabolic and heat-production rates can be measured in caves when the sample is collected from microbial mats (Rohwerder et al., 2003). Although organic acid and glucose have received a lot of attention with respect to their degradation rate in the environment, other carbon sources, such as mannitol, starch, xanthan, or humic acid, have been neglected in the literature. Therefore, we cannot compare their measured degradation and associated apparent growth rates from our study with data from other hypogean environments or soils.

With respect to the formation of moonmilk, these results point to metabolic activities capable of creating conditions favorable for the precipitation of calcium carbonate. Physicochemical characterization of the water percolating in this cave during rainfall has shown that it is undersaturated with respect to calcite (Perrin, 2003), and consequently, able to dissolve carbonate minerals. Similarly, the same study has shown that this percolating water is characterized by an increasing content of total organic carbon. In this context, it can be assumed that the microbial consumption of this organic carbon might provide sufficient carbonate ions and alkalinity to promote calcium carbonate formation. Indeed, the growth of cave microbial populations in a diluted medium such as nutrient broth was shown to increase the pH to values close to or above carbonate mineral stability (i.e., pH = 8.4; Portillo and Gonzalez, 2011). Microbial metabolism of organic acids imported in the system through the percolating water will contribute to the increase in pH since many organic acids have higher pHs than carbonic acid. This increase in pH has previously been demonstrated for oxalate (Braissant et al., 2002, 2004). Similarly, Curry et al. (2009) have demonstrated that use of calcium succinate by bacteria isolated from cottonballs (a specific type of moonmilk) yielded a significant production of calcium carbonate. Turnover of humic acids or exopolymeric substances such as xanthan could also favor the precipitation of carbonate minerals in the same way. In addition, such processes will also favor precipitation of carbonate minerals by releasing the calcium bound to the exopolymers (Braissant et al., 2007; 2009; Dupraz et al., 2009) or the humic acids and by removing precipitation inhibitors.

The large proportion of actinobacteria observed in this study, as well as in others (Laiz et al., 2000; Stomeo et al.,
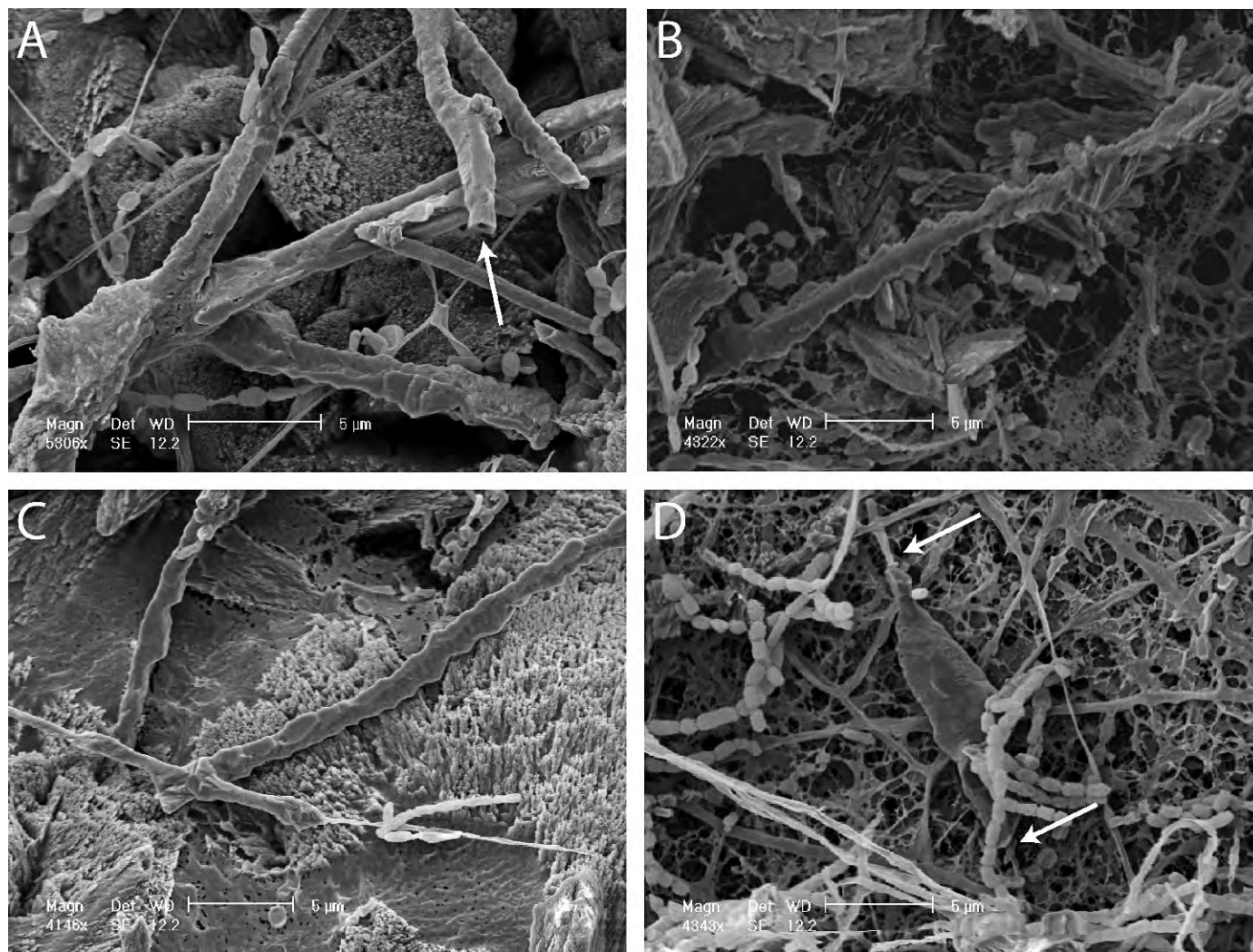
Figure 6. Indurate hyphae and "filament shaped" crystals produced by *Streptomyces* sp. growing on B4 agar plates. Note the similarities between these crystals and the features that can be observed in moonmilk. A. Typical indurated hyphae with a smooth appearance. A central hole may be seen on these structures (arrow). B. Straight calcified hyphae showing indentations due to epitactic growth of calcium carbonate. C. Curved indurated hyphae showing serrated edges due to epitactic growth of calcium carbonate only on one side. D. Epitaxy forming a large crystal around a mineralized hypha; arrows indicate the hyphae going through the crystal.

2008; Cuezva et al., 2009), and their strong ability to degrade oxalate (Sahin 2003, 2004), exopolymeric substances (Qian et al., 2007; Muchová et al., 2009; Tan et al., 2009; Gaskell et al., 2010), and humic acid (Badis et al., 2009; Dari et al., 1995) emphasize once more their potential role in the formation of moonmilk by creating the necessary physico-chemical conditions for carbonate-mineral precipitation. The role of actinobacteria in the formation of moonmilk was previously discussed by Cañaveras et al. (2006). According to their proposed model, the formation of a microbial biofilm would lead to a step-by-step formation of moonmilk using bacterial and/or fungal hyphae as the template. Filamentous actinobacteria were shown to produce needle-shaped crystals in cultures, but the needles resulting from such cultures have different sizes and shapes than those

observed in moonmilk (Fig. 6). Therefore, another process is thought to be at the origin of the calcitic features observed in the cave Vers chez le Brandt. No biofilm has been observed in the samples collected in that cave, and consequently the model proposed by Bindschedler et al. (2010) or by Cailleau et al. (2009a,b) involving calcite pseudomorphosis of fungal, bacterial, or plant cell-wall fibrous material seems more appropriate in that cave. In addition, the model of Bindschedler et al. (2010) could also explain the formation of nanofibers.

CONCLUSIONS

Microcalorimetric investigations on moonmilk samples allowed us to gain additional insights into the active

bacterial population as a whole. This study demonstrates that it is possible to estimate the size of the metabolically active microbial population in moonmilk samples. In addition, we determined the growth rate of the metabolically active microbial population with various carbon sources added, as well as the maximum consumption rate of these carbon sources. Obtaining information on growth rates and consumption rates allows for inferring what processes might be important to understanding the microbiology and biogeochemistry of moonmilk. In our study, organic acids were rapidly consumed, with citric acid sustaining the highest growth rate, emphasizing the crucial role of organic-acid input for the carbonate microfabric processes driven by this microbial community. Further use of microcalorimetry, in combination with molecular techniques, will undoubtedly lead to a better understanding of moonmilk formation by linking measurements of the rate and extent of metabolic processes and growth to the composition of the microbial community.

References

Amann, R.I., Ludwig, W., and Schleifer, H.K., 1995, Phylogenetic identification and in situ detection of individual microbial cells without cultivation: Microbiological Reviews, v. 59, p. 143–169.

Badis, A., Ferradji, F.Z., Boucherit, A., Fodil, D., and Boutoumi, H., 2009, Characterization and biodegradation of soil humic acids and preliminary identification of decolorizing actinomycetes at Mitidja plain soils (Algeria): African Journal of Microbiology Research, v. 3, p. 997–1007.

Barros, N., Feijóo, S., Simoni, J.A., Prado, A.G.S., Barboza, F.D., and Airoldi, C., 1999, Microcalorimetric study of some Amazonian soils: Thermochimica Acta, v. 328, p. 99–103. doi: 10.1016/S0040-6031(98)00629-7.

Barros, N., Gomez-Orellana, I., Feijbóo, S., and Balsa, R., 1995, The effect of soil moisture on soil microbial activity studied by microcalorimetry: Thermochimica Acta, v. 249, p. 161–168. doi: 10.1016/0040-6031(95)90686-X.

Barton, H.A., and Northup, D.E., 2007, Geomicrobiology in cave environments: past, current and future perspectives: Journal of Cave and Karst Studies, v. 69, p. 163–178.

Bindschedler, S., Millière, L., Cailleau, G., Job, D., and Verrecchia, E.P., 2010, Calcitic nanofibres in soils and caves: a putative fungal contribution to carbonatogenesis, in Pedley, H.M., and Rogerson, M., eds., Tufas and Speleothems: Unraveling the Microbial and Physical Controls: Geological Society of London Special Publications 336, p. 225–238. doi: 10.1144/SP336.11.

Boquet, E., Boronat, A., and Ramos-Cormenzana, A., 1973, Production of calcite (calcium carbonate) crystals by soil bacteria is a general phenomenon: Nature, v. 246, p. 527—529. doi: 10.1038/246527a0.

Borsato, A., Frisia, S., Jones, B., and Van Der Borg, K., 2000, Calcite moonmilk: crystal morphology and environment of formation in caves in the Italian Alps: Journal of Sedimentary Research, v. 70, p. 1171–1182. doi: 10.1306/032300701171.

Braissant, O., Cailleau, G., Aragno, M., and Verrecchia, E.P., 2004, Biologically induced mineralization in the tree Milicia excelsa (Moraceae): its causes and consequences to the environment: Geobiology, v. 2, p. 59–66. doi: 10.1111/j.1472-4677.2004.00019.x.

Braissant, O., Decho, A.W., Dupraz, C., Glunk, C., Przekop, K.M., and Visscher, P.T., 2007, Exopolymeric substances of sulfate-reducing bacteria: Interactions with calcium at alkaline pH and implication for formation of carbonate minerals: Geobiology, v. 5, p. 401–411. doi: 10.1111/j.1472-4669.2007.00117.x.

Braissant, O., Decho, A.W., Przekop, K.M., Gallagher, K.L., Glunk, C., Dupraz, C., and Visscher, P.T., 2009, Characteristics and turnover of exopolymeric substances in a hypersaline microbial mat: FEMS Microbiology Ecology, v. 67, p. 293–307. doi: 10.1111/j.1574-6941.2008.00614.x.

Braissant, O., Verrecchia, E.P., and Aragno, M., 2002, Is the contribution of bacteria to terrestrial carbon budget greatly underestimated?: Naturwissenschaften, v. 89, p. 366–370. doi: 10.1007/s00114-002-0340-0.

Braissant, O., Wirz, D., Göpfert, B., and Daniels, A.U., 2010, Use of isothermal microcalorimetry to monitor microbial activities: FEMS Microbiology Letters, v. 303, p. 1–8. doi: 10.1111/j.1574-6968.2009.01819.x.

Bull, A.T., 2004, Microbial Diversity and Bioprospecting, Washington, American Society of Microbiology, 496 p.

Cailleau, G., Dadras, M., Abolhassani-Dadras, S., Braissant, O., and Verrecchia, E.P., 2009a, Evidence for an organic origin of pedogenic calcitic nanofibres: Journal of Crystal Growth, v. 311, p. 2490–2495. doi: 10.1016/j.jcrysgro.2009.02.029.

Cailleau, G., Verrecchia, E.P., Braissant, O., and Emmanuel, L., 2009b, The biogenic origin of needle fibre calcite: Sedimentology, v. 56, p. 1858–1875. doi: 10.1111/j.1365-3091.2009.01060.x.

Callot, G., Guyon, A., and Mousain, D., 1985, Inter-relations entre aiguilles de calcite et hyphes mycéliens: Agronomie, v. 5, p. 209–216.

Cañavaras, J.C., Cuezva, S., Sanchez-Moral, S., Lario, J., Laiz, L., Gonzalez, J.M., and Saiz-Jimenez, C., 2006, On the origin of fiber calcite crystals in moonmilk deposits: Naturwissenschaften, v. 93, p. 27–32. doi: 10.1007/s00114-005-0052-3.

Colwell, R.R., and Grimes, D.J., 2000, Nonculturable Microorganisms in the Environment, Washington, American Society of Microbiology, 354 p.

Costerton, J.W., Lewandowski, Z., Caldwell, D.E., Korber, D.R., and Lappin-Scott, H.M., 1995, Microbial biofilms: Annual Review of Microbiology, v. 49, p. 711–745. doi: 10.1146/annurev.mi.49.100195.003431.

Cuezva, S., Sanchez-Moral, S., Saiz-Jimenez, C., and Cañaveras, J.C., 2009, Microbial communities and associated mineral fabrics in Altamira Cave, Spain: International Journal of Speleology, v. 38, p. 83–92.

Curry, M.D., Boston, P.J., Spilde, M.N., Baichtal, J.F., and Campbell, A.R., 2009, Cottonballs, a unique subaqueous moonmilk and abundant subaerial moonmilk in Cataract Cave, Tongass National Forest, Alaska: International Journal of Speleology, v. 38, p. 111–128.

Dari, K., Béchet, M., and Blondeau, R., 1995, Isolation of soil Streptomyces strains capable of degrading humic acids and analysis of their peroxidase activity: FEMS Microbiology Ecology, v. 16, p. 115–122. doi: 10.1111/j.1574-6941.1995.tb00275.x.

Dupraz, C., Reid, R.P., Braissant, O., Decho, A.W., Norman, R.S., and Visscher, P.T., 2009, Processes of carbonate precipitation in modern microbial mats: Earth-Science Reviews, v. 96, p. 141–162. doi:10.1016/j.earscirev.2008.10.005.

Engel, A.S., and Northup, D.E., 2008, Caves and Karst as Model Systems for Advancing the Microbial Sciences, in Martin, J.B., and White, W.B., eds., Frontiers of Karst Research, Leesburg, Virginia, Karst Waters Institute Special Publication 13, p. 37–48.

Fujii, K., Hayakawa, C., Van Hees, P.A.W., Funakawa, S., and Kosaki, T., 2010, Biodegradation of low molecular weight organic compounds and their contribution to heterotrophic soil respiration in three Japanese forest soils: Plant and Soil, v. 334, p. 475–489. doi: 10.1007/s11104-010-0398-y.

Gaskell, E.E., Sihanonth, P., Rostron, C., Hutcheon, G.A., and Hobbs, G., 2010, Isolation and identification of mucinolytic actinomycetes: Antonie van Leeuwenhoek, v. 97, p. 211–220. doi: 10.1007/s10482-009-9402-z.

Gigon, R., 1976, Inventaire spéléologique de la Suisse, tome 1, Canton de Neuchâtel, Neuchâtel, Commission de Spéléologie de la Société helvétique des Sciences naturelles, 223 p.

Goodfellow, M., and Williams, S.T., 1983, Ecology of actinomycetes: Annual Reviews in Microbiology, v. 37, p. 189–216.

Higuera-Guisset, J., Rodríguez-Viejo, J., Chacón, M., Muñoz, F.J., Vigués, N., and Mas, J., 2005, Calorimetry of microbial growth using a thermopile based microreactor: Thermochimica Acta, v. 427, p. 187–191. doi: 10.1016/j.tca.2004.09.010.

Holt, J.G., Krieg, N.R., Sneath, P.H.A., Staley, J.T., and Williams, S.T., 1994, Bergey's Manual of Determinative Bacteriology, ninth edition, New York, London, Lippincott Williams & Wilkins, 791 p.

James, A.M., ed., 1987, Thermal and Energetic Studies of Cellular Biological Systems, Bristol, John Wright, 221 p.

Janssen, P.H., Yates, P.S., Grinton, B.E., Taylor, P.M., and Sait, M., 2002, Improved culturability of soil bacteria and isolation in pure culture of novel members of the divisions Acidobacteria, Actinobacteria, Proteobacteria, and Verrucomicrobia: Applied and Environmental Microbiology, v. 68, p. 2391–2396. doi: 10.1128/AEM.68.5.2391-2396.2002.

Jones, S.E., and Lennon, J.T., 2010, Dormancy contributes to the maintenance of microbial diversity: Proceedings of the National Academy of Sciences of the United States of America, v. 107, p. 5881–5886. doi: 10.1073/pnas.0912765107.

Kawai, M., Yamaguchi, N., and Nasu, M., 1999, Rapid enumeration of physiologically active bacteria in purified water used in the pharmaceutical manufacturing process: Journal of Applied Microbiology, v. 86, p. 496–504. doi: 10.1046/j.1365-2672.1999.00689.x.

Kimura, T., and Takahashi, K., 1985, Calorimetric studies of soil microbes: quantitative relation between heat evolution during microbial degradation of glucose and changes in microbial activity in soil: Journal of General Microbiology, v. 131, p. 3083–3089. doi: 10.1099/00221287-131-11-3083.

Konhauser, K., 2007, Introduction to Geomicrobiology, Oxford, Blackwell Publishing Co., 433 p.

Lacelle, D., 2010, Discussion: "The biogenic origin of needle fibre calcite" by G. Cailleau et al. (2009), Sedimentology, 56, 1858–1875: Sedimentology, v. 57, p. 1147–1149. doi: 10.1111/j.1365-3091.2009.01134.x.

Laiz, L., Groth, I., Schumann, P., Zezza, F., Felske, A., Hermosin, B., and Saiz-Jimenez, C., 2000, Microbiology of the stalactites from Grotta dei Cervi, Porto Badisco, Italy: International Microbiology, v. 3, p. 25–30.

Muchová, M., Růžička, J., Julinová, M., Doležalová, M., Houser, J., Koutný, M., and Buňková, L., 2009, Xanthan and gellan degradation by bacteria of activated sludge: Water Science and Technology, v. 60, p. 965–973. doi: 10.2166/wst.2009.443.

Mulec, J., 2008, Microorganisms in hypogeon: examples from Slovenian karst caves: Acta Carsologica, v. 37, p. 153–160.

Mulec, J., Zalar, P., Hajna, N.Z., and Rupnik, M., 2002, Screening for culturable microorganisms from cave environments (Slovenia): Acta Carsologica, v. 31, no. 2, p. 177–187.

Northup, D.E., and Lavoie, K.H., 2001, Geomicrobiology of caves: a review: Geomicrobiology Journal, v. 18, p. 199–222. doi: 10.1080/01490450152467750.

Parinkina, O.M., 1973, Determination of bacterial growth rates in tundra soils: Bulletins from the Ecological Research Committee (Stockholm), v. 17, p. 303–309.

Pašić, L., Kovče, B., Sket, B., and Herzog-Velikonja, B., 2009, Diversity of microbial communities colonizing the walls of a Karstic cave in Slovenia: FEMS Microbiology Ecology, v. 71, p. 50–60.

Perrin, J., 2003, A conceptual model of flow and transport in a karst aquifer based on spatial and temporal variations of natural tracers [Ph.D. thesis]: Neuchatel, University of Neuchatel.

Phillips, S.E., Milnes, A.R., and Foster, R.C., 1987, Calcified filaments - an example of biological influences in the formation of calcrete in south Australia: Australian Journal of Soil Research, v. 25, p. 405–428. doi: 10.1071/SR9870405.

Phillips, S.E., and Self, P.G., 1987, Morphology, crystallography and origin of needle fiber calcite in Quaternary pedogenic calcretes of south Australia: Australian Journal of Soil Research, v. 25, p. 429–444. doi: 10.1071/SR9870429.

Pirt, J.S., 1987, The energetics of microbes at slow growth rates: maintenance energies and dormant organisms: Journal of Fermentation Technology, v. 65, p. 173–177. doi: 10.1016/0385-6380(87)90161-0.

Portillo, M.C., and Gonzalez, J.M., 2011, Moonmilk deposits originate from specific bacterial communities in Altamira Cave (Spain): Microbial Ecology, v. 61, p. 182–189. doi: 10.1007/s00248-010-9731-5.

Portillo, M.C., Gonzalez, J.M., and Saiz-Jimenez, C., 2008, Metabolically active microbial communities of yellow and grey colonizations on the walls of Altamira Cave, Spain: Journal of Applied Microbiology, v. 104, p. 681–691. doi: 10.1111/j.1365-2672.2007.03594.x.

Qian, F., An, L., Wang, M., Li, C., and Li, X., 2007, Isolation and characterization of a xanthan-degrading Microbacterium sp. strain XT11 from garden soil: Journal of Applied Microbiology, v. 102, p. 1362–1371.

Rohwerder, T., Sand, W., and Lascu, C., 2003, Preliminary evidence for a sulphur cycle in Movile Cave, Romania: Acta Biotechnologica, v. 23, p. 101–107. doi: 10.1002/abio.200390000.

Rong, X.-M., Huang, Q.-Y., Jiang, D.-H., Cai, P., and Liang, W., 2007, Isothermal microcalorimetry: a review of applications in soil and environmental sciences: Pedosphere, v. 17, p. 137–145. doi: 10.1016/S1002-0160(07)60019-8.

Sahin, N., 2003, Oxalotrophic bacteria: Research in Microbiology, v. 154, p. 399–407. doi: 10.1016/S0923-2508(03)00112-8.

Sahin, N., 2004, Isolation and characterization of mesophilic, oxalate-degrading Streptomyces from plant rhizosphere and forest soils: Naturwissenschaften, v. 91, p. 498–502. doi: 10.1007/s00114-004-0562-4.

Segawa, T., Yoshimura, Y., Watanabe, K., Kanda, H., and Kohshima, S., 2011, Community structure of culturable bacteria on surface of Gulkana Glacier, Alaska: Polar Science, v. 5, p. 41–51. doi: 10.1016/j.polar.2010.12.002.

Shaw, W.V., and Hopwood, D.A., 1976, Chloramphenicol acetylation in Streptomyces: Journal of General Microbiology, v. 94, p. 159–166. doi: 10.1099/00221287-94-1-159.

Stomeo, F., Portillo, M.C., Gonzalez, J.M., Laiz, L., and Saiz-Jimenez, C., 2008, Pseudonocardia in white colonizations in two caves with Paleolithic paintings: International Biodeterioration & Biodegradation, v. 62, p. 483–486. doi: 10.1016/j.ibiod.2007.12.011.

Tan, H., Deng, Z., and Cao, L., 2009, Isolation and characterization of actinomycetes from healthy goat faeces: Letters in Applied Microbiology, v. 49, p. 248–253. doi: 10.1111/j.1472-765X.2009.02649.x.

van Hees, P.A.W., Jones, D.L., and Godbold, D.L., 2002, Biodegradation of low molecular weight organic acids in coniferous forest podzolic soils: Soil Biology and Biochemistry, v. 34, p. 1261–1272. doi: 10.1016/S0038-0717(02)00068-8.

Wadsö, I., 2002, Isothermal microcalorimetry in applied biology: Thermochimica Acta, v. 394, p. 305–311. doi: 10.1016/S0040-6031(02)00263-0.

Wadsö, I., 2009, Characterization of microbial activity in soil by use of isothermal microcalorimetry: Journal of Thermal Analysis and Calorimetry, v. 95, p. 843–850. doi: 10.1007/s10973-008-9467-3.

IMPORTANCE OF KARST SINKHOLES IN PRESERVING RELICT, MOUNTAIN, AND WET-WOODLAND PLANT SPECIES UNDER SUB-MEDITERRANEAN CLIMATE: A CASE STUDY FROM SOUTHERN HUNGARY

ZOLTÁN BÁTORI[1]*, LÁSZLÓ KÖRMÖCZI[1], LÁSZLÓ ERDŐS[1], MÁRTA ZALATNAI[1], AND JÁNOS CSIKY[2]

Abstract: Species composition and the vegetation pattern of the understory were investigated in different sized solution sinkholes in a woodland area of the Mecsek Mountains (southern Hungary). Vegetation data together with topographic variables were collected along transects to reveal the vegetation patterns on the slopes, and a species list was compiled for each sinkhole. The results indicate that the vegetation pattern significantly correlates with sinkhole size. In smaller sinkholes, vegetation does not change substantially along the transects; in larger sinkholes, however, vegetation inversion is pronounced. We also found that sinkhole size clearly influences the number of vascular plant species, in accordance with the well-known relationship between species number and area. In the forest landscape, many medium-sized and large sinkholes have developed into excellent refuge areas for glacial relicts, mountain, and wet-woodland plant species.

INTRODUCTION

Climate-induced species extinction has become a major topic in conservation biology. Articles and books focusing on climate change have appeared (e.g., Iverson and Prasad, 1998; Sagarin et al., 1999; Cowie, 2007), and a rapidly increasing amount of information is available about current and potential refuge areas (e.g., Köhn and Waterstraat, 1990; Schindler et al., 1996; Sheldon et al., 2008) where many species may survive unfavorable regional environmental conditions. During glacial periods, a major part of Europe was largely covered by cold habitats, and only cold-adapted species were able to survive under these extreme conditions (Habel et al., 2010). However, after glacial retreat, sites with cold and humid climates became important to preserving glacial relicts and high mountain and mountain species, mainly in lower mountain and hill ranges.

On a global scale, extensive karst limestone bedrock plays an important role in the preservation of rare, endangered, or specialized species (e.g., Christiansen and Bellinger, 1996; Wolowski, 2003; Judson, 2007; Lewis and Bowman, 2010). Karst landforms like caves, wells and sinkholes (also known as dolines) determine the geomorphologic, microclimatic, and vegetation features of karst surfaces and influence the karst aquifer system. Moreover, caves and wells are hotspots of subterranean biodiversity (Culver and Sket, 2000; Elliott, 2007); sinkholes preserve relicts (Horvat, 1953; Lazarević et al., 2009), high mountain, mountain, (Beck v. Mannagetta, 1906; Horvat, 1953; Pericin and Hürlimann, 2001; Dakskobler et al., 2008) and endemic (Egli et al., 1990; Brullo and Giusso del Galdo, 2001; Özkan et al., 2010) species, and, in many cases, they are an important source of knowledge about

vegetation history. For example, *Dracocephalum ruyschiana*, a glacial relict in the sinkhole flora of northern Hungary, indicates a former periglacial climate (Király, 2009), but some high mountain elements (e.g. *Lilium martagon* subsp. *alpinum*, *Ribes alpinum*) also occur in the low-lying sinkholes (between 400 and 600 masl) of the area (Szmorad, 1999; Vojtkó, 1997).

Understanding the patterns of sinkhole vegetation requires an understanding of the surrounding vegetation patterns. According to Horvat (1953), the cool and humid microclimate of sinkholes may affect their flora and vegetation in two different ways. In many cases, thermal inversion leads to an inversion of surrounding vegetation zones. On the other hand, edaphic vegetation types may also appear on the bottom of sinkholes under special ecological conditions (Egli, 1991; Bátori et al., 2009). From an ecological point of view, the latter is more important, as it may provide primary habitats for many species absent in the surrounding vegetation.

The purpose of the present study is to determine and compare the vegetation pattern and species composition in solution sinkholes of the sub-Mediterranean part of Hungary with regard to sinkhole size and to offer some useful explanations for their role in nature conservation. The following questions are addressed: (i) What is the extent of vegetation inversion in different-sized sinkholes in a woodland area? (ii) How does the extent of refuge areas change with sinkhole size? (iii) How many relict, mountain,

* Corresponding author: zbatory@gmail.com
[1] Department of Ecology, University of Szeged, 6726 Szeged, Közép fasor 52, Hungary
[2] Department of Plant Taxonomy and Geobotany, University of Pécs, 7624 Pécs, Ifjúság útja 6, Hungary

Figure 1. Location of the study site in the Mecsek Mountains (southern Hungary).

and wet-woodland plant species can be found in the different sized sinkholes?

METHODS

The study was carried out in the karst area of 30 km^2 in the Mecsek Mountains (southern Hungary), near the city of Pécs (Fig. 1). On the karst surface, there are more than two thousand sinkholes located between 250 and 500 m above sea level (Fig. 2). The formation of these depressions started during the Pleistocene, and it is still intensive due to the abundant precipitation on the fissured bedrock underlying the woodland. The diameter of the largest sinkhole is over 200 m and its depth exceeds 30 m (Lovász, 1971), but more than fifteen hundred of these sinkholes are quite small (diameter < 20 m). The sinkhole density of this area is extremely high, with the maximum of 380 sinkholes per km^2. These depressions are in primitive stages of development, shown by their steep slopes and a funnel-like form (Hoyk, 1999).

The average annual rainfall of the study site exceeds 700 mm, with considerable interannual variation. Due to the sub-Mediterranean climate, the monthly maximum values occur during summer and autumn (May and June 77 mm, October 72 mm). The annual mean temperature is about 8.8 °C, with the highest monthly mean temperature of 19.3 °C in July. Winters are moderately cold with −1.1 °C

Figure 2. A large solution sinkhole (sinkhole O) of the Mecsek Mountains in the winter of 2008.

mean temperature from December to February (Ádám et al., 1981).

Sub-Mediterranean type, middle-aged (70 to 110 years old) mixed-oak and beech forests dominate the present vegetation of the plateaus and slopes of the study site. The most important Atlantic-Mediterranean, sub-Mediterranean, and Mediterranean plants include *Aremonia agrimonoides*, *Asperula taurina*, *Helleborus odorus*, *Lathyrus venetus*, *Luzula forsteri*, *Potentilla micrantha*, *Rosa arvensis*, *Ruscus aculeatus*, *Ruscus hypoglossum*, *Scutellaria altissima*, *Tamus communis*, and *Tilia tomentosa*. Hotspots of mountain species of the area can be found in the forests of the deep, humid, and rocky ravines and valleys.

Our surveys were conducted between 2006 and 2011 from early June to mid-September on the karst surface of the Mecsek Mountains. Sinkholes were selected in sites that did not show signs of recent wood-cutting. Sinkholes ranked by diameter are identified with capital letters from A to T (Table 1).

Transects for sampling understory were established across the twenty sinkholes in a north-south direction, passing through the deepest point of the depressions. Transects consisted of series of 1 m square contiguous plots. In the larger sinkholes, the transects were 2 m wide, with individual plots side-by-side along them. In the smaller sinkholes, only a 1 m wide series was surveyed. Percentage cover of each vascular plant species was estimated visually in the plots. Furthermore, a flora list for each sinkhole was completed by a systematic search through the total area of the sinkhole. The total area included the area of the slopes (where the slope angle was over 10°) and the area of the edges, an approximately 1 to 5 m wide strip around the smaller sinkholes, and an approximately 10 to 20 m wide strip around the larger sinkholes where the slope angle was less than 10°. For comparison, 405 1 m square plots were randomly taken from the three habitat types, mixed-oak forests, beech

Table 1. Diameters and depths of the studied sinkholes of the Mecsek Mountains.

Sinkhole Dimensions, m	A	B	C	D	E	F	G	H	I	J	K	L	M	N	O	P	Q	R	S	T
Diameter	9.5	14.5	15	18	21	23	43	60	69	76	81	85	92	124	135	145	158	167	187	229
Depth	1	2.5	2.5	3	4.5	3.5	7	12	12	12	15	15	13	17	19	25	22	22	21	31

forests, and forests in the deep ravines and valleys (called ravine forests below), occurring in the neighborhood of the sinkholes. We studied a total of 4017 plots on the karst of Mecsek Mountains: 3612 plots in sinkholes and 405 plots in their surroundings. A total of 251 vascular plant species were included in the analyses. In addition, the diameter and depth of the sinkholes were measured (Table 1). Plant species were named according to Simon (2000).

Diagnostic (or differential) species include species with high occurrence within a given vegetation type (or within some vegetation types) and low occurrence in other vegetation types. Diagnostic species of the different forest types surrounding the sinkholes were determined by statistical fidelity measures (Chytrý et al., 2002). The phi coefficient (Φ) for all species was computed with the JUICE 7.0.25 program (Tichý, 2002). This coefficient ranges from −1 to 1, but for convenience, it is multiplied by 100 in the program. The highest phi value of 1 is achieved if the species occurs in all plots of the target vegetation type and is absent elsewhere. For the comparison of mixed-oak forests, beech forests, and ravine forests (405 total plots), we used the $\Phi \geq 0.1$ threshold (Fisher's exact test, $p < 0.05$) during analyses. The classified data set contained only site groups of equal size (135 plots for each group). In this scale, fidelity measurement resulted in three groups of diagnostic species in the understories of the mixed-oak forests, the beech forests, and the ravine forests (Table 2). Finally, we classified each 1 m square plot along the sinkhole transects into plot types with the use of the diagnostic species groups. For example, if the number of diagnostic species of the ravine forests was the highest in the target sinkhole plot, we considered it a plot dominated by ravine forest species. Hence, this method resulted in five sinkhole-plot types: plots dominated by ravine forest species, plots dominated by beech forest species, plots dominated by mixed-oak forest species, transitional plots, and empty plots. Transitional plots were those which were dominated by an equal number of diagnostic species of two or three groups. Empty plots did not contain any plant species. From an ecological point of view, plots dominated by ravine forest species can be considered potential refuge areas for many species adapted to cool and moist habitats (e.g., Fig. 3). Moreover, field observations were performed to verify the result of fidelity measurement.

Species-area relations were assessed for all plant species, as well as for the group of relict, mountain, wet-woodland species and other diagnostic species of the ravine forests. In this study, twenty sinkholes, representative of sinkholes of all sizes, were included in the species-area analyses.

Results

The number of 1 m square plots dominated by ravine forest species generally increased with sinkhole size (Fig. 4; Table 3). In the small and shallow sinkholes A to G, only plots dominated by beech forest and mixed-oak forest species were found. In contrast, in larger sinkholes, the lower parts of the slopes were covered mainly by plots dominated by ravine forest species; while the upper parts of the slopes were covered by plots dominated by beech forest or mixed-oak forest species. In some sinkholes, the proportion of mixed-oak forest species was very high on the edges and south-facing slopes. Accordingly, vegetation inversion was pronounced, especially in the case of sinkholes N, S, Q, and T, followed by a gradual change in floristic composition.

Of the forty-one diagnostic species of the ravine forests found, five were mountain species, ten were wet-woodland species, and twenty-six were other diagnostic species (e.g., gap-species) (Table 2). In addition, a glacial relict (*Stachys alpina*), six other mountain species (*Actaea spicata, Aruncus sylvestris, Dryopteris affinis, Dryopteris dilatata, Dryopteris expansa*, and *Polystichum × bicknelli*), and six other wet-woodland species (*Deschampsia caespitosa, Eupatorium cannabinum, Festuca gigantea, Lycopus europaeus, Rumex sanguineus*, and *Solanum dulcamara*) were found in the ravine forests, although they were not diagnostic according to the test.

The relationship between sinkhole size ($\log_{10}$transformed) and species number ($\log_{10}$transformed) is shown in Fig. 5. When all species were considered, the correlation between species number and sinkhole size was positive and significant ($R^2 = 0.9302$, $p < 0.001$). For example, the highest number of species (141) was found in the largest sinkhole (T), while the lowest number of species (23) was found in two of the smallest sinkholes (A and C) (Table 3). The result was basically the same if only the group of relict, mountain, wet-woodland species and other diagnostic species of the ravine forests was considered ($R^2 = 0.9006$, $p < 0.001$). From a floristic point of view, sinkholes R and T were the most important, because they contained the highest number of both relicts and mountain species (R: *Dryopteris affinis, Dryopteris expansa, Dryopteris dilatata, Polystichum aculeatum, Polystichum × bicknelli* and *Stachys alpina*; T: *Aconitum vulparia, Actaea spicata, Asplenium scolopendrium, Dryopteris affinis, Polystichum aculeatum, Polystichum × bicknelli* and *Stachys alpina*).

Table 2. Diagnostic species of the types of forest surrounding sinkholes in the Mecsek Mountains, defined by Φ × 100 ≥ 10. If a species is in the list for more than one forest type, its Φ value is shown in both parts of the table.

Vegetation Type and Species	Φ × 100		
	MOF	BF	RF
Diagnostic species of the mixed-oak forests			
Lathyrus vernus	10.3	21.5	…
Festuca drymeja	11.1	…	…
Melittis carpatica	11.1	…	…
Galium mollugo	12.2	…	…
Poa nemoralis	12.2	…	…
Moehringia trinervia	12.9	…	…
Campanula persicifolia	14.1	…	…
Carex divulsa	14.1	…	…
Symphytum tuberosum	14.1	…	…
Torilis japonica	14.1	…	…
Brachypodium sylvaticum	14.2	…	…
Sorbus torminalis	14.2	…	…
Galium aparine	15.8	…	…
Luzula forsteri	15.8	…	…
Prunella vulgaris	15.8	…	…
Alliaria petiolata	16.2	…	…
Ruscus aculeatus	16.3	…	…
Carex pilosa	16.4	51.1	…
Quercus petraea	18.4	14.2	…
Potentilla micrantha	20.1	…	…
Viola alba	20.1	…	…
Viola odorata	20.1	…	…
Buglossoides purpureo-coerulea	22.5	…	…
Lysimachia nummularia	22.5	…	…
Veronica chamaedrys	23.3	…	…
Tamus communis	23.6	…	…
Festuca heterophylla	24.7	…	…
Fragaria vesca	26.4	…	…
Galium schultesii	26.8	…	…
Geum urbanum	29.1	…	…
Campanula rapunculoides	30.5	…	…
Crataegus laevigata	30.6	…	…
Acer campestre	30.8	…	…
Carpinus betulus	31.3	…	…
Helleborus odorus	33.3	…	…
Quercus cerris	34.4	…	…
Convallaria majalis	34.7	…	…
Euphorbia amygdaloides	35.0	…	…
Fallopia dumetorum	39.3	…	…
Euonymus verrucosus	40.0	…	…
Bromus ramosus agg.	43.5	…	…
Melica uniflora	45.1	39.8	…
Rosa arvensis	45.3	…	…
Glechoma hirsuta	54.9	…	…
Ligustrum vulgare	56.9	…	…
Stellaria holostea	60.6	…	…

Table 2. Continued.

Vegetation Type and Species	Φ × 100		
	MOF	BF	RF
Fraxinus ornus	66.4	…	…
Dactylis polygama	72.9	…	…
Diagnostic species of the beech forests			
Ulmus glabra	…	12.4	…
Milium effusum	…	14.1	…
Quercus petraea	18.4	14.2	…
Galeobdolon luteum s.l.	…	14.7	59.8
Asarum europaeum	…	15.1	…
Viola reichenbachiana	…	15.1	…
Carex digitata	…	16.3	…
Hepatica nobilis	…	20.9	…
Lathyrus vernus	10.3	21.5	…
Ruscus hypoglossus	…	21.8	…
Prunus avium	…	24.7	…
Tilia tomentosa	…	25.6	…
Tilia cordata	…	31.4	…
Rubus hirtus agg.	…	32.4	…
Fraxinus excelsior	…	32.6	…
Melica uniflora	45.1	39.8	…
Hedera helix	…	43.5	…
Fagus sylvatica	…	49.2	…
Carex pilosa	16.1	51.1	…
Galium odoratum	…	53.9	…
Diagnostic species of the ravine forests			
Mountain species			
Polystichum aculeatum	…	…	22.5
Aconitum vulparia	…	…	26.8
Lunaria rediviva	…	…	27.7
Silene dioica	…	…	30.5
Asplenium scolopendrium	…	…	37.8
Wet woodland species			
Dryopteris carthusiana	…	…	15.8
Myosoton aquaticum	…	…	15.8
Persicaria dubia	…	…	15.8
Carex pendula	…	…	17.3
Ranunculus repens	…	…	25.8
Carex remota	…	…	27.7
Urtica dioica	…	…	42.8
Aegopodium podagraria	…	…	44.8
Athyrium filix-femina	…	…	46.2
Chrysosplenium alternifolium	…	…	64.9
Other diagnostic species of the ravine forests			
Mercurialis perennis	…	…	11.1
Galeopsis speciosa	…	…	12.2
Erigeron annuus	…	…	12.2
Pulmonaria officinalis	…	…	12.4
Cerastium sylvaticum	…	…	14.1
Knautia drymeia	…	…	14.1

Table 2. Continued.

Vegetation Type and Species	Φ × 100		
	MOF	BF	RF
Atropa bella-donna	…	…	15.8
Salvia glutinosa	…	…	15.8
Clematis vitalba	…	…	16.3
Lamium maculatum	…	…	16.6
Chelidonium majus	…	…	18.8
Geranium phaeum	…	…	18.8
Stachy sylvatica	…	…	20.1
Cardamine impatiens	…	…	20.4
Polystichum setiferum	…	…	21.3
Asplenium trichomanes	…	…	26.8
Veronica montana	…	…	27.4
Geranium robertianum	…	…	27.5
Sambucus nigra	…	…	31.4
Dryopteris filix-mas	…	…	32.2
Mycelis muralis	…	…	33.3
Stellaria media	…	…	33.9
Acer pseudoplatanus	…	…	35.5
Circaea lutetiana	…	…	52.2
Oxalis acetosella	…	…	54.7
Galeobdolon luteum s.l.	…	14.7	59.8
Totals			
No. of plots	135	135	135
No. of diagnostic species	48	20	41

Note Abbreviations: MOF: mixed-oak forests, BF: beech forests, RF: ravine forests.

Discussion and Conclusions

Studying the ecological conditions, vegetation pattern, and species composition of karst depressions may provide important information for the conservation and management of karst surfaces. Many studies in vegetation science have focused on the large-scale vegetation patterns of karst forms (e.g. Lausi, 1964; Bátori et al., 2009), but only relatively few studies deal with the fine-scale vegetation pattern of sinkholes and the use of transects to reveal them (e.g., Gargano et al., 2010). In our study, the species composition and vegetation pattern of solution sinkholes were analyzed in relation to sinkhole size in a sub-Mediterranean woodland area of Hungary. The vegetation pattern of sinkholes can be summarized and the questions posed in the Introduction can be answered as follows.

(i) Vegetation inversion is a well known phenomenon in karst depressions (Beck v. Mannagetta, 1906; Lausi, 1964; Horvat, 1953; Favretto and Poldini, 1985). In Hungary, south-facing slopes receive much more solar radiation, and thus, are warmer than north-facing slopes (Jakucs, 1977). In smaller sinkholes of the study site, the vegetation pattern does not change substantially along the transects, and the slopes are floored

Figure 3. *Stachys alpina* **(left), a glacial relict, and** *Lunaria rediviva* **(right), a mountain species, in the sinkholes of the Mecsek Mountains, southern Hungary.**

by vegetation characteristic only of beech forests or mixed-oak forests. In contrast, south-facing slopes in larger sinkholes are dominated by mixed-oak forests or beech forests, north-facing slopes by beech forests, and the bottom of sinkholes by ravine forests. Vegetation inversion is well pronounced only in the largest sinkholes, where beech forest vegetation replaces that of mixed-oak forests on the deeper parts of the slopes. This phenomenon was also confirmed by field observations. Similar results were published by Bátori et al. (2009, 2011) in different scales.

(ii) Climate change has already produced and will continue to produce numerous shifts in the distributions of species (Walther et al., 2002), which highlights the role of current and potential refuge areas. A prominent finding in our study is that the low-lying sinkholes (250 to 500 masl) of the Mecsek Mountains provide good refuge areas for many species adapted to cool and moist habitats. This is a consequence of the morphologic characteristics of karst depressions, which strongly determine both abiotic (e.g., air humidity, air temperature, soil moisture) and biotic (e.g., vegetation pattern) parameters of sinkholes (see also, Geiger, 1950; Antonić et al., 1997; Bárány-Kevei, 1999; Antonić et al., 2001, Whiteman et al., 2004; Gargano et al., 2010). The extent of refuge areas shows a positive correlation with sinkhole size in the Mecsek Mountains. In general, the extent of cool and moist habitats in the sinkholes increases with sinkhole diameter, due to the fact that wider sinkholes are usually deeper.

(iii) Sinkholes of the Mecsek Mountains harbor many vascular plant species that are missing or are very rare in the surrounding habitats, and they can be considered habitat islands in the "ocean" of local
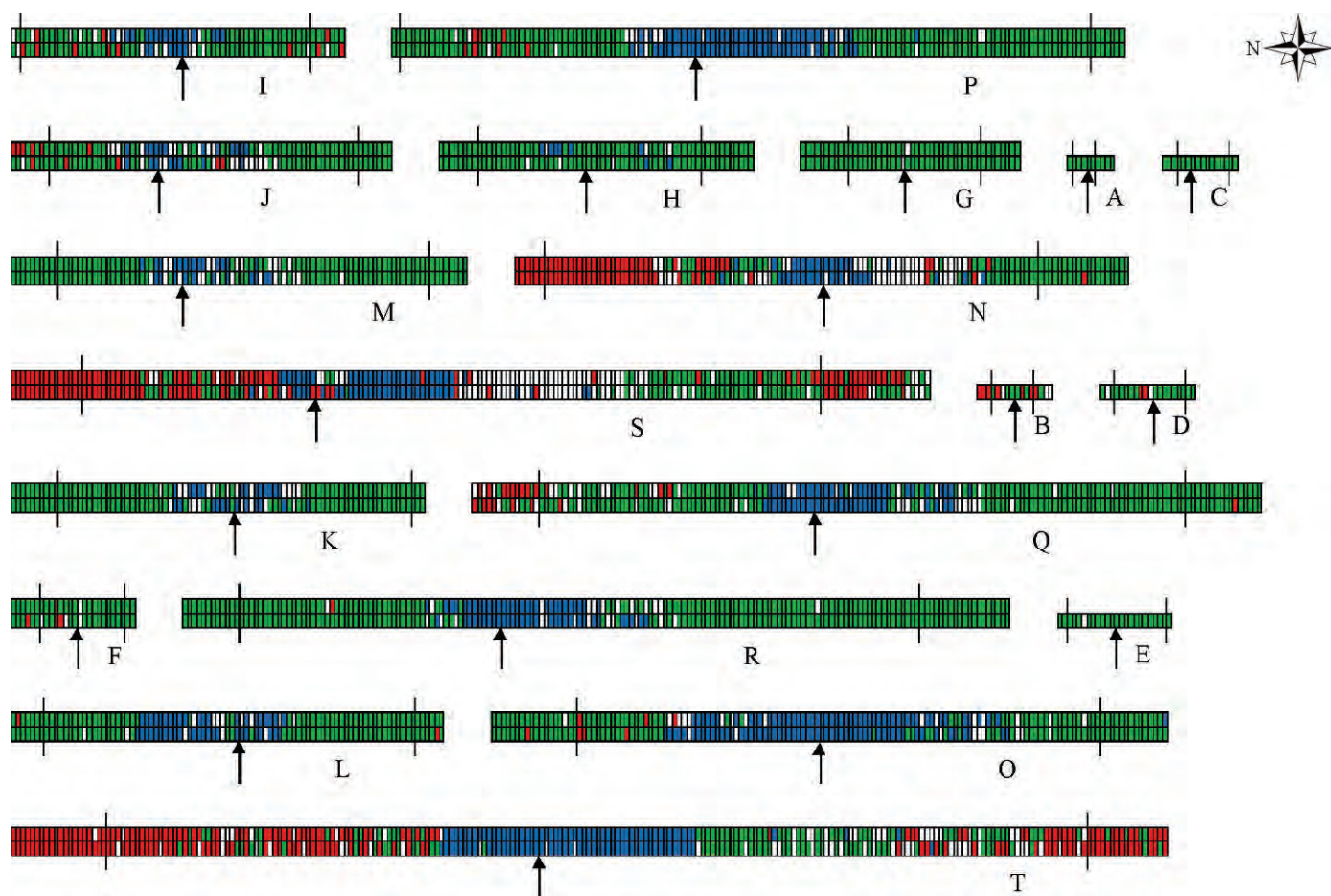
Figure 4. Plots in the north-south transects, with north to the left, that are dominated by mixed-oak forest (red), beech forest (green), or ravine forest (blue) species in the sinkholes (A-T) of the Mecsek Mountains. White plots are transitional or empty. Short vertical lines indicate where the slope falls below 10° at the edges of the sinkholes, and arrows mark the deepest point of the sinkholes, where slope exposure changes.

Table 3. Total number of plant species and cool-adapted species of various types, as well as the number of plots dominated by ravine forest species for the sinkholes, which increase in size from A to T.

Sinkhole	A	B	C	D	E	F	G	H	I	J	K	L	M	N	O	P	Q	R	S	T
Total number of plant species	23	37	23	30	32	43	39	58	68	68	66	72	63	97	82	91	86	93	113	141
Glacial relicts	···	···	···	···	···	···	···	···	···	···	···	···	···	···	···	1	···	1	···	1
Mountain species	···	···	···	···	···	···	···	1	2	1	2	2	2	3	2	3	3	5	3	6
Wet woodland species	···	···	···	···	···	···	···	2	3	4	2	3	2	7	5	6	6	8	6	8
Other diagnostic species of the ravine forests	4	3	2	2	4	8	7	11	12	11	10	11	12	16	15	13	16	16	16	18
Plots dominated by ravine forest species	···	···	···	···	···	···	···	8	22	20	25	46	25	39	109	79	59	61	65	107
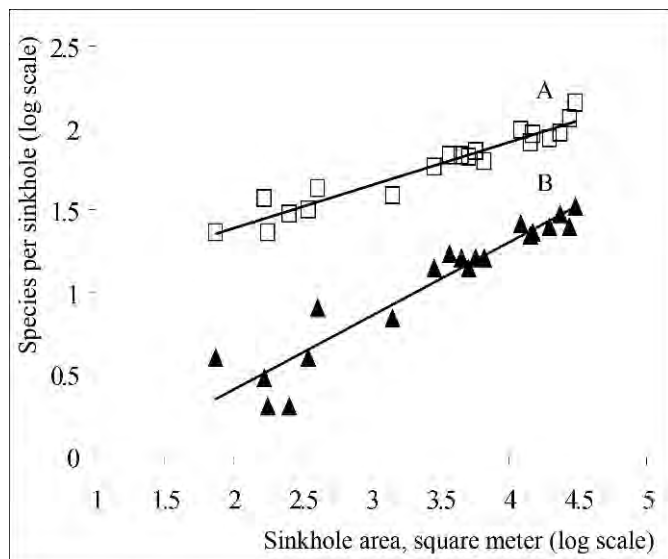
Figure 5. Relationship between sinkhole area (log$_{10}$transformed) and species number (log$_{10}$ transformed) for vascular vegetation of the Mecsek Mountains ($N = 20$). Species-area lines were determined for all species (A: $y = 0.2612x + 0.8670$, $R^2 = 0.9302$) and the group of relict, mountain, wet-woodland species and other diagnostic species of the ravine forests (B: $y = 0.4465x − 0.4868$, $R^2 = 0.9006$).

beech and mixed-oak forests. According to the well-known species-area relationship (Arrhenius, 1921), species number is related to area by the function $S = CA^z$, where S is species number, A is area of island, and C and z are positive constants. C and z constants were calculated by linear regression on the logarithmic form of the equation, $\log S = \log C + z \log A$, where $\log C$ represents the y-intercept and z the slope. When all species of the studied sinkholes are considered, the z value is 0.26, which is in good agreement with the z values received for many oceanic and habitat islands ($z = 0.20$ to 0.35) in island biogeography (MacArthur and Wilson, 1967; Simberloff and Abele, 1976; Begon et al., 2005). In contrast, when only the group of relict, mountain, wet-woodland species and other diagnostic species of the ravine forests is considered, the z value is considerably higher ($z = 0.45$). According to Rockwood (2006), z values larger than expected arise when islands have a large habitat diversity and are more or less isolated. For example, Culver et al. (1973) found a relatively high z value for terrestrial invertebrates in caves ($z = 0.72$), Trejo-Torres and Ackerman (2001) for endemic orchid species on geologically diverse montane islands ($z = 0.68$), and Brown (1971) for small boreal mammals on isolated mountaintops ($z = 0.43$). Accordingly, our results suggest that the habitat topography of large sinkholes is complex and the extent of cool and moist habitats

considerably increases with sinkhole size (Fig. 4), so larger sinkholes may preserve many more vascular plant species adapted to cool and moist habitats than smaller sinkholes.

Therefore, conservation management must focus on protecting habitats of larger sinkholes and their surroundings in the Mecsek Mountains. This management should include establishing a buffer zone around all sinkholes, in accordance with the proposal of the Forest Sinkhole Manual (Kiernan, 2002).

References

Ádám, L., Marosi, S., and Szilárd, J., eds., 1981, A Dunántúli-dombság (Dél-Dunántúl). Magyarország tájföldrajza 4: Budapest, Akadémiai Kiadó, 704 p.

Antonić, O., Kušan, V., and Hrašovec, B., 1997, Microclimatic and topoclimatic differences between the phytocoenoses in the Viljska Ponikva Sinkhole, Mt. Risnjak, Croatia: Hrvatski Meteorološki časopis, v. 32, p. 37–49.

Antonić, O., Hatic, D., and Pernar, R., 2001, DEM-based depth in sink as an environmental estimator: Ecological Modeling, v. 138, p. 247–254. doi:10.1016/S0304-3800(00)00405-1.

Arrhenius, O., 1921, Species and area: Journal of Ecology, v. 9, p. 95–99.

Bárány-Kevei, I., 1999, Microclimate of karstic dolines: Acta Climatologica Universitatis Szegediensis, v. 32–33, p. 19–27.

Bátori, Z., Gallé, R., Erdős, L., and Körmöczi, L., 2011, Ecological conditions, flora and vegetation of a large doline in the Mecsek Mountains (South Hungary): Acta Botanica Croatica, v. 70, p. 147–155. doi:10.2478/v10184-010-0018-1.

Bátori, Z., Csiky, J., Erdős, L., Morschhauser, T., Török, P., and Körmöczi, L., 2009, Vegetation of the dolines in Mecsek Mountains (South Hungary) in relation to the local plant communities: Acta Carsologica, v. 38, no. 2–3, p. 237–252.

Beck v. Mannagetta, G., 1906, Die Umkehrung der Pflanzenregionen in den Dolinen des Karstes: Sitzungsberichte der Kaiserliche Akademie der Wissenschaften in Wien–Mathematisch-Naturwissenschaftliche Klasse, v. 115, p. 3–20.

Begon, M., Townsend, C.R., and Harper, J.L., 2006, Ecology: From Individuals to Ecosystems: Oxford, Blackwell, 738 p.

Brown, J.H., 1971, Mammals on mountaintops: nonequilibrium insular biogeography: The American Naturalist, v. 105, no. 945, p. 467–478.

Brullo, S., and Giusso del Galdo, G., 2001, Astracantha dolinicola (Fabaceae), a new species from Crete: Nordic Journal of Botany, v. 21, p. 475–480. doi:10.1111/j.1756-1051.2001.tb00799.x.

Christiansen, K., and Bellinger, P., 1996, Cave Pseudosinella and Oncopodura new to science: Journal of Cave and Karst Studies, v. 58, no. 1, p. 38–53.

Chytrý, M., Tichý, L., Holt, J., and Botta-Dukát, Z., 2002, Determination of diagnostic species with statistical fidelity measures: Journal of Vegetation Science, v. 13, no. 1, p. 79–90. doi:10.1111/j.1654-1103.2002.tb02025.x.

Cowie, J., 2007, Climate Change: Biological and Human Aspects: New York, Cambridge University Press, 504 p.

Culver, D.C., Holsinger, J.R., and Baroody, R., 1973, Toward a predictive cave biogeography: the Greenbrier valley as a case study: Evolution, v. 27, p. 689–695.

Culver, D.C., and Sket, B., 2000, Hotspots of subterranean biodiversity in caves and wells: Journal of Cave and Karst Studies, v. 62, no. 1, p. 11–17.

Dakskobler, I., Sinjur, I., Veber, I., and Zupan, B., 2008, Localities and sites of *Pulsatilla vernalis* in the Julian Alps: Hacquetia, v. 7, p. 47–69.

Egli, B.R., 1991, The special flora, ecological and edaphic conditions of dolines in the mountain of Crete: Botanica Chronika, v. 10, p. 325–335.

Egli, B.R., Gerstberger, P., Greuter, W., and Risse, H., 1990, *Horstrissea dolinicola*, a new genus and species of umbels (Umbelliferae, Apiaceae) from Kriti (Greece): Willdenowia, v. 19, no. 2, p. 389–399.

Elliott, W.R., 2007, Zoogeography and biodiversity of Missouri caves and karst: Journal of Cave and Karst Studies, v. 69, no. 1, p. 135–162.

Favretto, D., and Poldini, L., 1985, The vegetation in the dolinas of the karst region near Trieste (Italy): Studia Geobotanica, v. 5, p. 5–18.

Gargano, D., Vecchio, G., and Bernardo, L., 2010, Plant-soil relationships in fragments of Mediterranean snow-beds: ecological and conservation implications: Plant Ecology, v. 207, no. 1, p. 175–189. doi:10.1007/s11258-009-9663-7.

Geiger, R., 1950, Das Klima der bodennahen Luftschicht: Ein Lehrbuch der Mikroklimatologie, third edition: Braunschweig, Friedr. Vieweg & Sohn, 460 p.

Habel, J.C., and Assmann, T., eds., 2010, Relict species: Phylogeography and Conservation Biology: Heidelberg, Springer, 449 p. doi:10.1007/978-3-540-92160-8.

Horvat, I., 1953, Vegetacija ponikava: Hrvatski Geografski Glasnik, v. 14–15, p. 1–25.

Hoyk, E., 1999, Investigation of the vegetation and soil in the dolinas of Western Mecsek Mountains, South Hungary: Acta Carsologica, v. 28, no. 1, p. 105–113.

Iverson, L.R., and Prasad, A.M., 1998, Predicting abundance of 80 tree species following climate change in the Eastern United States: Ecological Monographs, v. 68, no. 4, p. 465–485. doi:10.1890/0012-9615(1998)068[0465:PAOTSF]2.0.CO;2.

Jakucs, L., 1977, A karsztok morfogenetikája: A karsztfejlődés varienciái: Budapest, Akadémiai Kiadó, 284 p.

Judson, M.L.I., 2007, A new and endangered species of the pseudoscorpion genus *Lagynochthonius* from a cave in Vietnam, with notes on chelal morphology and the composition of the Tyrannochthoniini (Arachnida, Chelonethi, Chthoniidae): Zootaxa, no. 1627, p. 53–68.

Kiernan, K., 2002, Forest Sinkhole Manual: Tasmania, Hobart, Forest Practices Board, 35 p.

Király, G., ed., 2009, Új Magyar Füvészkönyv. Magyarország hajtásos növényei. Határozókulcsok: Jósvafő, Aggteleki Nemzeti Park Igazgatóság, 616 p.

Köhn, J., and Waterstraat, A., 1990, Recent distribution of glacial relict Malacostraca in the lakes of Mecklenburg: Annales Zoologici Fennici, v. 27, p. 237–240.

Lausi, D., 1964, Vorläufiger Überblick über die Vegetation der Triester Karstdolinen: Acta Botanica Croatica, v. 4, p. 65–71.

Lazarević, P., Lazarević, M., Krivošej, Z., and Stevanović, V., 2009, On the distribution of *Dracocephalum ruyschiana* (Lamiaceae) in the Balkan Peninsula: Phytologia Balcanica, v. 15, no. 2, p. 175–179.

Lewis, J.J., and Bowman, T.E., 2010, The subterranean asellids of Maryland: Description of *Caecidotea nordeni*, new species, and new records of *C. holsingeri* and *C. franzi* (Crustacea: Malacostraca:

Isopoda): Journal of Cave and Karst Studies, v. 72, no. 2, p. 100–104. doi:10.4311/jcks2009lsc0092.

Lovász, Gy., 1971, Adatok az Abaligeti-karszt geomorfológiai és hidrológiai jellemzéséhez: Földrajzi Értesítő, v. 20, p. 283–295.

MacArthur, R.H., and Wilson, E.O., 1967, The Theory of Island Biogeography: Princeton, Princeton University Press, 203 p.

Özkan, K., Gulsoy, S., Mert, A., Ozturk, M., and Muys, B., 2010, Plant distribution-altitude and landform relationships in karstic sinkholes of Mediterranean region of Turkey: Journal of Environmental Biology, v. 31, p. 51–60.

Pericin, C., and Hürlimann, H., 2001, Beobachtungen zur vertikalen Verteilung der Moosarten in der Doline Sterna-Filaria im Karstgebiet von Buje/Buie in Istrien (Kroatien): Bauhinia, v. 15, p. 91–96.

Rockwood, L.L., 2006, Introduction to Population Ecology: Oxford, Blackwell Scientific Publications, 339 p.

Sagarin, R.D., Barry, J.P., Gilman, S.E., and Baxter, C.H., 1999, Climate-related change in an intertidal community over short and long time scales: Ecological Monographs, v. 69, no. 4, p. 465–490. doi:10.1890/0012-9615(1999)069[0465:CRCIAI]2.0.CO;2.

Schindler, D.W., Bayley, S.E., Parker, B.R., Beaty, K.G., Cruikshank, D.R., Fee, E.J., Schindler, E.U., and Stainton, M.P., 1996, The effects of climatic warming on the properties of boreal lakes and streams at the Experimental Lakes Area, northwestern Ontario: Limnology and Oceanography, v. 41, no. 5, p. 1004–1017.

Sheldon, T.A., Mandrak, N.E., and Lovejoy, N.R., 2008, Biogeography of the deepwater sculpin (*Myoxocephalus thompsonii*), a Nearctic glacial relict: Canadian Journal of Zoology, v. 86, p. 108–115. doi:10.1139/Z07-125.

Simberloff, D.S., and Abele, L.G., 1976, Island biogeography theory and conservation practice: Science, v. 191, no. 4224, p. 285–286. doi:10.1126/science.191.4224.285.

Simon, T., 2000, A magyarországi edényes flóra határozója: harasztok, virágos növények: Budapest, Nemzeti Tankönyvkiadó, 845 p.

Szmorad, F., 1999, Adatok az Aggteleki-karszt és a Galyaság flórájához I.: Kitaibelia, v. 4, no. 1, p. 77–82.

Tichý, L., 2002, JUICE, software for vegetation classification: Journal of Vegetation Science, v. 13, no. 3, p. 451–453. doi:10.1111/j.1654-1103.2002.tb02069.x.

Trejo-Torres, J.C., and Ackerman, J.D., 2001, Biogeography of the Antilles based on a parsimony analysis of orchid distributions: Journal of Biogeography, v. 28, p. 775–794. doi:10.1046/j.1365-2699.2001.00576.x.

Vojtkó, A., 1997, Új adatok a Tornai-karszt flórájához és vegetációjához: Kitaibelia, v. 2, no. 2, p. 248–249.

Walther, G.-R., Post, E., Convey, P., Menzel, A., Parmesan, C., Beebee, T.J.C., Fromentin, J.-M., Hoegh-Guldberg, O., and Bairlein, F., 2002, Ecological responses to recent climate change: Nature, v. 416, p. 389–437. doi:10.1038/416389a.

Whiteman, C.D., Haiden, T., Pospichal, B., Eisenbach, S., and Steinacker, R., 2004, Minimum temperatures, diurnal temperature ranges, and temperature inversion in limestone sinkholes of different sizes and shapes: Journal of Applied Meteorology, v. 43, p. 1224–1236. doi:10.1175/1520-0450(2004)043<1224:MTDTRA>2.0.CO;2.

Wolowski, K., 2003, Euglenophytes reported from karst sink-holes in the Malopolska Upland (Poland, Central Europe): Annales de Limnologie - International Journal of Limnology, v. 39, no. 4, p. 333–346. doi:10.1051/limn/2003027.

GUIDE TO AUTHORS

The *Journal of Cave and Karst Studies* is a multidisciplinary journal devoted to cave and karst research. The *Journal* is seeking original, unpublished manuscripts concerning the scientific study of caves or other karst features. Authors do not need to be members of the National Speleological Society, but preference is given to manuscripts of importance to North American speleology.

LANGUAGES: The *Journal of Cave and Karst Studies* uses American-style English as its standard language and spelling style, with the exception of allowing a second abstract in another language when room allows. In the case of proper names, the *Journal* tries to accommodate other spellings and punctuation styles. In cases where the Editor-in-Chief finds it appropriate to use non-English words outside of proper names (generally where no equivalent English word exists), the *Journal* italicizes them. However, the common abbreviations i.e., e.g., et al., and etc. should appear in roman text. Authors are encouraged to write for our combined professional and amateur readerships.

CONTENT: Each paper will contain a title with the authors' names and addresses, an abstract, and the text of the paper, including a summary or conclusions section. Acknowledgments and references follow the text.

ABSTRACTS: An abstract stating the essential points and results must accompany all articles. An abstract is a summary, not a promise of what topics are covered in the paper.

STYLE: The *Journal* consults The Chicago Manual of Style on most general style issues.

REFERENCES: In the text, references to previously published work should be followed by the relevant author's name and date (and page number, when appropriate) in parentheses. All cited references are alphabetical at the end of the manuscript with senior author's last name first, followed by date of publication, title, publisher, volume, and page numbers. Geological Society of America format should be used (see http://www.geosociety.org/pubs/geoguid5. htm). Please do not abbreviate periodical titles. Web references are acceptable when deemed appropriate. The references should follow the style of: Author (or publisher), year, Webpage title: Publisher (if a specific author is available), full URL (e.g., http://www. usgs.gov/citguide.html) and date when the web site was accessed in brackets; for example [accessed July 16, 2002]. If there are specific authors given, use their name and list the responsible organization as publisher. Because of the ephemeral nature of websites, please provide the specific date. Citations within the text should read: (Author, Year).

SUBMISSION: Effective February 2011, all manuscripts are to be submitted via Peertrack, a web-based system for online submission. The web address is http://www.edmgr.com/jcks. Instructions are provided at that address. At your first visit, you will be prompted to establish a login and password, after which you will enter information about your manuscript (e.g., authors and addresses, manuscript title, abstract, etc.). You will then enter your manuscript, tables, and figure files separately or all together as part of the manuscript. Manuscript files can be uploaded as DOC, WPD, RTF, TXT, or LaTeX. A DOC template with additional manuscript specifications may be downloaded. (Note: LaTeX files should not use any unusual style files; a LaTeX template and BiBTeX file for the *Journal* may be downloaded or obtained from the Editor-in-Chief.) Table files can be uploaded as DOC, WPD, RTF, TXT, or LaTeX files, and figure files can be uploaded as TIFF, EPS, AI, or CDR files. Alternatively, authors may submit manuscripts as PDF or HTML files, but if the manuscript is accepted for publication, the manuscript will need to be submitted as one of the accepted file types listed above. Manuscripts must be typed, double spaced, and single-sided. Manuscripts should be no longer than 6,000 words plus tables and figures, but exceptions are permitted on a case-by-case basis. Authors of accepted papers exceeding this limit may have to pay a current page charge for the extra pages unless decided otherwise by the Editor-in-Chief. Extensive supporting data will be placed on the *Journal*'s website with a paper copy placed in the NSS archives and library. The data that are used within a paper must be made available. Authors may be required to provide supporting data in a fundamental format, such as ASCII for text data or comma-delimited ASCII for tabular data.

DISCUSSIONS: Critical discussions of papers previously published in the *Journal* are welcome. Authors will be given an opportunity to reply. Discussions and replies must be limited to a maximum of 1000 words and discussions will be subject to review before publication. Discussions must be within 6 months after the original article appears.

MEASUREMENTS: All measurements will be in Systeme Internationale (metric) except when quoting historical references. Other units will be allowed where necessary if placed in parentheses and following the SI units.

FIGURES: Figures and lettering must be neat and legible. Figure captions should be on a separate sheet of paper and not within the figure. Figures should be numbered in sequence and referred to in the text by inserting (Fig. x). Most figures will be reduced, hence the lettering should be large. Photographs must be sharp and high contrast. Color will generally only be printed at author's expense.

TABLES: See http://www.caves.org/pub/journal/PDF/Tables. pdf to get guidelines for table layout.

COPYRIGHT AND AUTHOR'S RESPONSIBILITIES: It is the author's responsibility to clear any copyright or acknowledgement matters concerning text, tables, or figures used. Authors should also ensure adequate attention to sensitive or legal issues such as land owner and land manager concerns or policies.

PROCESS: All submitted manuscripts are sent out to at least two experts in the field. Reviewed manuscripts are then returned to the author for consideration of the referees' remarks and revision, where appropriate. Revised manuscripts are returned to the appropriate Associate Editor who then recommends acceptance or rejection. The Editor-in-Chief makes final decisions regarding publication. Upon acceptance, the senior author will be sent one set of PDF proofs for review. Examine the current issue for more information about the format used.

ELECTRONIC FILES: The *Journal* is printed at high resolution. Illustrations must be a minimum of 300 dpi for acceptance.

Journal of Cave and Karst Studies

Volume 74   Number 1   April 2012